GATE-TURN-OFF THYRISTOR COMMUTATION OF DC MACHINES

The development of a rotating DC machine with
static commutation of armature coil current
using Gate-Turn-Off thyristor devices

by

ABDULMAJEED HABIB MOHAMMED KARIM

MSc(Eng), DipEE, AMIEE

A Thesis submitted to the University of Bradford for the Degree of
Doctor of Philosophy

Postgraduate School of Studies
in Electrical and Electronic Engineering
University of Bradford
Bradford - England

1986

To the memory of my father, Habib, who sadly died on Sunday the
28 September 1986, just before the completion of this work,
and who provided much support and encouragement
during my years of study in England.

To my dearest mother, Rabab, who
supported me equally, and to
whom I shall always
be indebted.

Majeed

A C K N O W L E D G E M E N T S

The author would like to express his deep gratitude to his supervisor, Dr Clifford B Gray, for his invaluable help and encouragement during the research period and during the preparation of this thesis. The author owes a special debt of gratitude to him for the provision of material from his book, to be published in 1987, from which the author greatly benefited.

The author would also like to thank Professors William Shepherd and Denis O'Kelly, professors in the Postgraduate School of Studies in Electrical and Electronic Engineering, University of Bradford for their continuous encouragement and support during his study period at the University and for making available the facilities of the School.

Thanks are also due to all the technicians of the School Laboratories and School Workshop for their help in building and provision of equipment for developing the prototype system.

The author is very much indebted to the Government of Bahrain and in particular, the Electricity Directorate, Ministry of Works, Power and Water, Manama, Bahrain, for the financial support in accomplishing this work.

The Director Personal Support, Eng. Abdulla Juma, is very much appreciated.

A B S T R A C T

The thesis is concerned with the development of a separately excited DC machine in which gate turn-off thyristor devices with their associated firing and protective circuits are used to provide the static commutation of armature coil current. The developed machine has its armature winding with 24 tapping points located on the stator and interconnected in "Lap" configuration. The initiation of the conduction periods of armature switching devices is defined by a digital control logic circuit, in conjunction with an incremental rotary encoder which provides the necessary feedback information relating to shaft speed and shaft angular position. This is arranged such that, under normal running conditions of the machine, the axis of the radial field of the armature winding maintains the normal space-quadrature relationship with that of the main field winding, giving the optimal torque angle of 90°. Provision is made, however, within the digital control circuit for controlled departure of the armature switch tapping points from the quadrature axis positions, and the effect of this, in improving commutation is investigated. The effect of interpoles is also explored. On the basis of the analysis carried out, a proposal is made for the future development of the machine employing a reduced number of armature switching devices without the need for interpole windings.

GLOSSARY OF PRINCIPAL SYMBOLS

Aa	Armature winding electric loading, A/m
AC, A.C.	Alternating current
ASCR	Asymmetrical thyristor
a	Number of parallel paths
a_b	Total surface area of a brush
Bn	Radial (normal) component of magnetic flux density, Wb/m^2
Bn_a	"Armature" winding radial magnetic flux density, Wb/m^2
Bn_f	"Field" winding radial magnetic flux density, Wb/m^2
Bn_{cp}	"Interpole" winding radial magnetic flux density, Wb/m^2
Bn_r	Resultant magnetic flux density in the airgap, Wb/m^2
β	Extinction angle
α	Firing (delay) angle
C	Number of commutator segments
C_k	K^{th} armature coil
C_s	Snubber capacitance, F
c	Number of coils
D	Duty cycle
Da	Diameter of the armature, m
DC, D.C.	Direct current
dV/dt	Rate of rise of off-state voltage, V/μsec
E_a	Motor generated (back) e.m.f., V
e_{cp}	Interpole induced e.m.f, V
e_r	Mean e.m.f. in a coil undergoing commutation, V
F_a , F_f	Armature, field winding m.m.f, At/pole

f_{clock}	Digital clock frequency, Hz
f_s	GTO switch switching frequency, Hz
$\emptyset$	Magnetic flux, Wb
G.T.O.	Gate turn-off Thyristor
g	Length of the airgap, m
H_n	Radial (normal) component of radial field intensity, A/m
H_t	Tangential component of radial field intensity, A/m
H_{n_a}	Armature winding radial field intensity, A/m
H_{n_f}	Field winding radial field intensity, A/m
$H_{n_{cp}}$	Interpole winding radial field intensity, A/m
H_{n_r}	Resultant radial field in the airgap, A/m
I_a	Armature load current, A
I_b	Armature current per brush, A
I_T (av)	Average on-state current of the switching device, A
I_{GF}	Gate turn-on (forward) current, A
I_{GR}	Gate turn-off (reverse) current, A
I.G.R.	Insulated gate rectifier
L_1	Self inductance of coil C1 undergoing commutation, H
l_w, l_s	Stray inductance of wiring and snubber, H
MOSFET	Metal-oxide semiconductor field effect transistor
m	Number of coil sides per slot
N_a	Number of armature winding conductors
N_f	Number of field winding conductors
n_c	Total number of turns of coil C undergoing commutation
n	Rotor speed, r.p.m.
P_{tot}	Total power loss in a GTO switching device
P.W.M.	Pulse width modulation
Q_1 Q_2 etc	Output Q of a flip-flop
$\bar{Q}_1, \bar{Q}_2$	Inverted output of a flip-flop

R_a	Motor armature resistance, Ohms
Rc	Ripple-carry output of a counter
S_1 S_2 etc	Negative rail connected armature switches
S_R	Digital control circuit reseting switch
s	Slip
s	Number of slots
T_1 T_2 etc	Positive rail connected armature switches
T_j	Junction temperature, °C
T_{hs}	Temperature of heat sink, °C
μo	Permeability of free-space
V_a	Motor armature voltage, V
V_T	On-state voltage of a GTO device, V
ΔV	Overshoot voltage, V
v	Rotor peripheral velocity, m/sec
y_c	Commutator pitch
y_b	Back pitch in coil sides
y_f	Front pitch in coil sides
y_r	Resultant pitch in coil sides

C O N T E N T S

CHAPTER ONE

INTRODUCTION

CHAPTER ONE

INTRODUCTION

1.1 VARIABLE SPEED MOTOR DRIVE SYSTEMS

The basic requirement that the most cost-effective electro-mechanical scheme of implementation be selected for a particular process dictates that serious consideration should be given to the various alternative drive schemes available, bearing in mind the essential features of drive economics, energy consumption and system efficiency.

The mere control of rotational speed is a requirement in many application areas and desirable in numerous others. Historically, this has been achieved through the selection of suitable prime movers, use of mechanical devices, special purpose electrical machines, variable speed couplings or electrical/electronic solutions.

The key to successful control of motor speed is the ability to vary in a fast, efficient and stable manner the voltages and currents applied to the motor. Closed loop control is often incorporated to maintain stability and accuracy as well as the ability to control other indirect variables such as the torque.

The selection of a drive type is further dependent on a number of other factors including power rating, speed range, operating

environment, maintenance considerations, accuracy requirements and general performance characteristics.

There are two major drive schemes, namely the DC and the AC drive systems. Since torque production is the ultimate requirement in any drive scheme, it should be appreciated that :

(i) For uniform airgap machines, torque production is the result of the interaction between the (radial) component fields of stator and rotor members facing each other across the airgap - called the "alignment torque", because the torque acts in a direction as to encourage the alignment of the stator and rotor field components.

(ii) Where the airgap is not uniform, "saliency" or "reluctance" torque is produced, if the system is "single-excited" and the excited member produces a field which is not symmetrically distributed about the magnetic axis of the salient pole structure on the other side of the airgap. Where the machine is salient pole "double-excited", both types of torque development are generally present.

DC drive systems should be discriminated by being excited from a DC source only and of having the armature current uniformly spread over the appropriate iron/airgap boundary. The polarity of this current reverses at each "brush" position. Where the airgap of the machine is uniform, such current distribution generates a triangular radial field distribution (Hn) with peaks coincident with the positions of the brushes (details of this will be given in chapter 2). The unique characteristic of the DC machine is its capability of maintaining a 90^{o} (electrical) torque angle between this axis of armature radial field and the axis of the radial field due to main

field winding excitation.

The tangential field component (H_t) on the other hand, varies linearly across the airgap where its peak occurs at the excited boundary of the airgap (equal to the current density (A/m)) to zero at the other [Gray 4] .

The radial and tangential field components established in the airgap by a DC armature winding is usually shown as triangular and rectangular distributions respectively.

AC drive systems, on the other hand, are characterised by having sinusoidally distributed current sheets on the surface of the rotor, thereby giving sinusoidal distributions of Hn and H_t with a 90° phase lead between the former and the latter.

It is therefore, the author's opinion that to abide with the fundamental machine theory, classification of variable speed motor drive systems should be in terms of the tangential field distribution and the radial flux distribution and not in terms of the electrical supply alone.

In the following sections, these two schemes will be reviewed with an attempt to assess relevant advantages of the DC and the AC systems.

1.2 DC DRIVE SYSTEMS

The excellent speed/torque characteristics and variable speed capacity of DC machines account for their continued and wide-ranging industrial use.

An excellent property of a DC separately-excited or shunt motor is that its steady-state speed is proportional to the armature voltage, provided the field current is held constant, the DC motor is the simplest motor to which electronic speed control may be applied since the control of the DC power is required. Therefore the earliest electronic speed control methods were those applied to DC motors and many have been successfully operating for over twenty years.

Good control of DC motors is achieved through the control of the armature voltage and current. This has made available motor sizes up to around 2500 KW, the limitation to a larger extent being to brushgear design.

The applied motor voltage is generally controlled in one of two ways [5]. The first method, is the DC "chopper" circuit [7,8] of which the present variant is known as the P.W.M. (Pulse Width Modulated) system [Tez 7]. The method is based on chopping of a DC voltage into a train of pulses which are variable in width using semiconductor devices such as transistors or thyristors. The switching frequency may be in the range 500 to 4000 Hz. If thyristors are used, forced-commutation of the anode current becomes necessary therefore increasing the complexity of the scheme. However the high rate of switching can provide a smoother output waveform.

In many industrial applications, DC drives are required to operate from an available alternating current source; the phase controlled converter (the second method) is used. This method is relatively easy and straight-forward to apply [1,5]: an alternating

input voltage is converted to a direct output voltage. The DC output voltage level is controlled by varying the point in time at which a thyristor is fired to allow it to conduct during each AC cycle of the input voltage. In this scheme, there is no need for artificially commutating the thyristors as current-commutation is achieved by the so called "natural" or "line" commutation.

The converter is referred to as "fully-controlled" if all the semiconductor devices are thyristors and "half-controlled" or "semi-converters" if some elements are thyristors and others are diodes.

Appropriate design of the converter circuit is required to permit operation in either 1, 2 or 4-quadrant operating mode, Fig. 1.1. The 4-quadrant operating mode is essential in cases where regenerative braking is required with speed control in both directions. Regenerative braking is called for in some industrial applications such as drives using frequent braking. If the field current direction is kept unchanged, then the armature current must be reversed in the regenerative mode to reverse the motor torque. The separately-excited DC motor is very flexible from the point of view of regenerative braking. This is because its field terminals can be reversed independently of its armature circuit. The field can be reversed either manually by contactors [9], or using dual converter, Fig. 1.1(d).

The variable speed DC drive has a number of distinct advantages in addition to the comparatively simple control: Very low speed operation is possible down to 1 rpm; overall efficiency is high particularly in the converter where 98% is achieved with 90% overall regularly achieved [6].

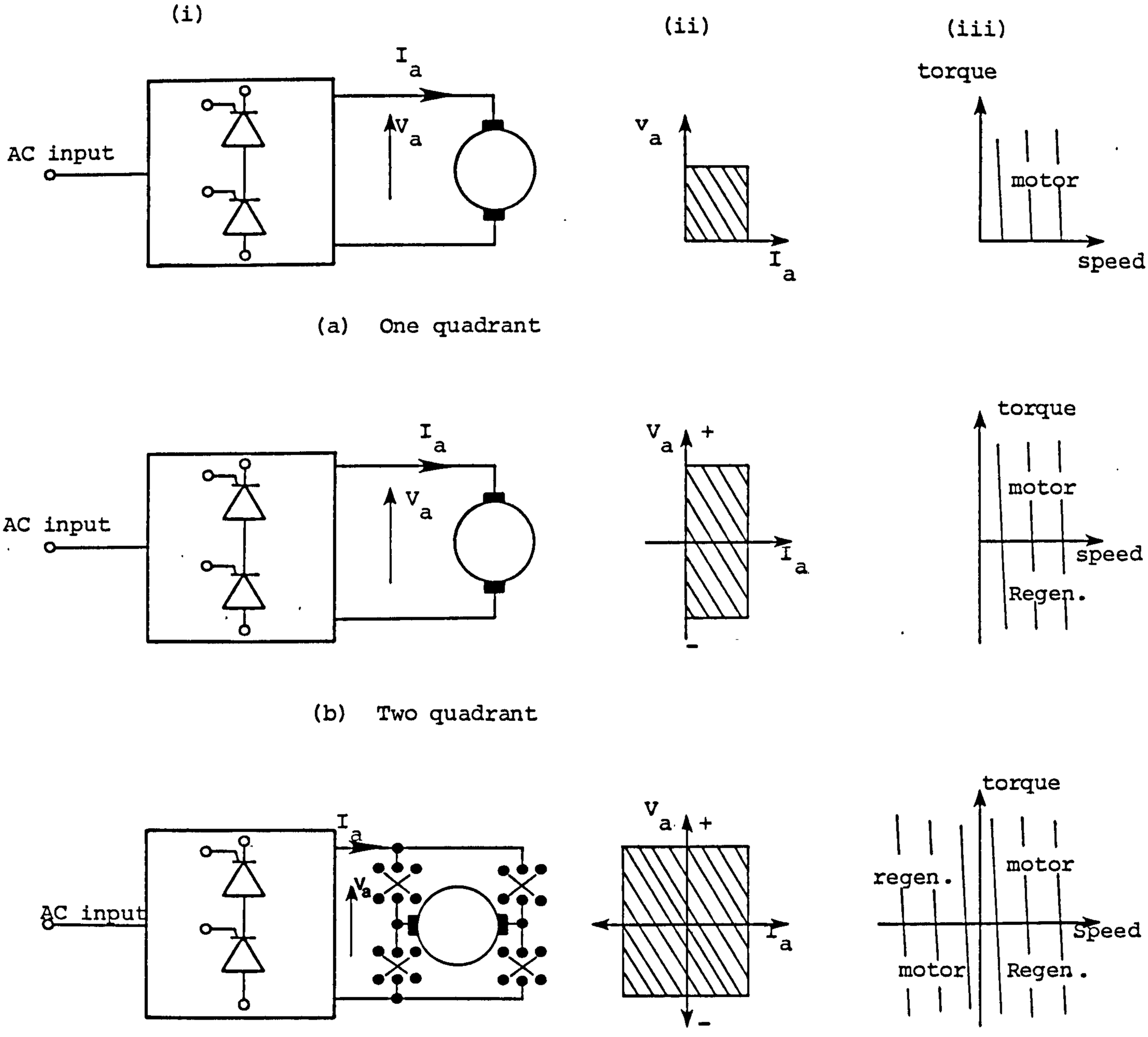

Fig. 1.1 Schematic representation of thyristor phase-controlled converter

(i) Block diagram
(ii) V_a versus I_a characteristics
(iii) Torque versus speed characteristics

Historically, the DC motor drive has dominated the market due to its desirable properties. Its one major drawback over the years has been the mechanical commutator which places substantial design and environmental limitations on their operation.

A summary of these limitations is given below.

1.2.1 MAJOR DRAWBACKS OF "BRUSH/COMMUTATOR" IN DC MACHINES

From the view point of the power-electronics engineer, the conventional rotating insulated copper segments in contact with stationary carbon brushes carry out an arduous duty with remarkable reliability. It, however, does have the following drawbacks :

(i) The commutator and brushes are prone to sparking necessitating periodic mechanical maintenance and overhaul therefore reducing the overall reliability of the drive system.

(ii) The arcing problem with mechanical commutation limits machine size to a KW x rpm product of between 2 and 3, x 10^6 [10].

(iii) Since the commutator is on the rotating element, the maximum speed at which it can run is limited due to centrifugal force, to values (in normal design) of perhaps 1500 rpm at 1 MW, 5000rpm at 50 KW. Higher speed may be obtained by very special design, the limit being probably 15000 rpm in the low power rating range [10].

(iv) Dirt and moisture attack the commutator and the machine needs to be specially protected in hazardous atmosphers.

1.3 AC DRIVE SYSTEMS

1.3.1 CAGE INDUCTION MOTOR DRIVES

A simple method of controlling the speed of a cage induction motor is by the reduction of the voltage (at line frequency) applied to the stator winding of the machine. Thyristors may be used in a fully controlled arrangement shown in Fig. 1.2 (i), where firing (delay) of the thyristors removes sections of the supply voltage so reducing the r.m.s. value of the voltage to the motor.
Voltage and current waveforms for phase (a) of a thyristor controller with a star connected load is shown in Fig. 1.2 (ii) [Shepherd 2]. The firing delay angle in the figure shown is approximately 30^{o}. The angle β is the extinction angle of the thyristor and is measured with respect to the preceding voltage zero.

The scheme has the advantage of low initial cost and continuous speed adjustment with a recommended operating range of 70% to 100% .

Where voltage reduction is obtained by semiconductor switching, the line voltage is rich with harmonics. Further, the low speed power factor is inherently poor and is made worse if the thyristor phase control is used to vary the voltage.

An alternative scheme is to vary the frequency of the voltage and current supplied to the motor. This is achieved using electronic controllers which modify the incoming supply frequency and synthesise a variable frequency pseudo-sine wave. Voltage is also required to be controlled in order to maintain the ratio between voltage and frequency constant over the speed range to maintain

(a)

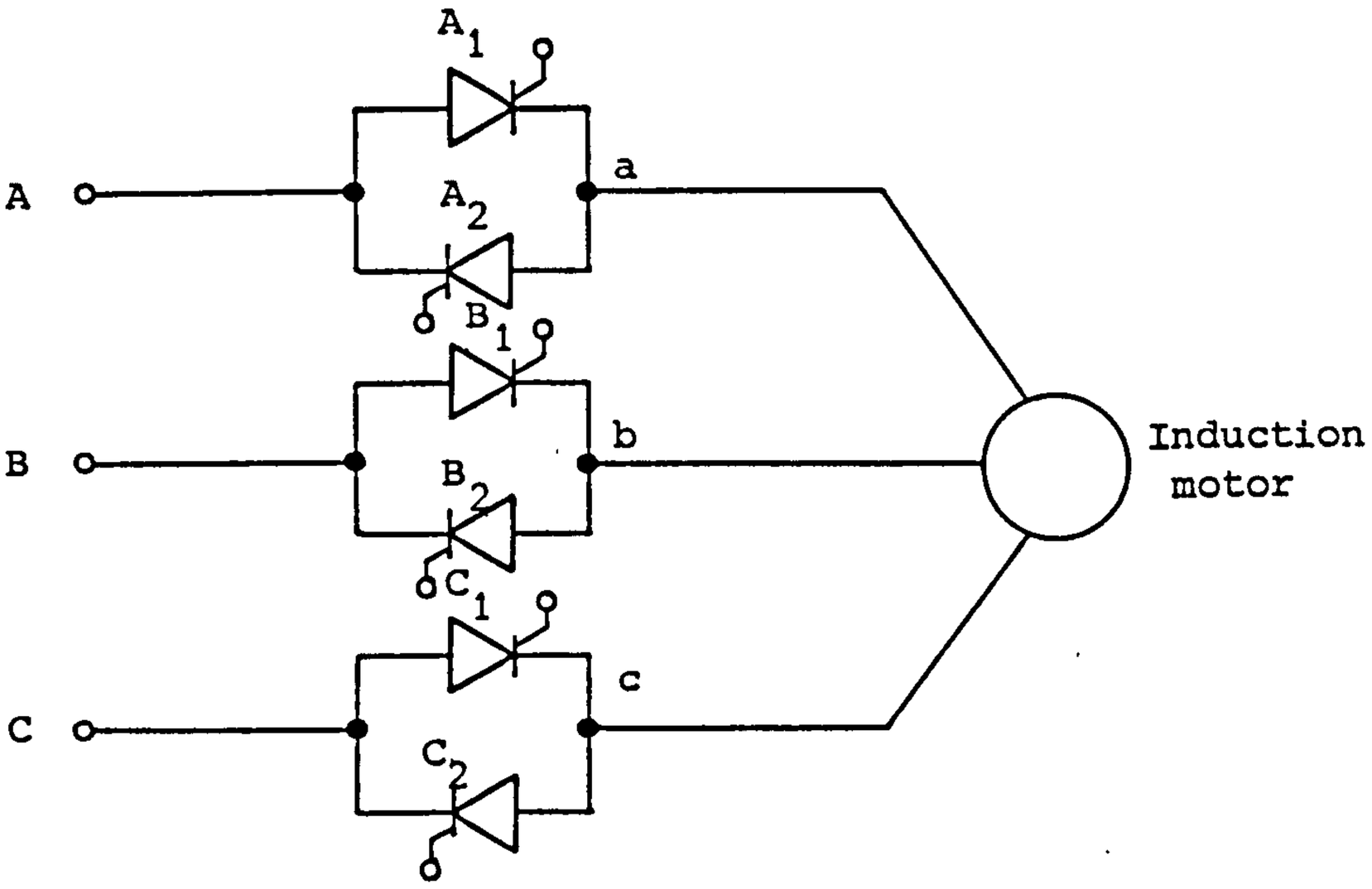

Thyristor triggering

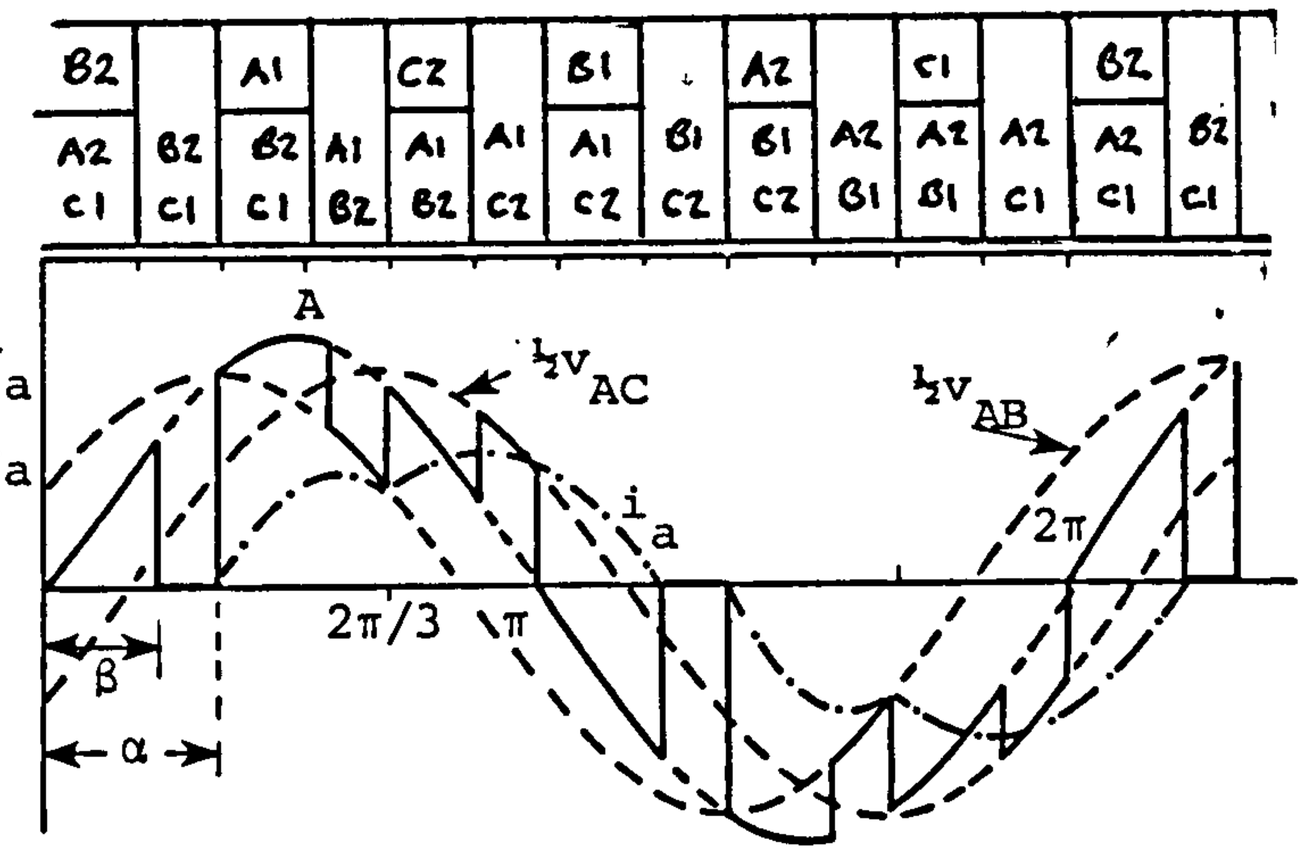

(b)

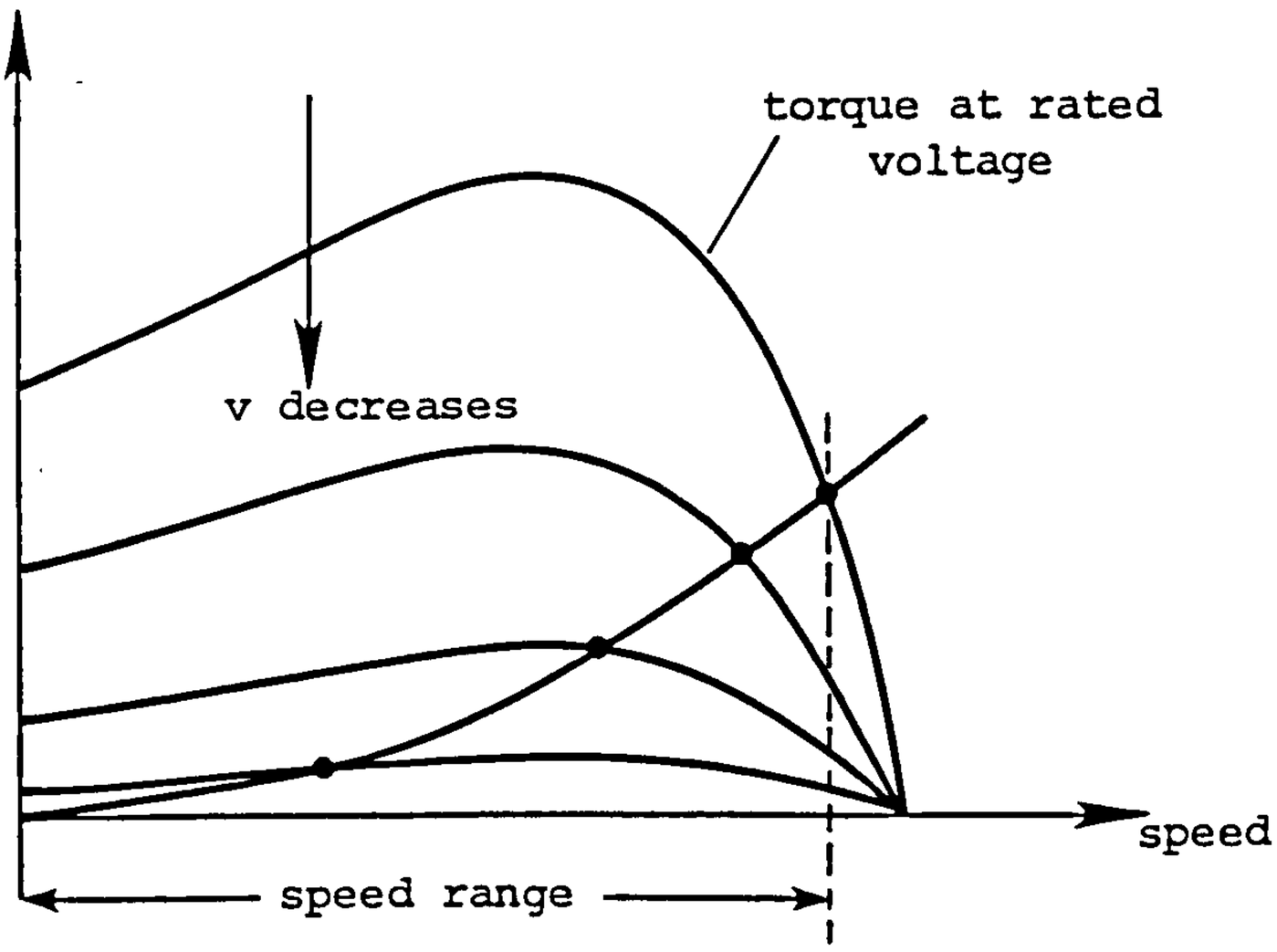

(c)

Fig. 1.2 Induction motor speed control by voltage control

(a) Thyristor controller
(b) Voltage and current waveform for phase (a)
(c) Speed/torque characteristics

(Shepherd ref-2)

optimum magnetic flux in the induction machine. Hence any variation in the inverter frequency must be accompanied by a voltage change. Three basic controllers designs are utilised :

- Cycloconverters.
- Voltage source inverters.
- Current source inverters.

1.3.1.1 Cycloconverters

The basic scheme of a cycloconverter [11] is that two three phase thyristor bridges are connected in inverse-parallel across the incoming supply as demonstrated by the block diagram of figure 1.3(i), and (ii) shows the connection circuit of a 3-pulse configuration; although there is a number of more complex connections involving further sets of bridges. By varying the timing of the switching of the thyristors an approximately sinusoidal waveform may be synthesised at a different frequency to the incoming supply as shown in figure 1.3(iii).

The maximum output frequency is generally limited to about one-half to one third of the input supply frequency although this range may be extended at a significant cost by introducing extra bridge circuits.

The peak value of the output voltage that a cycloconverter can supply is determined by the mean level of the direct voltage which the positive and the negative converter groups can supply. Hence for a "p" pulse cycloconverter, the peak value of the output voltage is [11] :

$$V_o(pk) = (p/\pi)\mathrm{Sin}(\pi/p)\ V_s(pk)\ \mathrm{Cos}\,\alpha$$

Where $V_s(pk)$ is the peak value of the supply voltage.

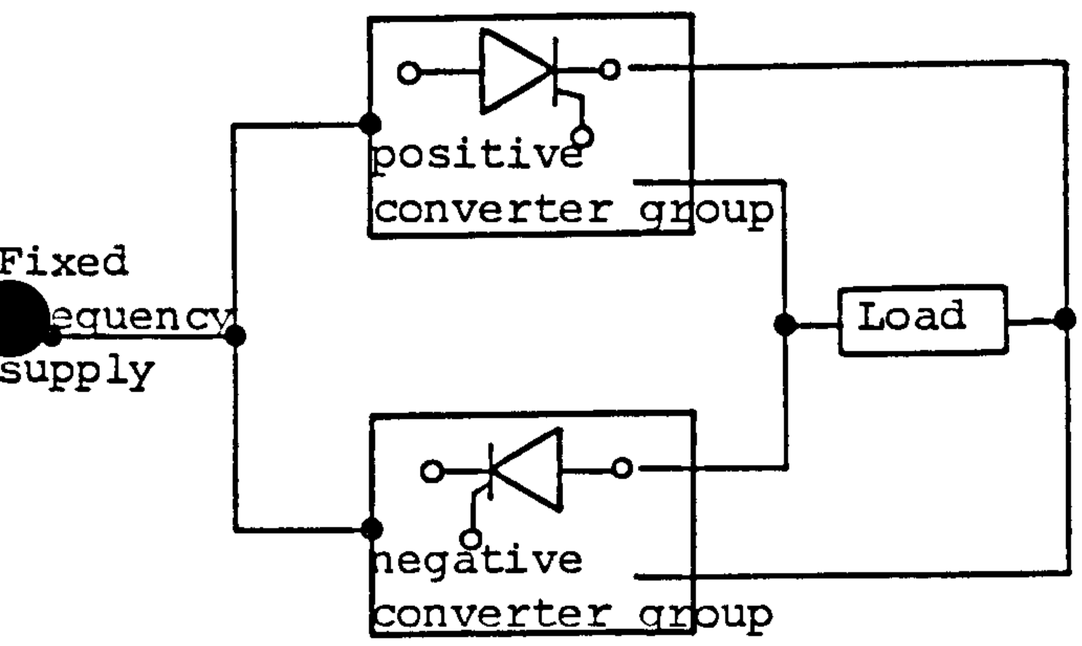

(i) Block diagram

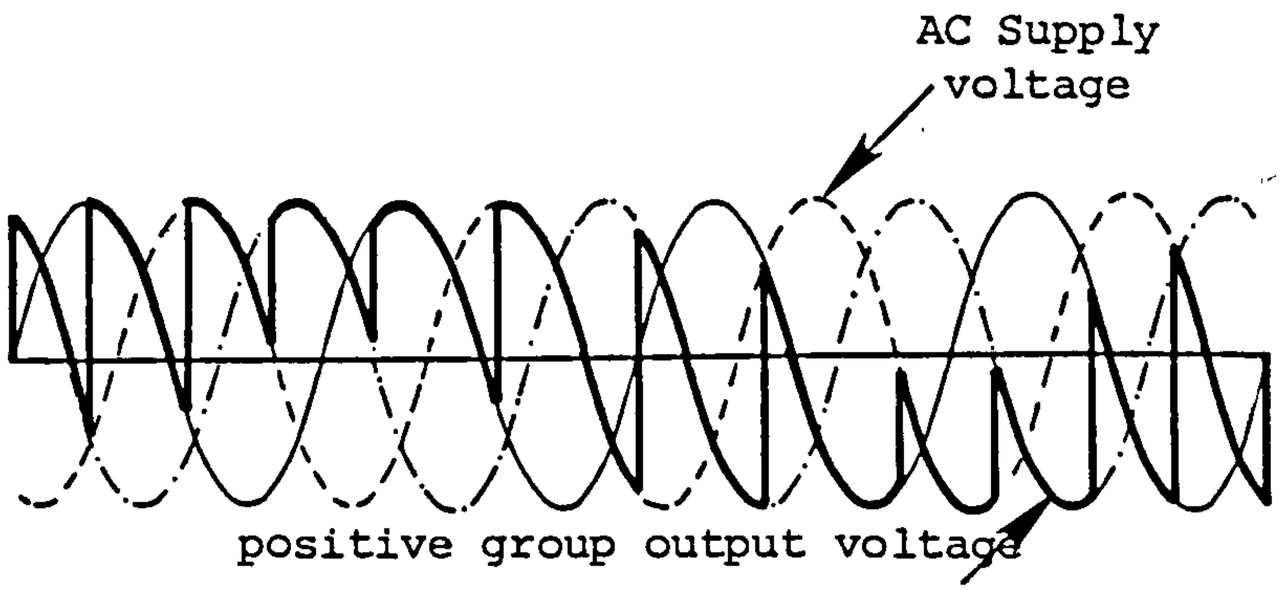

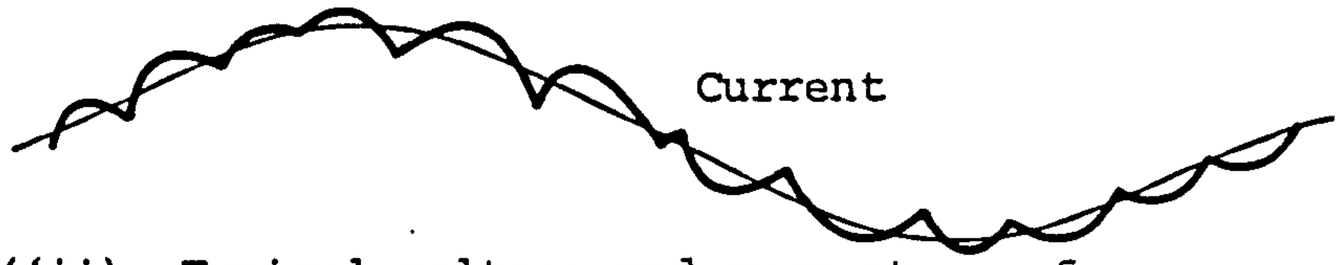

(iii) Typical voltage and current waveform in phase (a)

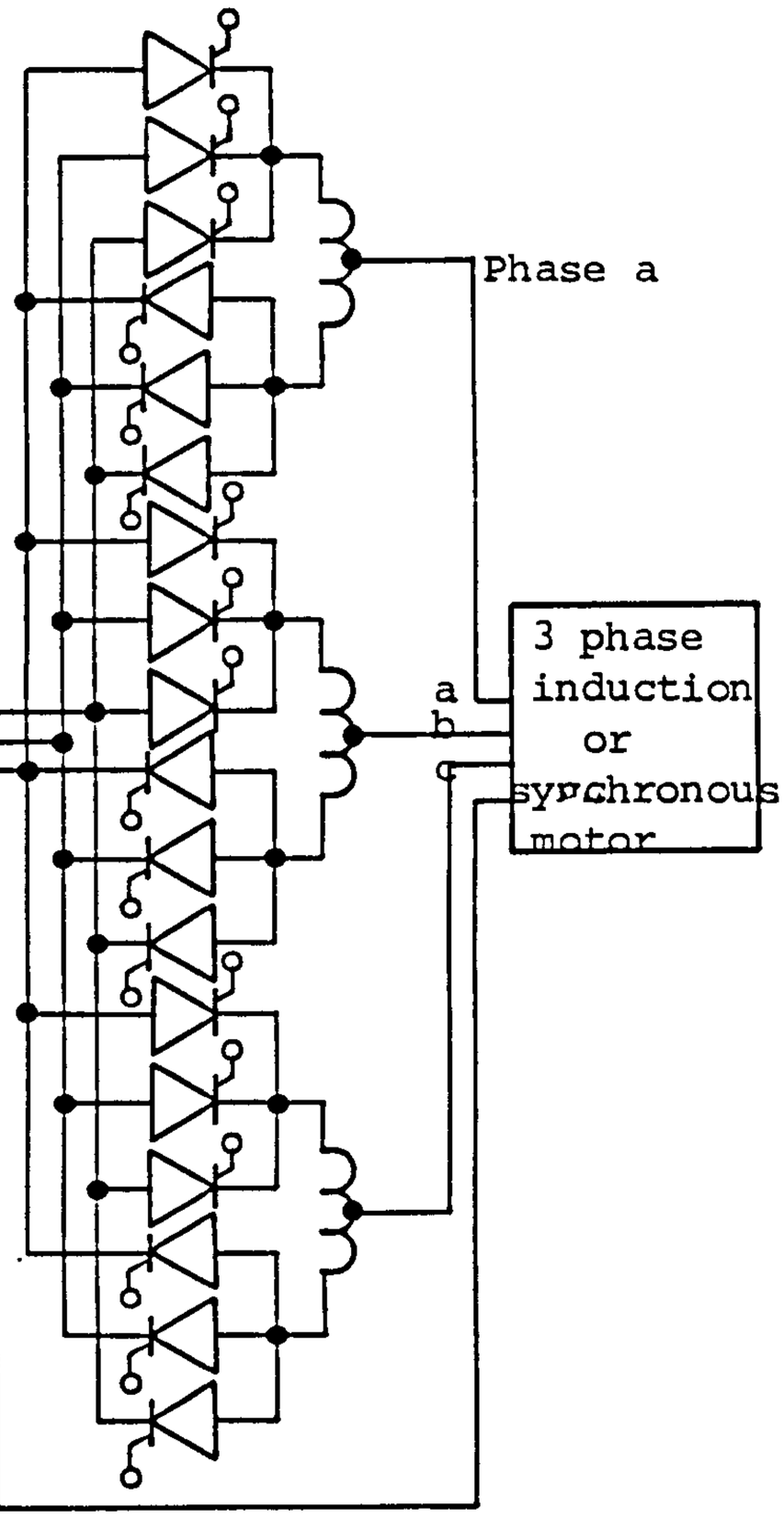

(ii) 3-pulse connection with 3-phase output

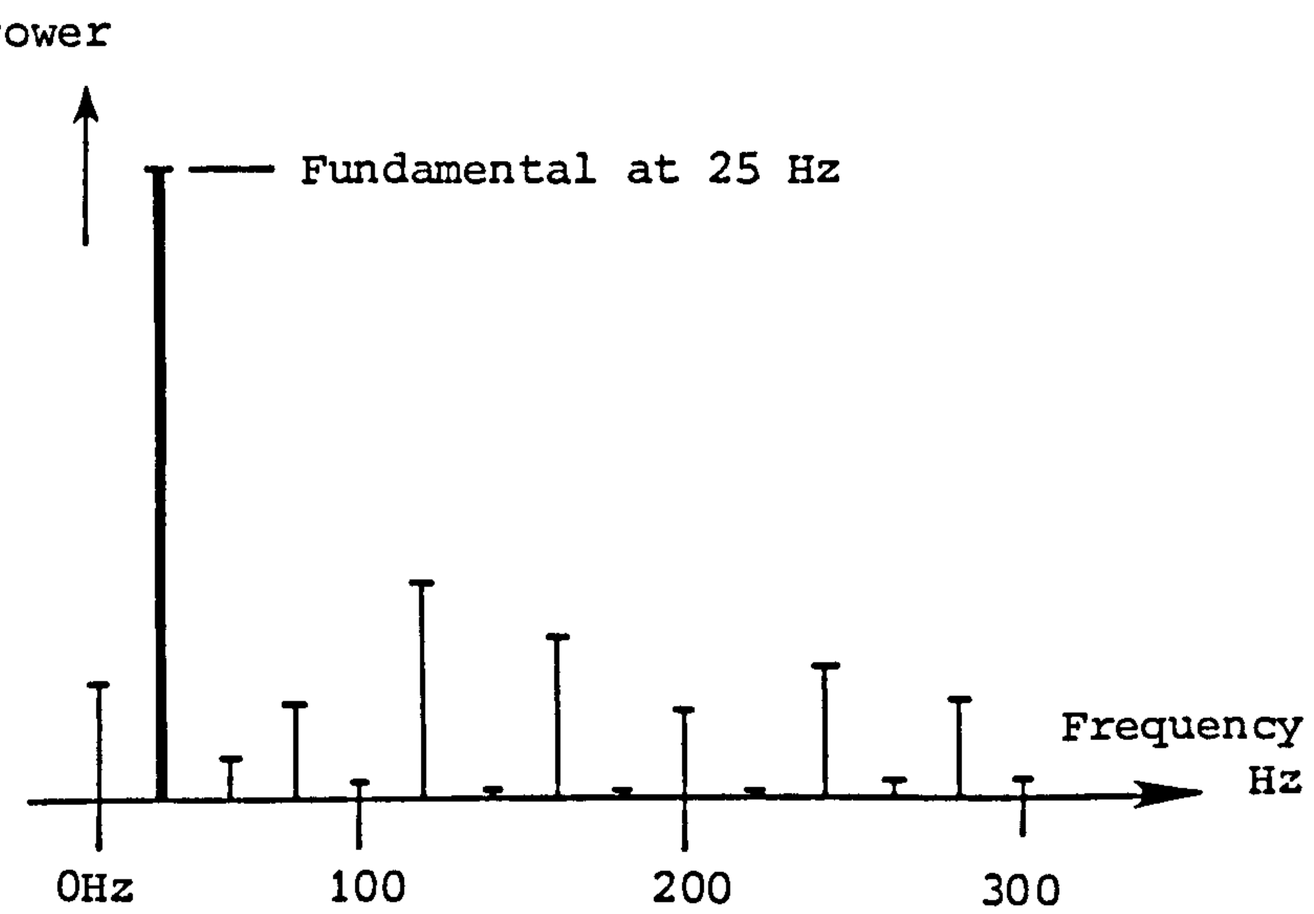

(iv) Spectrum for (ii)

Fig. 1.3 The cycloconverter scheme

and α is the firing (delay) angle measured from the crossing point of two input supply phases.

The cycloconverter is complex in that the synthesis of the new waveform requires careful control over the generation of firing pulses to the thyristors, and complex algorithms such as the Venturini converter have been developed to improve response, reduce harmonics and yield a good performance/cost ratio.

Technically, the cycloconverter use is limited by the low output frequency range, and by the quite severe harmonic and power factor demands. Fig 1.3(iv) shows typical harmonic spectrum for the case when the cycloconverter provides output at half the frequency of the incoming supply.

1.3.1.2 Voltage-source inverters

In this scheme, the inverter synthesises an AC voltage from a DC voltage by controlled switching of devices connected to DC supply [1,12]. All inverters operating off an AC supply therefore consist of a rectifier, an interconnecting section and an inverter to supply AC to the machine, Fig. 1.4 .

The interconnecting section between the rectifier and the inverter is known as the "DC link" and the presence of the capacitor is to emphasise that the DC feed to the inverter is nominally at constant voltage over each cyclic change in the inverter.

The power supplied to the motor is voltage-controlled; the level may be controlled in one of three ways :

(i) A controlled thyristor bridge rectifier on the input side of the DC link [12] as depicted in the block diagram of Fig. 1.4(a).

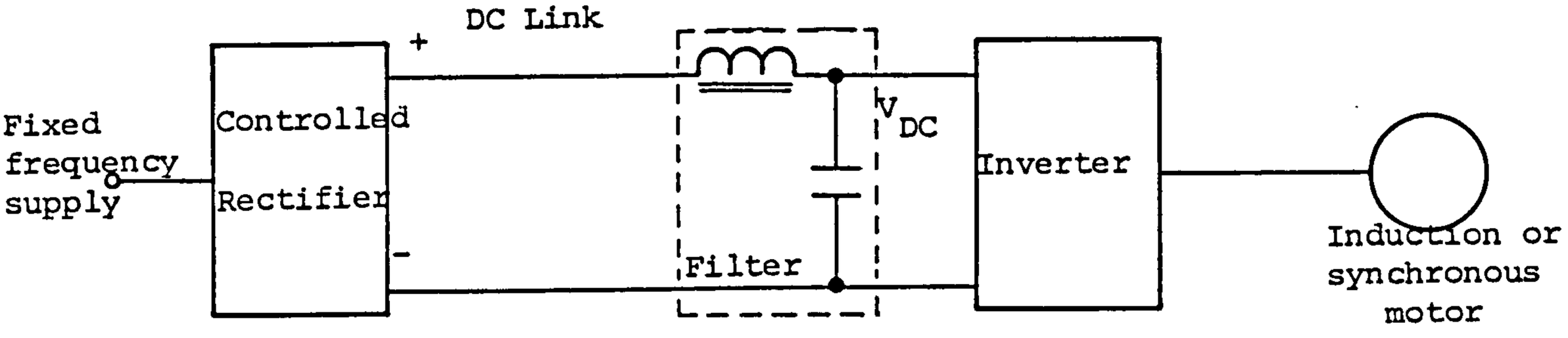

(i) Block diagram

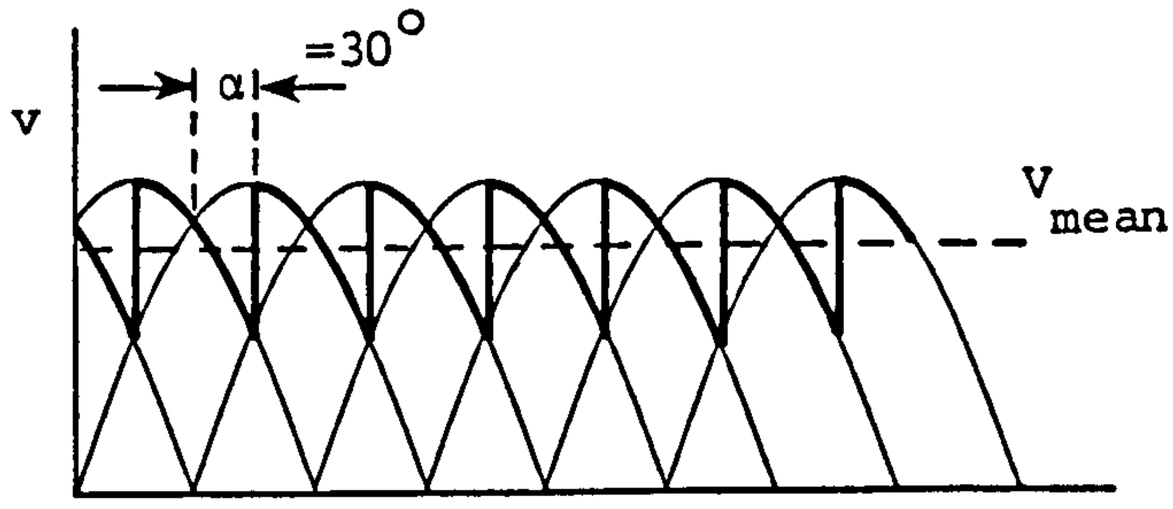

(ii) DC Link voltage adjustment : small firing delay angle

(a) Controlled rectifier scheme

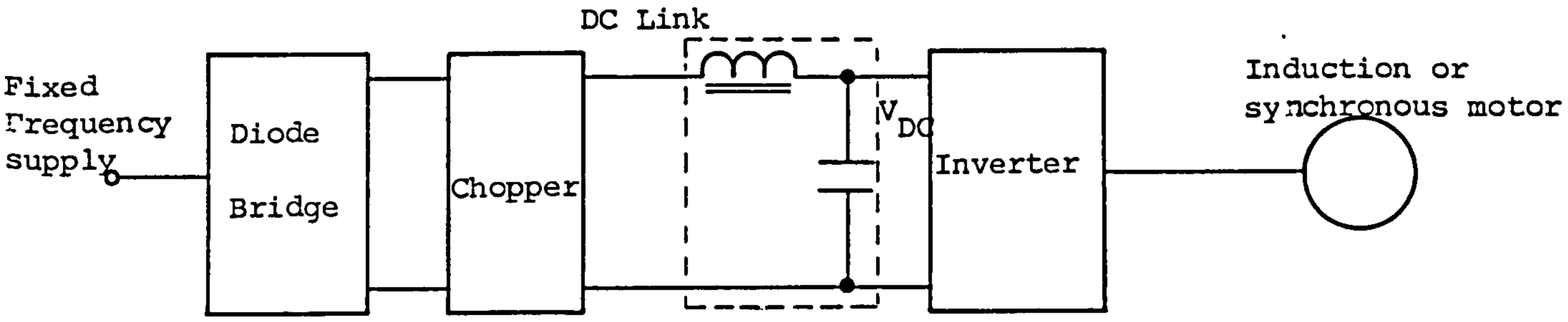

(i) Block diagram

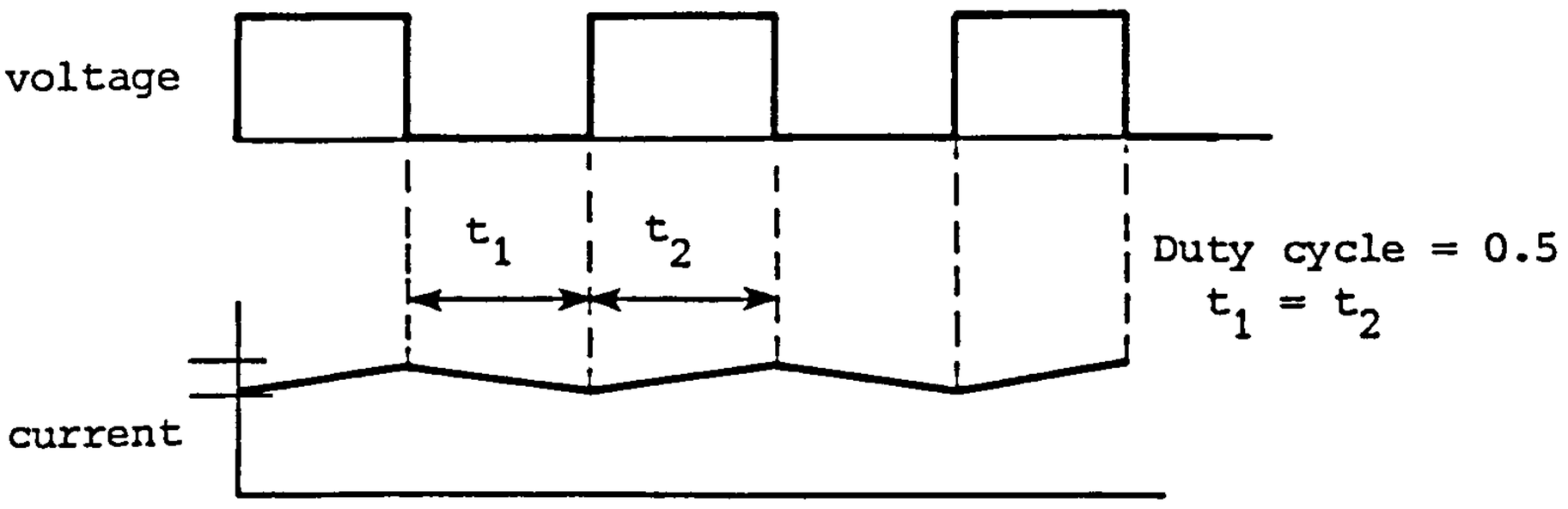

(ii) DC link voltage and current waveforms

(b) Intermediate chopper regulator scheme

Fig. 1.4 Quasi-square wave voltage controlled inverter

The voltage in the DC link is adjusted by varying the firing (delay) angle α. Fig. 1.4(a) also shows the DC link voltage waveform for the case when the firing delay angle is small ($\alpha = 30^{\circ}$); this output is filtered before reaching the inverter.

The scheme has the advantage that any speed control demand is met by fast response.

(ii) A DC "chopper" between the rectifier and the inverter as shown in the block diagram of Fig. 1.4(b). In this scheme, diode rectifiers are used giving a fixed DC busbar voltage. The voltage in the DC link is regulated by the DC chopper on/off action. The voltage and current waveform in the DC link for this scheme is also shown in (b) for the case when the chopper on/off duty cycle is set at 0.5 .

(iii) Adjustment of the voltage by the inverter.

In the voltage-source inverter, the reverse connected diodes across each power switch prevent DC link voltage reversal, so any regeneration has to involve current reversal. Current reversal is not possible in the chopper scheme (the second method), unless a dual circuit arrangement is employed; therefore confining its use in applications which do not require regeneration. The selection of the method then depends on the type of the inverter. The two common inverter designs synthesise the AC waveform either using multi-step method (quasi-square wave) or the technique of pulse-width modulation. The current and voltage waveforms for both of these methods are given in Fig. 1.5.

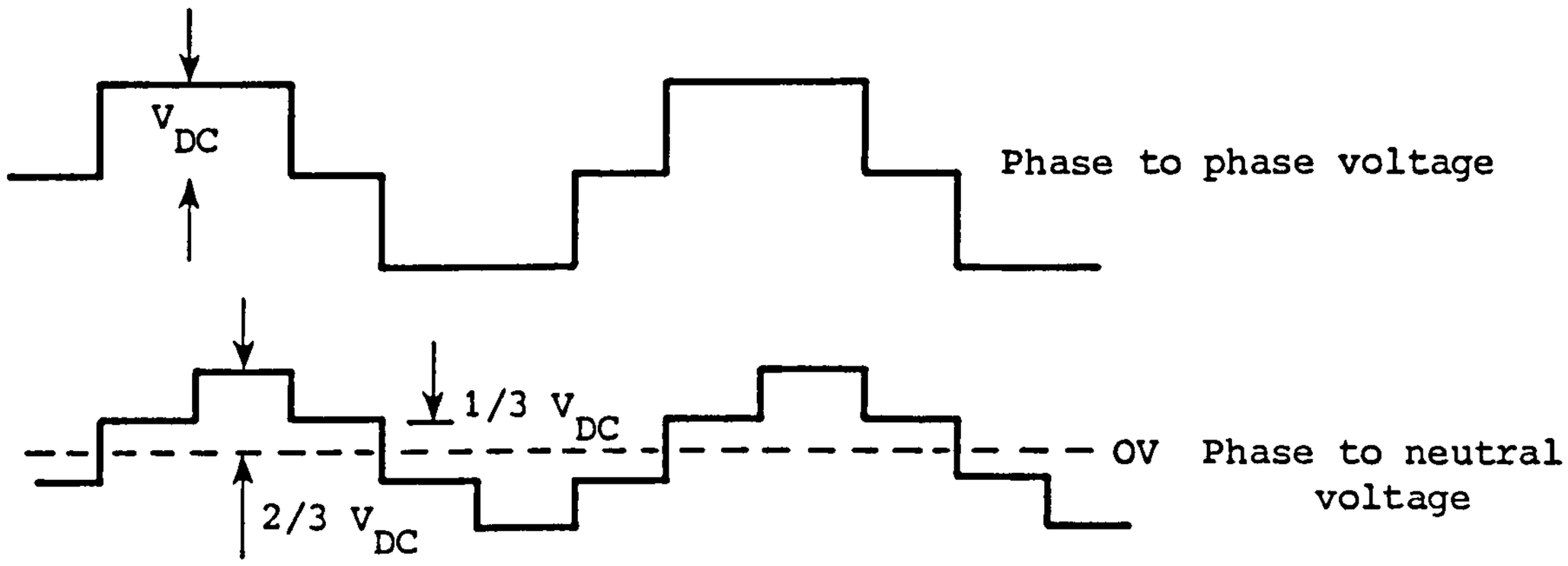

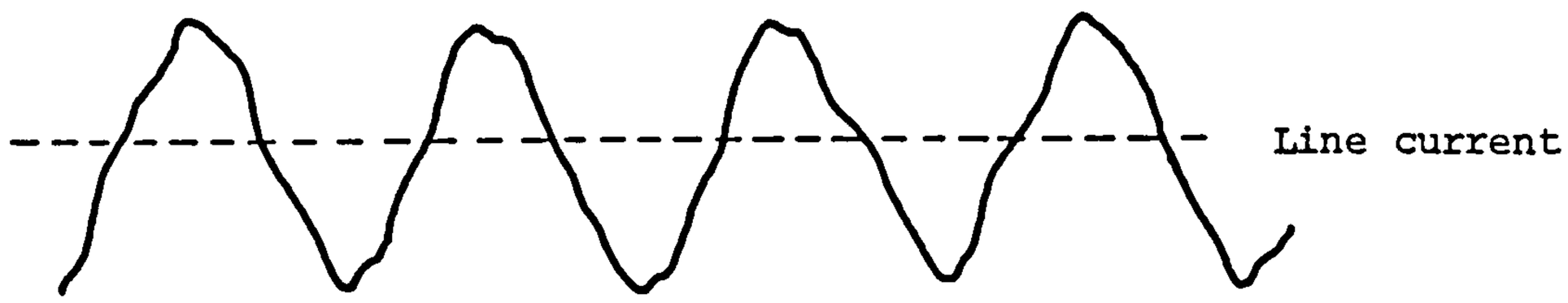

(i) 6-pulse quasi-square wave inverter voltage and current waveforms

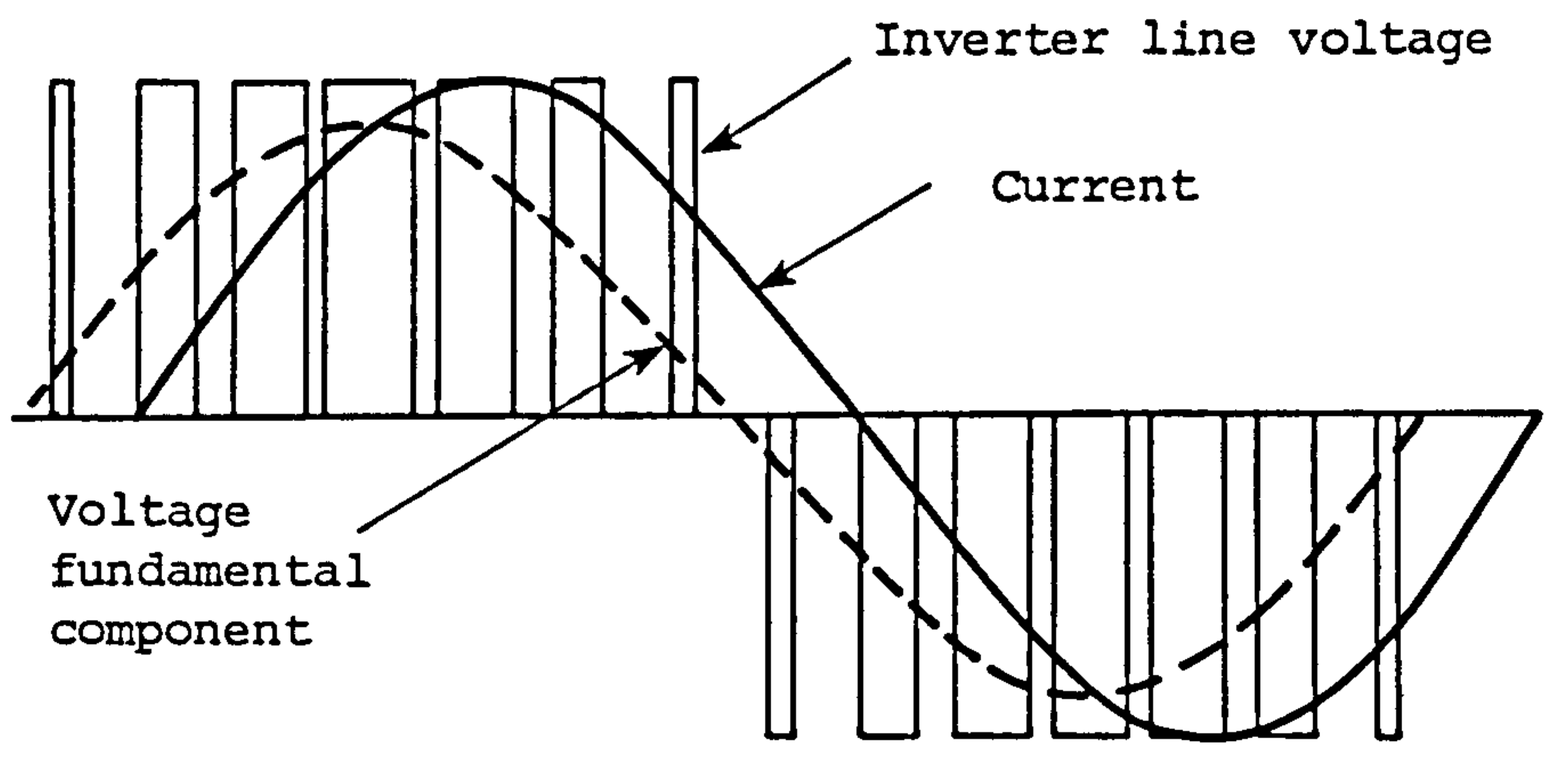

(ii) Voltage and current waveforms for a sinusoidally weighted PWM

Fig. 1.5 Voltage-source inverter output waveforms

1.3.1.3 Current-source inverters

Current-source inverters are basically very similar to voltage source inverters using quasi-square wave outputs [Farrer 12] Fig. 1.5(i), except that the input converter is used to control the level of the current fed to the inverter rather than the voltage.

Fig. 1.6(i) illustrates the application of a current-source inverter to a cage induction motor. Compared to the constant voltage source inverter, it is clear that the capacitor in the DC link is not present in this scheme, the reactor being the dominant feature. The purpose of the DC link reactor is to smooth the DC input to the inverter and prevent any sudden current changes resulting from violent changes in the shaft torque.
The waveform of the inverter output current and voltage is shown in Fig. 1.6(ii).

The inverter frequency is set by the speed demand with the voltage adjusted to obtain the constant voltage/frequency ratio. The current (and hence the torque) is adjusted too during the acceleration period. The current source inverter has several good features, for example, the power circuit is rugged and reliable and no high-speed switching is required for the power switches. However, these advantages are outweighed by several serious drawbacks:

There is a requirement for a large choke in the input circuit. Severe voltage spikes appear during commutation leading to the need for higher voltage rating power switches. The response time of the current source inverter is slow and it is difficult to use with multi-motor systems.

A typical application of the current source inverter to a synchronous motor drive system will be presented in section 1.5.1.

1.3.2 SLIP-RING INDUCTION MOTOR DRIVES

In theory, the methods just described for the cage induction motor are equally applicable to the slip ring machine. These methods are not generally applied unless an existing wound-rotor machine is already installed. In considering the wound rotor machine, it is the access to the rotor windings via the slip-ring which enables some specific forms of speed control to be applied to these devices.

The main scheme for these type of machines is to convert the slip power in the rotor circuit (Pr), into useful energy, i.e. feeding back to the supply the electrical power generated in the rotor circuit; such schemes are usually referred to as Kramer drives. The voltage at the slip rings, Fig. 1.6(iii), is at slip frequency which is incompatible with the stator frequency, therefore the slip-voltage is rectified by means of a diode bridge (converter A) into a DC link. The DC link power is transferred back into the mains supply via a thyristor converter (converter B) operating in the inverting mode.

The main limitation of Kramer drive systems is that the rotor power (Pr) is uni-directional; hence rotor power reversal is not possible confining the operation to subsynchronous speeds only.

A variation of this scheme is the Scherbius drive which has the facility for slip power reversal by using an inverter in the rotor circuit instead of a bridge rectifier. i.e. converter A, Fig.

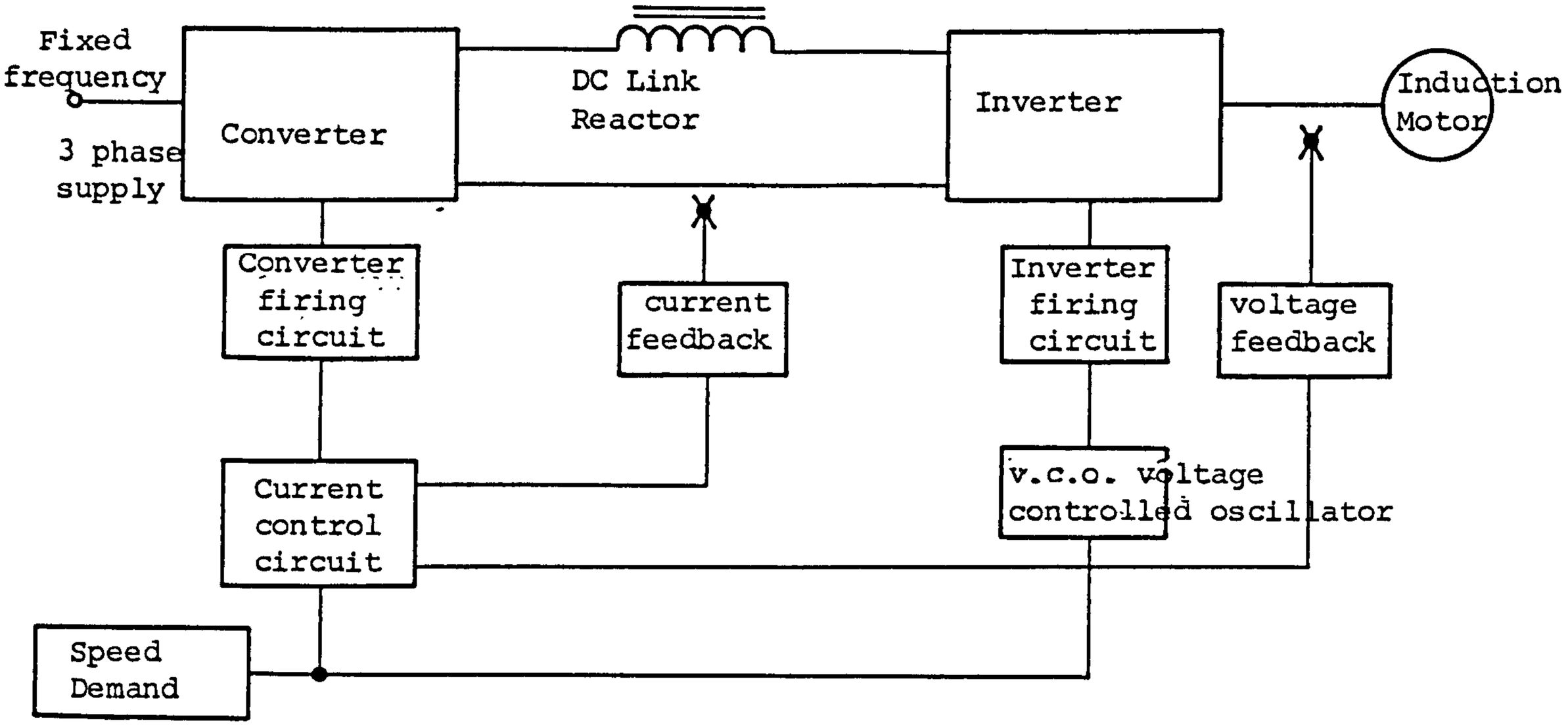

(i) Block diagram - current-source inverter

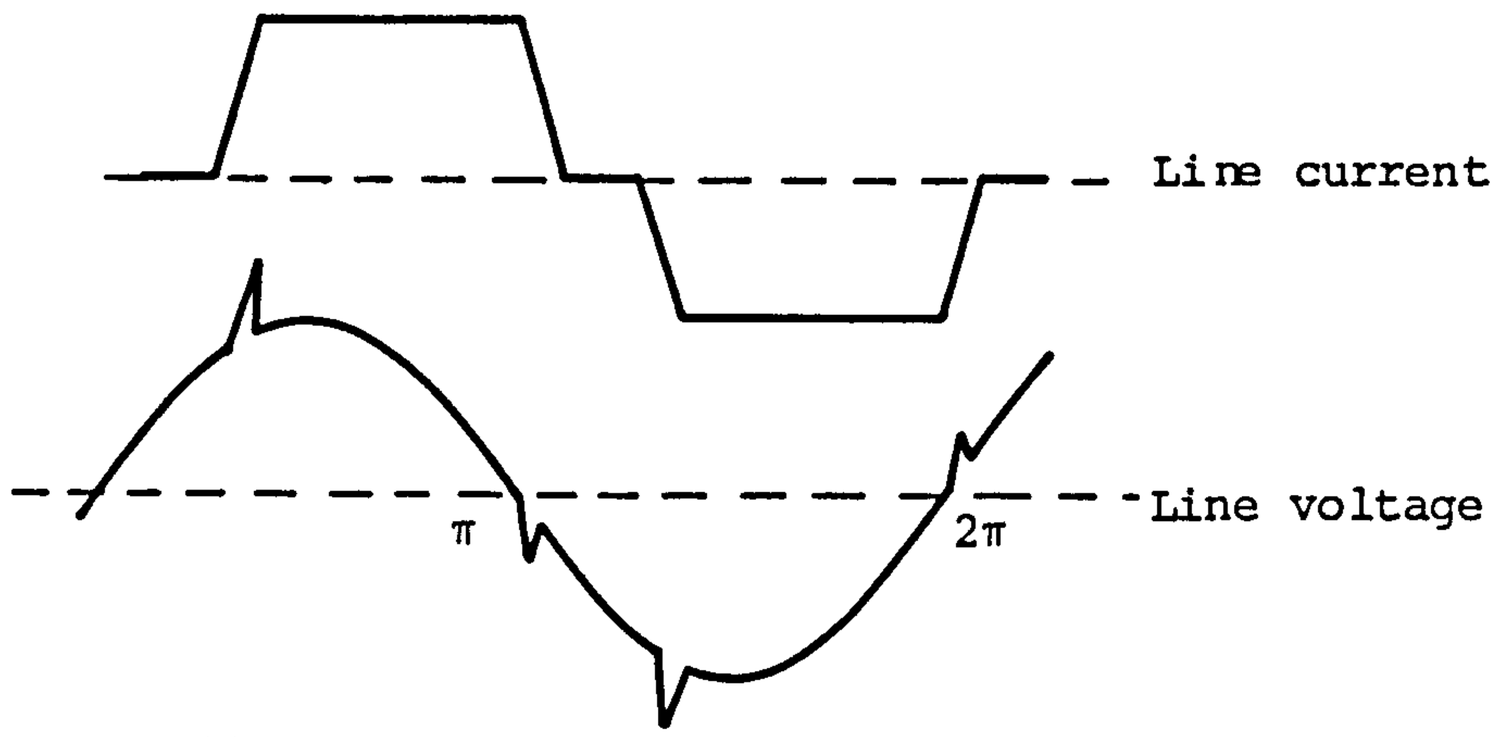

(ii) Output line current and voltage waveform

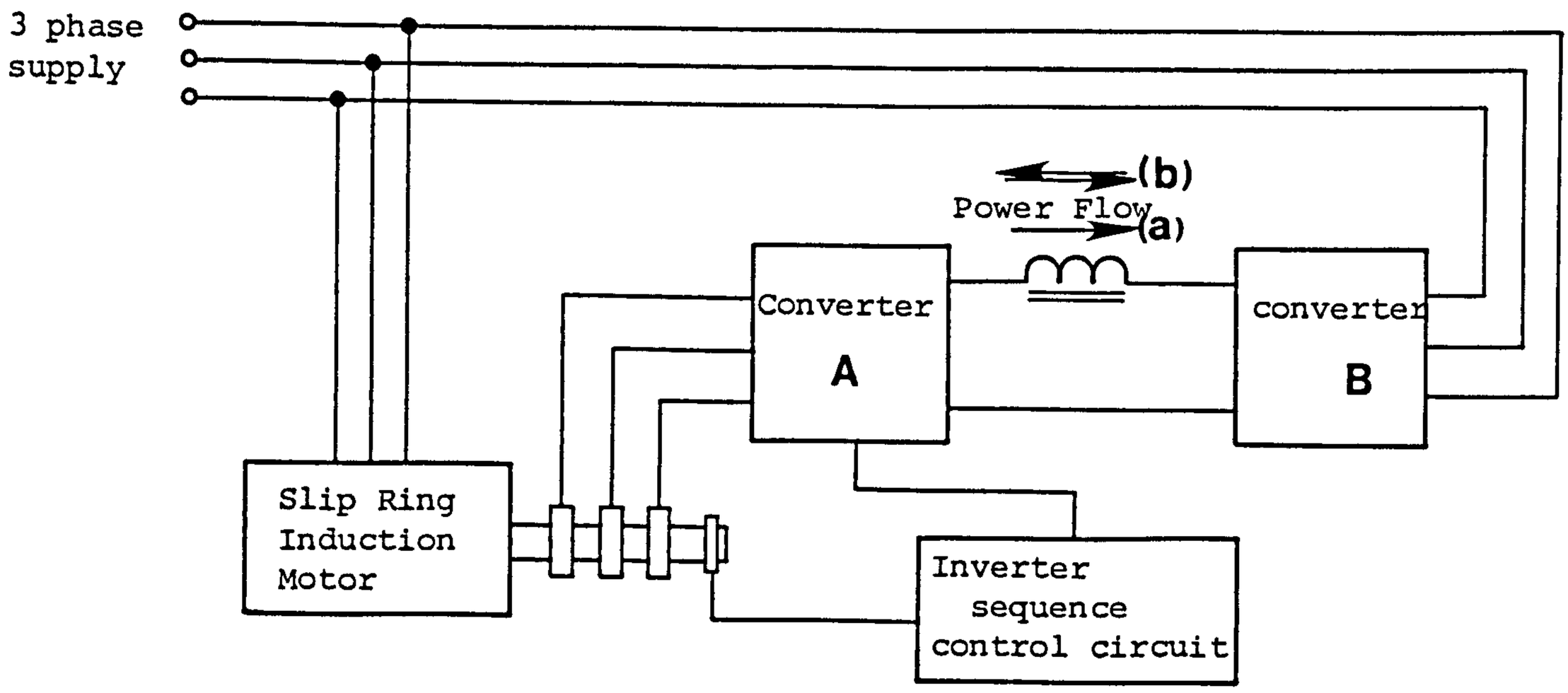

(iii) Slip ring schemes : (a) Kramer and (b) Scherbuis Drive

Fig. 1.6 Induction motor drive schemes

1.6(iii), is an inverter. This allows rotor power to flow in both directions.

Sub, Super-synchronous operation is possible in the range ± 50% nominal.

1.3.3 SYNCHRONOUS MOTOR DRIVES

The three schemes of varying the input frequency to the motor i.e. the voltage fed inverter, the current fed inverter and the cycloconverter can all be applied to synchronous machines.

However, to become worthwhile, a scheme must have some advantage over induction motor drives to offset the higher cost of synchronous motors.

Such an advantage is obtained if the current source system is used because with the synchronous motor drive, "load-commutation" can be be employed, whereby the thyristors are turned OFF by the reverse bias of the back e.m.f. of the machine, although special conditions apply at zero speed [23]. Furthermore, the thyristors are turned ON or OFF corresponding to the rotor angular position using shaft position feedback system in the form of a rotary encoder provided on the shaft of the machine; this ensuring that the inverter frequency is always kept in synchronism with the motor speed.

The constant-current inverter/synchronous motor drive scheme is often referred to, in the literature, as DC "Commutatorless" (DC CLM) or "Brushless" (DC BLM) motor. The reason for this terminology will be discussed in section 1.5 where this drive scheme will be described and compared with the conventional DC motor with its

commutator replaced by an electronic switching system.

At this stage, it is appropriate to discuss drive systems which come under the "brushless" heading.

1.4 VARIABLE SPEED BRUSHLESS SYSTEMS

In recent years, there has been a great proliferation of brushless motors of various kinds [15-28] .

In a paper published five years ago [13], Persson categorised variable speed brushless, three phase wound armature machines according to the basic inverter system and motor configurations.

1.4.1 MOTOR CONFIGURATIONS

The basic nomenclature in this general area is not yet established. On surveying the literature, one often comes across a variety of different names :

- Variable frequency drives.
- Variable frequency AC drives.
- Brushless AC motors.
- Brushless DC motors, to name a few.

To clarify the difference, the brushless three phase wound armature machines will be discriminated according to the basic motor scheme :

- AC induction motor.
- AC synchronous motor.
- AC synchronous motor with rotor position feedback: "Brushless DC motor".

1.4.1.1 AC induction motor

Fig. 1.7(i) shows a simplified circuit diagram of an AC induction motor drive system supplied from an inverter. The figure depicts a short-circuited rotor implying the use of a cage induction motor. While this motor can be controlled by several methods, the most efficient way of controlling it is to vary the applied frequency. These schemes are therefore often referred to as variable frequency AC induction motor.

The frequency of the induced rotor current (f_r) is equal to the slip (s) times that of the stator frequency (f_s)

i.e. $f_r = s\ f_s$

where the slip is defined as :

(Synchronous speed - Rotor speed)/(Synchronous speed)

The developed torque is a function of the slip. This means that if a voltage of a certain frequency is applied to the motor, the rotor angular velocity i.e. shaft speed, will vary depending on torque loading on the motor such that the higher the loading torque, the lower the shaft velocity.

Other schemes include the variation of speed by electronically controlling the slip energy at slip rings of a wound-rotor induction motor (static Kramer or Scherbius system). Slip rings are needed in such schemes and therefore the term "brushless" does not apply.

1.4.1.2 AC synchronous motor

Fig 1.7(ii) shows an inverter scheme supplying an AC synchronous motor. The major difference between this motor and the AC induction motor is that its rotor is a permanent magnet. Because of this, a

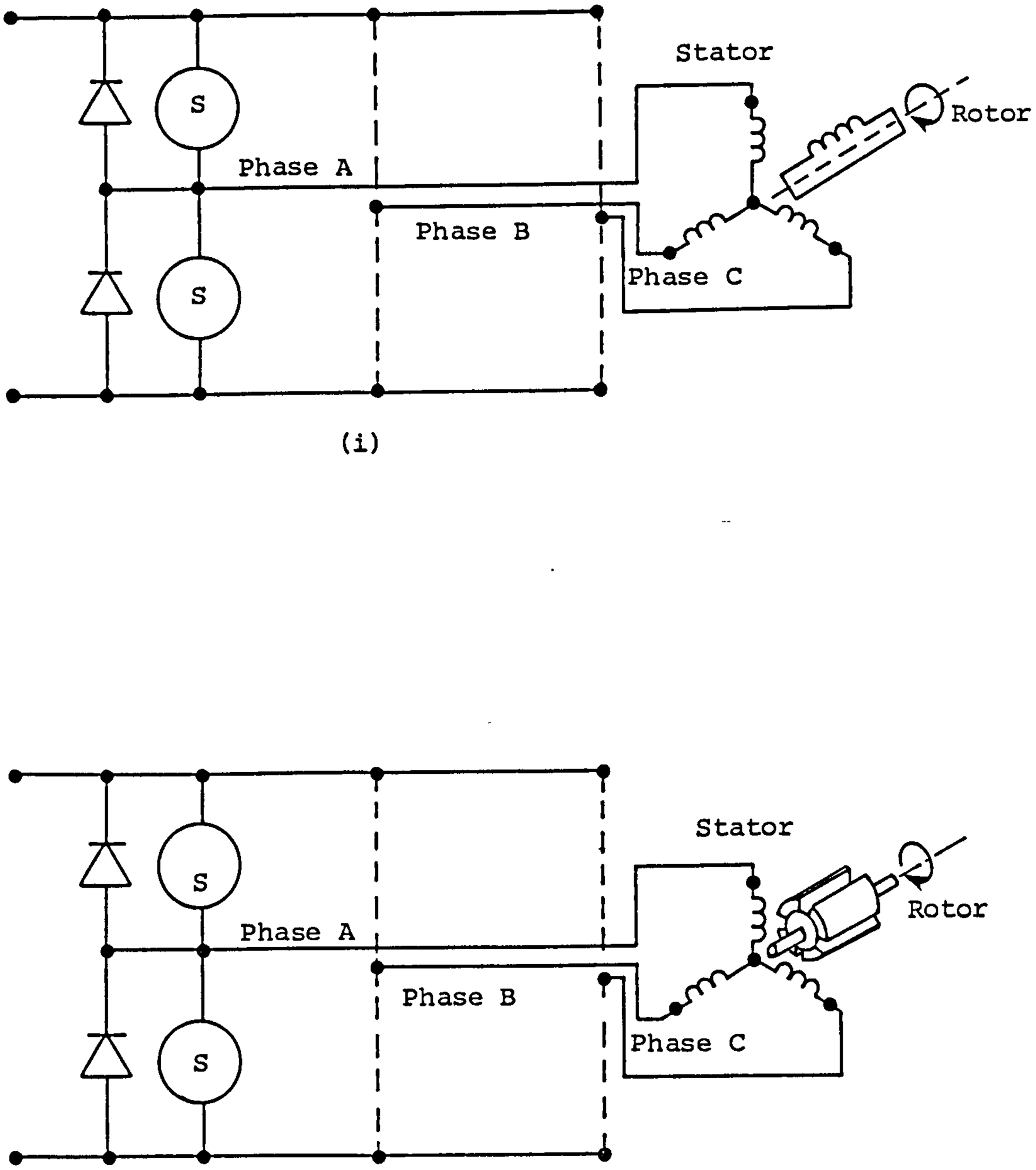

Fig. 1.7 Brushless three-phase wound armature

(i) A.C. induction motor scheme
(ii) A.C. synchronous motor scheme

Symbol (S) denotes a semiconductor switch

significant difference exists between the torque producing characteristics of this motor compared with the AC induction motor. In this case, the torque/speed relationship is simply that the shaft torque is a function of the angle between the axis of the stator rotational field and the rotor magnetic field. Thus in normal operation, no slippage occurs between the imposed frequency to the motor and the rotational frequency of the rotor shaft. In effect the motor shaft will change its "lag angle" with respect to the stator field in response to a load.

The two schemes discussed above are based on "open-loop" configuration i.e. there exists no feedback between the input frequency and the output shaft rotation.

1.4.1.3 AC Synchronous motor with rotor position feedback

The stator and rotor in this drive scheme is identical to the synchronous motor system described in 1.4.1.2, the only difference being the use of a shaft position sensor. The function of the sensor, as stated earlier, is to organise the switching sequence (ON or OFF) of the inverter switching devices corresponding to the angular position of the rotor. The term "brushless" applies because the rotor is a permanent magnet.

On surveying the literature [23,28], it was found that these drive schemes are usually referred to as being DC commutatorless motors, for the reason that rotor positional feedback is employed which may be considered to perform the same function as the brush/ commutator arrangement in a conventional DC machine.

System definition has therefore become muddled when considering

this example of a synchronous AC motor with a coupled shaft encoder (or "distributor", the term used by Matsui [23]) which provides shaft position information to the controller.

To clarify the situation, the intrinsic definition of the DC and AC machine according to the fundamental machine theory was stated in section 1.1 .

In considering the case of an AC synchronous motor with rotor position feedback, Matsui[23] states that these machines have the problem of high torque pulsation, hence large variation in the torque angle as the machine is loaded.

Such drives may be therefore more appropriately called "variable frequency AC synchronous motors" as referred to by Stoken [22], due to the fact that their speed is changed by adjusting the inverter frequency in a closed-loop arrangement; such drives are usually characterised of having [23] :

- low starting torque
- high pulsation torque
- small overload capacity.

some properties not associated at all with conventional DC machines.

1.4.2 INVERTER SYSTEMS

Referring to Fig. 1.7, it can be seen that the stator winding of both the AC induction and synchronous motor is supplied via an inverter. The symbol (S) is used to denote a semiconductor switch such as a transistor, a thyristor, etc.

The basic function of the inverter is to provide the appropriate supplies needed to run the above motor schemes. Two basic needs must be satisfied by the inverter. One is to provide a suitable voltage to the motor windings (or in some cases it is a question of suitable current to this winding) and the other is to supply a suitable frequency commutation sequence for the windings.

The two basic systems of voltage or current controller schemes were previously described.

The first two examples of the AC motor drive schemes, Fig. 1.7, involves the generation of a three phase voltage {see waveforms Fig. 1.5(i) and (ii)}. One such system introduced earlier, uses the technique of six-step generation of three phase voltage (shown in Fig. 1.5(i)). The disadvantage of this technique is that the "corners" of the waveform consist of harmonic frequency voltages which can only contribute to additional harmonic copper loss and reduction of efficiency.

The other method more desirable, is the PWM (Pulse Width Modulation) technique, Fig. 1.5(ii), in which the output waveform is generated near to the desired sinusoidal waveform by controlling the width of the discrete pulses.

1.5 SOLID-STATE COMMUTATION IN DC MACHINES

The brush/commutator assembly of a conventional DC motor can be regarded as a system of controlled switches whose function is to pass a current through the sliding contact between a stationary carbon brush and rotating circular assembly of copper segments

(commutator sectors) connected to the armature winding coils. As the bars pass under the brush the current in the coils to which they are attached is reversed. The function of this will be dealt with in chapter 2.

The main limitations of such electro-mechanical switching system were discussed in section 1.2.1. Solid-state commutation of the armature coils may be used to mitigate many of these limitations. An immediate advantage to be gained is the inversion of the machine: the armature winding may be placed on the stator and the field winding made to rotate. This will consequently lead to the following:

(i) Easing of problems of insulation and securing of the armature conductors.

(ii) The complete elimination of the brushes is possible, for example by using a permanent magnet field rotor system.

(iii) If commutation is achieved without the need of interpoles, a very simple rotor assembly is possible.

The inverted structure in this case offers other useful thermal advantages [10]: Heat generated in the armature winding can be more easily dissipated; brushgear heating eliminated and armature winding temperature monitoring made easier.

The rotor tends to be lighter in machine size in the range 5W-5KW, thus giving higher torque/inertia ratio.

With the field poles rotating, the axis of the magnetic field produced by the armature current must also be made to rotate and to do so at exactly the same speed as the rotor in order to maintain the space-quadrature relationship between the axis of the radial

fields of the stator and rotor, as is natural for the DC machine with quadrature axis brushes. To this end, the position of the rotor should be made to control the armature supply switches.

Replacement of the commutator by static switches was first proposed by Alexanderson, some fifty years ago [14], when thyratrons were used as the switching elements. Little progress was made until the introduction of solid-state devices, a quarter of a century later [15] . Since that time, a large number of research papers have been published on commutatorless DC machines; these can be broadly classified into two groups:

(i) Machines with three phase wound armatures.

(ii) Multi-coil armature DC machines.

1.5.1 THREE PHASE WOUND ARMATURE MACHINES

Machines in this category were introduced earlier; Fig. 1.8(i) taken from reference 10, shows the drive in its simplest form, with the main thyristors of the supply system shown, ancillary circuits (e.g. thyristor turn-off circuits, gate drive circuits) not included. Such drive systems have been comprehensively studied elsewhere and an extensive range of literature is available - [reference 21 - 28 inclusive]. The system comprises a supply converter (controlled rectifier), a DC link (smoothing) reactor, feeding a thyristor converter bridge connected to a three phase excited synchronous motor. From earlier description of inverters, one can recognise the electronic scheme to be the current-fed-DC-link inverter, producing quasi-square machine line currents. The machine converter firing sequence is tied to the rotation of the

machine by using feedback signals obtained from a shaft encoder. By this means the stator line currents are switched round in sympathy with the rotor rotation, thereby forcing the machine to operate synchronously at all speeds.

The machine's excitation can either be applied via slip-rings or by brushless 3-phase exciter incorporating rotating diodes. Permanent magnet excitation may also be used for smaller drives.

Commutation (turning-off) of the current in the thyristors of the current source inverter shown in Fig. 1.8 can be achieved in one of two ways :

(i) "Line-commutation" where the machine back e.m.f. is utilised.

(ii) "Forced commutation", where auxiliary thyristors and L-C circuits are required.

Line commutation is the mechanism of transfer of current from one inverter phase to another, achieved naturally through the AC voltages of the machine. The supply converter is naturally line-commutated from the AC power source.

At all speeds above 5 to 10% of rated speed, the machine converter thyristors may also be naturally line-commutated from the stator voltage. During motoring operation, The machine converter operates in its inversion mode, with the power being extracted from the DC link and applied to the machine. When operating in this manner, the machine converter thyristors must be fired at an angle to give safe commutation so that time is allowed for current overlap and thyristor recovery before forward voltage appears across the outgoing thyristor [22]. The operating firing angle results in the machine running at a leading power factor when motoring irrespective

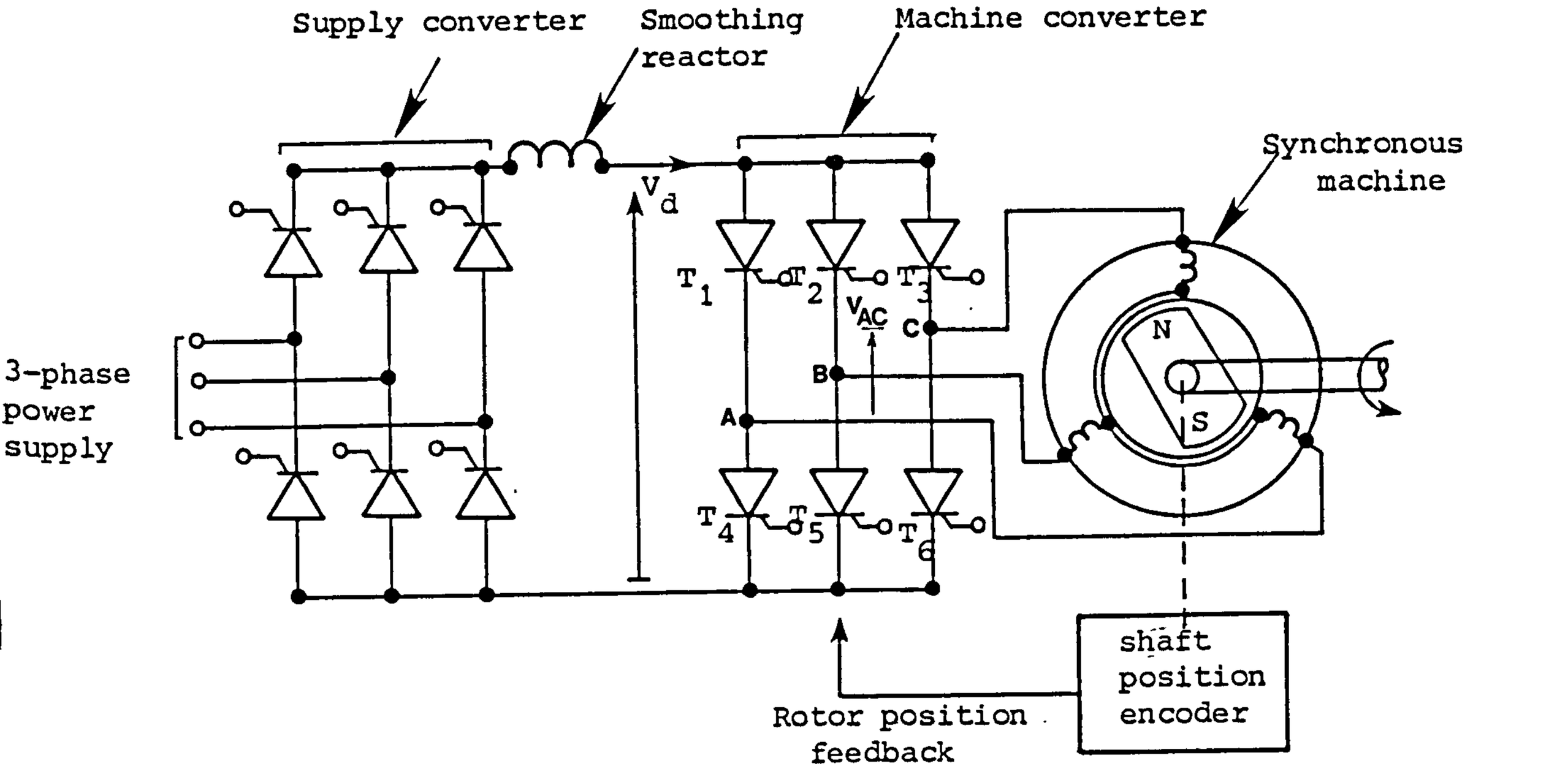

(i) Circuit Diagram

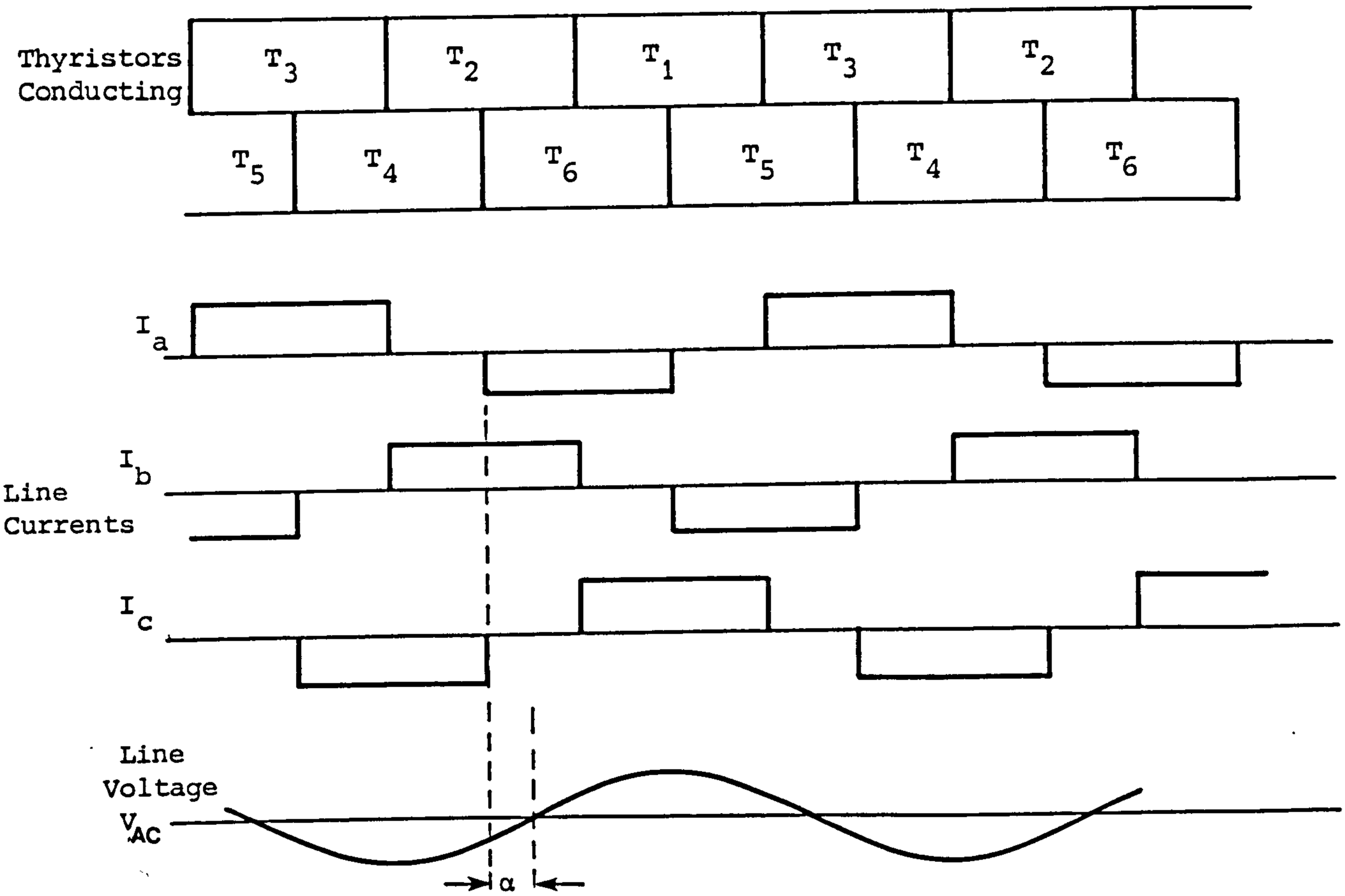

Fig. 1.8 Thyristor switch commutatorless motor drive

of its excitation level. The firing system can be best explained by referring to Fig. 1.8 and considering the instant when thyristors T_2 and T_4 are conducting :

It is required to switch-off T_4 and switch-on T_6 . When the gating signal is applied to T_6, it assumes an on-state and both T_4 and T_6 conduct for some period called the commutation period. Such an interval is necessary in order to establish magnetic energy in the associated phases. If the induced voltage between terminals A and C is negative, the current in T_4 gradually decreases to zero and T_4 is turned-off [26] .

Successful operation depends on angle α (the angle by which machine phase current leads phase voltage) which is determined by the setting of the position sensor. If α is larger than the commutation angle plus the thyristor turn-off time, the transition is completed successfully. In such schemes it is essential to maintain a minimum phase angle between fundamental components of voltage and current of about 30° (this large value of α results in high output torque ripple [26]).

1.5.2 MULTI-COIL ARMATURE DC MACHINES

A number of attempts have been made to replace directly the function of the mechanical commutator in a DC machine by an electronic switching facility [references 15 - 20].

Fig. 1.9 synthesises a normal multi-coil armature winding of a DC motor with the commutation interpoles omitted for simplicity; the machine shown has 8 commutator segments.

The armature winding described by Trickey in reference 15, shown

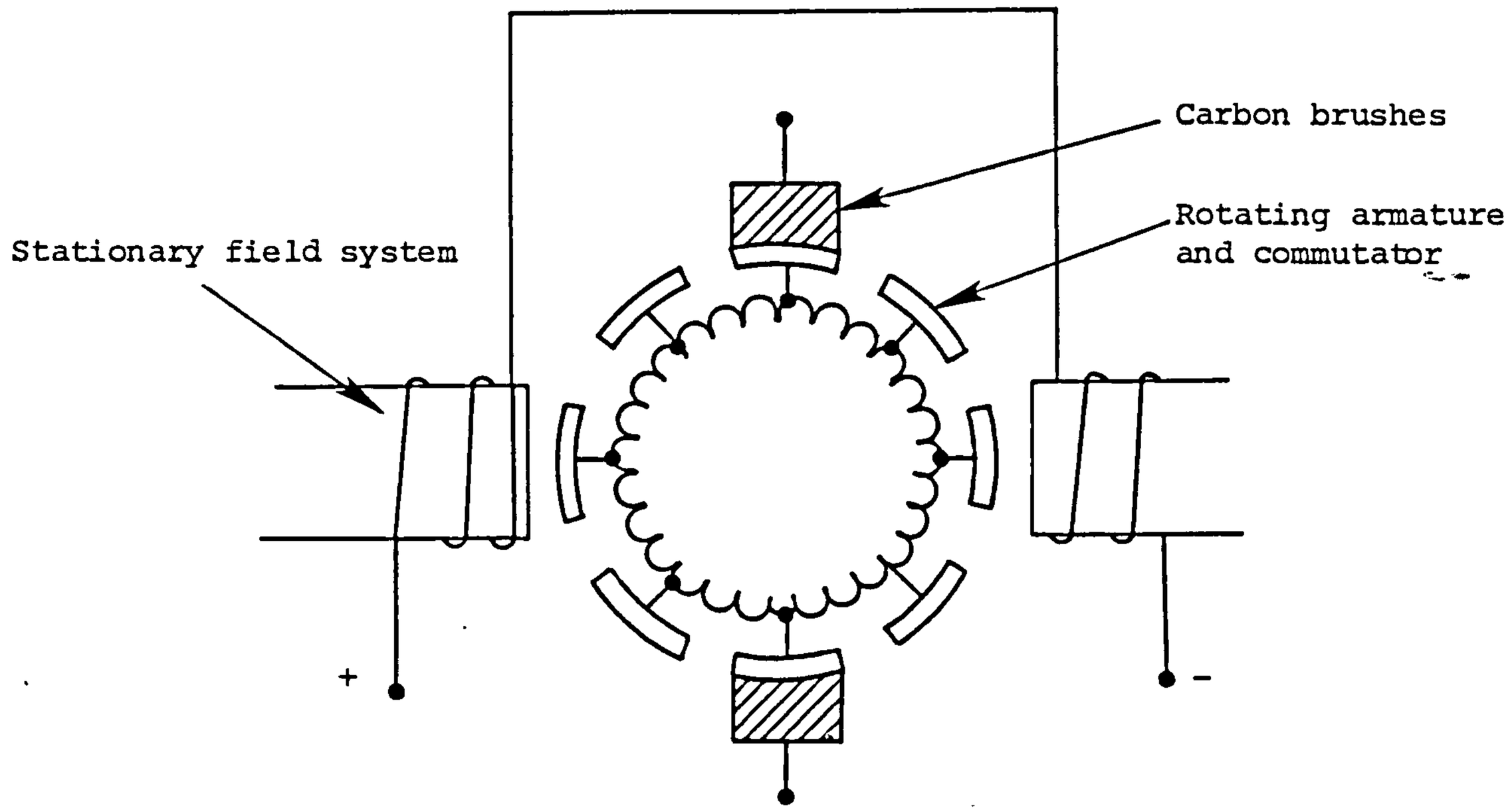

(i) Brush/Commutator arrangement in dc machine

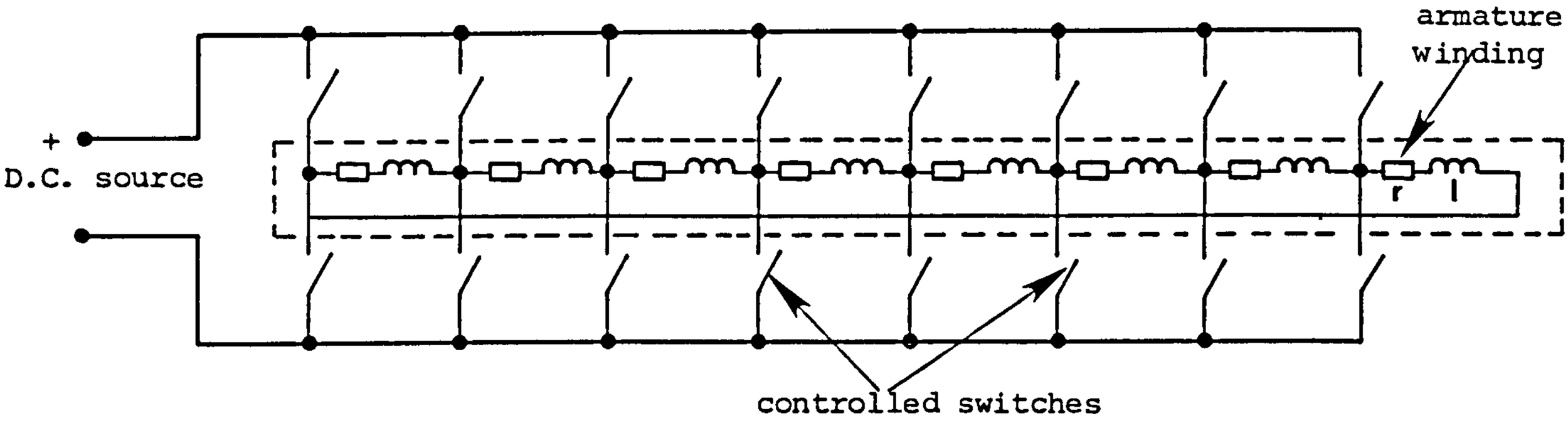

(ii) Statically commutated armature circuit

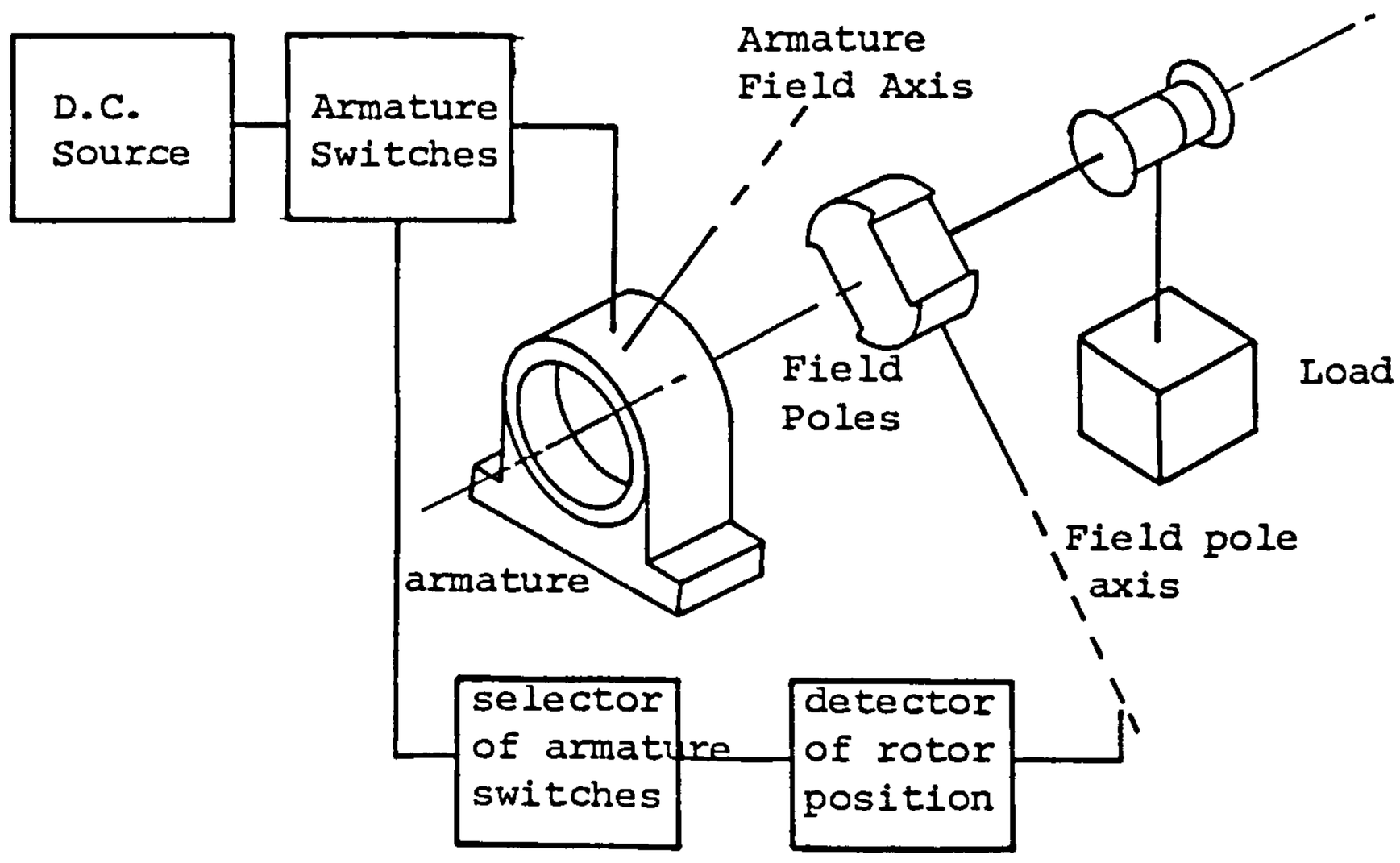

(iii) Block diagram of a brushless d.c. motor

Fig. 1.9 Synthesis of multi-coil armature commutatorless d.c. machine

in Fig. 1.9(ii) also corresponds to conventional multi-coil armature winding of a DC machine, but located on the stator. The coils can be either lap or wave wound, full or fractional pitch. Static commutation using solid-state devices (e.g. thyristors) can be obtained with two controlled switches required per coil, which corresponds to twice as many switches as segments of the commutator being replaced. Thyristors were used as the switching devices in Trickey's system; this requiring forced commutation of the anode current. The turning-off procedure was based on turning-on an auxiliary thyristor causing a charged capacitor to be switched across the main thyristor, as shown in Fig. 1.10(i). The charged capacitor reverses the voltage across the thyristor which have been carrying armature current causing it to switch-off.

Another scheme described by Zabar [16] was also based on a similar concept in which light-triggered thyristors were used as the switching elements. The firing sequence of the devices was effected cyclically with each input device turned-on simultaneously with its output counterpart. The firing system was controlled by an "information collector" consisting of a rotating-light beam and light activated thyristors.

Thyristor turning-off in Zabar's system was different. This was done by feeding a rectangular alternating voltage to coils wound on auxiliary poles on the rotor, in quadrature with the main magnetic field - coils A shown in Fig. 1.10(iii). The voltage induced in the armature coil C_k is fed to the conducting thyristor i.e. T_k, forcing it to turn-off if the voltage across the thyristor becomes negative.

In both Trickey's and Zabar's scheme, turning-off of the current

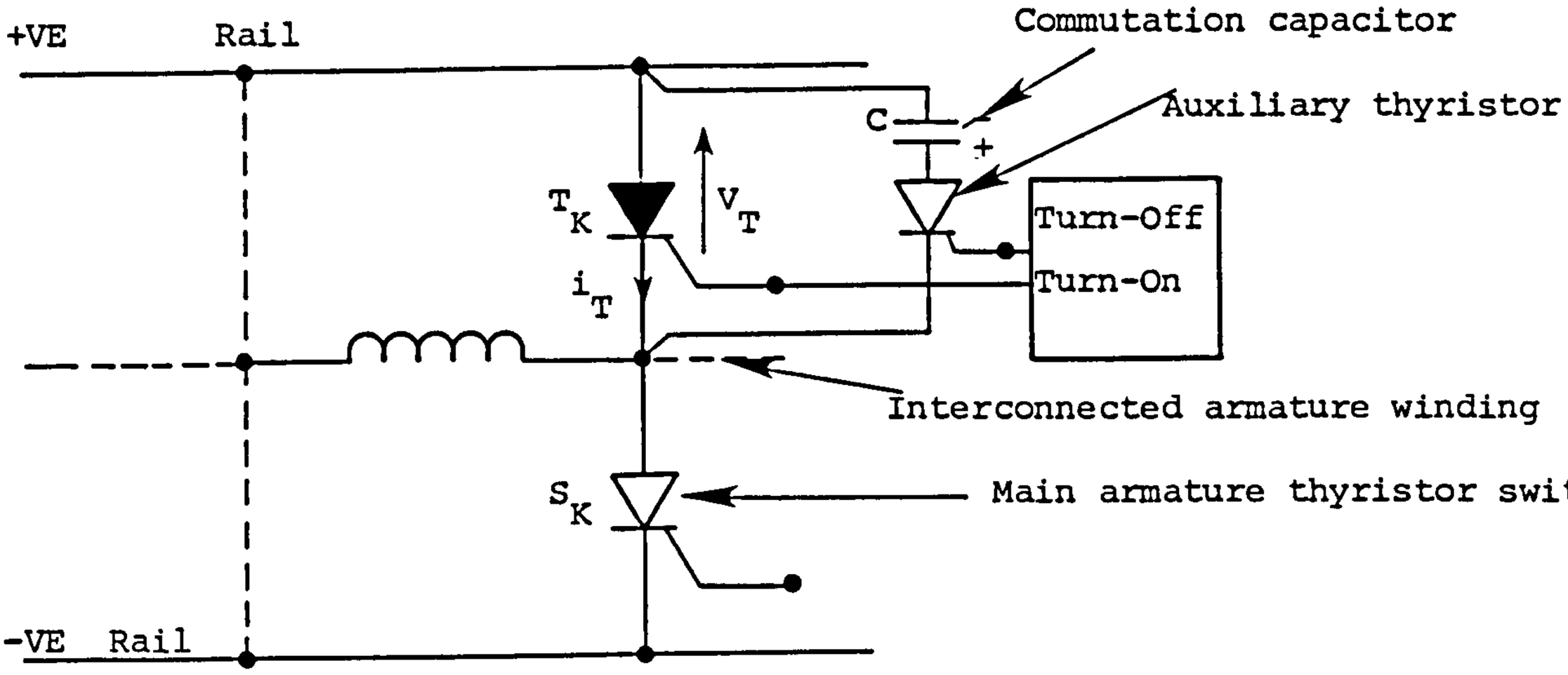

(i) Trickey's Turn on/off scheme

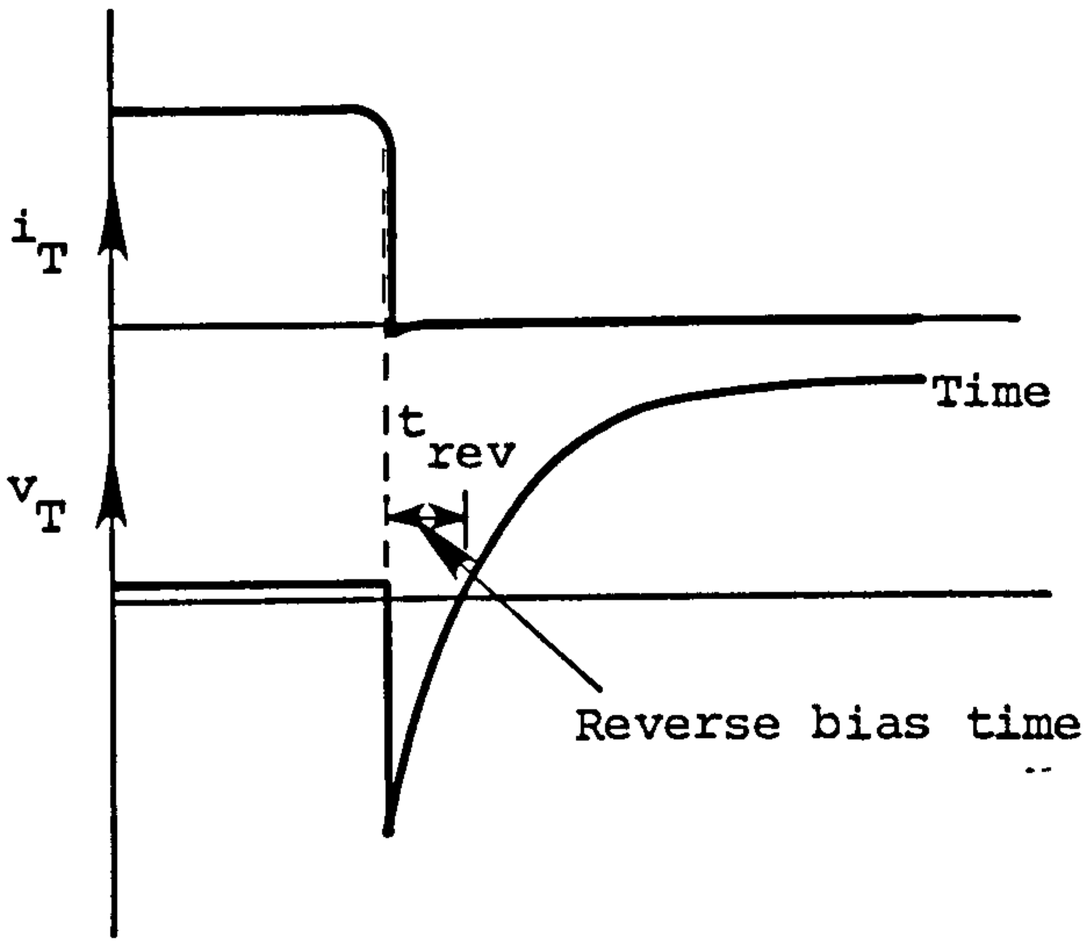

(ii) Voltage and current waveform for (i)

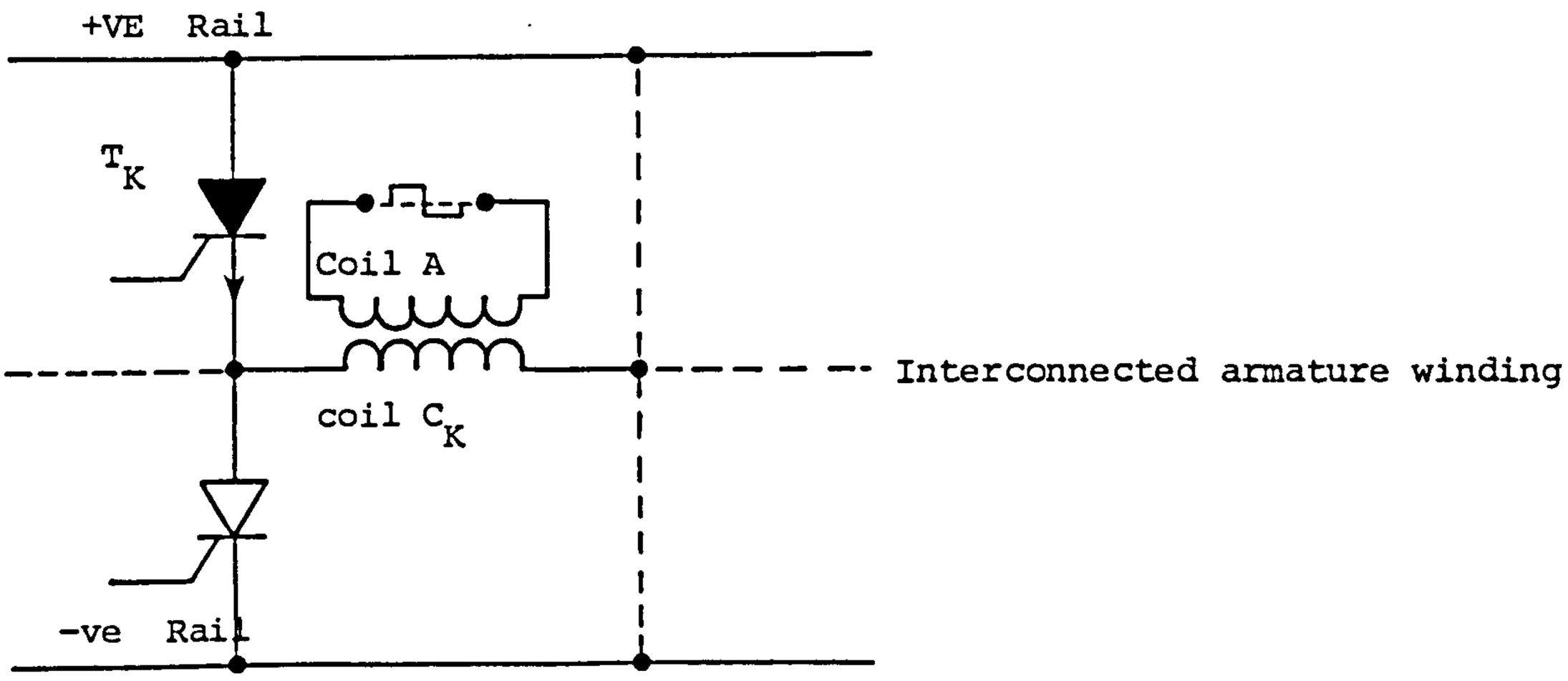

(iii) Zabar turn-off scheme

Fig. 1.10 Gate control schemes in thyristor armature switch DC motor

after conduction has been achieved was a prime difficulty as shown by the need for extra circuit elements such as forced commutation circuitry in the former and rectangular AC voltages applied to auxiliary coils on the rotor, in the latter. Zabar described a case which he referred to as "accidental commutation lag" in which a thyristor regains its conduction status before it is fully turned-off.

A generalised block diagram of such brushless scheme is shown in Fig. 1.9(iii). Completely brushless operation is achieved by using a permanent-magnet rotor of the salient-pole construction [15,16,17] or cylindrical [18].

1.6 THE OBJECT OF THIS WORK

The continuing technological development of semiconductor device technology has made available substantially improved switching devices suitable for electronic commutation. The recent addition of Gate-Turn Off thyristors (G.T.O's) to the established families of thyristors, bi-polar transistors and darlingtons widened the scope of new investigation into the viability of replacing the mechanical commutator of a DC machine by such devices.

The two attempts by Zabar and Trickey described earlier were both based on the use of the thyristor as the switching device. The principal difficulty with the use of thyristors in DC applications is that of extinguishing the current after conduction has been achieved.

The G.T.O. on the other hand, combines the most desirable

characteristics of the conventional thyristor with those of the bi-polar transistor. Like the transistor, it can be switched-ON and -OFF by a low power gate drive, but like the thyristor, it can pass high forward currents when turned-on and block high forward voltage when turned-off.

This work presents the systematic development of a DC machine with its mechanical commutator device being replaced by a system of electronic switching using gate-turn-off thyristors. The developed machine, like Trickey's scheme, is inverted i.e. the armature winding is on the stator and the field poles rotate.

A digital control circuit has been designed which, in conjunction with an incremental shaft encoder, defines the instant of switching of a particular G.T.O. armature switch, its conduction period and the correct sequential triggering order of all the devices to maintain the optimal 90^{o} (electrical) torque angle between stator and rotor fields.

Also incorporated within the digital closed-loop control circuit is the possibility of controlled departure from the 90^{o} torque angle and the effect of this on the commutation is thoroughly investigated both experimentally and theoretically.

Operation of the machine in the motoring mode, the generating mode, the effect of interpoles provision on machines performance is also investigated.

A detailed analysis of machines rating requirements is given together with choice of the switching devices, their rating, their drive circuit and protection circuit requirements.

A proposal for developing the machine with a fewer number of switching devices is suggested on the basis of the results obtained

1.7 SUMMARY OF THE REMAINDER OF THE THESIS

Chapter 2 describes the process of current reversal in an armature coil of a conventional DC machine and discusses the methods of improving the commutation process. Chapter 3 gives a detailed description and rating evaluation analysis of the machine "original" and "inverted" formats, for the windings on both sides of the airgap. The distributions of the radial field in the airgap of the machine is also analysed. Chapter 4 specifically deals with the reasons for the choice of gate turn-off thyristors as the armature switching devices detailing the design considerations of gate drive and protection circuit requirements of the devices. An empirical formula is derived for predicting the overshoot voltage on the devices at the end of the commutation period of a particular armature coil. Chapter 5 is devoted to the design of the digital control circuit for controlling the switching system of the GTO armature devices such that under normal operation, the radial fields of the armature and main field windings are kept in space quadrature. Provision is made within the design of the digital control circuit for controlled departure from the quadrature axis position; this is also detailed in chapter 5. Experimental tests on the machine describing and analysing the operation of the machine in the motoring and generating modes, effect of controlled departure from the optimal torque angle (q-axis) position and the effect of the provision of interpoles on the commutation is thoroughly

investigated in chapter 6. Finally, conclusions of the present study are presented and the design specification for future development of the machine is given in chapter 7.

CHAPTER TWO

THE PROCESS OF COMMUTATION IN DC MACHINES

CHAPTER TWO

THE PROCESS OF COMMUTATION IN DC MACHINES

2.1 DESIGN CONSIDERATIONS OF DC MACHINES ARMATURE WINDING

To achieve optimum performance with DC machines, the armature winding is distributed over a large number of slots on the periphery of a cylindrical iron laminated core structure. The reason for this is the concern about the distribution of flux and field; this should be as uniform as possible, which will lead to:

(a) Uniform mechanical stressing of the armature iron.

(b) Avoidance of early magnetic saturation in iron teeth areas of high local flux density.

The desire to minimise ripple on the e.m.f. induced reinforces the need to distribute the armature winding.

Individual armature coils are interconnected with adjacent coils to form the armature winding. The resulting winding is continuous for the case of a DC machine with each coil connected to a commutator segment (via a "riser") for periodic connection via a "brush" to an external circuit, as shown in the diagram of Fig. 2.1(i). With full pitched coils, the induced e.m.f. in the coil passes through zero at the instant when the active side of the coil passes through the magnetic neutral zone.

The distributed nature of the armature winding gives the DC machine some unique properties [4], Fig. 2.1(ii):

(a) current-carrying axially-directed conductors of the armature winding may be represented as an axially directed current sheet uniformly spread over the appropriate iron/airgap boundary. Such current distribution and its associated tangential field distribution within the airgap (H_t) approximate to a square waveform. The peak value of the tangential field occurring at the excited boundary of the airgap is equal to the current density (in A/m) [proof of this is given in reference 4].

(b) The airgap radial field distribution due to current excitation of the armature winding approximates to a triangular waveform which may be considered uniform across the length of the airgap with the peak value occurring coincident with the brush position.

The periodic reversal of the load current in each armature coil should ideally take place over a period when the net e.m.f. induced in the coil is zero.

This reversing process is accomplished by means of the brush/ commutator arrangement. This is an assembly of insulated copper bars, mounted on the rotor shaft and connected individually to armature coils, each in cyclical contact with carbon (graphite) brushes as the rotor rotates. The function of the brush/commutator assembly is to translate the essentially alternating e.m.f. and current variation with time within the coils into steady values appropriate to direct current supply. A typical interconnection layout of the armature winding of a DC machine is shown in Fig.

2.1(i). The diagram shows each coil to be connected with adjacent coils and also to one commutator segment. The complete winding is continuous with each coil spanning a full pole pitch. The brushes are also separated by a pole pitch.

As the DC armature (rotor) rotates, the carbon brushes switch currents in the "phase" coils undergoing commutation. The coils undergoing commutation in the diagram of Fig. 2.1 are the ones shown in bold (marked with an asterisk). This continuous switching process ensures that the total pattern in space of rotor slot currents remain stationary thereby giving the commutator the following properties :

(i) All phase coils, other than those being switched, continuously carry full current and are therefore fully utilised for torque production.

(ii) The resultant square spatial waveform of slot currents around the armature periphery, is optimum for torque production via interaction with the (ideally) square radial field distribution due to main field winding excitation, and these two waveforms are always held in the correct relative position so that overall the greatest possible torque per watt of I^2R loss is achieved.

(iii) Torque ripple with shaft rotation is low, the same form of variation of torque with speed is obtained for all sets of no-load speeds (for the separately excited machine), including zero [10] .

(iv) All the above requires no special control signals, to initiate switching at the correct instant.

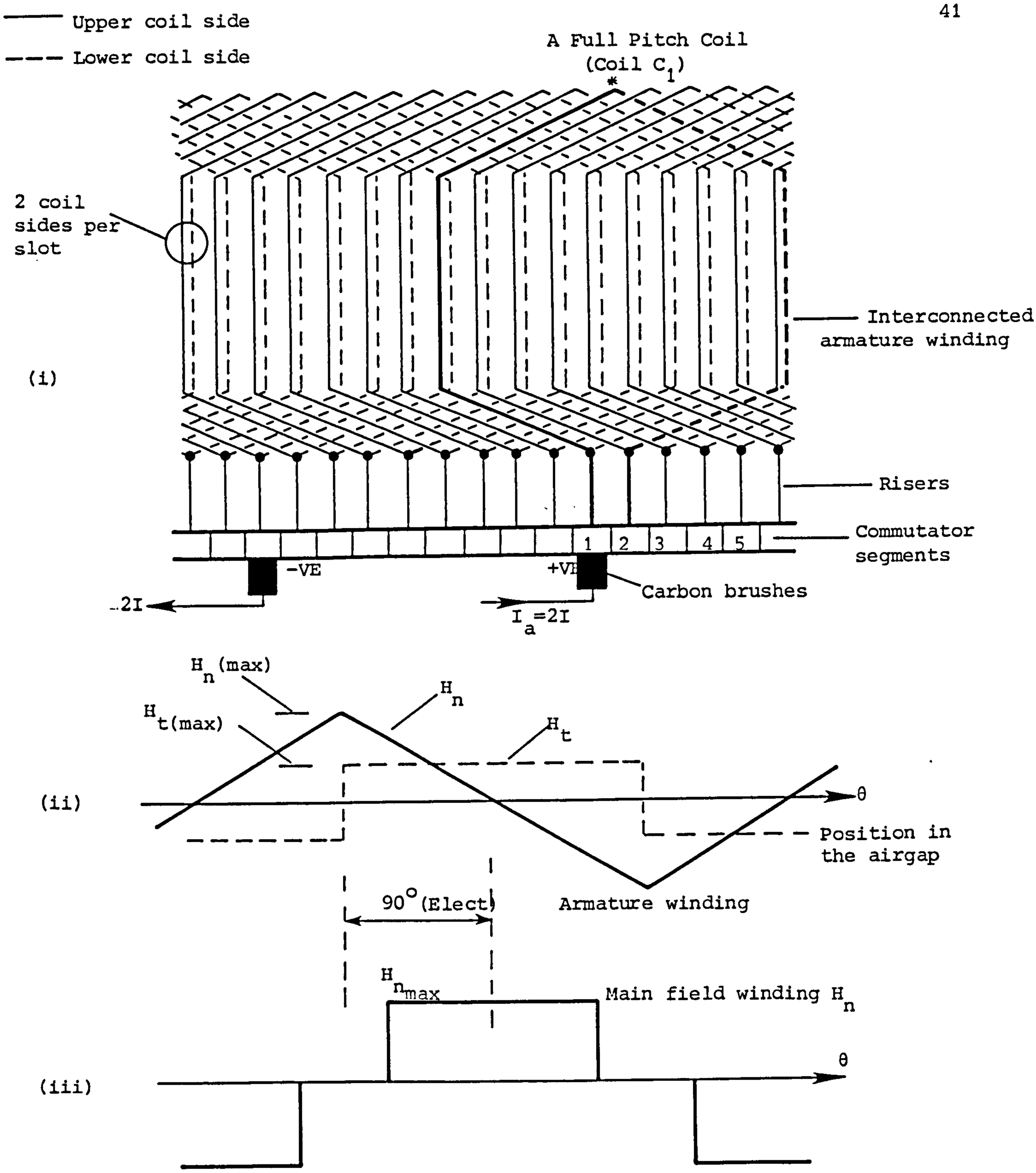

Fig. 2.1 Distributed armature winding of DC machine

(i) Interconnected armature winding layout
(ii) Radial and tangential field distribution due to armature winding excitation
(iii) Radial magnetic field due to main field winding excitation

(Gray Ref. 4)

2.2 CURRENT REVERSAL

The process of commutation involves passing armature current (I_a) through a sliding contact between a fixed brush and a rotating circular assembly of copper bars (commutator segments), each bar being connected to a pair of coil ends through "risers". As the segments pass under the brush, the current in the coils to which they are attached directly is reversed. The brush/commutator assembly may be therefore, regarded as an electro- mechanical switching system in which the switching is performed by making or breaking mechanically electrical contact between brush and commutator segment, a process that inherently occurs at any speed of rotation.

The process of current reversal in an armature coil (for example, a coil marked with an asterisk - Fig. 2.1), is shown in Fig. 2.2 for the case when coil C_1 is undergoing commutation. Coil C_1 in Fig. 2.2 (shown as a single turn but is often multi-turn) is a full pitch coil; the current is switched to this coil via the brush and commutator sector "1". As the armature rotates, sector "1" and "2" simultaneously pass under the brush surface. Thus, for a brief period, coil C_1 becomes bridged or short-circuited. It is during this brief interval that the current in the coil has to be reversed or "commutated".

The ideal case for current reversal is that it should take place at a uniform rate i.e. current linearly decay to zero and build up in the opposite direction. Such ideal current reversal is generally opposed by the e.m.f. of self induction of the armature coil, given by the product of the rate of current change and the effective self-

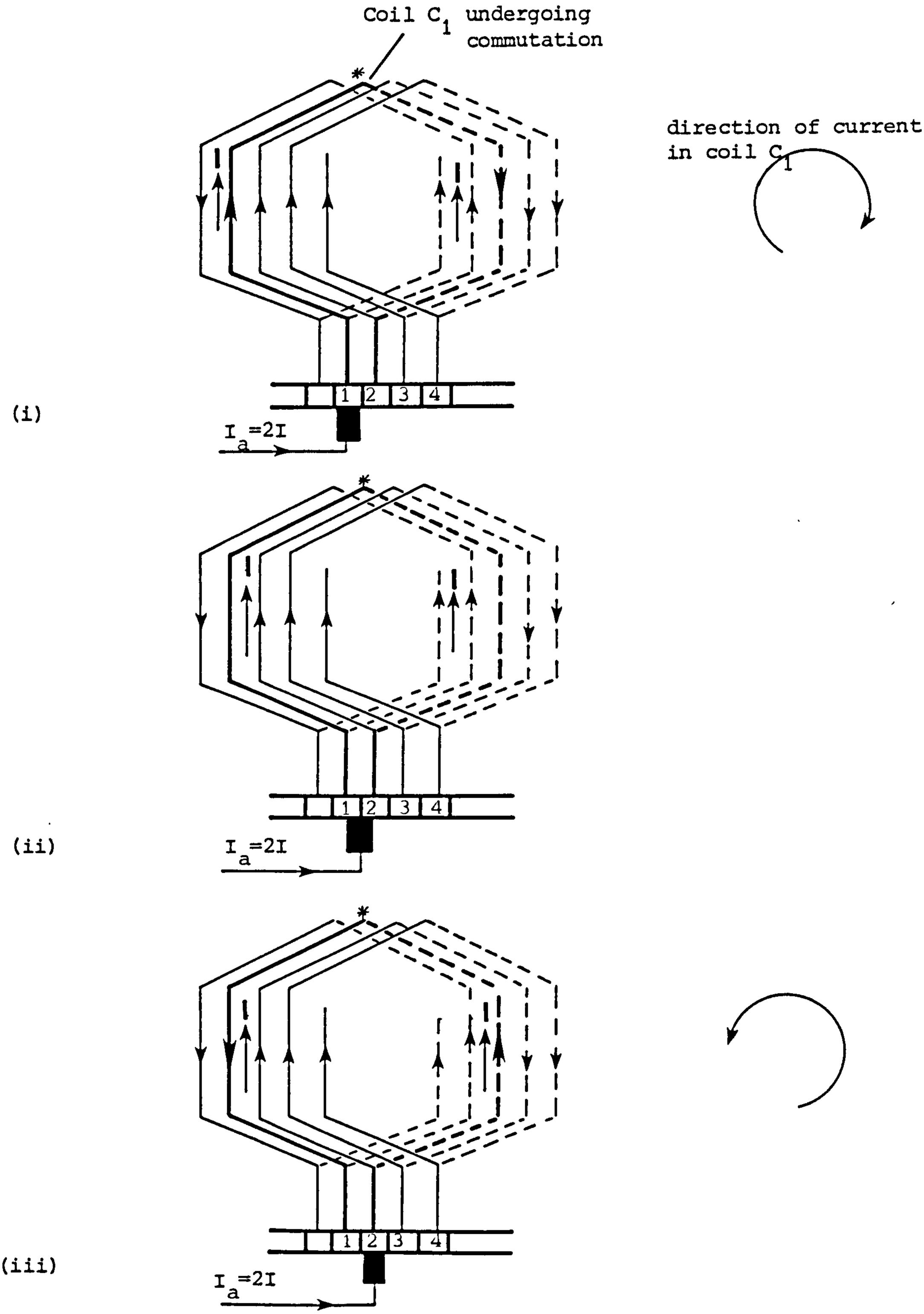

Fig. 2.2 Before and after coil C_1 subjected to commutation

induction of the coil, viz :

$$e_1 = L\ (di/dt) \qquad (2.1)$$

The problem of commutation of the current in a coil of a DC armature is more complicated by the fact that the commutated circuit is by no means of constant resistance owing to the nature of the brush contact resistance.

2.3 COMMUTATION IN SMALL MACHINES (WITHOUT INTERPOLES)

The value of the e.m.f. of self induction, expressed in terms of self flux $\emptyset$, and the number of turns N with which the flux is linked is:

$$N\ (d\emptyset/dt) \qquad (2.2)$$

From equation 2.1 and 2.2 it follows that the inductance has a value given by :

$$L = (N\ \emptyset)/I \qquad (2.3)$$

The product $(N\ \emptyset)$ of the flux and the number of turns with which it is linked is called the number of flux linkages.

If the self inductance of a coil undergoing commutation is assumed negligible (due to the small number of turns incorporated in each armature coil, for example coil C_1 Fig. 2.2), the division of the brush current I_b between the two adjacent commutator risers would be governed only by the combined resistance of the coil, the risers and the brush contact. The brush contact resistance usually predominates.

Referring to Fig. 2.3, if the total surface area of the brush is a_b

$$a_b = a_1 + a_2 \qquad (2.4)$$

i.e. sum of the contact surface areas, then the corresponding brush

contact surface resistances are :

$$r_1 = r_b \ (a_b/a_1) \qquad (2.5)$$

$$r_2 = r_b \ (a_b/a_2) \qquad (2.6)$$

The current division between the two commutator risers will be in direct proportion to the contact surface areas a_1 and a_2 (therefore, inversely proportional to the contact resistances).

$$\text{i.e.} \quad i_1 \propto (1/r_1) \qquad (2.7)$$

$$i_2 \propto (1/r_2) \qquad (2.8)$$

These contact resistances may be slightly influenced by such factors as the peripheral speed of the commutator and depend to some extent upon the pressure of the brushes upon the commutator.

The manner in which the current in a coil undergoing commutation changes (eq. 2.7 and 2.8) clearly determines the manner in which the current density under the brush varies. To obtain the so-called "straight-line commutation", the change should occur linearly with time. The brush current for this case, will be uniformly distributed over the whole brush surface area giving constant current density, Fig. 2.4(i). "Linear" commutation of this kind is relied upon for acceptable commutation in small machines without using interpoles.

Failure to achieve this ideal current reversal can lead to either "over" or "under-commutation". If the change in the current is too fast, this results in high current density near the leading edge of the brush. This leads to the so called "over-commutation" effect, Fig. 2.4(ii). If the current reversal is incomplete by the time the sector leaves the brush, the forcing to zero of the current is accompanied by a spark. Sparking occurs between the brush and the

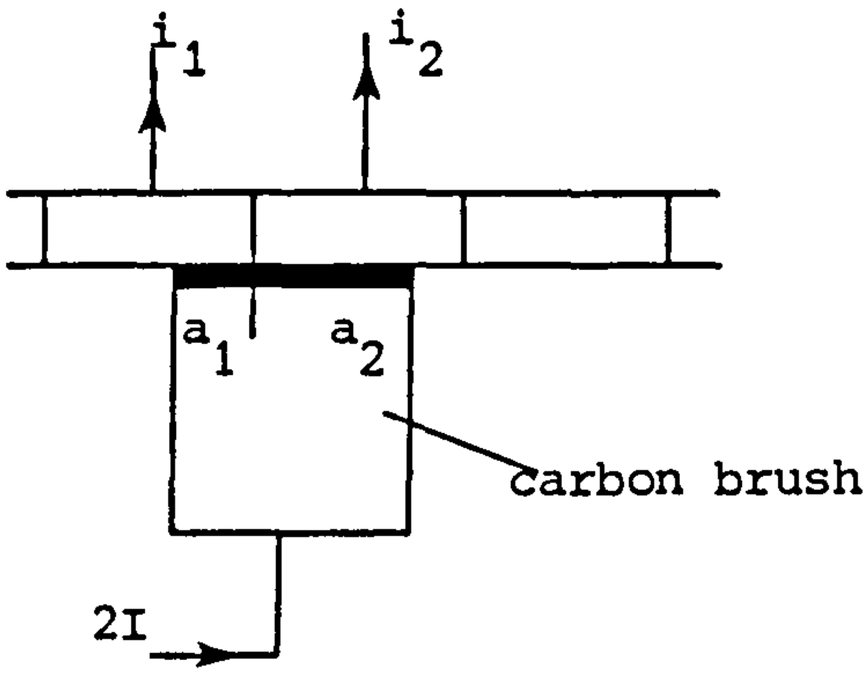

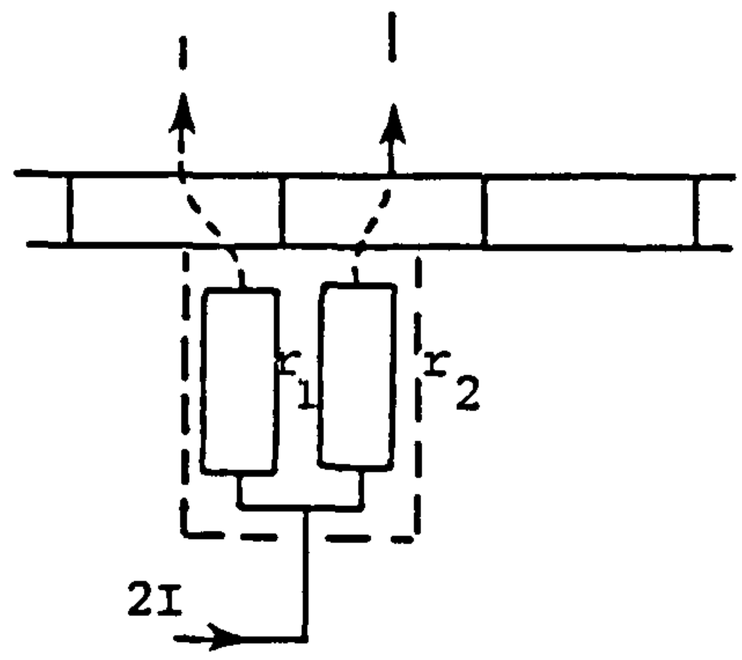

Figure 2.3 Resistance Commutation

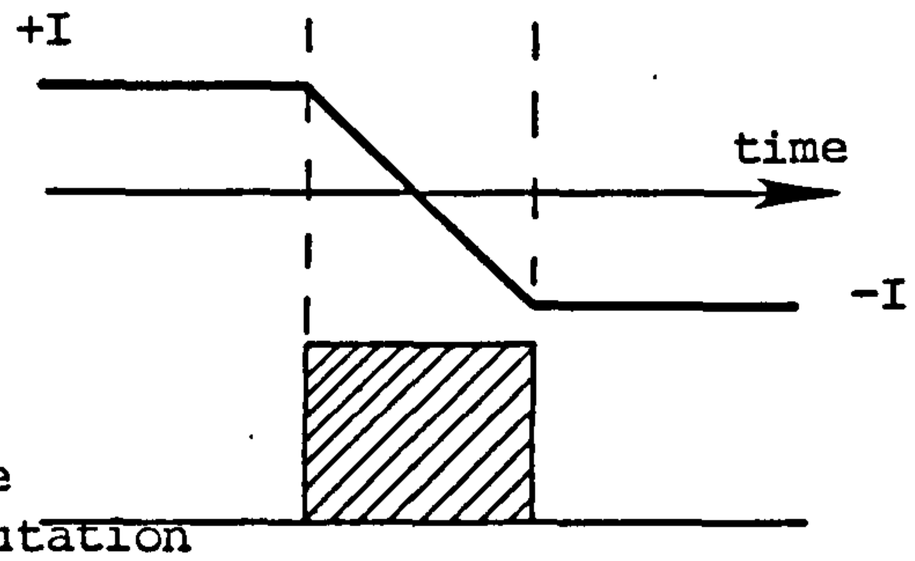

(i) Straight-line (linear) commutation

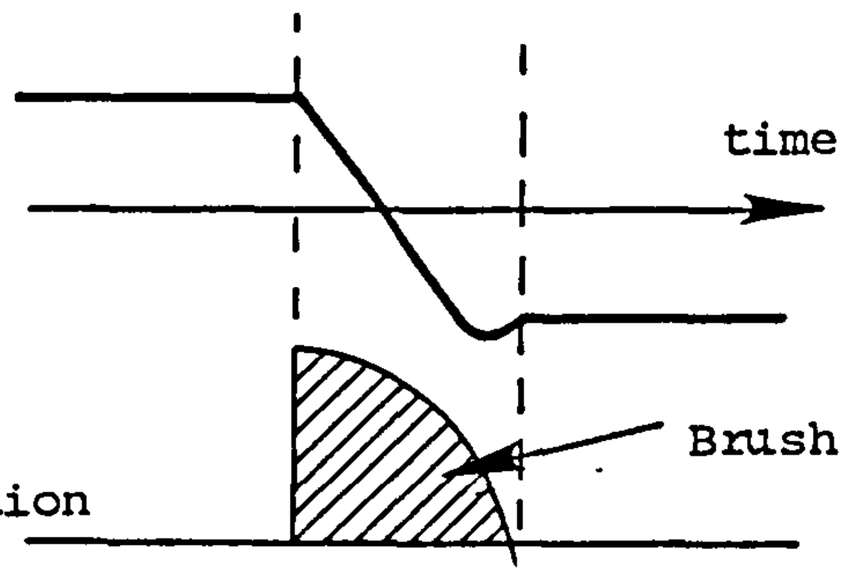

(ii) Over-commutation

commutation time

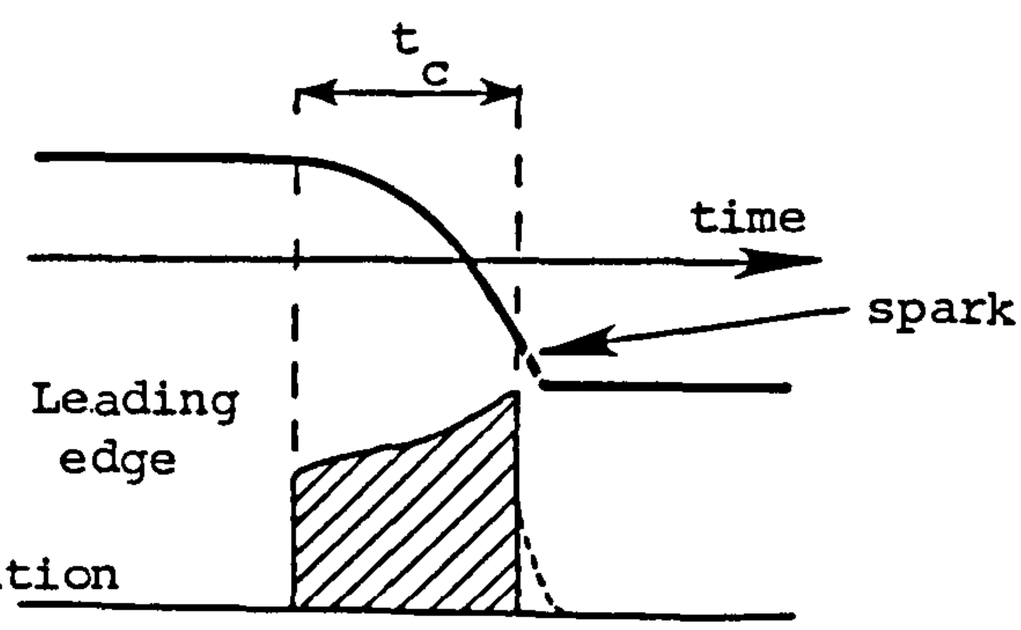

(iii) Under-commutation

Figure 2.4 Coil current change and brush current density (source: Say & Taylor - D.C. Machines)

receding commutator segment whose current transfer is incomplete within the commutation time allowed. This condition is known as "under-commutation".

In small rating DC machines the effective inductance/resistance ratio relationship of the commutated circuit is such that satisfactory commutation is achieved up to full load current without the need to use interpoles. Sparking, resulting at the trailing edge of the brush implies poor commutation. Sparking causes damage to the commutator, leading to still greater brush wear. Also the non-uniform current density within the brushes leads to greater power loss, temperature rise and hence brush damage.

2.4 COMMUTATION IN LARGE MACHINES (THE USE OF INTERPOLES)

It was stated earlier (section 2.3) that straight line commutation can only be achieved when the brush has a uniform current density. The condition for straight-line commutation was obtained on the assumption that the coil inductance was negligible. With large machines, with slotted armatures, each coil consisting of large number of turns has appreciable leakage inductance (as confirmed by equation 2.3).

As a result, during the time that the current in the slot is being commutated, the e.m.f. of self induction of the armature coil undergoing commutation (sometimes referred to as the "reactance e.m.f.") can be very large. In order to ensure that the current in the commutating coil is reversed by by the end of the commutation period, a rotational e.m.f. of opposite polarity to the coil self-induction e.m.f. is intentionally induced in the short-circuited

coil. This is done by fitting small, narrow poles to the frame of the machine, called interpoles or compoles (commutating poles). These poles are placed midway between the main poles and are excited in such a manner as to produce a commutation field of the required polarity and strength, confined to the quadrature axis where commutation is taking place, Fig. 2.5(ii). For a generator, to aid the current reversal, the polarity of the interpole must be the same as that of the main pole ahead (in the direction of rotation), and opposite for a motor.

The concept is best illustrated by referring to Fig. 2.5. The radial airgap field distribution (shown earlier in Fig. 2.1) due to the main field winding excitation (Hn_f), the armature winding (Hn_a) and their resultant is shown in (i). By arranging the radial field developed by the interpole to be confined to the quadrature axis - Fig. 2.5(ii), commutation will occur in the magnetic neutral position; the resultant radial field in the commutation zone is reduced to near zero.

The interpole winding is local in its action in that the winding develops radial field which should be confined to commutating zone only.

The interpole winding is energised with a definite fraction of the armature current so that its strength and polarity vary automatically as required with the changes in load or function, whether motoring or generating provided the direction of rotation and the polarity of main field remain unchanged.

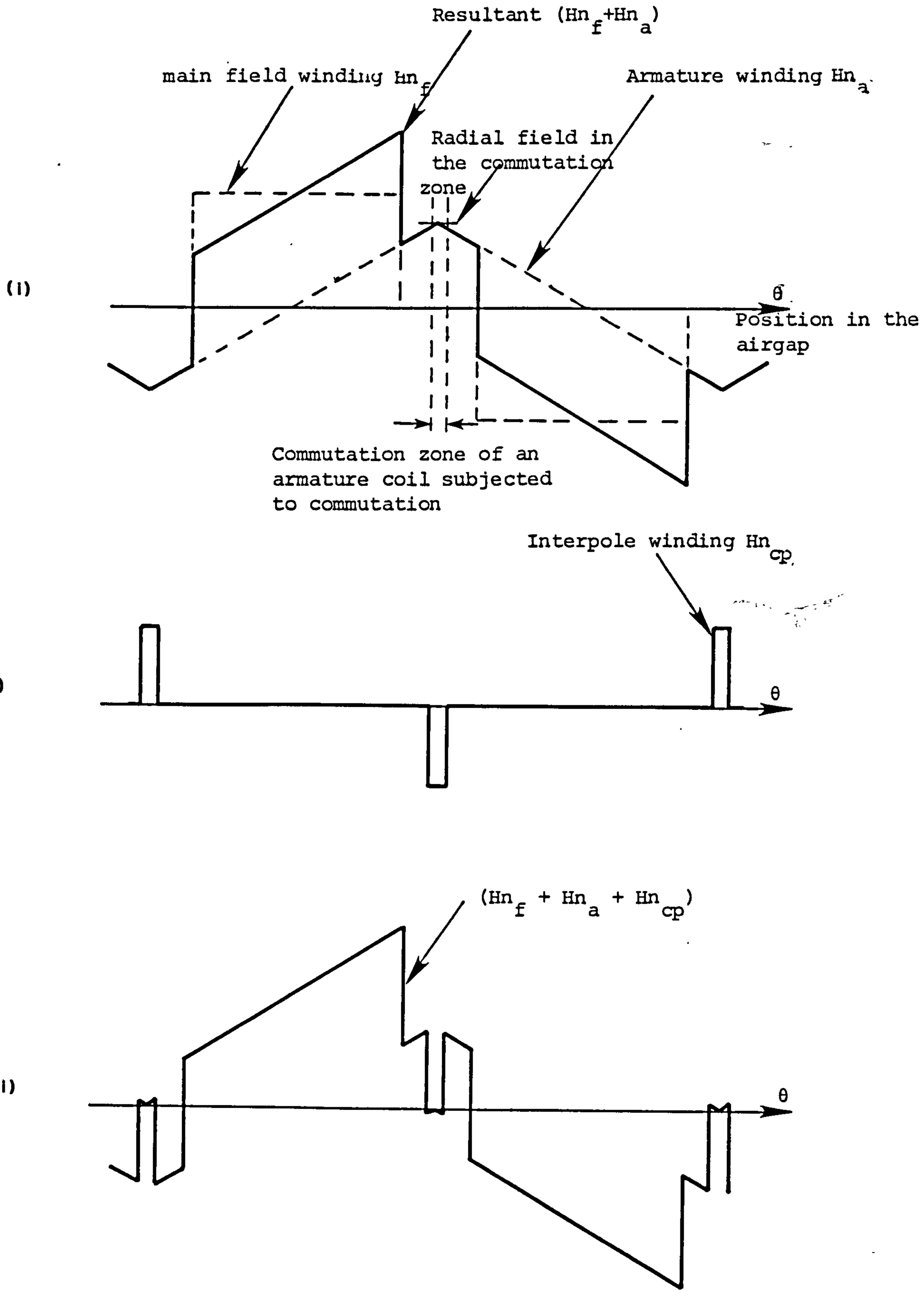

Fig. 2.5 Radial airgap field distributions
(Salient Pole - main field winding)

2.4.1 ESTIMATION OF THE RADIAL FIELD INTENSITY OF THE INTERPOLE WINDING :

If the mean e.m.f. in the coil undergoing commutation ($e_{r_{av}}$) is known from the knowledge of the resultant radial field in the commutation zone {this value is shown in Fig. 2.5(i)} including the reactance e.m.f., then the requirement is that the reversing e.m.f. induced by the interpoles (e_{cp}) should neutralise $e_{r_{av}}$.

The interpole induced e.m.f. (e_{cp}) can be calculated from the equation :

$$e_{cp} = 2 (Bn_{cp} \times l \times v) \text{ volts per turn} \qquad (2.9)$$

This is the equation for the e.m.f. induced in a single turn coil, derived from the more fundamental Lorentz equation for the electric field induced in a conductor moving in a magnetic field. It is given in terms of the axially directed coil side of length l, situated a pole pitch apart, the interpole radial gap flux density Bn_{cp} and peripheral speed of the armature v .

For the commutating coil with n_c turns :

$$e_{cp} = 2\ n_c\ (Bn_{cp}\ l\ \ v)\ \ V$$

If the interpole induced e.m.f. is to neutralise $e_{r_{av}}$, then

$$e_{r_{av}} = 2\ n_c\ (Bn_{cp}\ l\ \ v)$$

and $$Bn_{cp} = e_{r_{av}} /(2\ n_c\ l\ \ v) \qquad (2.10)$$

Using the relationship :

$$Bn = \mu o\ Hn \qquad (2.11)$$

where μ = permeability of the medium

μ = μo (permeability of free space in this case)

Bn = radial flux density (Wb/m^2)

Hn = radial magnetic field intensity (A/m)

$Bn_{cp} = \mu o \quad Hn_{cp}$ and

$$Hn_{cp} = e_{r_{av}} / (2 \mu o n_c \; 1 \quad v) \qquad A/m \qquad (2.12)$$

In the design of the interpole winding, equation 2.12 can be used in the evaluation of the value of the radial field intensity of the winding .

In conventional DC machines, exact compensation of the the commutating e.m.f.s ($e_{r_{av}}$) by the interpole induced voltage (e_{cp}) is difficult to achieve. Even in machines where these e.m.f.s are kept low by using extensive subdivision of armature coils, it is still difficult to achieve absolute compensation because of the complex nature of the electro-magnetic system and the uncertain nature of the brush contact. There is, in fact little factor of safety in the engineering problem of the interpole design that can be used to ensure that the effects of the uncertain and imperfectly understood phenomena are kept within satisfactory limits.

2.5 ASSISTED COMMUTATION USING SEMICONDUCTOR DEVICES

Attempts have been made to use solid-state devices for "assisting" the commutation process in an effort to overcome the physical limitations on conventional DC machines that are due to commutation difficulties.

The principle upon which Bate's schemes [34, 35, 36] are based is by division of the switching action of a conventional commutator into two parts: an entirely "off-load" switching by a sliding

contact and a complementary and synchronised "on-load" switching by use of semiconductor devices such as diodes or thyristors. It is for this reason that the method is referred to as being "assisted", since the switching function of the conventional mechanical commutator is partly achieved by the brush/commutator (off-load switching) and the other part by the semiconductor switching (on-load). This system of switching is illustrated in Fig. 2.6 . Here, the switches S_1, S_2,S_3 and S_4 are on- load switches which are required to be capable of switching the current, while switches T_1,T_2 --- etc, and their output counterpart T_1`, $T_2$` --- etc operate off load.

With the switches in the position as shown in the diagram, in order to commutate coil C_1, the following sequence of switching is followed [34] :

(a) Close T_2 and its output counterpart T_2`

(b) Close S_3 and S_4

(c) Open S_1 and S_2

(d) Open T_1 and T_1`

This will transfer the current from the previously conducting pair of switches T_1 and T_1` to $T_2$ and $T_2$`.

Diodes and thyristors have been used as switches for such systems; these two systems will be briefly reviewed.

2.5.1 DIODE-ASSISTED COMMUTATION

Fig. 2.7 shows the scheme based on assisted commutation using diodes as the switching devices. The commutator is constructed in

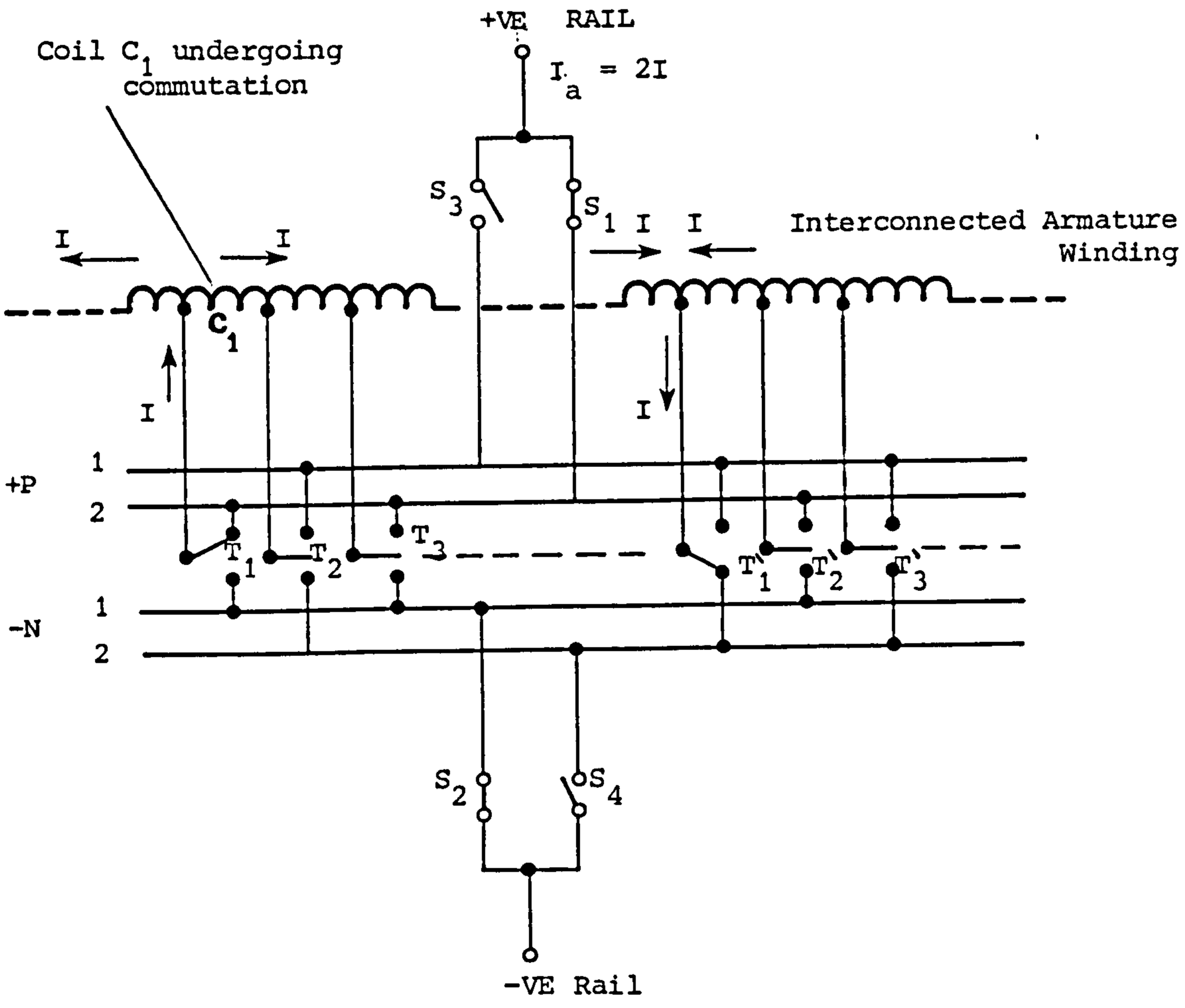

S denotes On-Load switch

T denotes Off-Load Switch

Figure 2.6 Division of switching process in assisted commutation

two parts, each with alternate "active" and "inactive" sectors. The winding tappings are connected to these alternate segments on two segmented rings, contact to the rings being made by conventional carbon brushes B_1 and B_2. Diodes D_1 and D_2 perform the on-load switching.

The armature current (I_a= 2I) is fed into the winding via the brush/ series diode arrangement. The brush position shown in Fig. 2.7(i) shows that all the armature current passes through brush B_1 . As the commutator moves to position shown in (ii), coil C_1 becomes short circuited through both brushes B_1 and B_2 and diodes D_1 and D_2 . With the introduction of an appropriate commutating voltage (e_{cp}) in this local short-circuited coil due to its passage in the compole flux region, a circulating current (i_c) will flow (in this local short-circuited coil) which will cause the current in brush B_2 to rise and in brush B_1 to decay towards zero. The reverse blocking characteristics of the diode ensures that the current in brush B_1 does not reverse. Hence, the whole armature load current 2I has been transferred from brush B_1 to B_2.

A similar argument applies at the brush position where the current leaves the armature except that the diodes have the reverse blocking direction. Certain features of the scheme: the voltage induced in the commutating section by the interpole (e_{cp}) should be sufficiently large to reverse bias the outgoing diode before the appropriate part brush leaves its segment.

i.e e_{cp} must be greater than the induced voltage in the commutating coil ($e_{r_{av}}$).

Other features essential to conventional commutation, such as

* Coil C_1

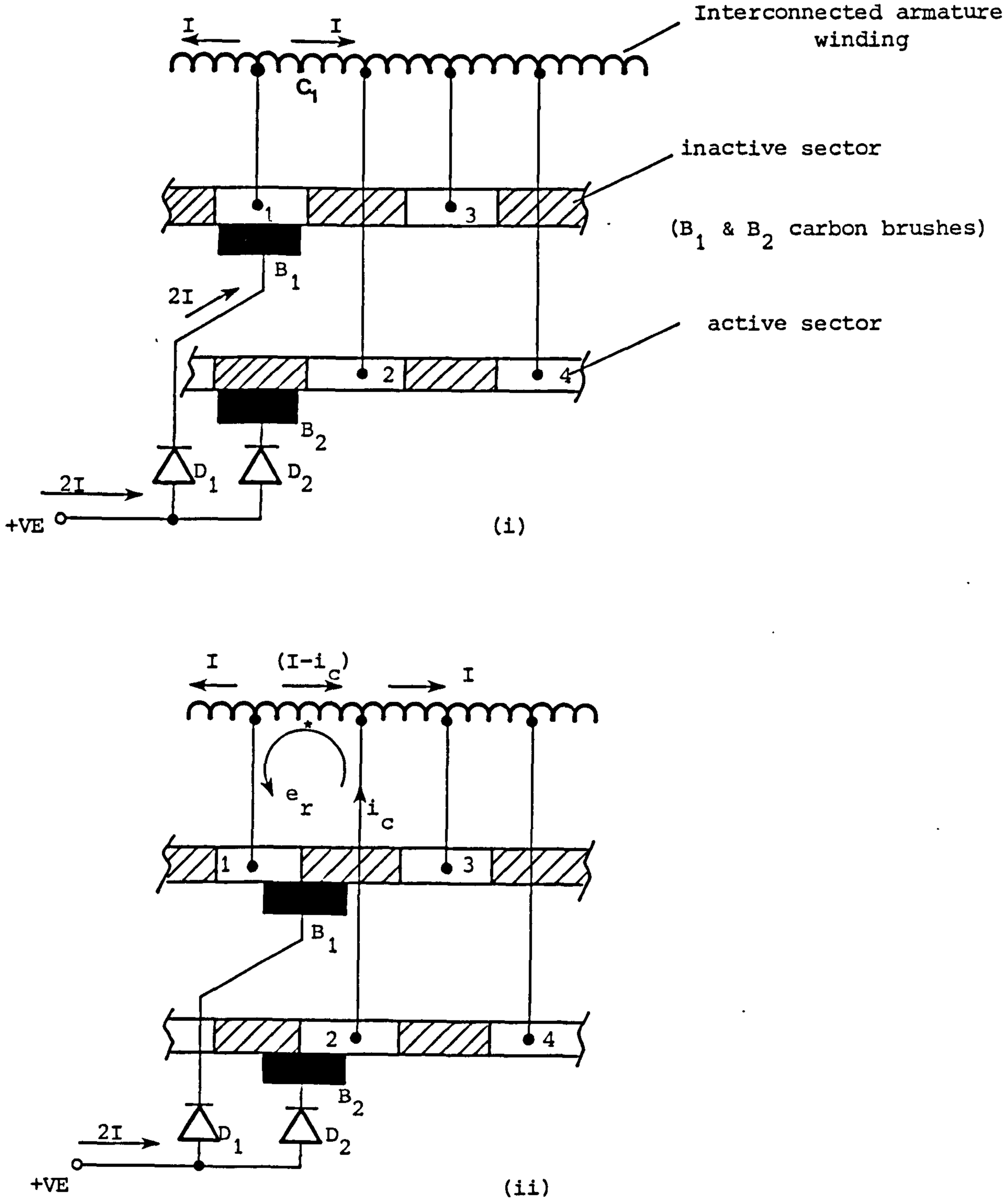

Fig. 2.7 Assisted commutation using diodes

careful balance of e_{cp} by $e_{r_{av}}$ not necessary .

The scheme of Fig. 2.7 has certain problems which prevent successful operation. These problems are those of uncertain contact of the brushes on the segments. Another apparent problem with the system is that the interpole induced e.m.f. (e_{cp}) is zero at starting and too small at low speeds. This might necessitate the introduction of an auxiliary commutating e.m.f. from an external source (see Fig. 2.9). A major practical difficulty is shown by the transfer of brush B_1 from an in-active segment to an active segment; the contact with the active segment may be very uncertain one. Thus uneven brush pressure, aggravated by the commutating voltage, may cause destructive sparking. A more reliable scheme replaces the diodes by controlled thyristors and waits until brush B_2 is fully in contact with segment 2 before any attempt is made to close switch D_2, and to open switch D_1 while brush B_1 is still fully on segment 1. This is the basis for "thyristorised" assisted commutation.

2.5.2 THYRISTOR ASSISTED COMMUTATION [BATES 34,35,36]

The entering-edge sparking associated with the use of diodes when the brush slides from an inactive to an active segment, can be avoided by replacing the diodes with thyristors. The basis of this method is to delay the gating of the thyristors until the brush B_2 (Fig. 2.7) is fully in contact with segment 2. The two brushes B_1 and B_2 are split into two parts (B_{11} , B_{12}) and (B_{21} , B_{22}) as shown in Fig. 2.8(i). This, together with the duplication of the thyristor switches, Fig. 2.8(i), allows the switching action to be

controlled in principle, so that a brush is never carrying current as it moves across from active to in-active segments, or viceversa. The duplication of the thyristors is, however, not necessary provided the links between the part brushes are short and non-inductive. This alternative arrangement is shown in Fig. 2.8(ii).

As brush B_{12} leaves the active segment 1, brush B_{11} must pick up all the current in order to avoid any sparking. In the same way, brush B_{21} must pick up its share of current from B_{22} as it comes into contact with segment 2 .

This arrangement requires that the thyristor should be turned off within a certain time in order that the brushes cease to carry current before they reach the end of a segment. Turning on thyristor S_2 and switching off S_1, Fig. 2.8(ii), implies a full reversal of the current in coil C_1 which can only be achieved by introduction of a commutating voltage into the short-circuited loop. The commutating loop is available outside the machine, hence a commutating voltage to complete the current reversal can be injected from outside. This feature is most important at low speeds when the interpole induced voltage is insufficient to bring about a complete reversal of current in the commutating zone and the thyristors will not turn off before the brushes leave the segment. A commutating transformer (Fig. 2.9) can be used to inject a voltage from an available AC supply at mains frequency, provided that the mean injected voltage is sufficient to effect commutation within one half-period and that three half periods is less than the time required for commutation.

i.e. the time before brush B_{11} reaches the end of the active

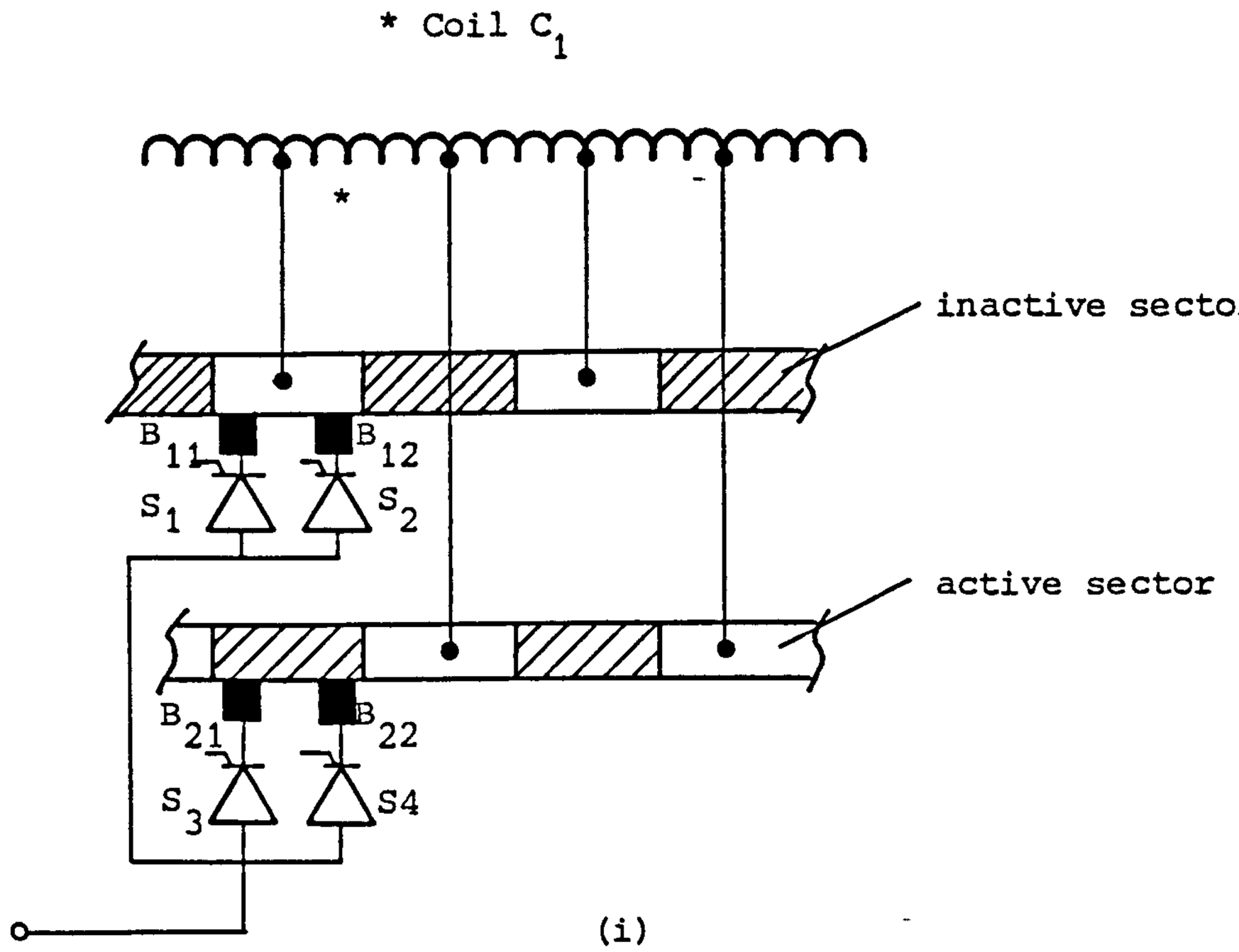

(i)

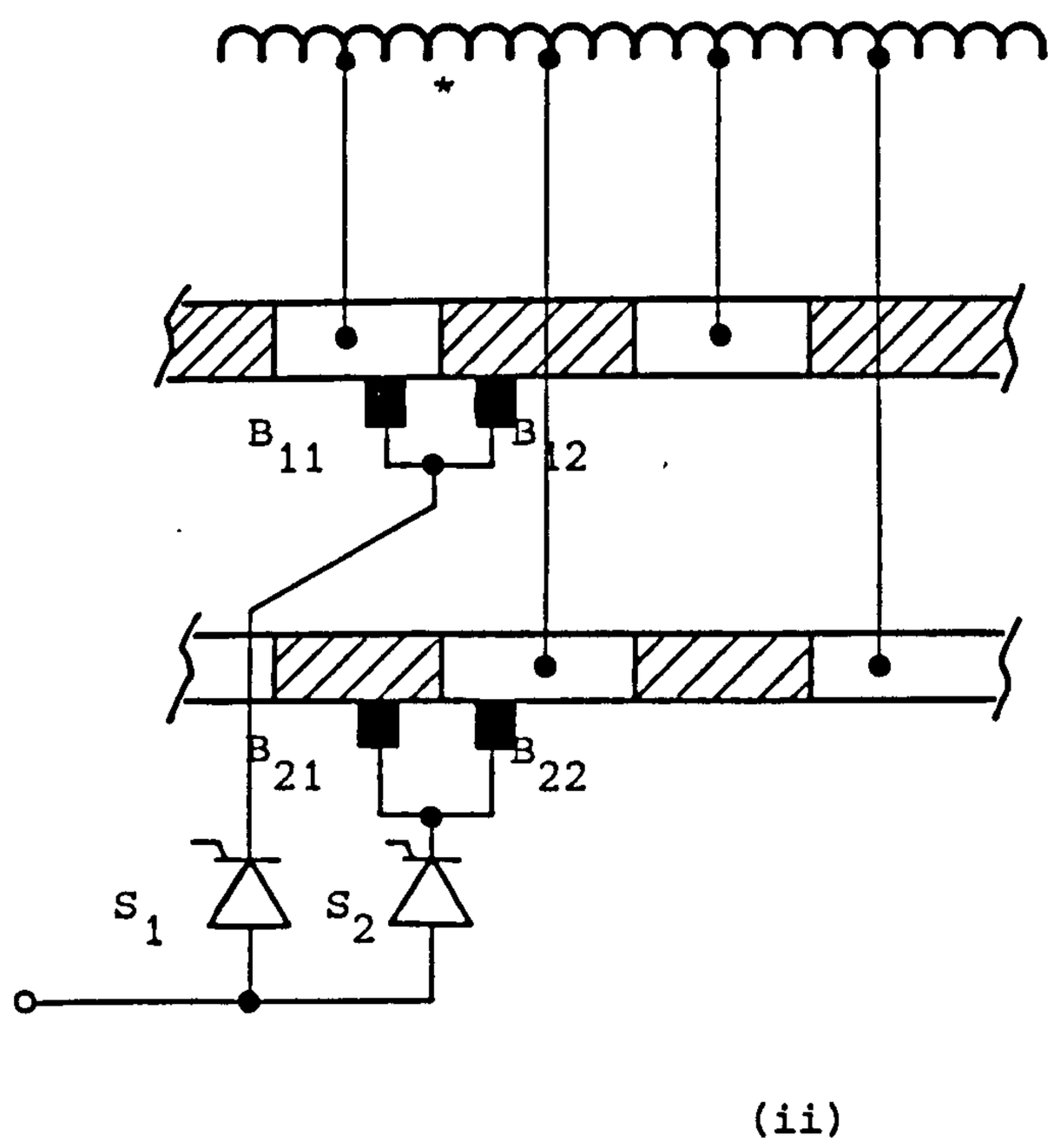

(ii)

Fig. 2.8 Assisted commutation using thyristors

segment must be greater than (3/2)f seconds.

One condition in the design of the armature which was not mentioned so far, is that it must have a small number of tappings, therefore a small number of segments on the commutator. This is to make sure that a brush is always on a segment before it has to carry current. An immediate consequence of this may be that the torque pulsation can be greater than the conventional many - segment commutator machine. However, Bates states that with 8 armature tappings per pole pair, torque pulsations are not substantially large to be a problem in many applications.

Proposals for the diode and thyristor assisted "sliding contact" commutation still depend upon successful sliding-contact current collection even though the switching problems of the contact have been eliminated. Sliding contacts of carbon brushes on metal surfaces have always been a weak feature in electrical machines.

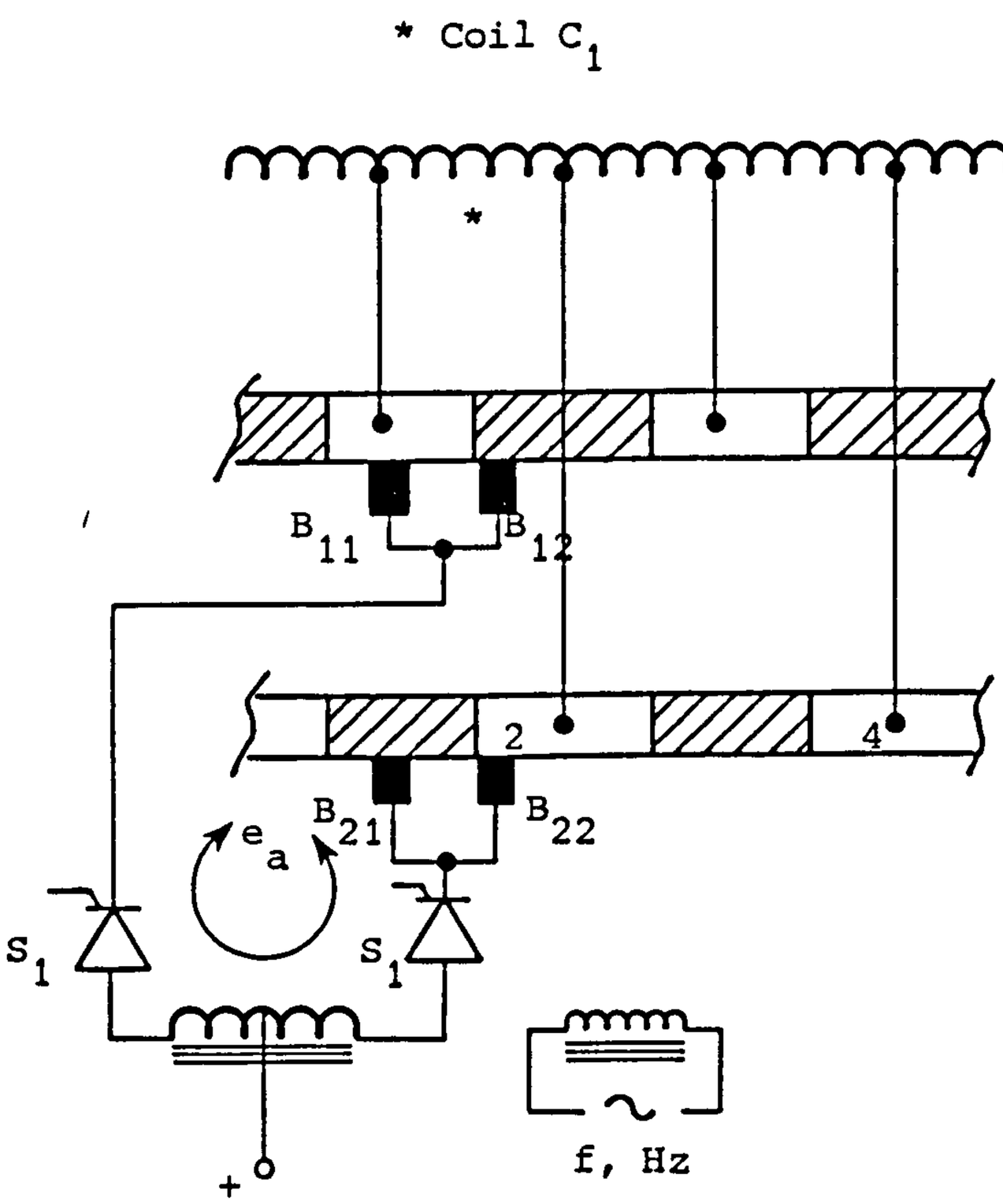

Fig. 2.9 Commutation by external AC injection

CHAPTER THREE

MACHINE WINDING STRUCTURE AND RATING CALCULATION

CHAPTER THREE

MACHINE WINDING STRUCTURE AND RATING CALCULATION

3.1 INTRODUCTION

This chapter gives a detailed description/analysis of the machine winding layout and rating evaluation on both sides of the airgap. It must be stated at the outset that a Mawdsley's Generalised Machine was used to carry out this work. The reasons for this choice were :

(i) The ready availability of such a machine for the research work.

(ii) The stator winding of this machine was ideal for this project because, as will be explained later, all the coil terminals are available outside the machine for interconnection in a satisfactory configuration.

(iii) The generalised machine is directly coupled to another DC machine (called DC Work Machine); the combination is necessary for experimentation in the motoring/generating mode.

(iv) The shaft encoder necessary for shaft position feedback was relatively easy to mount and adjust.

However, the original rotor available for this machine did not offer sufficient flexibility for interconnection as the main field winding, nor was there a provision for using interpoles, in case this latter is needed. The University of Bradford did, however,

agree to purchase a special rotor with both of these two facilities available plus the possibility of changing the ratio of the number of turns allocated to the main field winding to that available for an interpole winding. Full details of this will be explained in this chapter, together with the rating calculation of the machine.

At the outset, it will be necessary to explain two formats which will be used throughout this thesis :

(i) "ORIGINAL" format refers to the original status of the Mawdsley's Generalised Machine operated as a DC separately-excited or shunt machine according to the data supplied from Mawdsley's.

(ii) "INVERTED" format refers to the machine with the stator winding used as the armature winding and the rotor conductors constituting the main field/interpole winding.

3.2 GENERAL MACHINE LAYOUT

The Mawdsley's Generalised Machine used for experimentation consists of the generalised machine itself coupled directly to a DC work machine. The schematic diagram of Fig. 3.1(i) gives an impression of the general layout of the set.

The stator of the generalised machine has a conventional 4-pole winding set in 48 slots. The "start" and "finish" of all 48 coils are brought out to 96 terminals symmetrically arranged in four concentric circles on the main terminal panel of the machine.

Fig 3.1(ii) shows the layout of the stator coil terminals.

To illustrate the physical relationship between the position of a coil side and the arrangement of the terminals, Fig. 3.2(i) typically shows the physical position of coil $C_{1,13}$ {marked with a "star" in Fig. 3.1(ii)}.

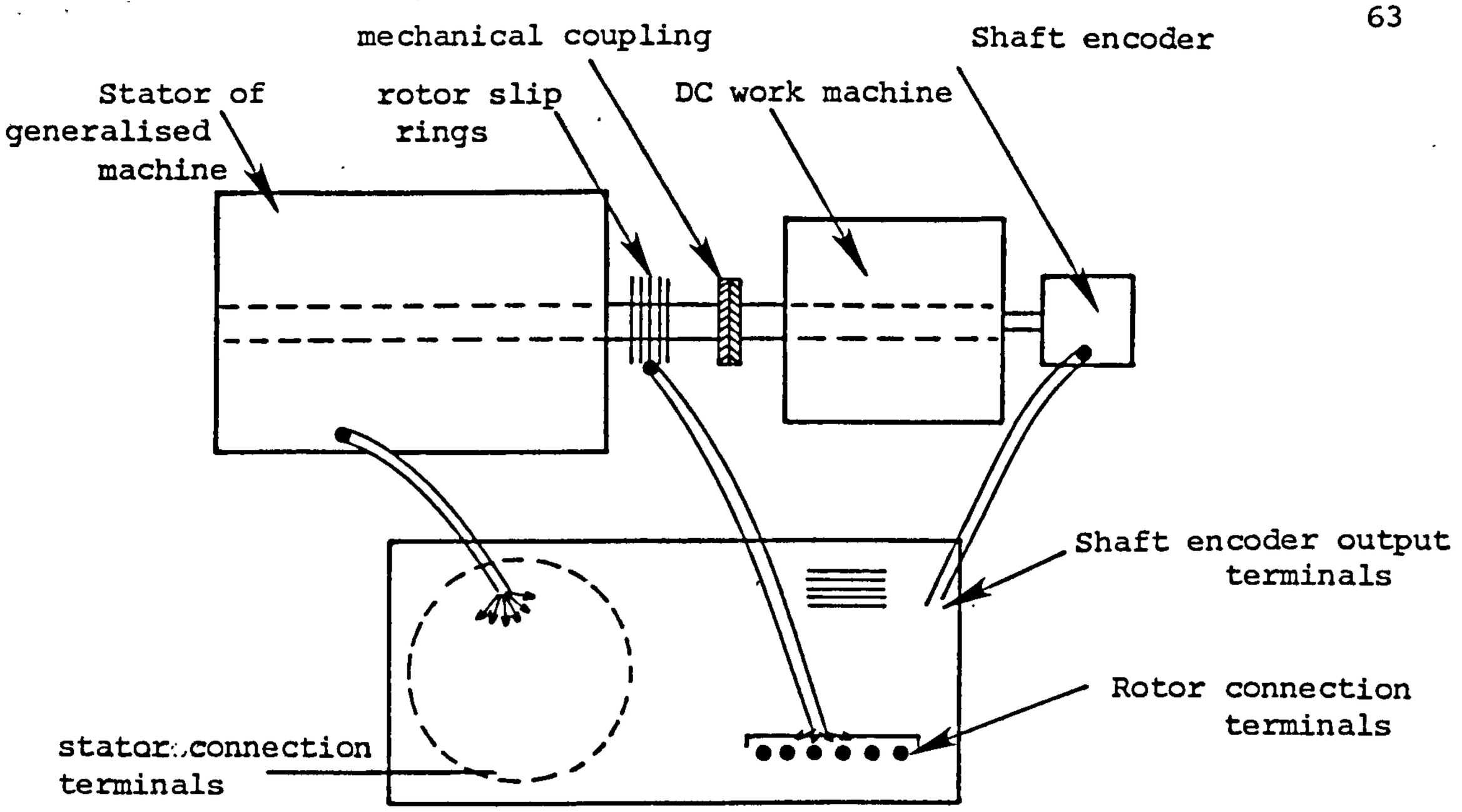

(i) Schematic diagram of the experimental set

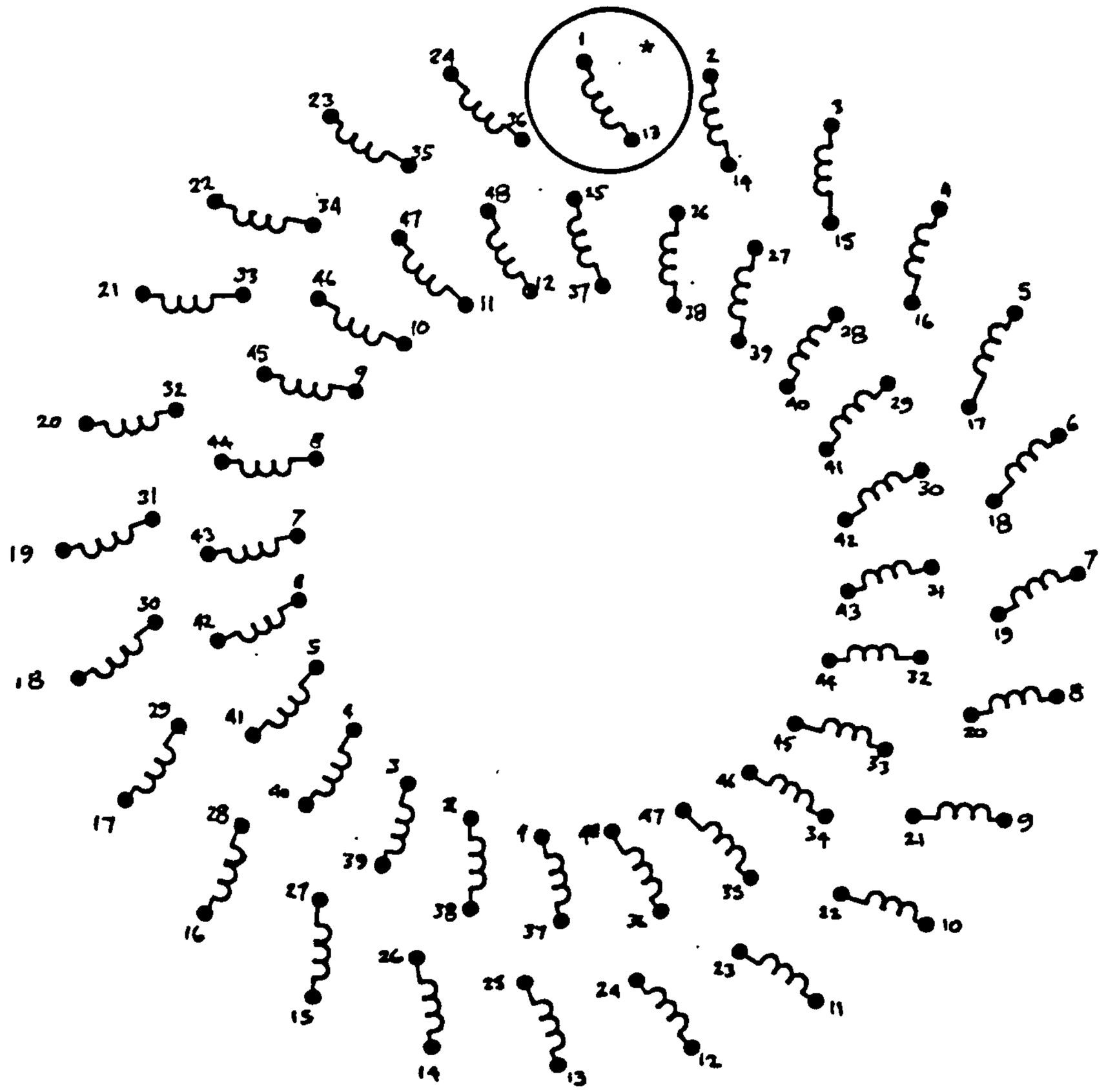

(ii) Arrangement of stator coil terminals

* a full pitch coil

Fig. 3.1 Layout of the Generalised Machine

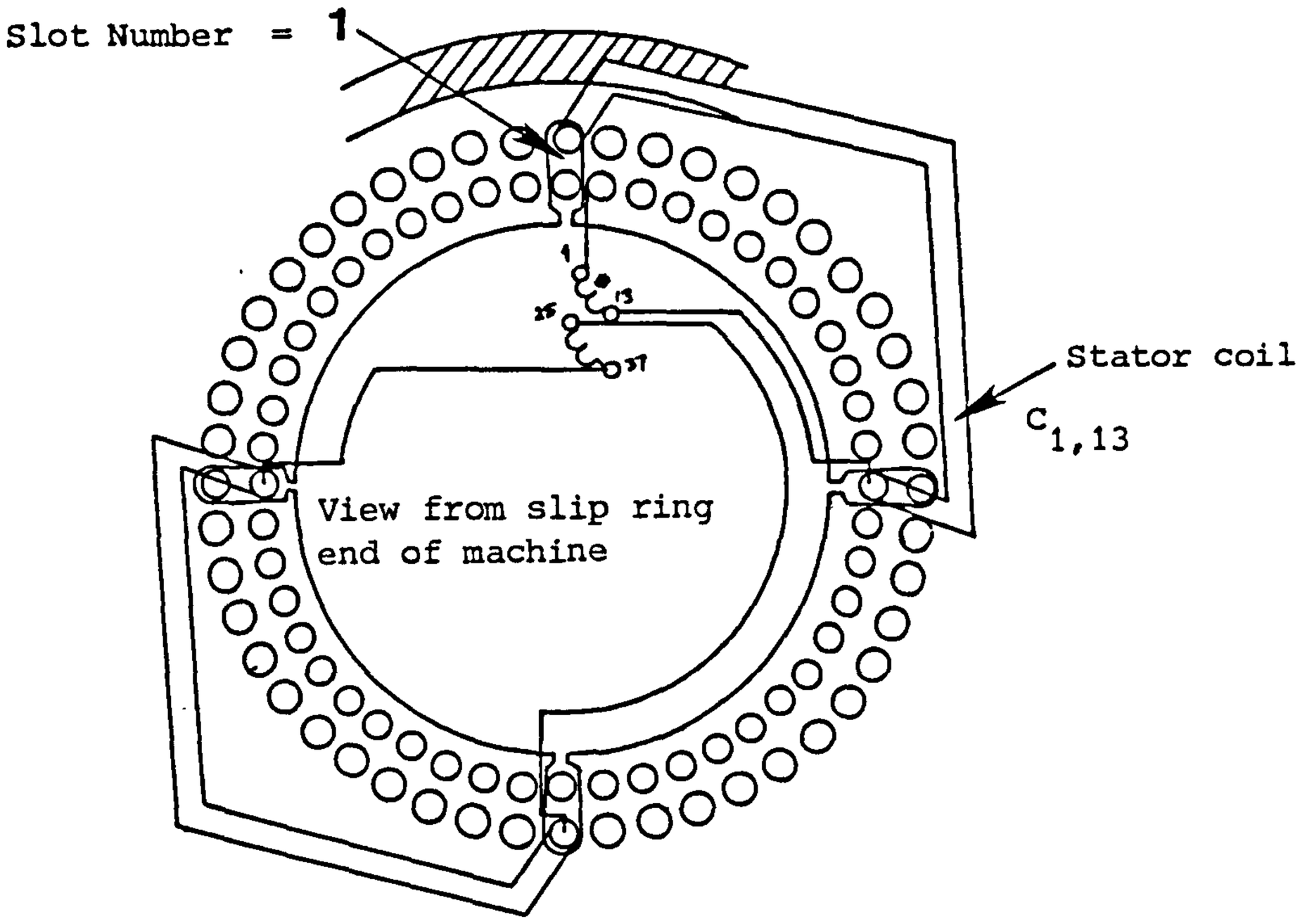

i) Position of an armature coil

Details of stator slot

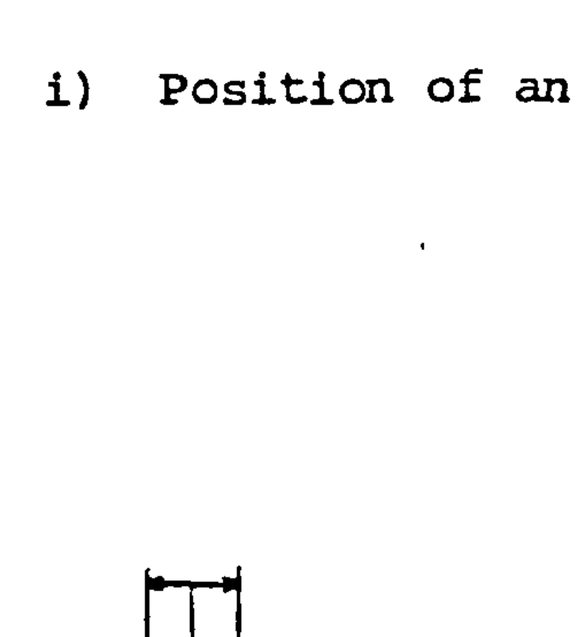

Details of rotor slot

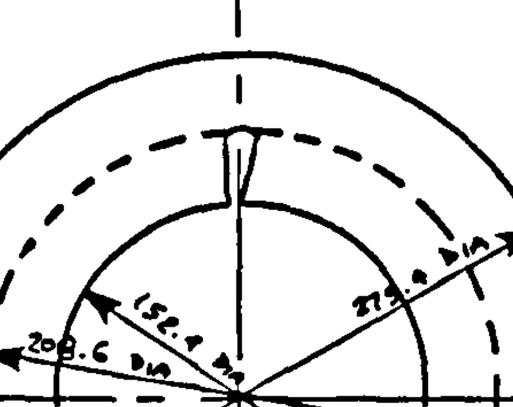

Rotor stamping

(ii) Rotor and stator stampings dimensions (in mm)

Fig. 3.2 Details of the Generalized Machine

Single-conductor search wires are also available, situated near the tops of stator slots 1, 7, 9, 12, 13. This is useful for observing the radial field distribution due to the main field, armature or interpole winding excitation. With this arrangement, it is possible to form search coils of various pitches; a full-pitch search coil will be 1 - 13 .

Some rotor and stator stamping dimensions are given in Fig. 3.2(1), see also Appendix C; this data is used in rating calculations later in this chapter.

The machine's "original" format will be briefly described and then the "inverted" interconnection layout will be shown in detailed form.

3.3 MACHINE ORIGINAL FORMAT

The original format of the generalised machine according to Mawdsley's data [37] is that it is operated as a conventional 4-pole DC machine with the stator used as the main field winding and the rotor used as the armature winding. The machine can be operated using either separate or shunt excitation with or without interpoles; all these modes can be achieved by suitable connection of the stator coils. The field and armature details are as follows:

3.3.1 MAIN FIELD WINDING

The main field winding of the machine is located on the stator. The interconnection diagram is shown in Fig. 3.3, for the case of a 4-pole with 8 coils per pole; with the possibility of connecting the remaining ones for the interpole winding.

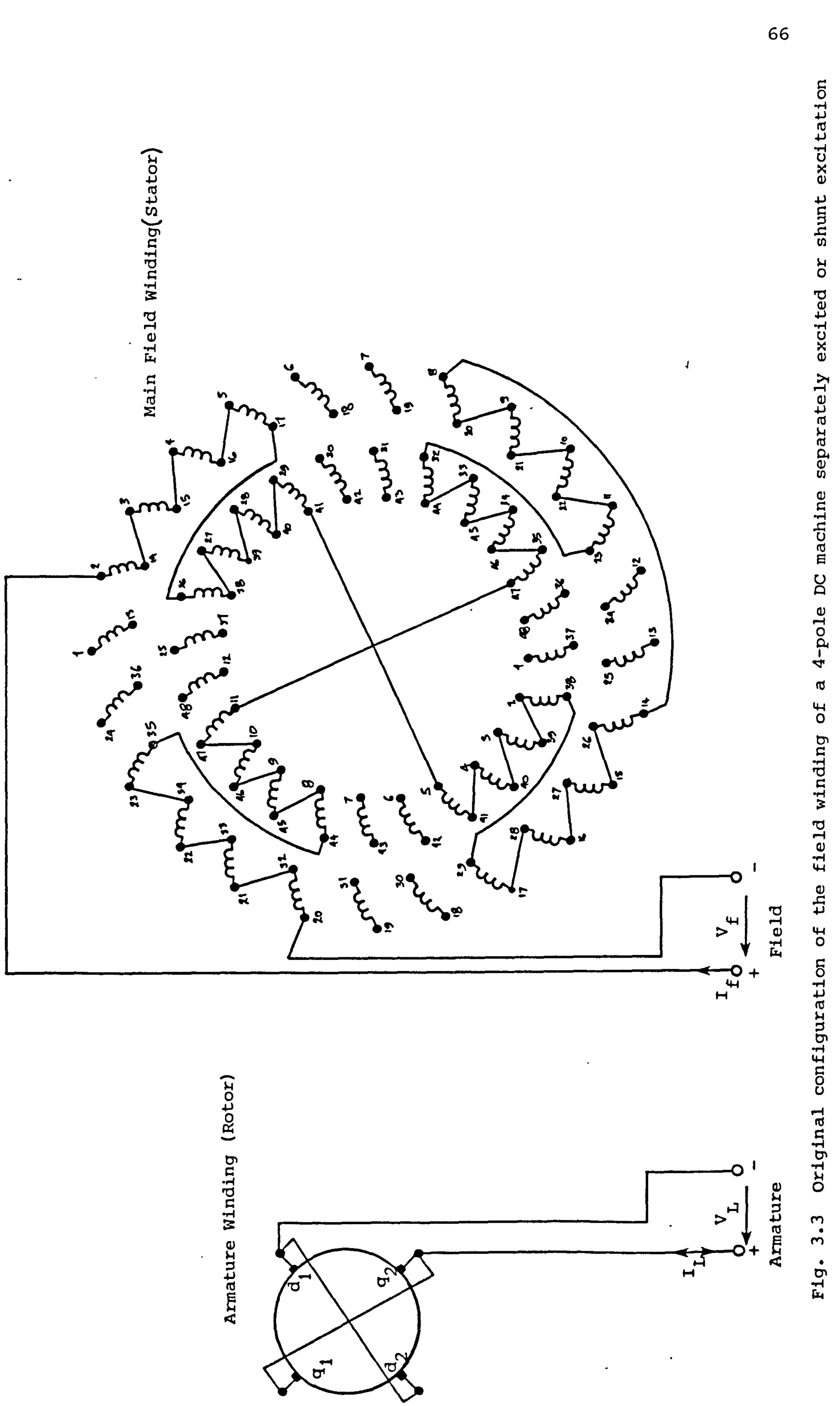

Fig. 3.3 Original configuration of the field winding of a 4-pole DC machine separately excited or shunt excitation

3.3.2 ARMATURE WINDING

This is incorporated in the rotor of the machine and has a 4-pole "lap" winding set in 36 slots. The developed layout of the winding is shown in Fig. 3.4; the interconnected armature winding has a commutator with 144 segments.

3.4 MACHINE INVERTED FORMAT

In the inverted format of the machine, the stator is used as armature winding and the rotor as main field/interpole winding :

3.4.1 MAIN FIELD/INTERPOLE WINDING

The original rotor of the Mawdsley's Generalised Machine was not suitable to be used as the main field winding because of the coil interconnecting in lap, accessed via the commutator. To facilitate maximum flexibility in the operation, a rotor with a special distributed winding was built to provide an interpole capability with the provision for changing the number of rotor coils allocated to main field/interpole winding. The new rotor has the same number of slots as the original rotor (36 slots) with 36 coils, full-pitched as a 4-pole, thus giving a total of 9 coils per pole. These 9 coils are further subdivided into groups of 5,2,1,1 coils as shown in Table 3.1 and with the provision of "rotor connection selector" a various proportion of coils can be allocated to main field : interpole winding.

From Table 3.1 it can be seen that the allocation can be changed in the ratios 5:2 , 7:2 , 6:3 and 5:4 .

Fig. 3.5 shows the physical interconnection of rotor coils for

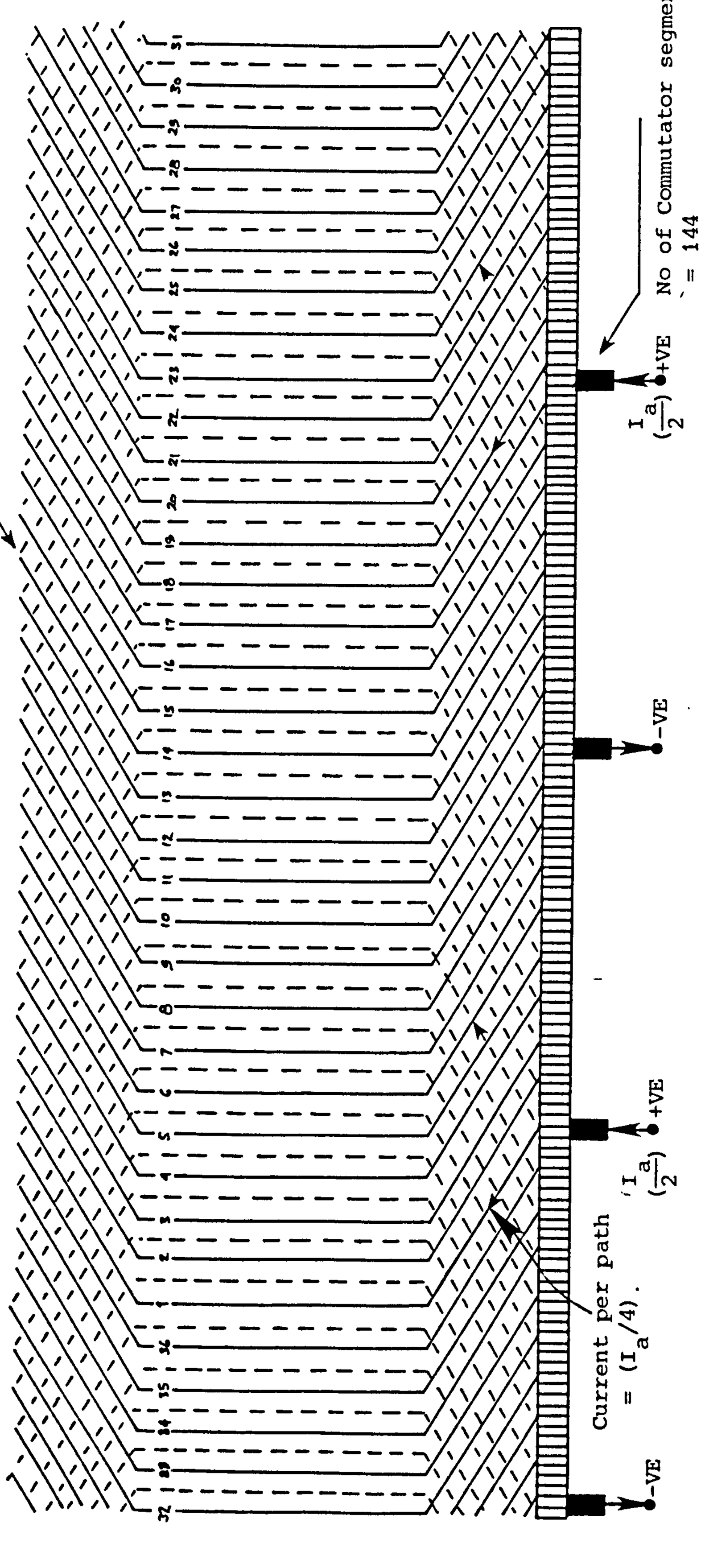

Fig. 3.4 Original Armature Winding of Mawdsley Machine - 4 pole lap

the case of 7 coils per pole used for the main field winding and 2 coils per pole for the interpole winding.

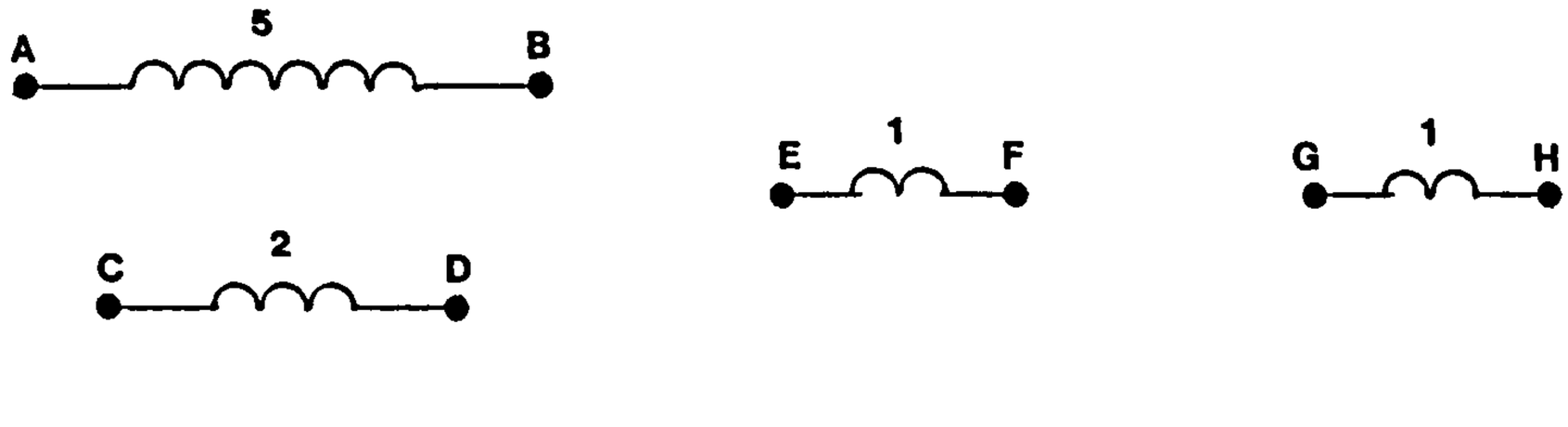

COILS/POLE		LINK		TERMINAL CONNECTIONS	
Main	I.P.			Main	I.P.
5	2	- - -	- - -	A & B	C & D
7	2	B & E	F & H	A & G	C & D
6	3	B & E	D & G	A & F	C & H
5	4	D & E	F & G	A & B	C & H

TABLE 3.1

3.4.2 ARMATURE WINDING

The armature winding for the inverted machine is located on the stator and, since all the stator coil terminals are conveniently available on the machine panel, it is necessary to provide a suitable interconnection of these coils to form the armature winding. The winding may be connected in either "Lap" or "Wave" configuration, whichever is most appropriate, as is conventional for normal DC machines.

There are certain winding rules [30] which must be satisfied

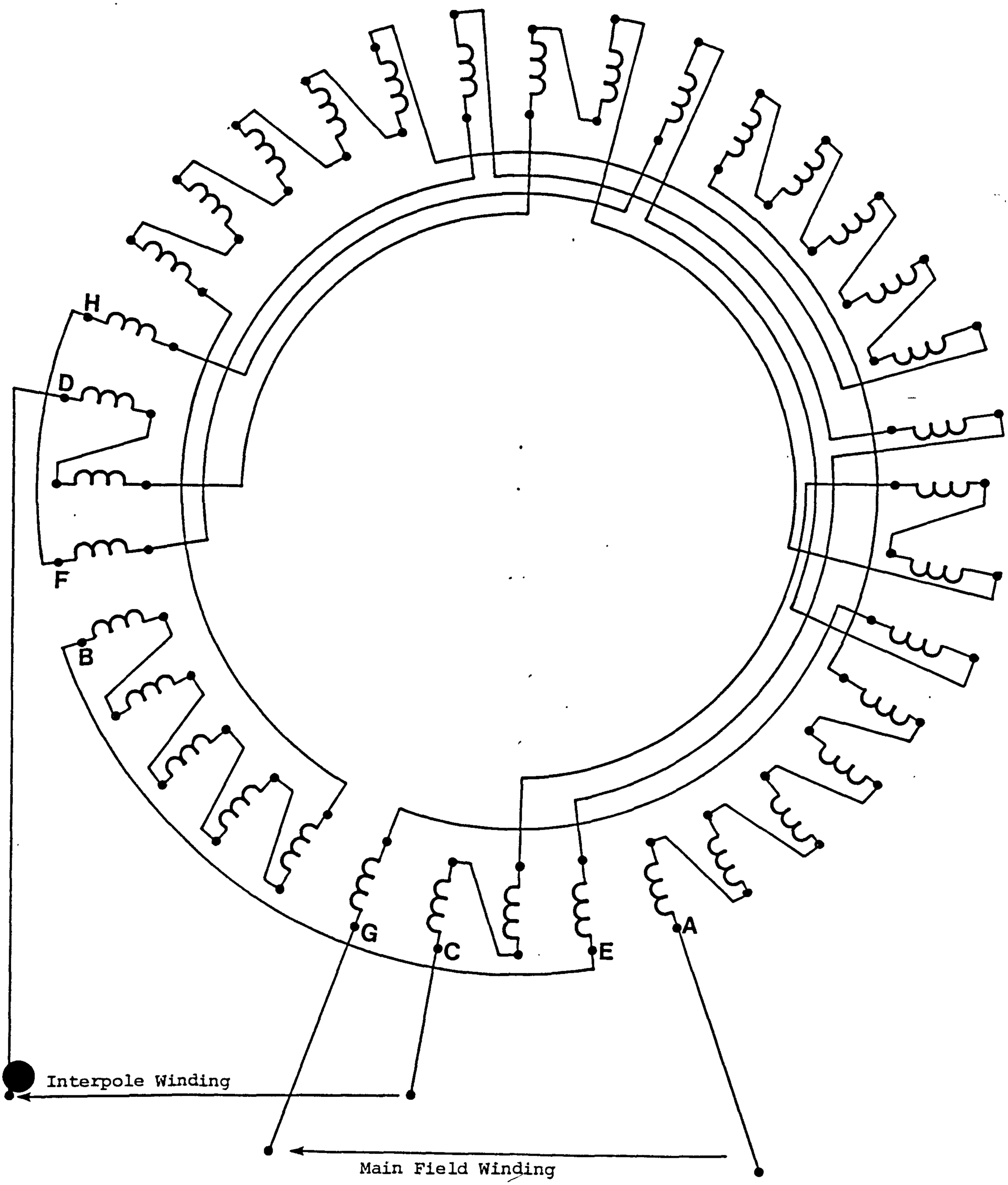

Fig. 3.5 Field and interpole winding of the inverted machine

before a decision is made as to which connection should be adopted

For this machine :

The number of coil sides per slot "m" = 2,

The machine is uniformly slotted with a total number

of slots "s" = 48

For the interconnection in Lap configuration, the number of coils or commutator segments (C) is not restricted except that it must conform to the number of slots (s) and the number of coil sides per slot (m) in accordance with the formula :

$$C = (m \times s)/2 \qquad (3.1)$$

This condition is satisfied in this case,

hence C = 48

Therefore Lap interconnection is possible.

Other winding rules also applies, viz :

commutator pitch (y_c) = 1

resultant pitch in coil sides (y_r) = $y_b - y_f$ (3.2)

where y_b = coil span (back pitch) in coil sides ,

y_f = front pitch in coil sides.

Therefore equation (3.2) gives :

$$y_r = y_b - y_f = 2$$

Hence the condition :

$$y_r = 2\ (y_c) \qquad (3.3)$$

is also satisfied.

On the other hand, the winding rules for interconnection in Wave configuration [30] are not supportable, hence it is possible to interconnect the stator (armature) winding only in Lap system.

The interconnected layout of the armature winding is shown in

Fig. 3.6, which is in accordance with the conditions specified by equations 3.1, 3.2 and 3.3. This interconnection refers to 4-pole with 48 commutator segments.

In conventional armature windings of DC machines, "equalisers" are used to balance the potential at points whose e.m.f's, at every instant should be the same (for example, at points x & x`, Fig. 3.6). Difference in potential occurs due to magnetic asymmetry, due for example to an eccentric shaft. A connection of this kind cannot be made in this case, because the armature coils are already imbedded in the stator.

Instead, paralleling connections were used; these connections are placed on similar coils which are a double pole pitch apart. Upon assessing the effect of this, it can be seen that it is two-fold :

i) Firstly, the e.m.f.s will be equalised at those points which are a double pole pitch apart.

ii) Secondly, the number of armature switching devices necessary will be halved for the 4-pole configuration.

Fig. 3.6 shows the complete interconnected armature winding; an example of a paralleling connection is also shown; coil $C_{1,13}$ to $C_{25,37}$.

Electronic commutation is used to replace the conventional mechanical switching system. This involves the replacement of each brush/commutator "switch" by a pair of solid state switching devices. Gate turn-off thyristors (G.T.Os) were selected as the armature switches because of the reasons briefly mentioned in chapter 1, and to be more fully discussed in chapter 4.

An alternative diagram showing the interconnected armature

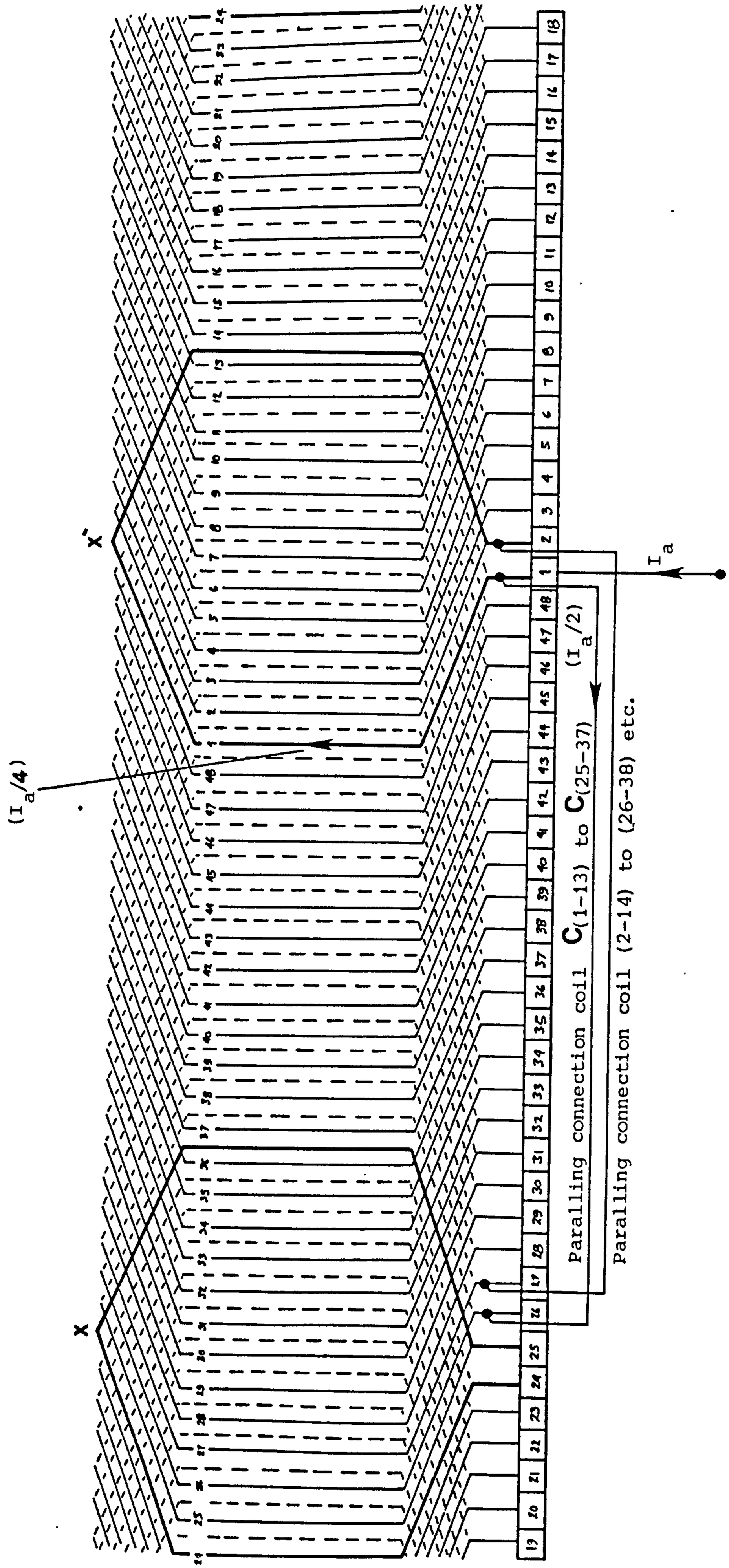

Fig. 3.6 Interconnection layout of the inverted format of the armature winding

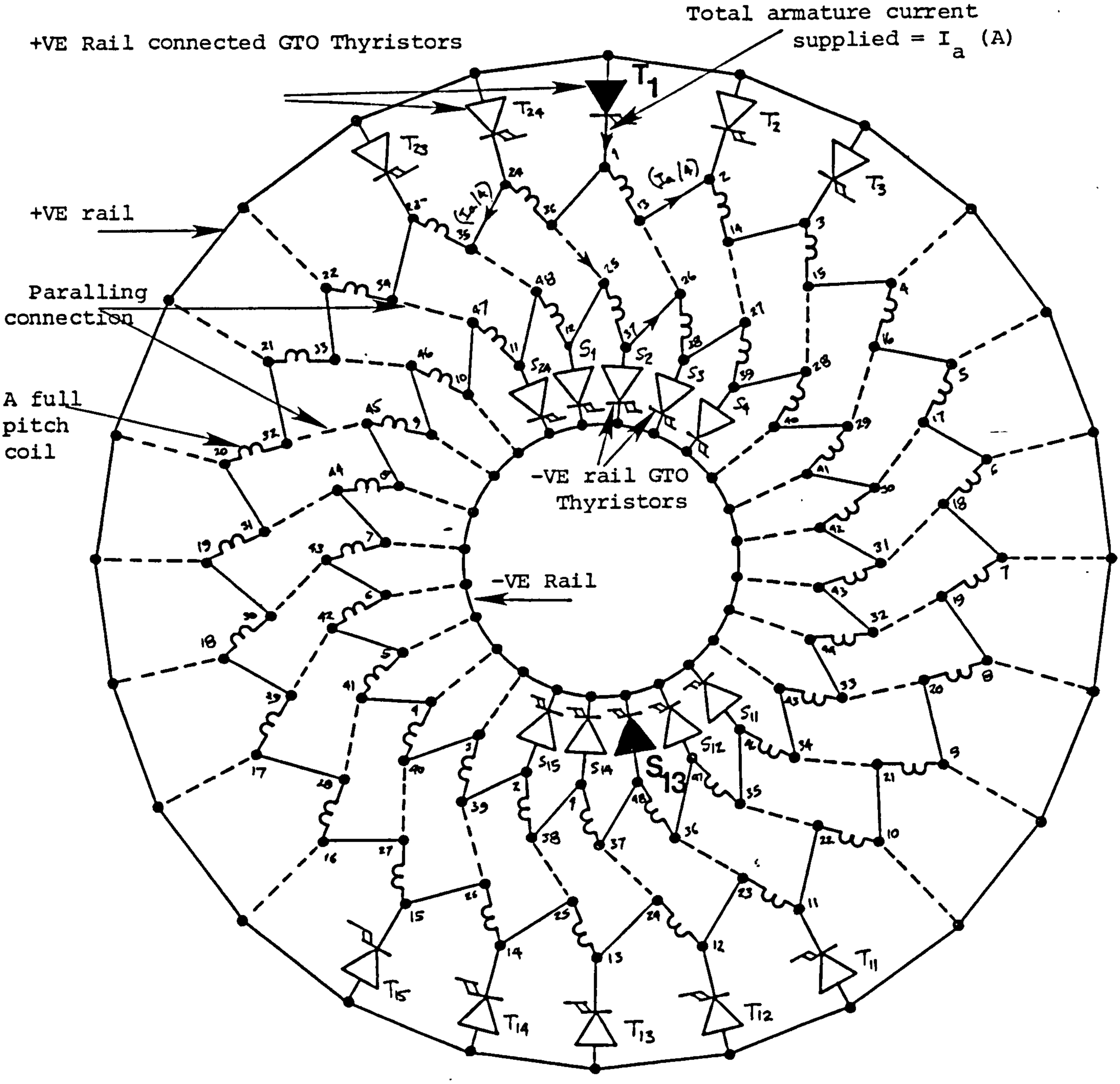

Fig. 3.7 Lap interconnected GTO thyristorized armature winding

winding with the GTO thyristor armature switches is shown in Fig. 3.7. This diagram shows typically, the position of a positive rail connected GTO (T_1) and its output counterpart (S_{13}); 180° (electrical) phase difference. The switching duty requirements of the devices will be considered in section 3.7.

For the purpose of this thesis, positive rail connected GTOs will be referred to as the "input" devices and "output" for their negative rail counterparts.

3.5 ANALYSIS AND CALCULATION OF MACHINE "ORIGINAL" & "INVERTED" RATINGS

The basic configurations of the machine original and inverted format have been explained. The electric loading on both sides of the airgap can be determined for the original format of the machine.

The requirement in the inverted format of the machine is to determine current values for both the stator (armature winding) and rotor (field winding) which will provide similar values of electric loading as given by the original Mawdsley's machine.

The following analysis details the method of estimation of the value of electric loading appropriate to both the field and armature windings for both the "original" and the "inverted" formats of the machine.

3.5.1 ELECTRIC LOADING FOR THE ORIGINAL FORMAT

3.5.1.1 Armature winding

The basic layout of the armature winding is shown in section 3.3. The coils are interconnected in Lap configuration connected to a commutator/brush gear assembly.

From Mawdsley's specification :

Total number of rotor slots = 36

The armature winding is connected as 4-pole, giving 9 slots per pole.

Each slot accommodates two coil sides, each coil having 8 conductors.

Therefore, total number of conductors per slot = 16

Total number of conductors per pole = 9 x 16 = 144

Referring to Fig. 3.4, if the total armature current supplied is I_a(A) ; this gives current per brush of $(I_a/2)$. Further, the current then distributes into two equal paths (for each brush).

Hence current per path = $I_a/4$ (3.4)

(This is current per path for a 4-pole configuration).

Since the armature winding is uniformly distributed over a number of slots, the radial "Hn" distribution over the airgap approximates to a triangular waveform with the peaks occurring at the q-axis position.

peak armature m.m.f. = $Fa_1 = (I_a/4) \times N_a$

$$Fa_1 = (I_a/4) \times 144$$

$$= 36\ I_a \quad \text{At/pole} \qquad (3.5)$$

The assembly of currents in the armature conductors gives axial current-sheet patterns of linear density Aa_1- called the specific

electric loading. These current sheets are uniform in this case where the rotor is cylindrical and given in A/m of periphery.

The value of the specific electric loading for the (rotor) armature winding :

Aa_l = m.m.f. per pole/length of a pole face

= $36\ I_a/(\frac{1}{4} \times \pi \times Da)$ (Da = diameter of the armature)

= $36\ I_a/(\frac{1}{4} \times \pi \times 151.4 \times 10^{-3}) = 302.8\ I_a$ A/m

Armature current at full load is $I_a = 22$ A

Hence the armature loading corresponding to full load condition

$$Aa_l = 302.8 \times 22 = 6660 \text{ A/m} \qquad (3.6)$$

3.5.1.2 Field winding

The basic configuration of the field winding is also described in section 3.3. Fig. 3.3 shows the field winding with 8 coils per pole; the winding interconnected in 4-pole arrangement. According to Mawdsley's data [37], the machine may be operated with a field current of around 2 A . .

Each coil has a total number of 31 turns

There are 2 coil-sides per coil.

Total number of conductors per coil = 2 x 31 = 62

Total number of conductors per pole = 8 x 62 = 496

Since the coils of the main field winding are connected in series (Fig. 3.3), the current in each conductor is equal to I_f=2 A

The radial field distribution in this case approximates to a trapezoidal space waveform. The peak field m.m.f. can be calculated as follows :

F_{f_l} = I_f x N_f (where N_f = total number of conductors per pole)

F_{f_l} = 2 x 496 = 992 At/pole (3.7)

Therefore, the electric loading corresponding to the current excitation to the field winding :

$$A_{f_1} = 992/(\tfrac{1}{4} \times \pi \times 152.4 \times 10^{-3}) = 8288 \quad A/m \qquad (3.8)$$

This compares with the value of electric loading calculated for the armature winding at full load, ($Aa_1 = 6660$ A/m given in equation 3.6).

3.5.2 ELECTRIC LOADING FOR THE INVERTED FORMAT

3.5.2.1 Stator armature winding

With the inverted formation of the machine, the stator is used as the armature winding. Fig. 3.7 shows the complete interconnected winding with the GTO thyristors replacing the commutator/brushes. To calculate the armature m.m.f. in this format:

The stator has a total of 48 slots connected as 4-pole :

Number of slots per pole = 12 slots

Each slot accommodates two coil sides placed axially in the slot, each having 31 turns.

Total number of conductors per slot = 62

Total number of conductors per pole = 12 x 62 = 744

The distribution of the total current supplied is shown in Fig. 3.7. The armature current per path (from equation 3.4)

$$= I_a/4 \quad A$$

The uniform distribution of armature conductors will set up a radial field distribution of triangular shape. The peak armature m.m.f. per pole in this case is given by :

$$Fa_2 = (I_a/4) \times N_a = (I_a/4) \times 744 = 186\ I_a \quad At/pole \qquad (3.9)$$

The specific electric loading for the armature winding in the

stator of the machine (A/m of periphery):

$$Aa_2 = 186\ I_a/(\tfrac{1}{4}\times\pi\times152.4\times10^{-3}) = 1554\ I_a\ A/m \qquad (3.10)$$

If the armature specific electric loading in this case (Aa_2 - equation 3.10)is required to be the same as that calculated for the original machine armature winding (Aa_1 - equation 3.6):

$$Aa_2 = Aa_1 = (1554\ I_a) = 6660;\ I_a = 4.3\ A$$

i.e the full load armature current for the case of the inverted format of the machine = 4.3 A

3.5.2.2 The field winding

The main field winding of the inverted machine was described in section 3.4.1. This is located on the rotor, with the following specification :

Total number of coils (rotor) = 36 coils

Since the winding is interconnected as 4-pole, this gives a total number of 9 coils per pole. The main field winding can be interconnected with a maximum of 7 coils per pole. The remaining two coils out of nine, can be utilised for the interpole winding. This is the interconnection adopted and is shown in Fig. 3.5.

Each coil has 13 turns, total number of conductors per pole for the main field winding

$$= (\ 2\ x\ 13\ )x(\ 7\ ) = 182 \text{ conductors}$$

The radial field distribution for excitation of current to this winding has a trapezoidal space distribution.

The peak m.m.f. of the main field :

$$F_{f_2} = I_f x\ N_f = (I_f)\ x\ (182) = 182\ I_f \quad At/pole \qquad (3.11)$$

The electric loading for this winding:

$$A_{f_2} = 182\ I_f/(\tfrac{1}{4}\times\pi\times151.4\times10^{-3}) = 1530\ I_f \quad A/m \qquad (3.12)$$

If the electric loading calculated in this case (A_{f_2}- equation 3.12) is required to be the same as that given by the original field winding of the machine (A_{f_1}- equation 3.8)

$$A_{f_2} = 8288 = 1530\ I_f \quad A/m$$

$$I_f = 8288/1530 = 5.4\ A$$

i.e. Field current needed for the inverted machine at full-load = 5.4 A.

3.6 CALCULATION OF RADIAL AIRGAP FIELD DISTRIBUTION

The radial airgap field distribution due to current excitation to either stator (armature) or rotor (field) windings of the machine can be monitored using a single-turn search coil. The search conductors are placed axially in the slots and hence at right angles to both the radial flux crossing the airgap and the direction of motion of this flux with respect to the conductors.

The theoretical radial (normal) field distribution can be calculated by the application of Ampere's law [4] which states that the line integral of magnetic field intensity $\bar{H}$ over any closed circuit is equal to the current enclosed :

$$\oint \bar{H} \cdot d\bar{l} = \bar{I} \qquad (3.13)$$

The radial field intensity is calculated on applying Ampere's law to an elementary closed loop which involves two traverses of the uniform airgap of length "g":

The peak value of the radial magnetic field intensity in the airgap, Hn (max) is given by:

$$Hn\ (max) = (n \times I)/(2 \times g) \qquad (3.14)$$

Where n = total number of turns of the winding

and I = current excitation to the winding

The rotational e.m.f. induced in a single turn full pitch search wire is recorded using an oscilloscope and compared with the distribution deduced theoretically. The e.m.f. induced between the ends of a search coil is given by:

$$e = 2 (Bn\ l\ v) \qquad (3.15)$$

This is equation 2.9 given in chapter 2; where Bn = radial flux density, l = axial length of the search conductor (101.6 mm), v = rotor peripheral speed (in m/sec)

The aim of the following analysis is to obtain the distribution of the radial flux density, hence the distribution of Hn, experimentally and, compare this with the distribution obtained theoretically using equation 3.13 and 3.14.

3.6.1 MAIN FIELD WINDING Hn_f

With the main field winding connected with a total of 7 coils per pole and excited with a constant current of 2.0 A, the radial field approximates to a trapezoidal distribution as shown in Fig. 3.8. The field winding is distributed over a number of slots in this case. The "stepped" nature of the theoretical radial field distribution is derived based on the following assumptions :

(i) The number of slots per pole is small, making the steps prominent.

(ii) All conductors in one slot i.e. top and bottom coil sides are so concentrated in that slot that are represented by a single conductor whose m.m.f. is equivalent to the total m.m.f. given by all the conductors in that slot.

These two assumptions will also be the basis for derivation of the theoretical radial field distributions of the armature and interpole winding.

The rotor was run at a constant speed of 300 r.p.m.

Peripheral speed = (π x D)(rpm/60) (3.16)

= (π x 151.4x10^{-3})(300/60) = 2.378 m/sec

The peak value of the radial magnetic intensity in the airgap for this current excitation to the field winding can be calculated using equation 3.14 :

$Hn_f(max)$= (7 x 13)(2)/(2 x 0.508x10^{-3})

(n = 7 coils per pole each having 13 turns)

(g = length of the airgap = 0.508 mm)

$Hn_f(max)$= 179134 A/m

This is the theoretical peak value of normal component of Hn_f

The observed oscillogram of the rotational e.m.f. is shown in Fig. 3.8; this depicts a peak value of voltage recorded of approximately 105 mV. The e.m.f. induced in the search coil is given by equation 3.15 :

e (max) = 105 x 10^{-3} = 2 {$Bn_f(max)$x 101.6x10^{-3}x 2.378}

$Bn_f(max)$ = 0.217 Wb/m^2

Using the relationship:

$Bn_f(max) = \mu o \times Hn_f(max)$ (equation 2.11 - Chapter 2)

0.217 = (4 π x 10^{-7}) x $Hn_f(max)$

$Hn_f(max)$ = 170000 A/m

This is the value of $Hn_f(max)$ obtained experimentally.

Fig. 3.8 depicts the theoretical radial field distribution in (i) and the experimental result in (ii) for current excitation to the main field winding. Examination of these two distributions, it

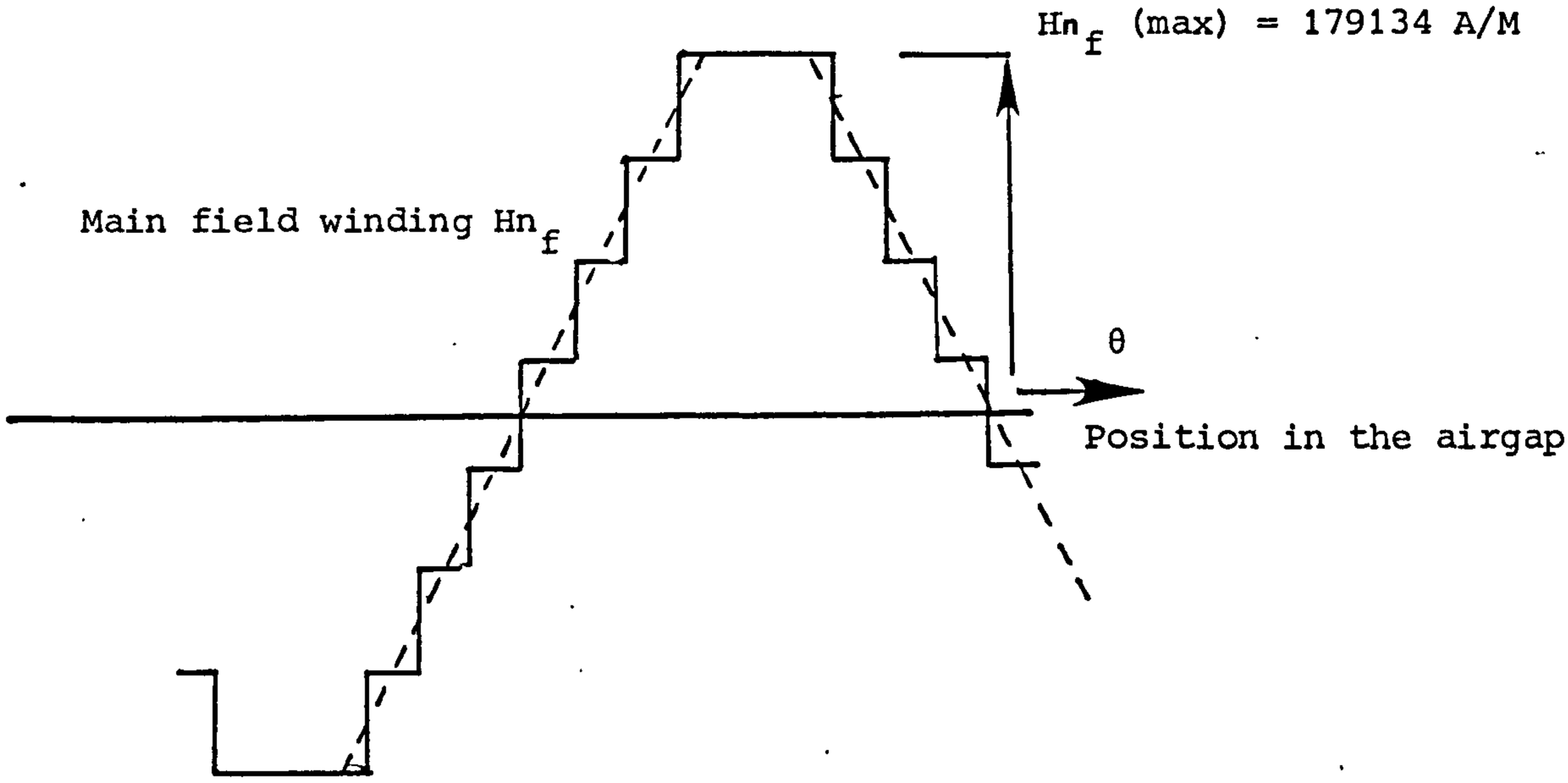

(i) Theoretical distribution

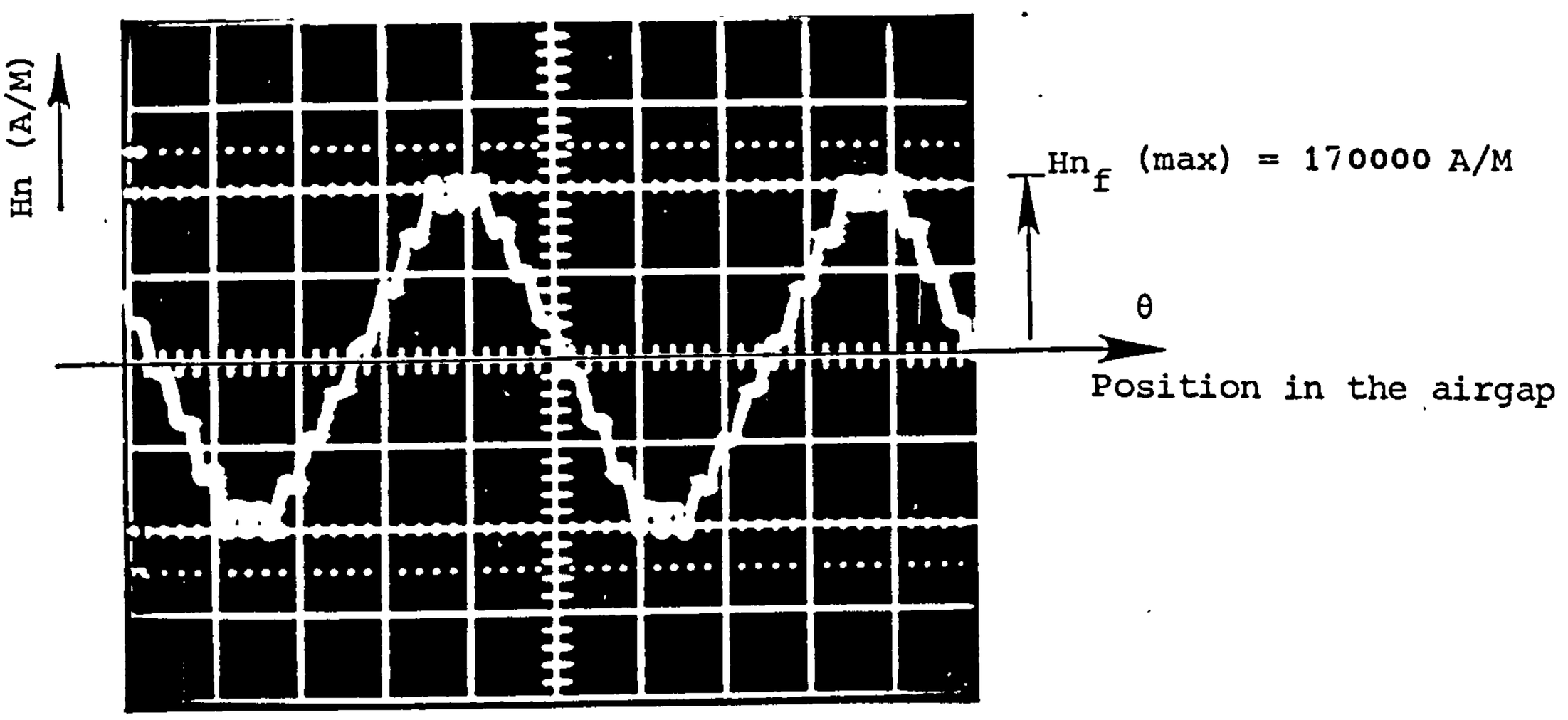

(ii) Experimental result

Fig. 3.8 Radial field distribution due to main field winding excitation

can be seen that the maximum value of the radial field obtained experimentally (170000A/m) is in close agreement with that obtained theoretically (179134 A/m). Comparison of these two results is shown at the end of this section (Table 3.2).

3.6.2 ARMATURE WINDING Hn_a

In a similar manner, the radial field distribution due to current excitation to the armature winding can be analysed. The armature winding in the stator of the machine has a uniform current distribution spread over the iron/airgap boundary. The machine has a uniform airgap, hence the current distribution generates a near-triangular radial field distribution with peaks occurring at the quadrature axis position.

The theoretical maximum value of the triangular waveform of the armature radial magnetic field intensity can be calculated using equation 3.14 :

$$Hn_a(max) = (12 \times 31)(I_a/4)/(2 \times 0.508\times10^{-3})$$

(n = 12 coils per pole each having 31 turns)

If the armature current is constant at 1.0 A

$$Hn_a(max) = 91535 \text{ A/m}$$

This is the theoretical peak value of armature radial field.

The rotational e.m.f. induced in the full-pitch search coil is given in Fig. 3.9 (ii). This is recorded for rotating the switching of the armature GTO's at a rate corresponding to 350 rpm.

Using eq. 3.16, $v = (\pi \times 151.4\times10^{-3})(350/60) = 2.78$ m/sec

The peak value of this recorded voltage is approximately 60 mV.

The e.m.f. induced in the single turn search coil whose sides are a pole-pitch apart is given by equation 3.15 :

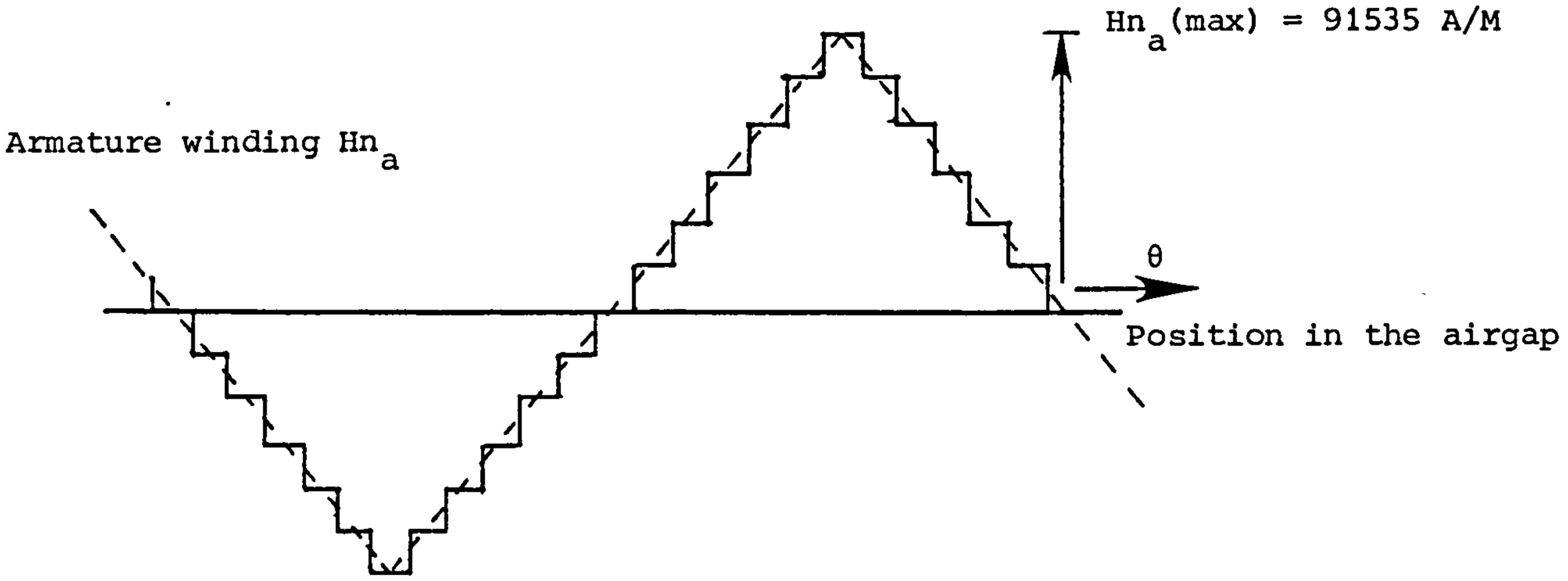

(i) Theoretical distribution

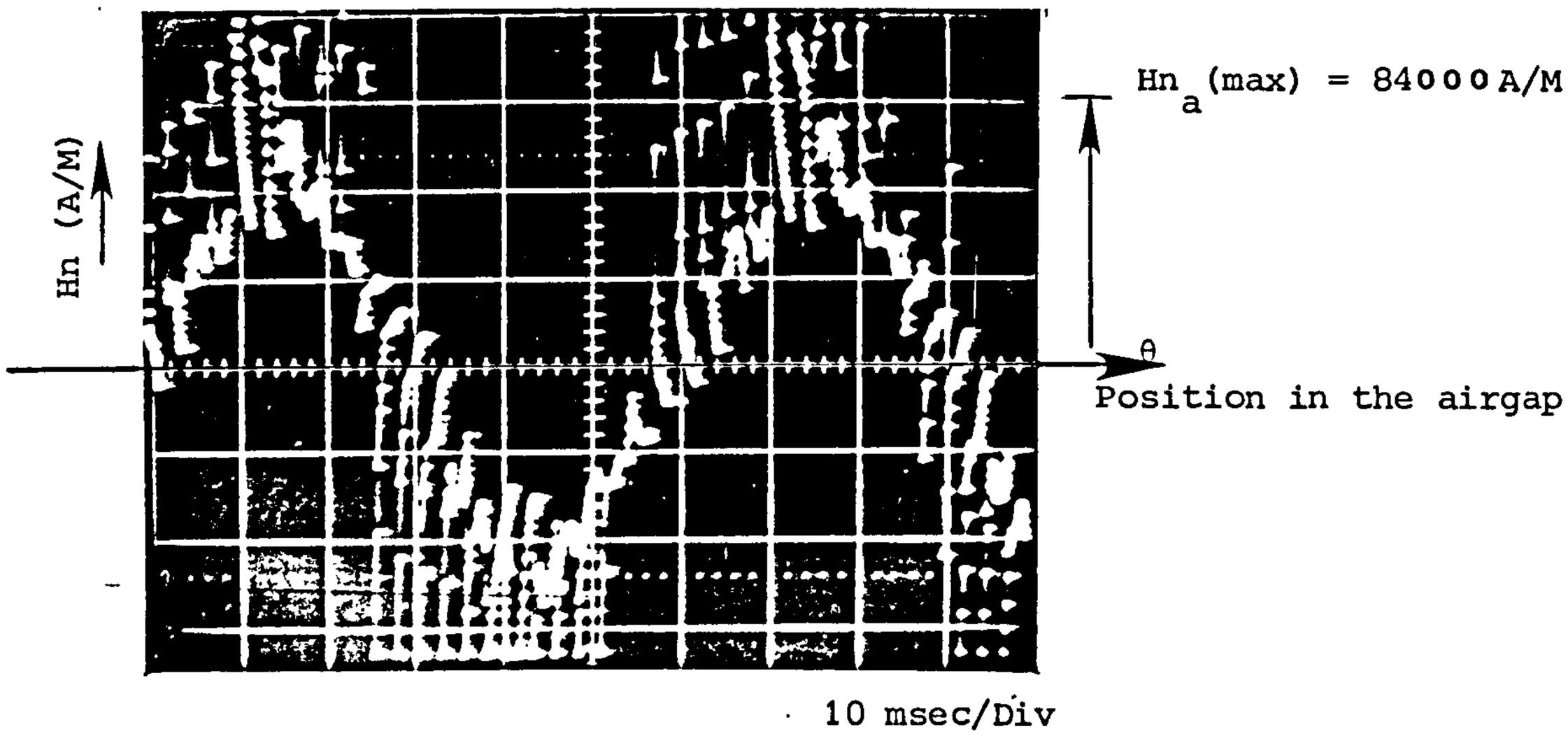

(ii) Experimental result

Fig. 3.9 Radial airgap field distribution due to armature winding excitation

$60 \times 10^{-3} = 2 \{ Bn_a(max) \times 101.6 \times 10^{-3} \times 2.78 \}$

$Bn_a(max) = 0.106 \quad Wb/m^2$

$Bn_a(max) = \mu o \times Hn_a(max)$

$0.106 = (4\pi \times 10^{-7}) \times Hn_a(max)$

$Hn_a(max) = 84000 \ A/m$

The radial field distribution for the armature winding obtained by monitoring the e.m.f. induced in a search coil confirms the triangular waveshape normally associated with armature windings of DC machines. The result obtained experimentally for the peak armature winding radial field (84000A/m) is in close agreement with the theoretical value (91535 A/m), see table 3.2 .

3.6.3 INTERPOLE WINDING Hn_{cp}

With the maximum possible 7 coils per pole used for the main field winding located on the rotor, the remaining two coils (per pole) can be utilised for the interpole winding - Fig. 3.5 shows this interconnection.

The anticipated "theoretical" radial field distribution and the oscillogram of the experimental result recorded for a constant current excitation of 1.5 A to the interpole winding, is shown in Fig. 3.10 . One immediate observation is that the interpole radial field is not confined to the commutation zone (quadrature axis) only, because of the distributed nature of the winding.

The theoretical maximum value of the radial magnetic field intensity of the interpole winding :

$$Hn_{cp}(max) = (2 \times 13)(1.5)/(2 \times 0.508 \times 10^{-3}) = 38386 \quad A/m$$

(n = 2 coils per pole, each having 13 turns)

The oscillogram of the e.m.f. recorded in the search coil (2

coil sides a pole pitch apart) shown in Fig. 3.10, gives a peak e.m.f. of approximately 20 mV

Rotor velocity "v" = 2.378 m/sec (n = 300 rpm)

Using the relationship of 3.15 :

$$20 \times 10^{-3} = 2 \{Bn_{cp}(max) \times 101.6 \times 10^{-3} \times 2.378\}$$

$$Bn_{cp}(max) = 0.0414 \quad Wb/m^2$$

The value of $Hn_{cp}(max)$ is then given by:

$$Bn_{cp}(max) = \mu o \times Hn_{cp}(max)$$

$$0.0414 = (4\pi \times 10^{-7}) \times Hn_{cp}(max)$$

$$Hn_{cp}(max) = 33000 \quad A/m$$

Comparison of the experimental value of the interpole winding radial field (33000A/m), with the theoretical value (38386 A/m) shows a slight discrepancy due to possibly the error incurred in the experimental recording of the e.m.f. induced in the search wire.

The radial field waveshape for the armature, main field and interpole winding are according to the anticipated distributions. The experimental result in each case is compared and found to be in close agreement with the theoretical values obtained by direct application of Ampere's law. Table 3.2 gives the discrepancy between the theoretical and experimental results.

WINDING	Hn (max) Radial field distribution (A/m)		Discrepancy (%)
	Theoretical	Experimental	
MAIN FIELD	179134	170000	5%
ARMATURE	91535	84000	8%
INTERPOLE	38386	33000	14%

TABLE 3.2

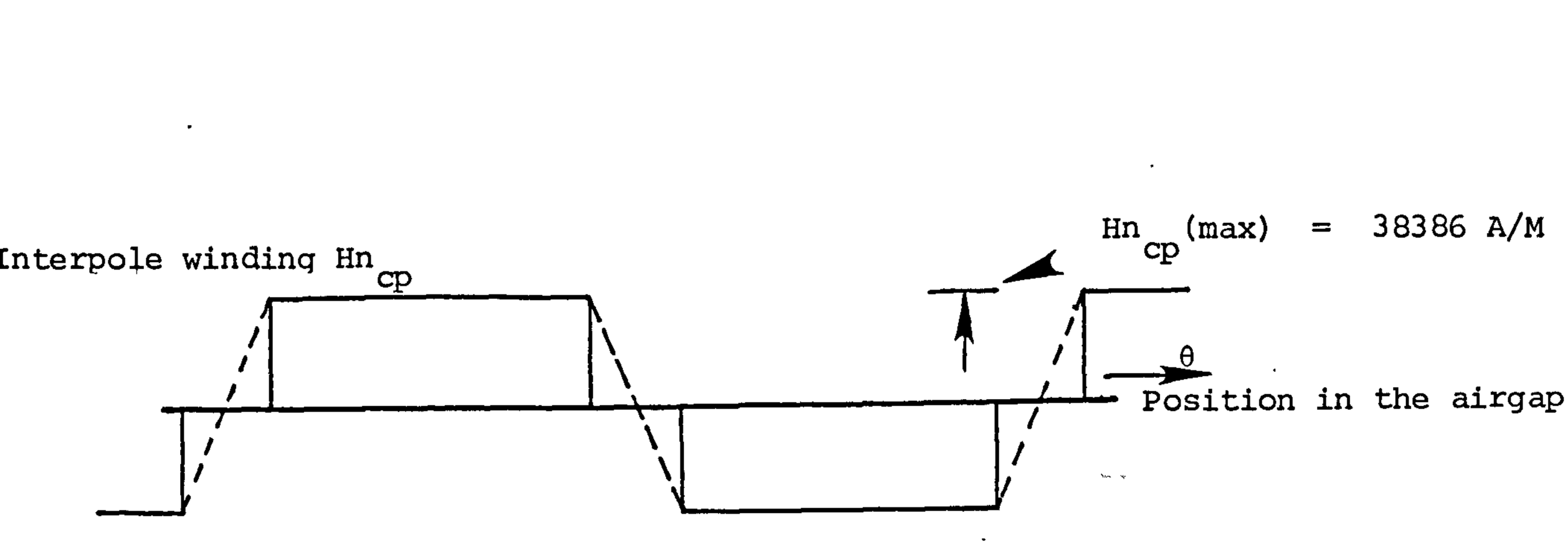

(i) Theoretical distribution

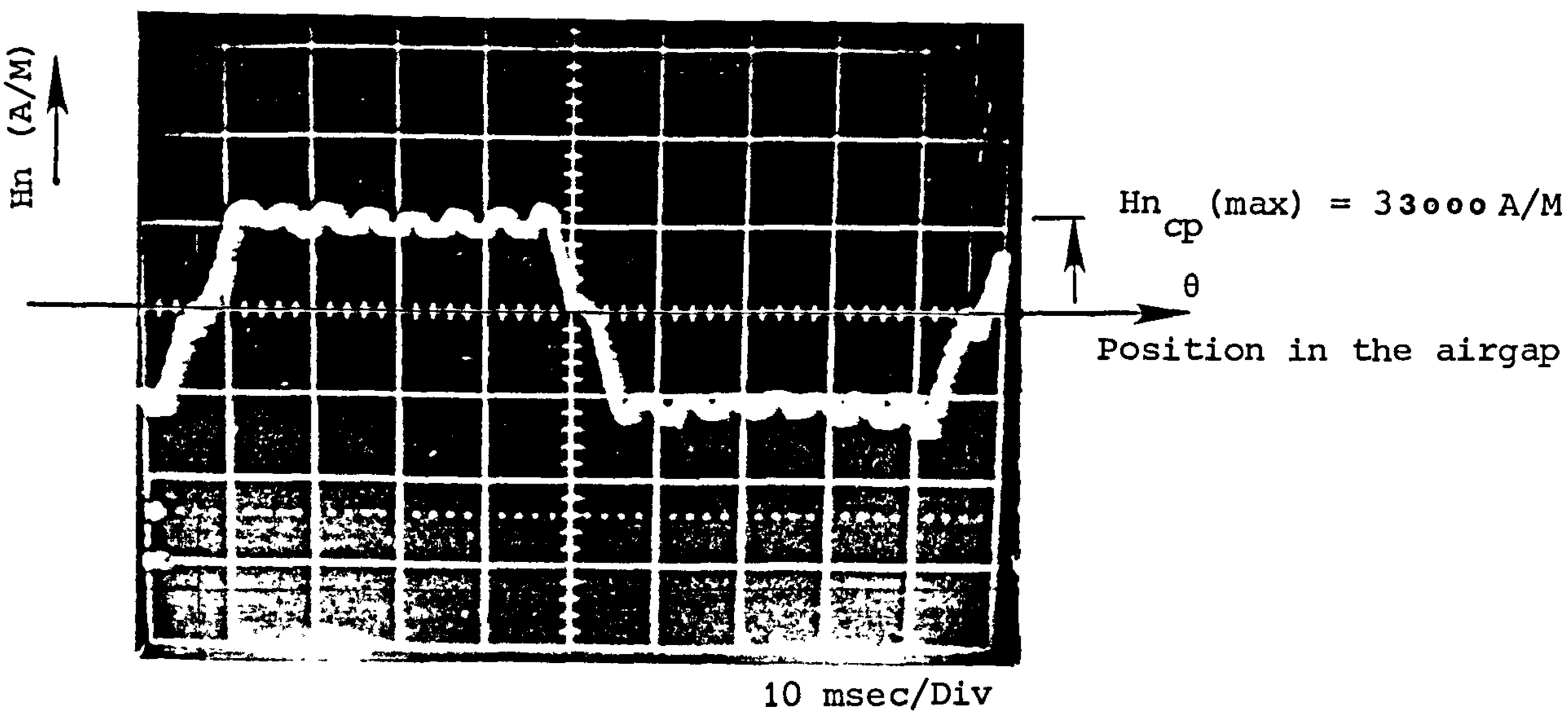

(ii) Experimental result

Fig. 3.10 Radial airgap field distribution due to interpole winding excitation

3.7 DUTY CYCLE OF ARMATURE SWITCHING DEVICES

The lap interconnected armature winding is described in section 3.4.2 . The developed view of the winding is clearly shown in Fig. 3.6, from whence it can be seen that the number of commutator segments is apparently 48. The number of GTO thyristor devices needed, however, was reduced by half by using the paralleling connections (as described earlier in section 3.4.2). The statically commutated armature winding with a pair of GTO thyristor devices replacing each commutator segment is shown in Fig. 3.7 .

The switching sequence is as follows :

With thyristor T_1 and its output counterpart S_{13} conducting, the current derived from the DC source is distributed between the stator coils as shown in Fig. 3.7 . After an appropriate interval, thyristors T_2 and S_{14} are triggered-on and the previously conducting pair turned-off. Variation of this switching procedure is possible (this will be dealt with in chapter 5). The interval over which each thyristor of Fig. 3.7 will conduct in a typical sequence is given by [68]:

$$T_{on} = tc = (p/a)(60/n\ c) \qquad (3.17)$$

where p = number of pole pairs

a = number of pairs of parallel paths

n = rotor speed in r.p.m.

c = number of armature coils

If the conduction period of each thyristor is defined by digital clock pulses such that each clock pulse is equal to T_{on} (equation 3.17), then the graph shown Fig. 3.11 gives the relationship between the clock frequency required and particular rotor speed.

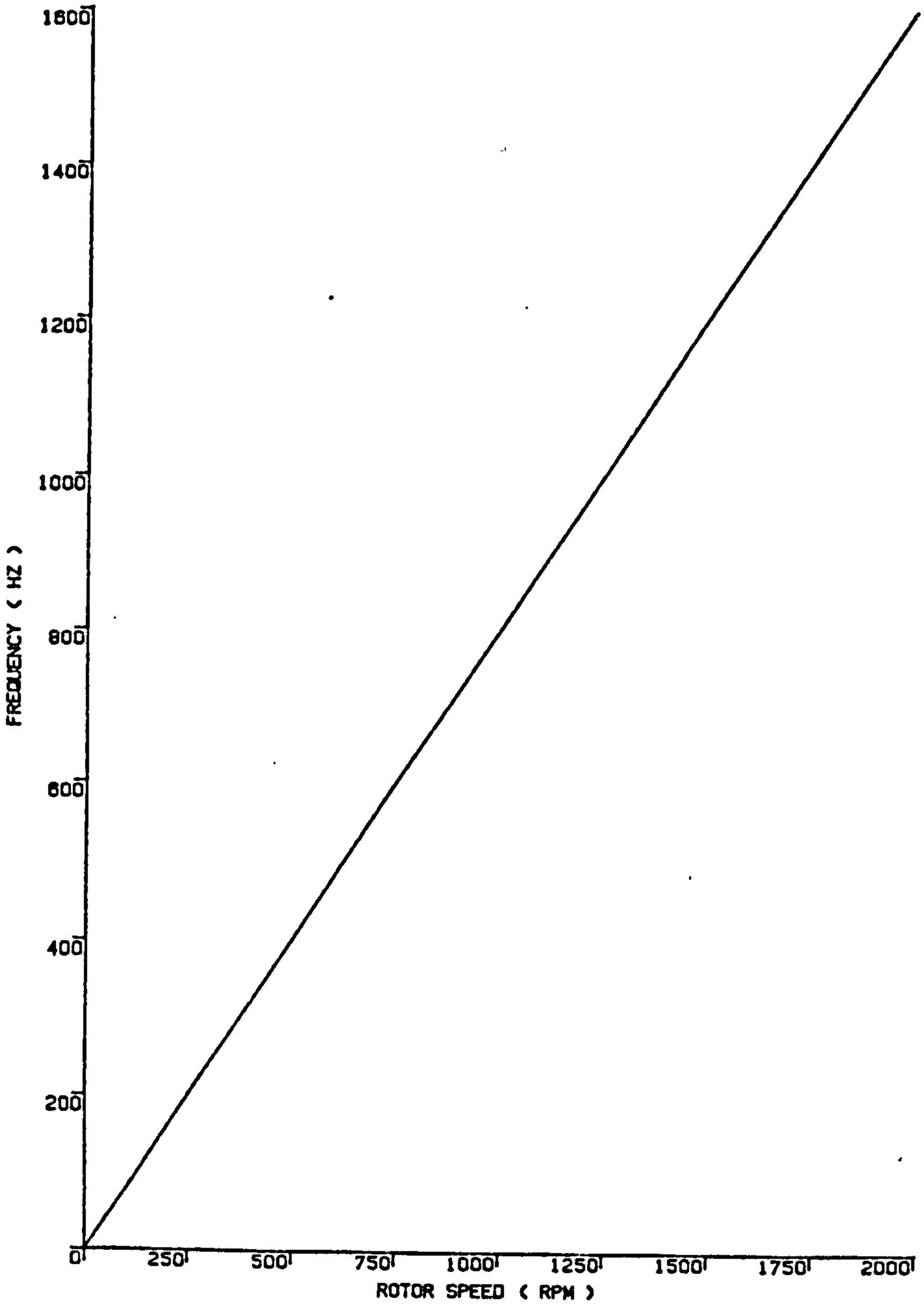

FIGURE 3.11
CLOCK FREQUENCY REQUIRED

CHAPTER FOUR

GATE TURN-OFF THYRISTORS AS ARMATURE SWITCHING DEVICES

CHAPTER FOUR

GATE TURN-OFF THYRISTORS AS ARMATURE SWITCHING DEVICES

In the previous chapter, a brief discussion was made concerning the layout of the inverted machine.

One of the fundamental requirements in the design of the developed machine is the selection of a suitable power switching device necessary to allow the flow of armature current at the appropriate instant when each particular armature coil traverses the neutral zone.

The ideal requirements needed for the power switches are summarised below :

(i) Fast switch-ON with zero impedance and high current gain.

(ii) Ease of switch-OFF with zero leakage current.

(iii) Zero switching losses with no radio interference.

(iv) Rugged construction with surge and fault current capability for ease of protection.

(v) Low cost and simple layout.

None of the existing commercial power switches have yet met all these requirements and it is likely that none ever will. Compromise and trade-offs are needed in the choice of suitable power switches for a particular application.

4.1 DISCUSSION ON THE CHOICE OF POWER SWITCHES

The main power switches commercially available are thyristors, bipolar power transistors [43], field-effect transistors (F.E.T) [42] or gate turn-off thyristors (G.T.O). Each of these have advantages and limitations relevant to possible use in this kind of application.

Thyristors are readily available with the required forward blocking voltage, over a wide range of current ratings. Internal regenerative action enables the device to be used at high surge currents with very low gate drive powers, therefore permitting easy isolation of the control signal.

However, the same regenerative feature means that the device cannot be turned off at the gate; forced commutation of the anode current is necessary in this kind of application where the supply is a DC source.

More recently, the Asymmetric thyristor (ASCR) has been designed specifically for circuits where anti-parallel diodes are connected across the thyristor (for example, inverter circuits driving inductive loads). This means that the reverse blocking requirements of the thyristor are reduced (to typically 2 V in the steady-state condition). The less stringent demands on the reverse blocking voltage allow improvements in the switching times and/or forward blocking voltage.

Bipolar Transistors may be used in DC applications of this kind. The saturated current gain of these devices is relatively low however, therefore making the base drive and isolation circuits quite complex.

The family of Field Effect Transistors of which the Power MOSFET is one, are devices capable of controlling a current of a few amperes with a gate voltage of a few volts and near zero gate power. At present, these devices are only available for use with low-voltage inputs and at low powers because of the "power-law" relationship between the forward blocking voltage and the on-state resistance [55]: for example, to achieve a doubling of the voltage rating, the chip area must be increased by a factor of about five. In other respects, they are rugged and have low switching losses with very short switching time.

Gate Turn-Off thyristors have the same high forward blocking voltage capability as the ASCR. Controlled internal regenerative action permits high range currents with moderately low gate drive, while allowing the device to be turned-off at the gate {the properties and characteristics of this device will be briefly explained in section 4.2 of this chapter}.

Among the above mentioned devices, it is clear that the design decision involved a choice between the bipolar power transistor switch, the MOSFET or the gate turn-off thyristor switch. The latter was chosen on the basis that its desirable properties are far superior for this application than the other two especially its voltage handling capability.

A summary of the properties of this device compared with the other mentioned is given in Appendix D [obtained from reference 46].

Under the discussion of suitable devices, it is worthwhile to mention an interesting and promising new power device called the Insulated Gate Rectifier (I.G.R), announced in 1982 by General

Electric Company to overcome most of the limitations and to sum the features mentioned above in one device [40]. This new IGR switch, which is still in the development stage, has been claimed to have the following characteristics :

(i) It can be switched with logic level signal due to its high gate impedance.

(ii) Controlled turn-OFF, as in a MOSFET .

(iii) Voltage blocking capability in both the forward and reverse direction as in a thyristor (MOSFET and bi-polar transistor can block only in the forward direction).

(iv) Current densities more than 10 times larger than the equivalent MOSFET and twice as large as a bi-polar transistor.

4.2 THE GTO THYRISTOR ARMATURE SWITCH

Since the beginning of this decade, a great interest has been shown in this recently developed device; well reflected by the large number of research papers which have been published in the literature, of which only 16 have been mentioned in this thesis [references 44 - 59 inclusive].

The physical operation of the device is well documented elsewhere [45,46,50]; the device characteristics will be briefly reviewed.

4.2.1 PROPERTIES OF THE DEVICE

Like the reverse blocking thyristor, the GTO can be switched ON via the gate with a current of certain polarity and switched OFF by reducing the anode current. In addition, because of the extreme

interdigitation of the gate electrode and the cathode, the GTO can be switched-off by a gate current of the opposite polarity to that of turn-on.

The GTO thyristor as depicted in Fig. 4.1(i) is a member of the diverse family of four layer (PNPN)switching devices. Like the thyristor, the GTO can be represented by a simplified two transistor model shown in Fig. 4.1(ii); the physical explanations of the functioning of the device using this model is well explained by Bosterling [reference - 46].

4.2.2 SWITCHING CHARACTERISTICS OF THE DEVICE [47]

The GTO thyristor turn-on and conduction process, are essentially very similar to those of the conventional thyristor; typical waveforms are shown in Fig. 4.2. Turn-on is achieved with the forward blocking voltage applied by the injection of a positive (forward) current to the gate of the device (the minimum value of this is usually specified in the device data sheets).

One of the main features of the GTO thyristor is that the anode (main) current in the on-state can be turned-off via a negative gate current (I_{GR}). The waveforms for this are shown in Fig. 4.2. When turn-off is required, a negative voltage is applied by the gate drive circuit. This produces a rising negative gate current to which the anode current does not respond until the end of the storage period. The anode current then falls rapidly (typically in the order of 1 μs or less) as it is diverted to the gate. The interdigitation of the gate structure pinches the current into thin filaments which extinguish in turn leaving only a small anode current "tail". The gate current reduces rapidly from its peak

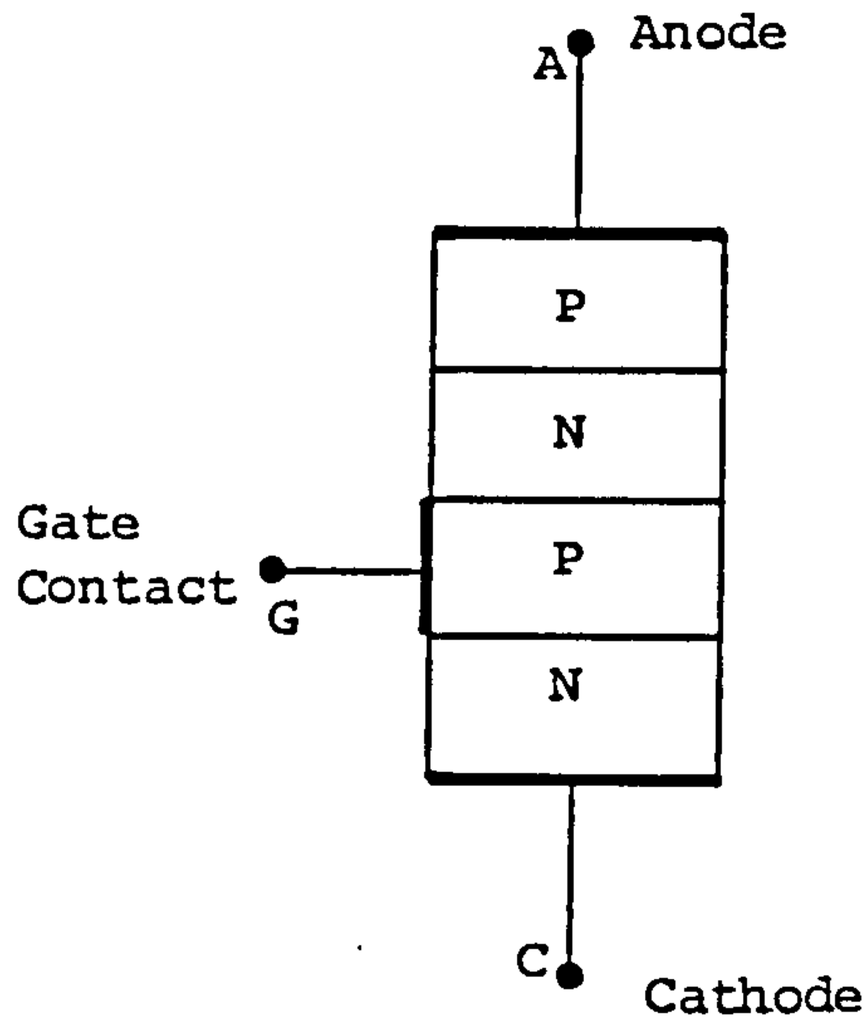

(i) PNPN layer structure of the GTO

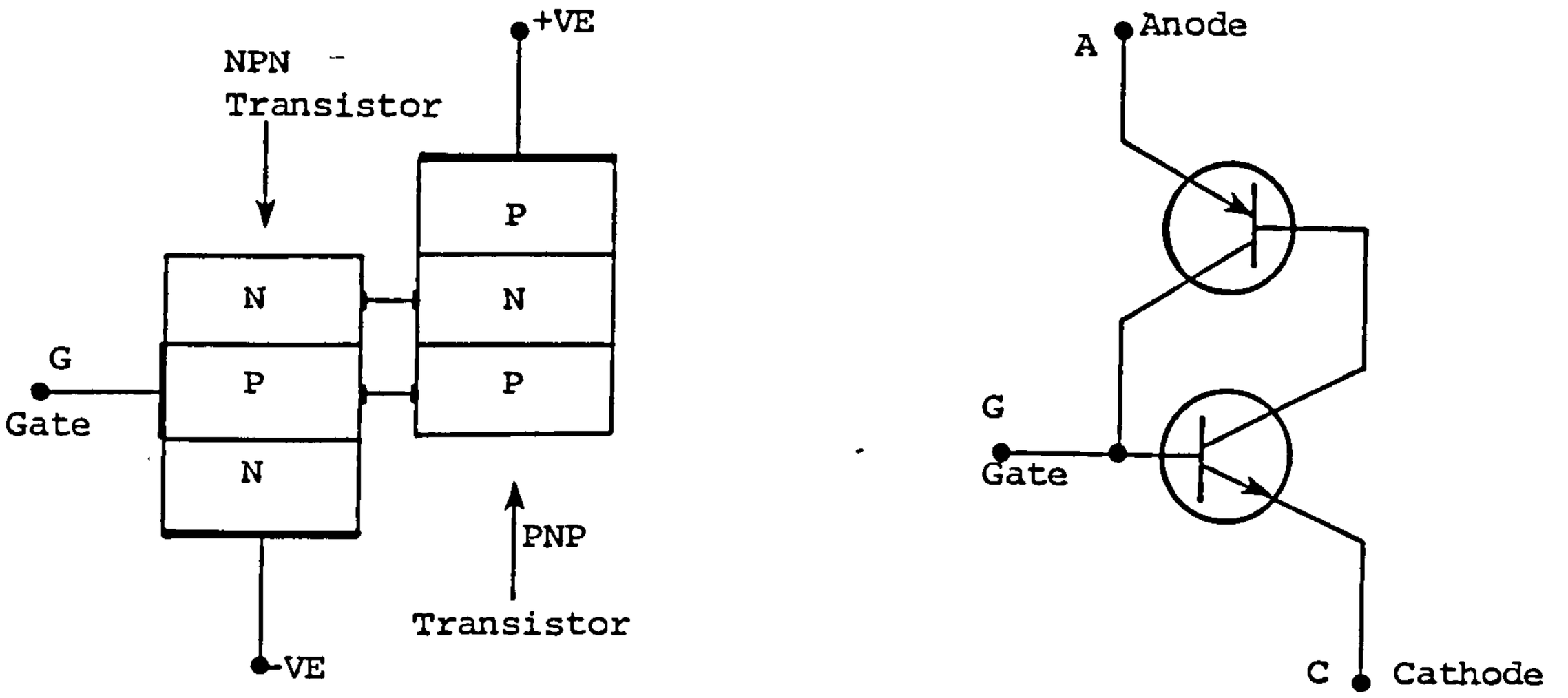

(ii) Two-transistor model of GTO

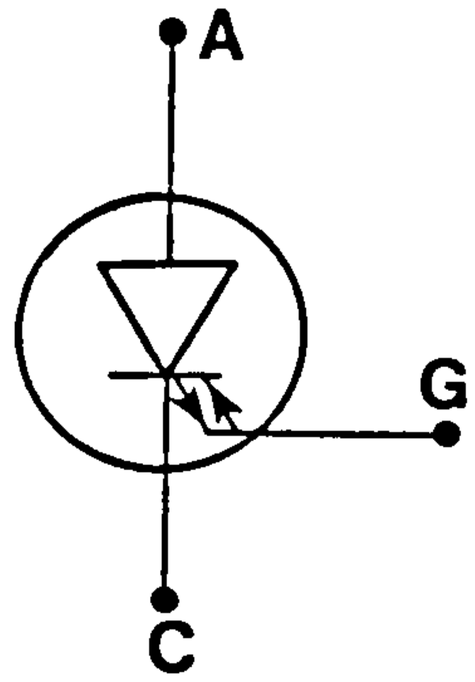

(iii) Symbol for GTO

Fig. 4.1 Representation of the GTO thyristor

value to its "tail" which removes the small amount of remaining internal charge. The anode and gate current tails decay to zero as forward blocking voltage builds up to its peak across anode and cathode.

4.3 DESIGN CONSIDERATIONS OF THE ARMATURE GTO THYRISTOR

The essential stages which has to be followed to ensure successful GTO circuit design of this kind are as follows [48, 53, 58] :

- Selection of the correct current rating (I_{TC}) and (dV/dt)
- Selection of the correct voltage rating
- Design of a suitable gate drive circuit
- Design of an adequate snubber circuit and suitable choice of a heat sink.

In the last chapter on the analysis of the machine rating, the armature current required to develop full load torque (similar to that given by the original machine was calculated to be around 4.5 Amperes. A suitable device which can handle this value of armature (anode) current is the Mullard BTW 58 series rated at 6.5 A (average on-state current). The voltage rating of this device is 1300 V (BTW 58 - 1300R). The data sheet is given in Appendix E, a summary of this is as follows :

- Average on state current $I_T(av)$ = 6.5 A (max)
- Repetitive peak off-state voltage = 1300 V (max)
- (dV/dt) < 10 KV/ μsec
- Typical gate trigger current I_{GT} > 200 mA

The interconnected armature winding with 48 of these GTO thyristors (24 positive rail and 24 negative rail) devices is shown in Fig. 3.7.

4.3.1 SLOW RISE (SNUBBER) CIRCUIT

The current switch-off in the GTO thyristor, device-controlled, produces certain features which are unique to this device. A slow rise or "snubber" circuit is of prime importance for turning off high currents - this has two major roles :

i) Firstly, to rapidly decrease the current which has flowed through the GTO device i.e. the on- state current, by diverting the current to the snubber circuit when the device is switched off. Unless there is a snubber circuit, the current continues to flow in the GTO device, causing a great loss to occur in it.

ii) Secondly, to limit the rate of rise of the voltage in the forward direction at turn off, and without it, the induced voltage due to the circuit inductance can be excessive and may lead to catastrophic failure. The snubber circuit used to protect the device is a standard RCD (resistor, capacitor, diode) shown in Fig. 4.3 (i). The value of the snubber capacitor can be calculated from the graph of controllable anode current (I_{TC}) versus (dV/dt), given in the data sheet {Appendix E, Fig. 10 & 11}. For safe operation, the GTO must never be switched off at a point which lies outside the relevant curve of the junction temperature and reverse gate voltage available.

The size of the snubber capacitor needed to give the required dV/dt is calculated from the equation :

$$C_s = I_T(pk)/(dV/dt) \qquad (4.1)$$

Where $I_T(pk)$ is the peak anode current to be switched-off = 6.5 A.

The reverse gate voltage used in the gate drive circuit (V_{GR}) = 10 V

Assuming a peak junction temperature of 120° C , the data sheet gives a value of dV/dt of 700 V/μsec.

$$C_s = 6.5/700 \times 10^6 = 10 \text{ nF} \qquad (4.2)$$

This value of capacitance reduces the rate of rise of voltage to within the specified limits but the snubber circuit components {L_s (stray inductance), C_s (snubber capacitor) and R_s (resistor)} that it forms may be under-damped resulting in high frequency oscillation as the off-state voltage rises. To minimise this problem, the value of the capacitance is increased to give a near critically-damped condition (C_s = 22 nF).

The energy that is stored in the capacitor ($\frac{1}{2}$ C_s V_p^2) is dissipated in the series resistor during the period that the GTO is ON. The value of R_s is chosen so that the capacitor is able to discharge itself and the rating of the resistor must be sufficient to handle the rate of change of stored energy :

$$\text{Rating} \quad > (\tfrac{1}{2} C_s V_p^2/T) \qquad (4.3)$$

where T = period of gate pulse.

The diode D_s is connected so that the current may flow rapidly into the capacitor C_s. To avoid large sudden voltage undershoot, it is recommended [47] to use a fast-recovery diode in the snubber circuit; i.e. D_s is fast recovery of the type BY 448 .

Also of prime importance is minimisation of stray inductance by mounting the snubber circuit very close to the GTO switch anode-cathode terminals.

4.3.2 GATE DRIVE CIRCUIT

The waveform of the gate current required for driving the GTO is shown in Fig. 4.2(i) . At turn-on, the gate is driven hard with a current higher than the gate trigger current (I_{GT}) {with a fast rise time} to ensure fast switching and minimum turn-on losses. During the steady conduction period of the GTO, it is essential to maintain the minimum gate trigger current to ensure that the GTO is kept in on-state.

Turn-off is achieved by applying a negative gate voltage (of around 10 V) between the gate and the cathode, this causing a negative gate current (I_{GR}) to flow.

The function of the gate drive circuit is to allow the flow of turn-on gate current (I_{GF}) and turn-off gate current (I_{GR}) as shown in Fig. 4.2. The gate drive circuit can be designed using either of the following two methods :

i)The first uses a single power supply system where the forward and the reverse gate currents are provided from a single gate power supply. The method uses a capacitor or a reactor to store energy for allowing the flow of current of the opposite polarity. ii)The other method is a dual-power supply system where the currents I_{GF} and I_{GR} are provided from two separate gate power supplies. This method is normally used for driving high current GTO thyristors and is expensive. The first method is used in this project on the account of the fact that it can turn-off the armature rated current of about 4.5 A and is cheap to build. The gate drive circuit is shown in Fig. 4.3(ii) was built and tested for switching both resistive and resistive/inductive loads. The capacitor Cn is used

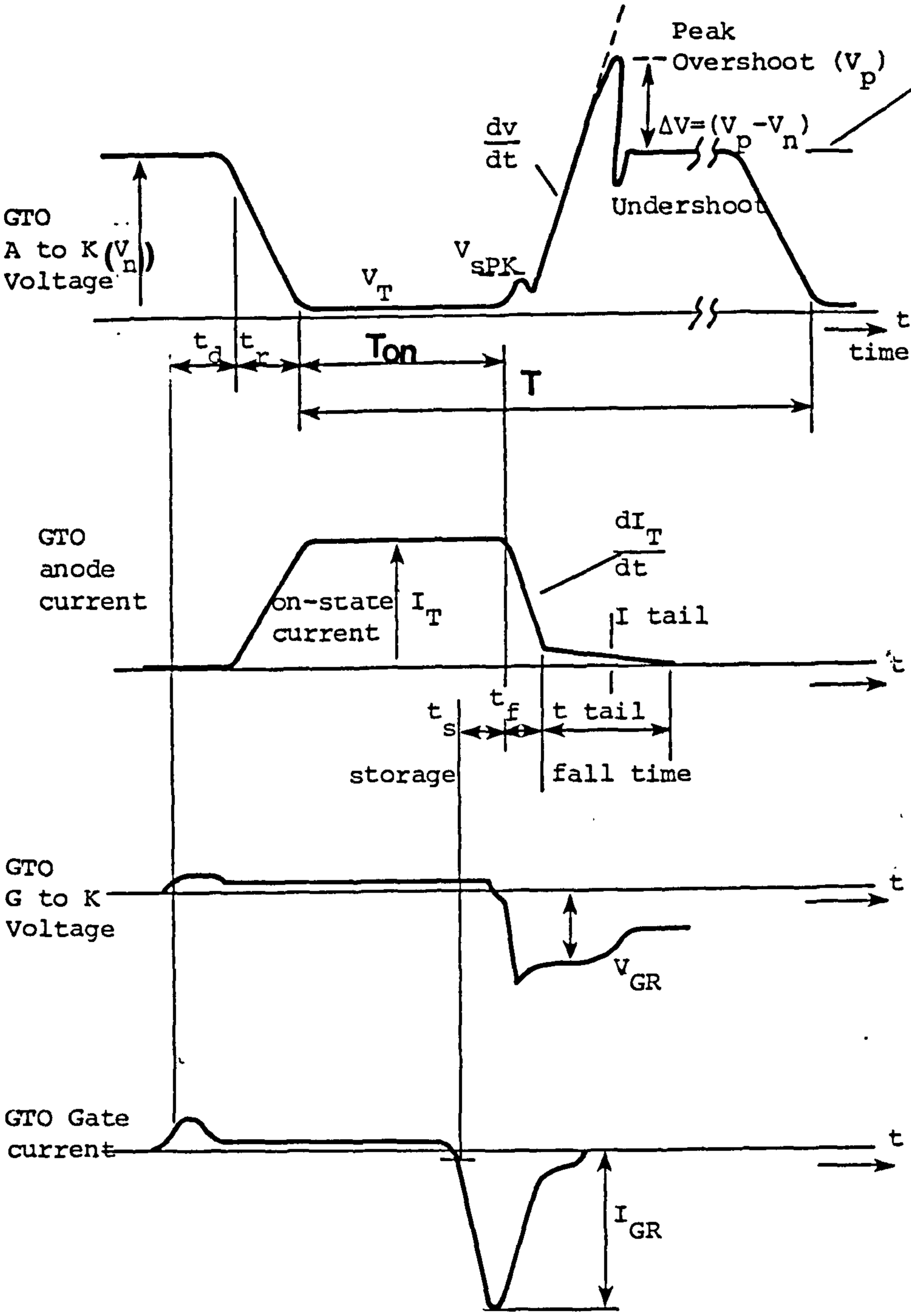

(i) GTO switching waveforms

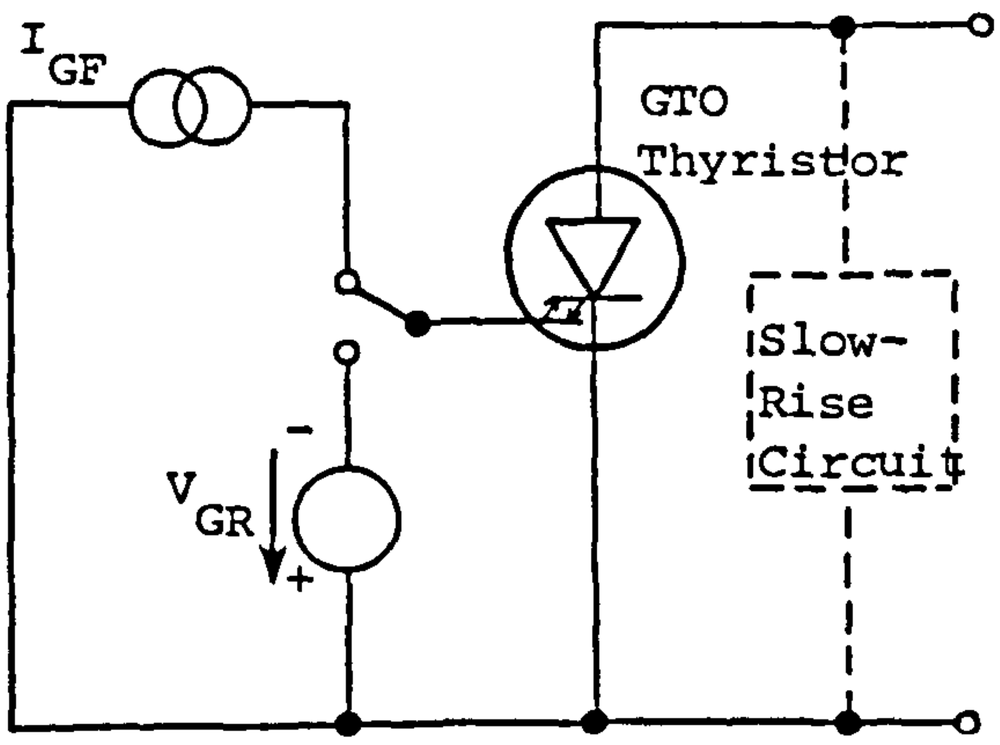

(ii) Basic drive circuit

Fig. 4.2 GTO Thyristor switching behaviour

to store the energy. When a pulse is applied via the opto-isolator to the base of transistor Tr_1, Tr_1 switches on causing subsequently Tr_3 to switch-on and Tr_4 to switch off. Positive gate drive current (I_{GF}) flows from the DC supply rail (+15 V), its steady-state value controlled by the value of emitter resistor R_5 causing the GTO to switch on. If the opto-isolator pulse is removed Tr_1, Tr_2 and Tr_3 all switch off and the darlington transistor (Tr_4) switches on. Capacitor Cn which has been charged to - 10 V during the on period of the GTO is now discharged between the gate and the cathode. The purpose of the zener diode is to limit the capacitor voltage to 10 V and the darlington transistor gives current amplification. Opto-isolators are used to provide effective isolation between the digital circuitry and the power electronic elements. The opto-isolation circuit is shown in Fig. 4.4(i), the optically coupled isolators [71] are of the dual type with each of its transistor output stage supplying one gate drive circuit.

The other design requirement for the GTO gate drive circuits is the provision of a DC power supply to these drive circuits. Negative-rail-connected GTO gate drive circuits can be supplied from one common power supply unit; however, positive-rail-connected GTO drive circuits need floating power supplies. These were provided as shown in Fig. 4.4(ii): small 20 VA transformers were used each with two secondary outputs rated at 15 V - 10 VA, to obtain two isolated 15 V DC supplies, each capable of supplying one individual gate drive circuit.

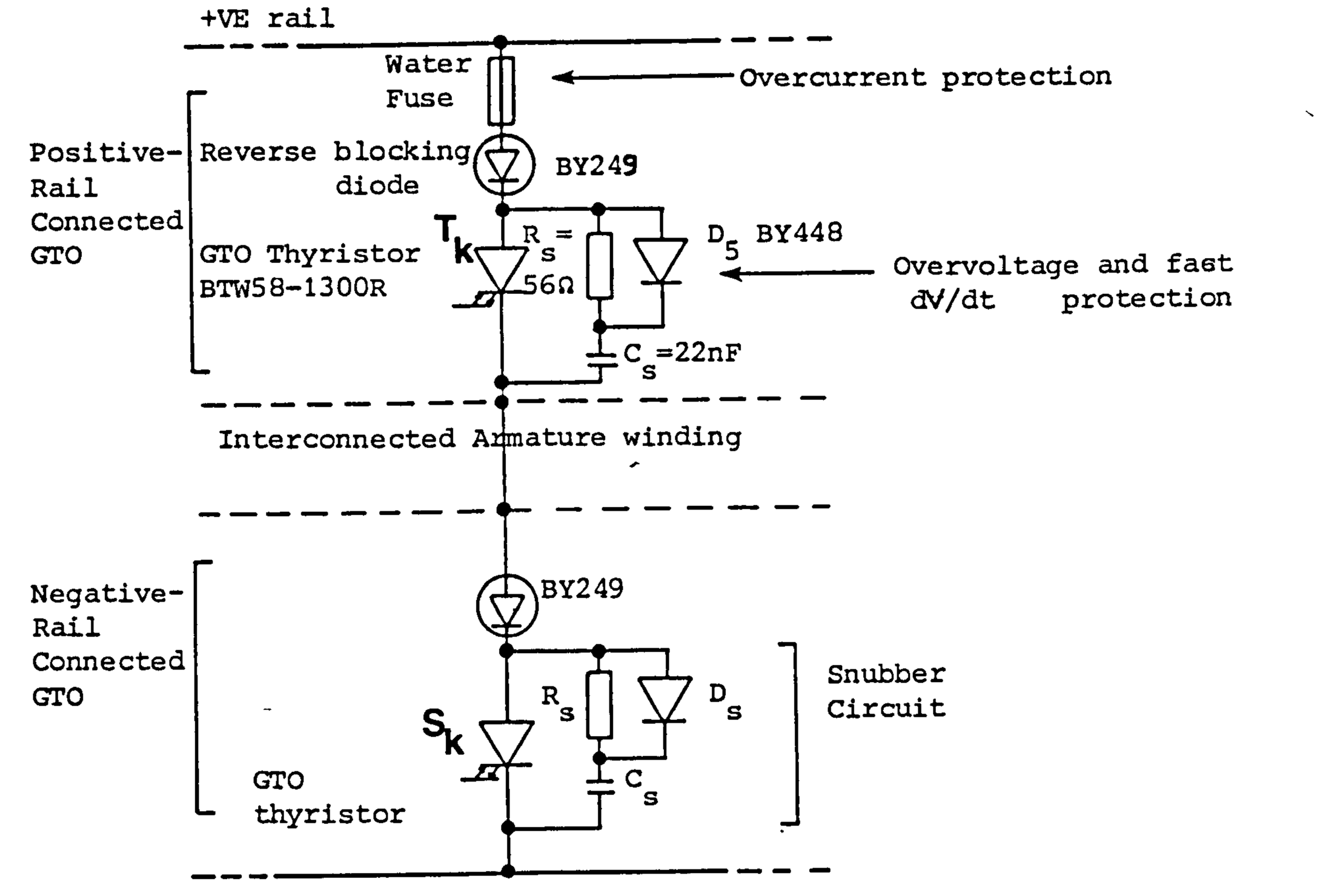

(i) GTO Protection Circuit

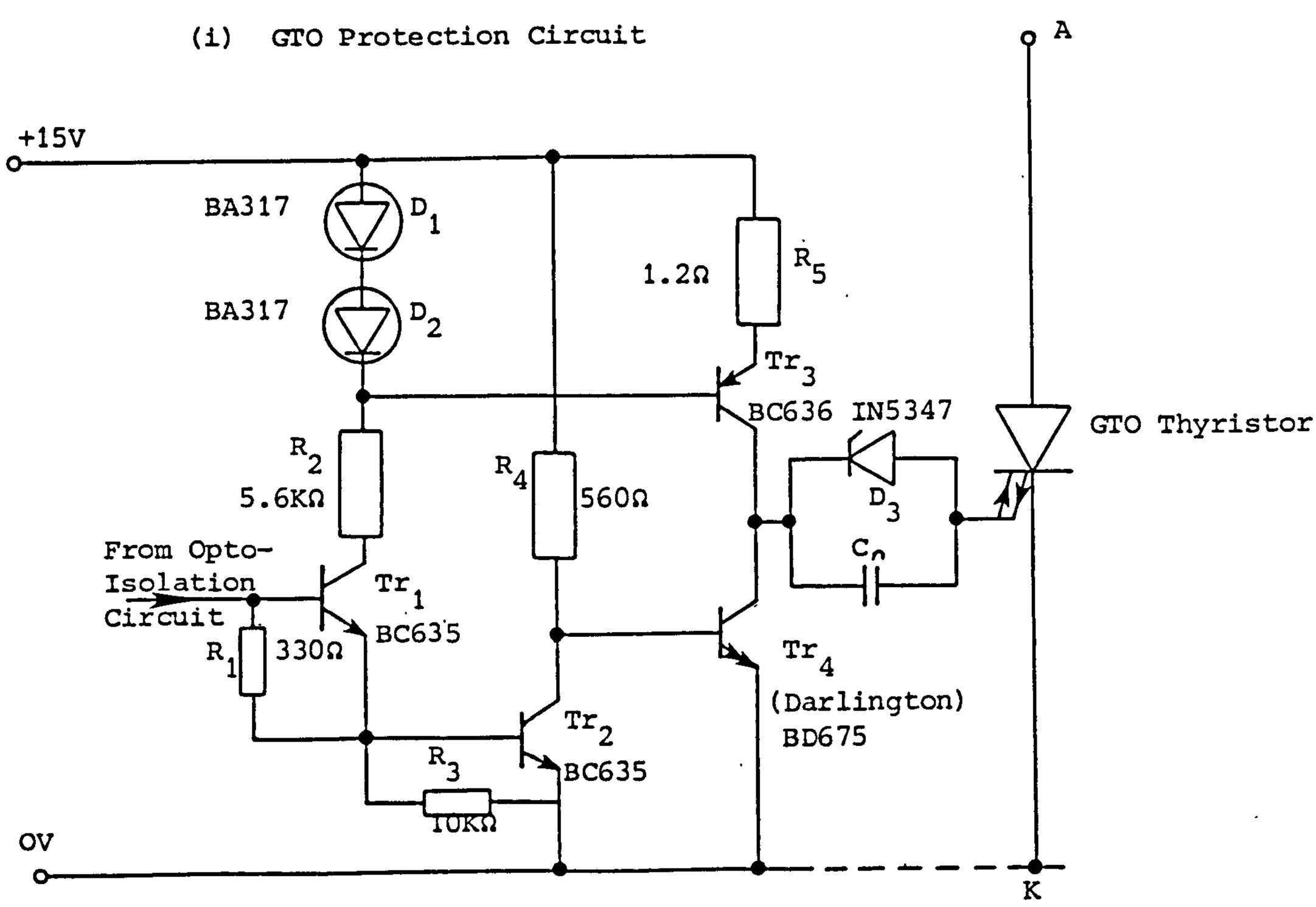

(ii) Gate Drive Circuit

Fig. 4.3 Gate drive and protection circuit for GTO armature switch

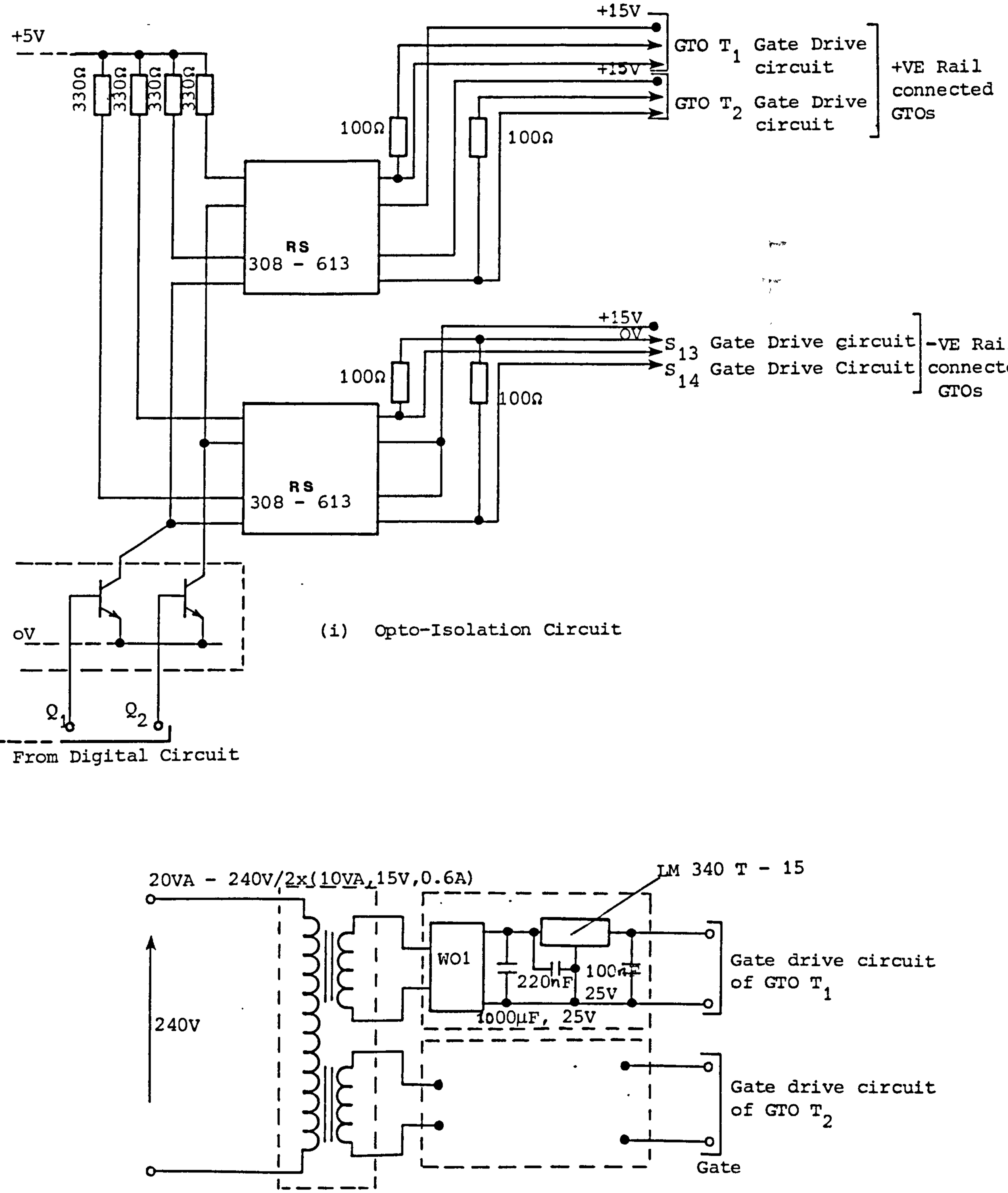

(i) Opto-Isolation Circuit

(ii) Positive rail GTO's isolated gate supply circuit

Fig. 4.4 Gate drive opto-isolation and isolated power supply circuits

4.3.3 DETERMINATION OF GTO TOTAL POWER DISSIPATION AND HEAT SINK REQUIREMENTS

To determine the size of the heat sink required for this application, the total GTO power dissipation must be calculated. The total power loss in in the GTO comprises of the on-state loss, off-state loss, switch-on loss and switch-off loss [48,53,58].

(i) On-state loss : this is due to the voltage-drop and current passing during forward conduction of the device and represents the major source of loss. It can be evaluated from the formula

$$P\ (on) = (V_T x\ I_T x\ D) \tag{4.4}$$

where D = duty cycle = t_{on}/T (4.5)

Some device manufacturers give nomograms in their data sheets from which the value of P (on) loss can be directly evaluated {Appendix E, Fig. 4}.

(ii) Off-state loss : this is due to the leakage during the blocking state and is given by the off-state anode leakage current I_D multiplied by the off-state anode voltage, allowing for the off state duty ratio {the value of I_D is stated in the manufacturer data sheets, Appendix E}.

$$P\ (off) = (1-D)\ x\ I_D x\ V_n \tag{4.6}$$

(iii) Switch-on loss : this depends significantly on the anode current and voltage waveforms at turn-on [48]

$$P_{sw}(on) = \frac{1}{6}\ x\ V_n x\ I_T x\ t_r\ x\ f_s \tag{4.7}$$

Using the snubber circuit shown in Fig. 4.3 (i), and since the switching frequency (f_s) is low, the switch-on power loss is small [48], as confirmed by equation 4.7 .

(iv) Switch-off loss : this also depends strongly on the anode

voltage and current waveforms as modified by the effect of the snubber, and is very much dominated by the tail losses. Again some manufacturers supply nomograms to evaluate this loss. Alternatively, this can be calculated from

$$P_{sw}(off) = \frac{1}{6} \times V_{spk} \times t_f \times (I_T + 2\ I_{Tail}) \times f_s \qquad (4.8)$$

Fig. 4.2 (i) shows the definition of the parameters in the above equations.

From the above equations: [$f_S = 50$ Hz]

P (on) = 1.25 W

P (off) = 0.4125 W

P_{sw}(on) = 6.25 mW

P_{sw}(off) = 0.375 mW

Total power loss (P_{tot}) = 1.669 W

Using the method given in reference 48 the size of the heatsink may be calculated, as follows :

The heat transfer P_{tot}, is directly proportional to the temperature difference between the junction and the ambient temperature. The ratio between the temperature difference and the amount of heat transfer gives what is known as the thermal resistance, R_{th} :

$$R_{th} = \{T_j\ (max) - T_{hs}\}/P_{tot} \qquad (4.9)$$

where T_{hs} is the temperature of the heatsink.

Assume the worst case of maximum operating junction temperature

$= T_j(max) = 120\ ^oC$

From the data sheet {Appendix E}, the thermal resistance from junction to mounting base (heat sink) = 1.5 $^oC/W$

Therefore $T_{hs} = T_j\ (max) - (P_{tot} \times R_{th})$

$$T_{hs} = 120 - (1.669 \times 1.5) = 117.5\ ^{o}C$$

Assuming a peak ambient temperature of 60 °C

Size of the heat sink = (117.5 - 60)/1.669 = 34.5 °C/W

The heat sink used was an aluminium plate of thickness 1.6 mm with the dimensions 80 x 40 mm calculated to give a minimum of 10 °C/W .

4.3.4 OTHER DESIGN FEATURES

(i) The GTO thyristor permits uni-directional current flow (from anode to cathode). This means that current cannot be reversed, hence for operating the machine in the generating mode, the polarity of the voltage has to be reversed.

The reverse characteristic of the GTO device is equivalent to that of a resistance which is incapable of blocking voltage or conducting significant current [48]. If the polarity of the voltage is to be reversed in the generating mode, reverse blocking will be required. For this reason, a diode {of the type BY 249-600, rated at 6.5 A - mean forward current} is connected in series with each GTO thyristor, as shown in Fig. 4.3(i) .

(ii) As the thermal capacity of the device is low, overcurrent or overload will soon raise its temperature, and lead to damage to the device [1]. Faults causing overcurrents must be cleared quickly. Mechanical contactors are not suitable to protect semiconductor devices, because of their low operating speeds. The best way to protect the devices is by using fuses. The main requirement of the fuses are : a) to be able to carry continuously the thyristor rated current, and b) the $\int i^2\,dt$ of the fuse should be less than that of

the device. Each pair of series connected positive and negative rail GTO devices is protected by one fuse {as shown in Fig. 4.3(i)}. The fuses used were water fuses with a nominal fusing current of 5A.

4.4 ANALYSIS OF CURRENT INTERRUPTION IN AN ARMATURE GTO THYRISTOR

The switching sequence of the armature GTO thyristors has been described in section 3.7 of chapter 3. Current commutation in an armature coil takes place when a conducting pair of armature GTO devices are switched-off and the following pair (in the sequence, in the direction of rotation) are switched-on.

Whilst commutation is taking place, the current flowing in the commutated coil, initially equal in magnitude to the current flowing in one of the parallel paths through the armature - has to reverse its direction of flow. The current reversal in the commutated coil results in an e.m.f. of self induction, which is applied as an overshoot (spike) voltage across the terminals of the switching device at turn-off. The purpose of the following analysis is to relate the peak value of this overshoot voltage to the parameters of the commutated coil and the snubber circuitry. Stiegerwald [57] developed formulae for calculating the peak overshoot voltage upon current interruption in a GTO thyristor circuit. The following analysis is based on those formulae with the appropriate simplifying assumptions.

The interconnected armature winding with the GTO thyristor armature switches has been shown in Fig. 3.7 of chapter 3. This

figure is now redrawn for the instant when GTO T_1 and its output counterpart S_{13} are conducting for the duration of the commutation period "tc " {equation 3.17} and the armature current (Ia = 2I) is resolved, at the node of T_1 cathode (i.e. node "a") into two equal branch currents "I", Fig. 4.5. From inspection of Fig. 4.5(i), it is clear that the branch inductance (L´) between nodes "b" and "c" and (L´´) between nodes "a" and "d" are very much larger than the inductance of the commutated coil itself.

At the end of period tc, GTOs T_2 and S_{14} are turned on and the previously conducting pair T_1 and S_{13} are switched off. This causes the reversal of the current in commutated coil C_1 and the stored magnetic field energy due to the self inductance of this coil is transferred to the capacitive element of the snubber circuit - C_s. Hence, the transition of switching from GTO pair T_1, S_{13} to T_2, S_{14} causes current reversal in this local commutated coil (coil C_1), the current in the armature circuit branches L´ and L´´ is assumed to be constant throughout the commutation interval. The two current sources I shown in Fig. 4.5 (ii) and (iii) represent the currents in these armature branches.

The stray inductances due to snubber circuit (l_s) and GTO circuit wiring (l_w), Fig. 4.5(ii) and (iii) are very small compared with the inductance of the commutated coil itself (L_1)

$$L_1 \gg l_s \quad \text{or} \quad l_w$$

When the GTO current falls abruptly from the on-state value, the current is momentarily diverted into the snubber circuit. The energy transfer is as follows :

The energy increase in C_s is equal to energy decrease in L_1

The energy increase in C_s is given by :

$$\frac{1}{2} C V^2 = \frac{1}{2} C_s (\Delta V)^2 \qquad (4.10)$$

where $(\Delta V) = (V_p - V_n)$ = peak overshoot voltage

The energy decrease in L_1 is given by :

$$\frac{1}{2} L I^2 = \frac{1}{2} L_1 (I_a/2)^2 \qquad (4.11)$$

Equating 4.10 and 4.11 :

$$\frac{1}{2} C_s (\Delta V)^2 = \frac{1}{2} L_1 (I_a/2)^2$$

$$\text{Hence} \quad (\Delta V) = (I_a/2)\sqrt{L_1/C_s} \qquad (4.12)$$

Equation 4.12 gives the value of peak overshoot voltage (ΔV)

$$\text{Hence} \quad (\Delta V) = V_p - V_n = (I_a/2)\sqrt{L_1/C_s}$$

$$V_p = V_n + (I_a/2)\sqrt{L_1/C_s} \qquad (4.13)$$

The voltage curve across an armature circuit GTO thyristor is shown in Fig. 6.2(c) of chapter 6 to illustrate this overshoot voltage upon experimental current interruption in the device. The value of overshoot voltage recorded experimentally is subsequently compared with that obtained using equation 4.12 and found to be in good agreement, (Section 6.2).

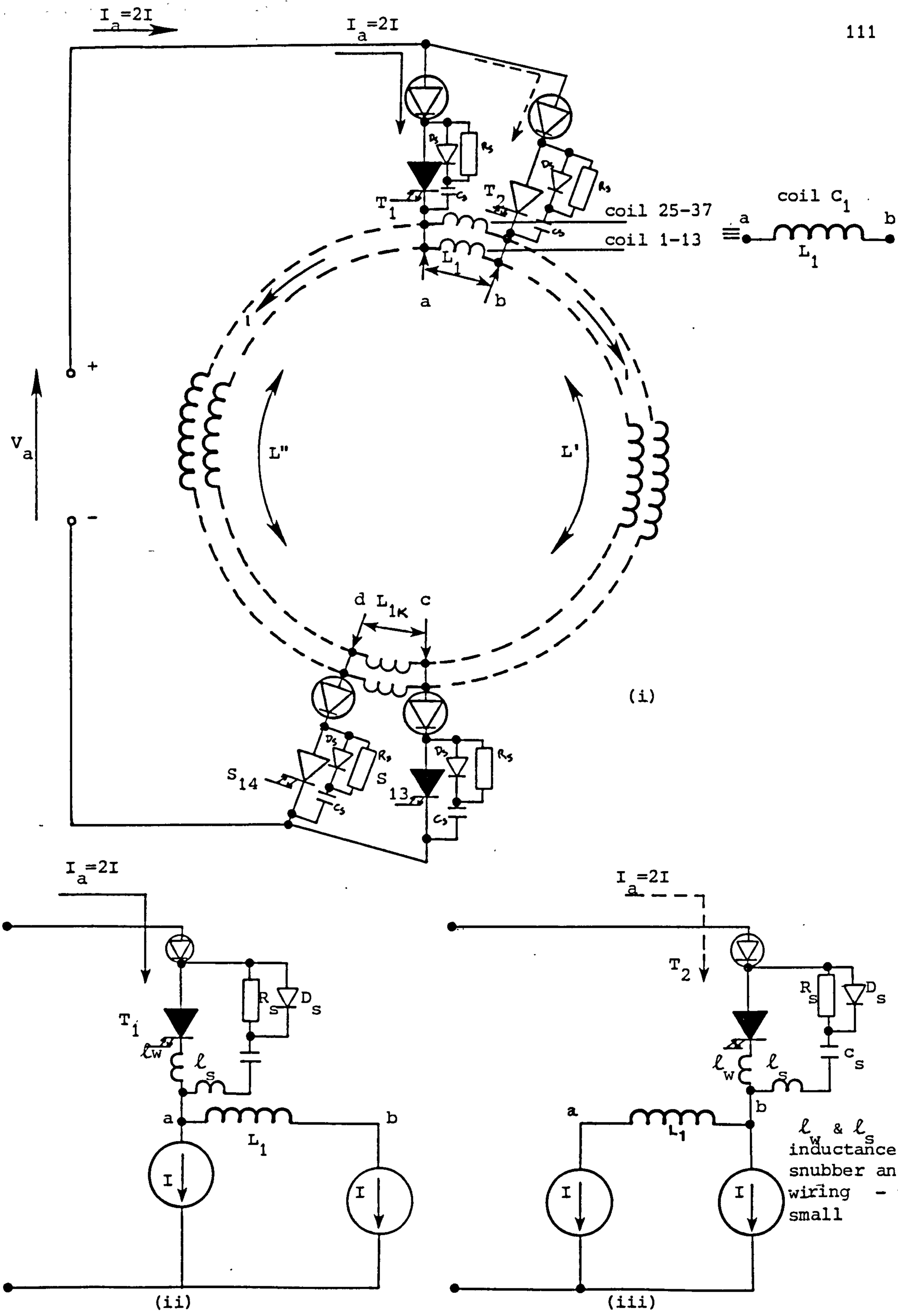

Fig. 4.5 Switching of armature GTO thyristors - instantaneous picture

CHAPTER FIVE

DESIGN OF THE DIGITAL CONTROL CIRCUIT

CHAPTER FIVE

DESIGN OF THE DIGITAL CONTROL CIRCUIT

5.1 BASIC CONSIDERATIONS

The main aim in the design of any control circuitry is to enable certain functional operations to be achieved and hence it is essential to accurately detail these functions prior to describing the electronic circuitry subsequently built.

Having discussed in the last chapter the overall design of the GTO armature switch circuits, it is evidently necessary to develop a control circuit capable of organising the switching sequence of these devices: (a) at the correct instant in time, (b) for the correct duration of period and (c) in the correct sequential order.

The following points are of importance in the design of the digital control circuit :

(i) The suitable selection of a velocity and positional feedback element to provide the necessary information for controlling the switching configuration of the armature GTO thyristors in a closed loop regime to maintain the required (optimal) torque angle.

(ii) The necessary complex pulse generation circuits required to initiate the conduction of the power switches should be incorporated within a digital electronic circuit.

(iii) Any possibility of malfunction should be considered and appropriate steps taken to avoid the same.

(iv) Incorporation of any secondary features within the control circuit without the need to change the hardware in the system.

(v) A requirement in any control circuit is the optimisation of the logic circuit necessary to perform the desired function.

In detailing the design of the digital control circuit an overall block diagram will first be described in general terms. Then, the required function of each block and the added flexibility incorporated within the control circuit will be explained in more detail.

5.2 GENERAL BLOCK DIAGRAM

Fig. 5.1 depicts a simplified block diagram of the digital control circuit. The individual blocks have been numbered for reference purposes. The block marked "1" is the shaft feedback element which is basically a rotary-type incremental encoder that outputs three types of signals (Details of these outputs will be given in the next section). These encoder output signals give the required information relating to shaft speed and the instantaneous angular position of the rotor.

Block "2" is the signal processing circuit. This block provides the conditioning of the signal outputs available from the encoder. It also gives a single ("reference") pulse, at the correct T.T.L. level, each time the rotor "traverses" a reference position determined as the instantaneous position of the quadrature-axis (see section 5.5 of this chapter).

(Determination of the q-axis will be detailed in section 5.5).

Block "3" is the "starting-routine circuit" in which a separate, low frequency clock is utilised to sequentially trigger the GTO armature switches if the rotor is at standstill : i.e. no phase outputs are available from the rotary encoder. This low frequency clock is "disabled" once shaft feedback information is available from the encoder.

Block "4" is basically a digital frequency comparator circuit whose function is to engage the feedback available from the rotary encoder as soon as the shaft has moved from standstill. Therefore, as soon as the "Index pulse" is generated and clock pulses are available from the shaft encoder, the input information to block "6" will be transferred to the feedback elements.

Block "5" is designed to permit "controlled departure" from the quadrature-axis position by re-direction of the Index pulse. This feature is analogous to rocking the brushes on a conventional armature of a DC machine.

Block "6" is the "heart" of the digital control circuit, in which the necessary signals are generated which define the exact conduction periods of the armature GTO thyristors.

Finally, the drive logic and interface circuits (Block 7) are necessary to interface the signals from the digital control circuit to the firing circuits of the appropriate armature GTO thyristors.

The individual elements of the control circuit will now be explained in more detail and their primary function will be outlined.

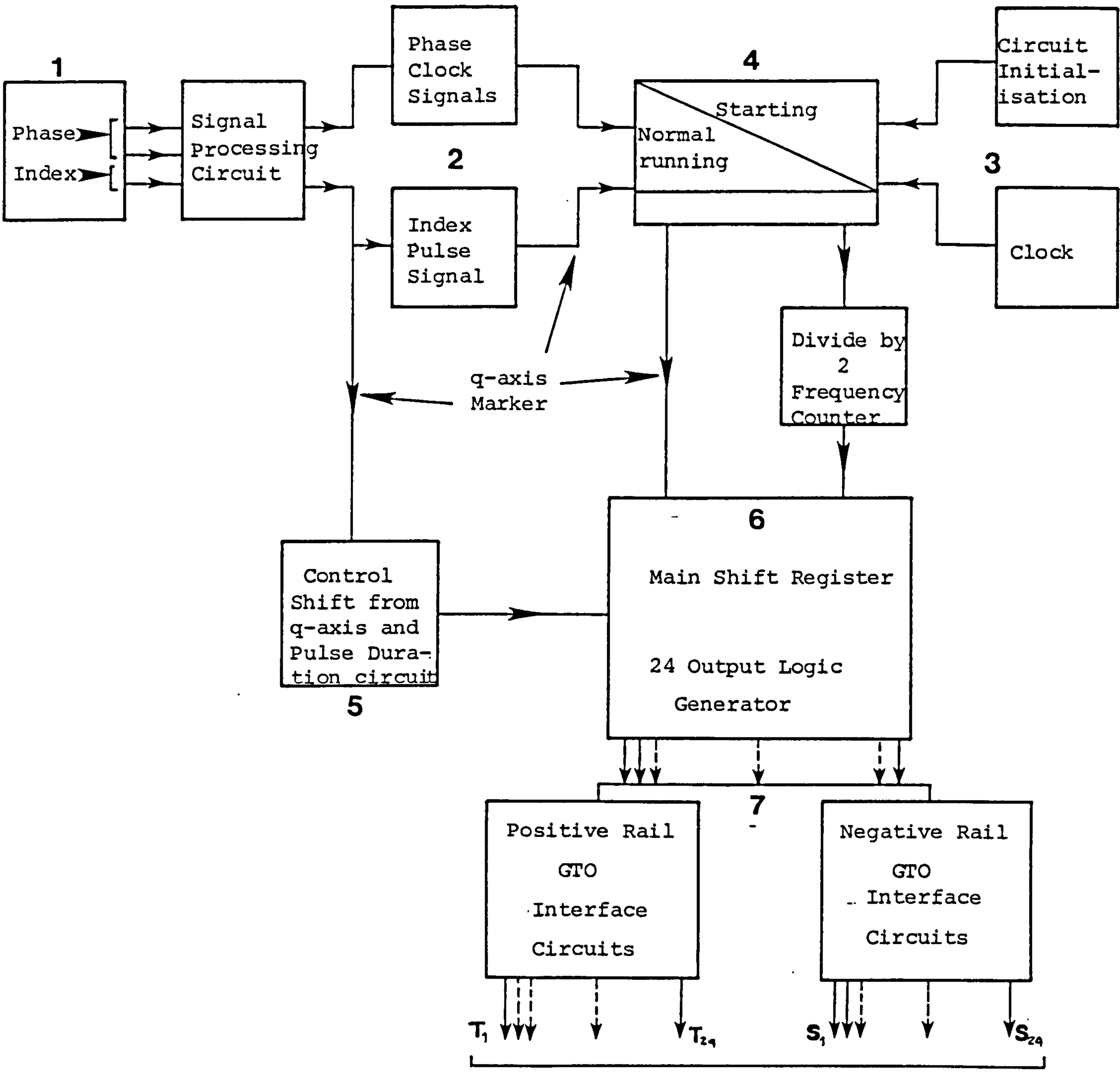

Firing Circuit Drive Logic and Interface

Fig. 5.1 Block Diagram of Digital Control Circuit

5.3 ROTOR VELOCITY AND POSITION FEEDBACK

The function of the feedback element is to control the switching sequence of the armature GTO thyristors in a closed loop system, thus enabling the radial field of the armature winding to maintain its normal space-quadrature relationship with that of the rotor field winding (hence giving optimal torque angle of 90°). A rotary encoder is used as a position sensor that generate pulses in accordance with incremental changes in the angular position of the rotor shaft. Optical rotary encoders are categorised into two main groups [61,62]:

The Absolute type and the Incremental type.

"Absolute type" rotary encoders output the absolute positions of the rotational angles of the input shaft in the form of a specified pulse string (such as Binary coded decimal - BCD codes).

"Incremental type" rotary encoders output pulse strings of two phases - designated as channels A and B; with a 90° phase difference between A and B, corresponding to the rotation of the rotor shaft. These two outputs give the necessary information relating to shaft velocity and rotational direction can be determined from the relative position of these two phases. The absolute position of the input shaft, however, cannot be output directly . To compensate for this, a third output signal - called the "index" pulse, is generated

once per rotation of the input shaft to serve as the reference position signal. The three outputs may then be used in a digital circuit to obtain the absolute position of the shaft.

5.3.1 THE ENCODER USED FOR THIS WORK

A shaft type, optical encoder has been used in this project. The encoder integrates the case, shaft, disc, light detecting/ emitting elements and bearing. Fig. 5.2(i) shows the basic structure of this encoder. The shaft is connected to the motor by a mechanical coupling method.

The essence of an optical rotary encoder [62] is a light beam which is interrupted by a rotating code wheel as shown in Fig. 5.2(i). .To allow for the higher resolution at a given diameter than that achievable by a simple direct-beam interruption method, a mask or "phase plate" is placed in the light path above the photo detectors. The light from the LED can reach the detectors only when the code wheel slits are aligned with the slits on the phase plate, and, since the code wheel is rotating, the detector receives alternating periods of light and dark.

The encoder outputs shown in Fig. 5.2(iii) are available only after the amplification of the photo detectors signals.

5.3.2 ENCODER OUTPUT WAVEFORMS

The rotary encoder used in this work was the Sharp GP1R52 incremental type rotary encoder.

{The data sheet for this encoder is given in Appendix F}.

The encoder gives the following output signals :

output A: an approximate sine wave displaced from the 0V axis, as shown in the oscillogram of Fig. 5.4(i). The peak voltage level of

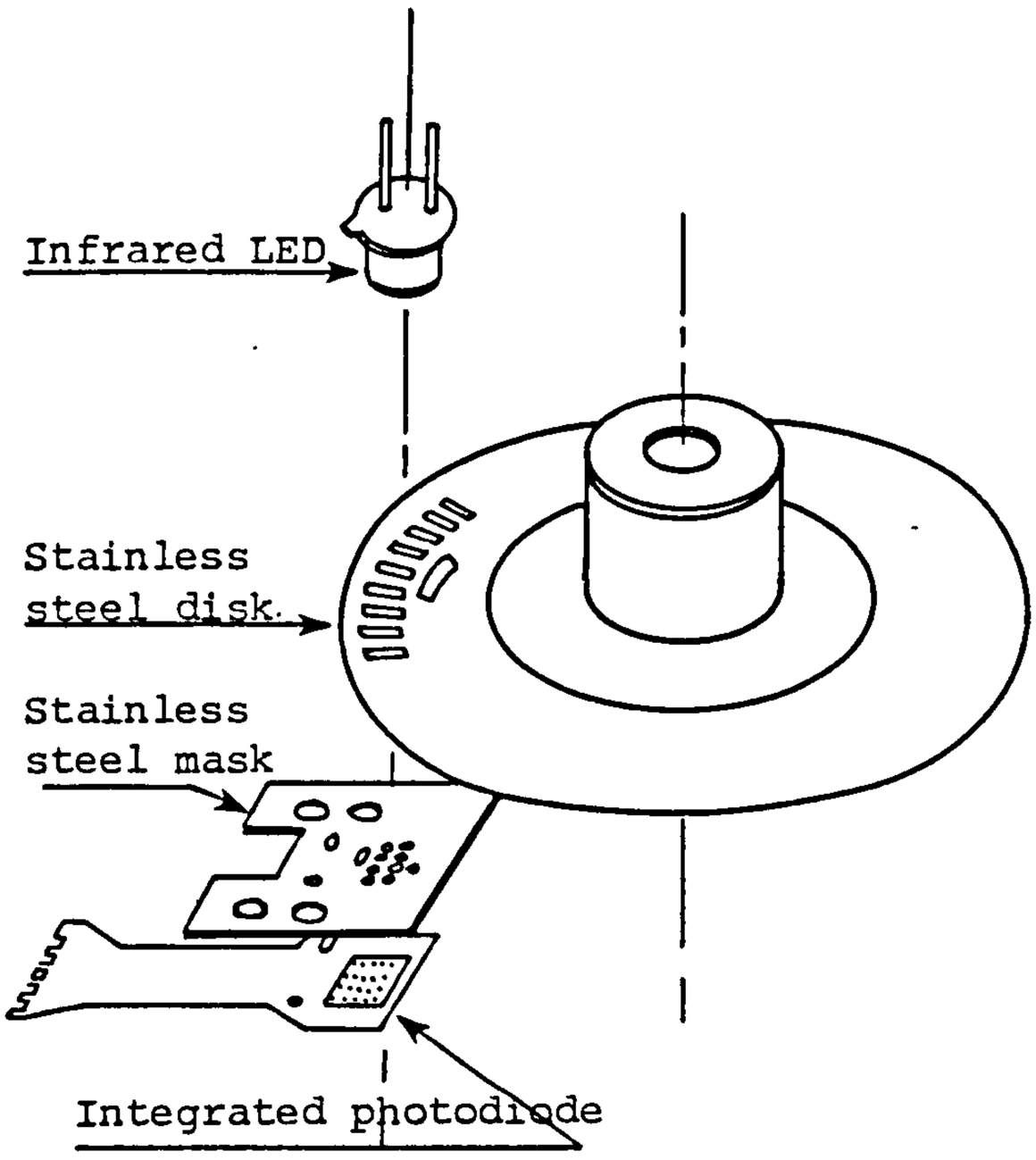

(i) Structure of optical rotary encoder

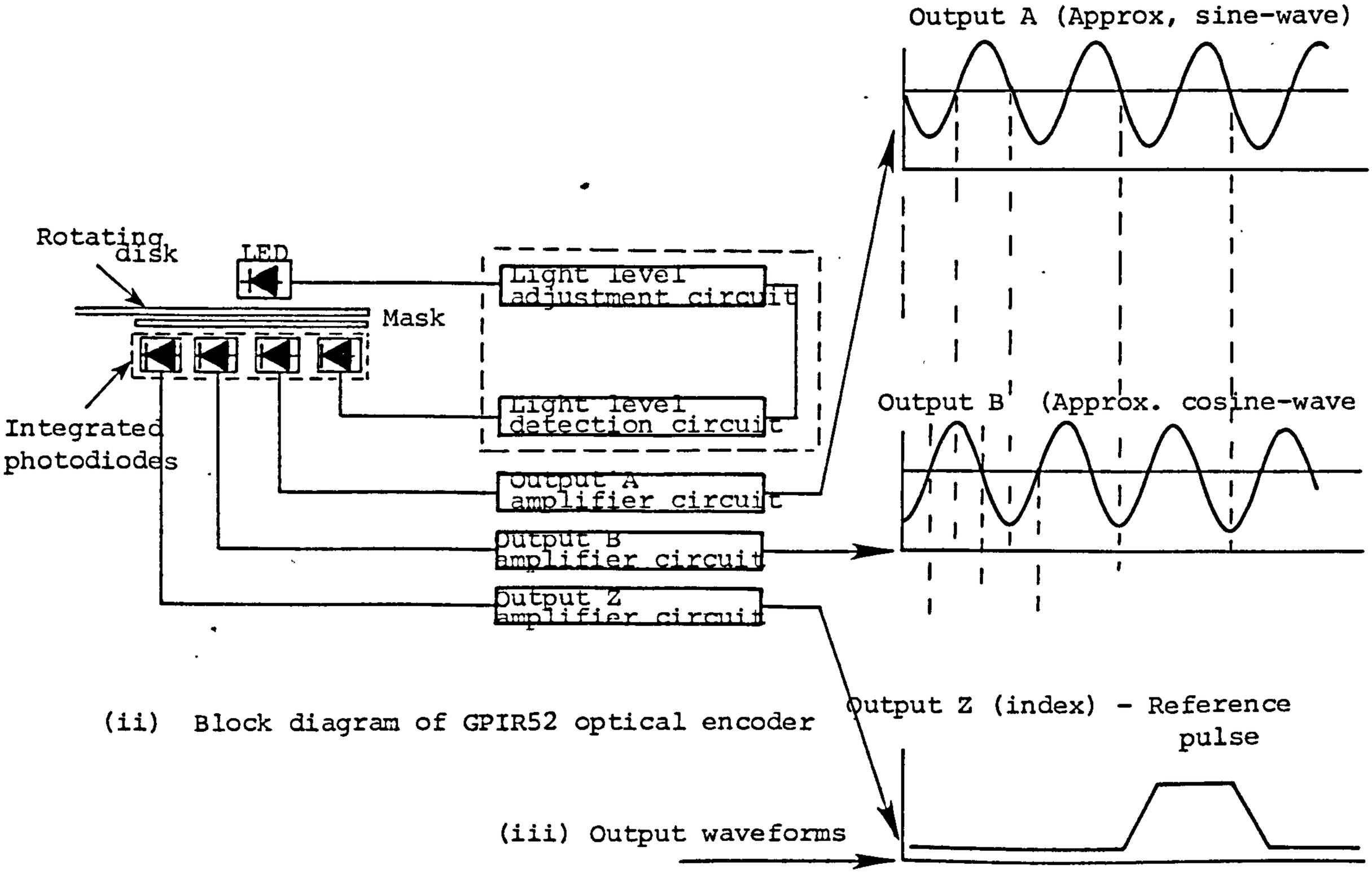

(ii) Block diagram of GPIR52 optical encoder

(iii) Output waveforms

Fig. 5.2 Details of the integrated rotary encoder used in the project

the wave is approximately 3V (measured from the 0V axis) and 96 pulses are generated every single revolution of the shaft.

output B: an approximate cosine wave of similar magnitude and number of pulses as that of output A.

output Z: an "index" pulse which is generated once every revolution of the input shaft, its waveform shown in Fig. 5.4(i).

A block diagram of this encoder with its available outputs is shown in Fig. 5.2 .

The number of pulses per revolution (the resolution) of either output A or B is 96, hence each pulse defines an angular displacement of :

$$360/96 = 3.75^{\circ} \text{ (mechanical)}$$

5.4 IMPLEMENTATION OF THE LOGIC CONTROL ROUTINE

5.4.1 THE SIGNAL PROCESSING CIRCUIT

The shaft encoder gives analog outputs {shown in oscillogram of Fig. 5.4(i)} which are not directly suitable for interfacing with the digital control circuit. A signal processing circuit is designed to obtain the correct TTL logic level signals.

The signal processing circuit is shown in Fig. 5.3(i). Schmitt trigger circuits are used to square the signals available from the encoder. The voltage level of the index pulse (output Z) is low (typically of the order of 1.25 V) thus unable to drive the Schmitt trigger circuit (G_3), hence a pulse amplifying circuit is used to

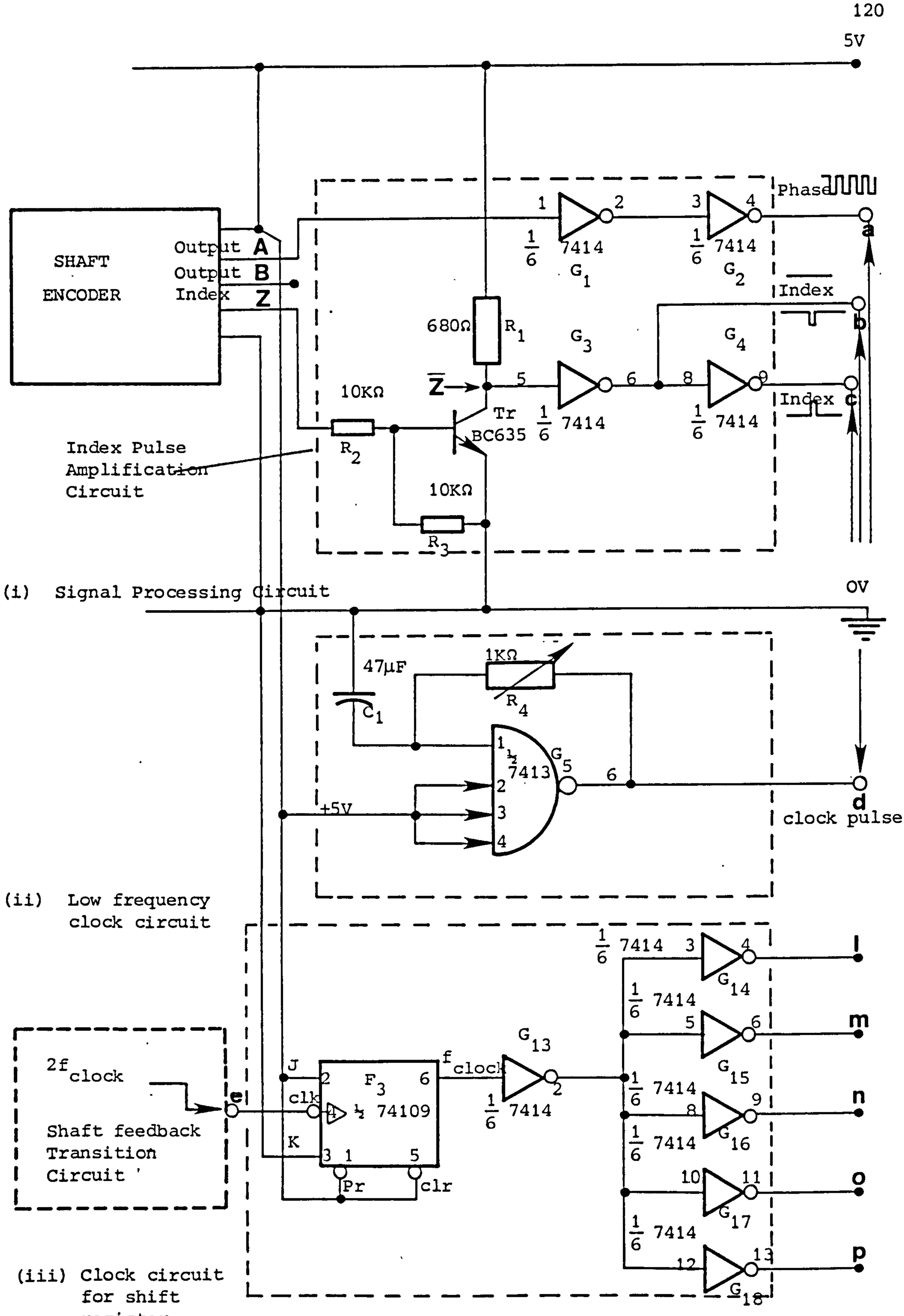

Fig. 5.3 Components of Digital Control Circuit

give the correct voltage level at Z`.

Fig. 5.4(ii) gives the oscillogram of the output of pulse shaping circuit.

5.4.2 STARTING ROUTINE

A problem is apparent at the instant of starting, when the shaft is at standstill, as no index or phase output is available from the encoder until the rotor has rotated through an indeterminate angle. The required switching procedure for the armature GTO thyristors is therefore, not known. The correct sequence of switching will only be known when the index pulse has arrived and output is available from encoder channels A or B (called the phase outputs). To overcome this problem, a separate, low frequency clock is used at the time of starting to rotate the switching of the armature devices, inching the armature field, corresponding to a limited armature current, in the desired direction of rotation. As the torque angle increases due to the relative movement between the stator and rotor fields, sufficient torque will sooner or later be developed to accelerate the rotor away from standstill and, once motion is established, output pulses are provided by the encoder. When the encoder index pulse is generated (implying also availability of phase outputs), the exact angular position of the rotor is known and clocking of the flip-flops of the main shift register (section 5.4.5) can be synchronised by the feedback information from the shaft encoder.

The circuit to obtain the low frequency clocking is shown in Fig. 5.3(ii). A quad-input NAND gate Schmitt trigger circuit (G_5) is

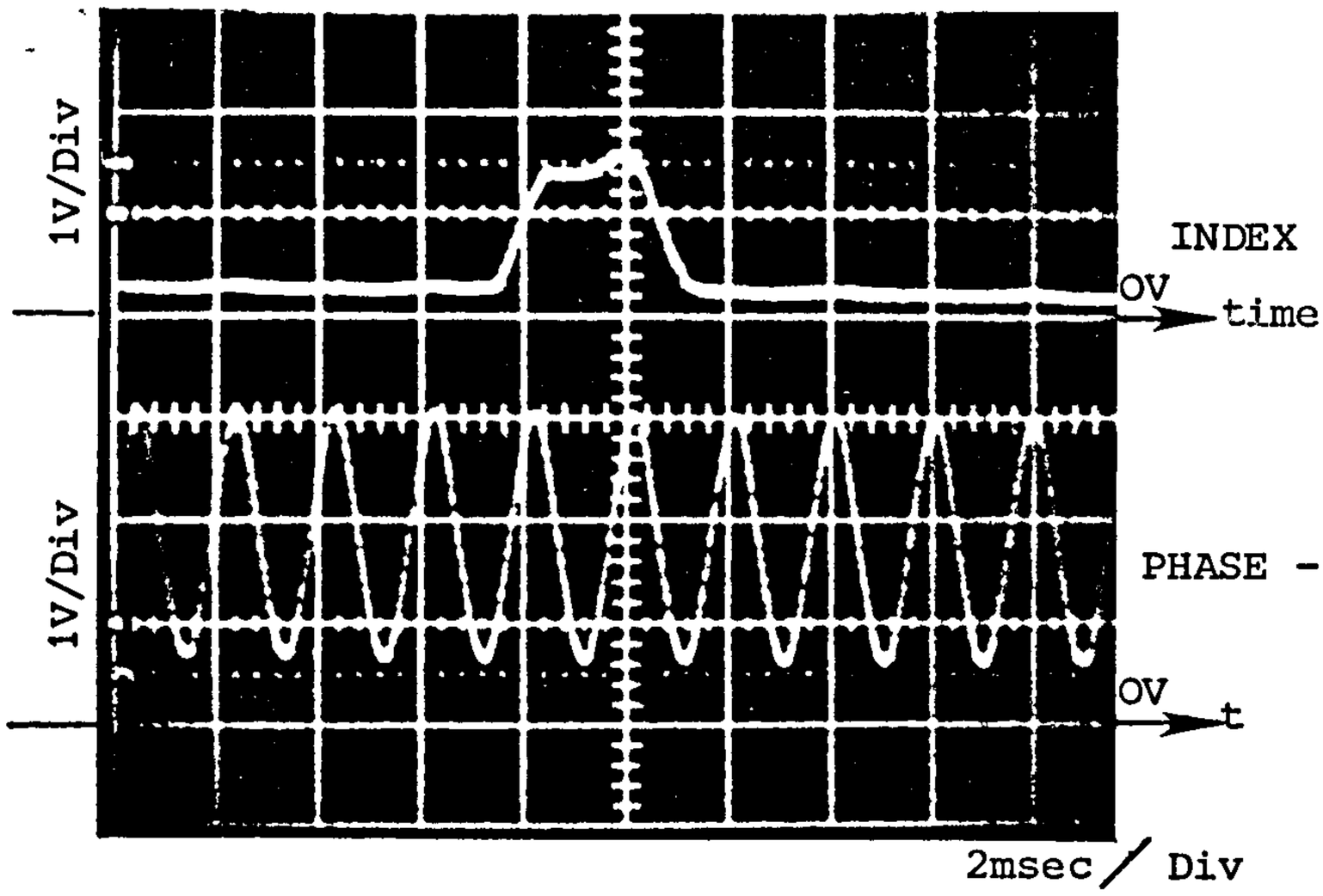

(i) Encoder Analog Output Waveforms

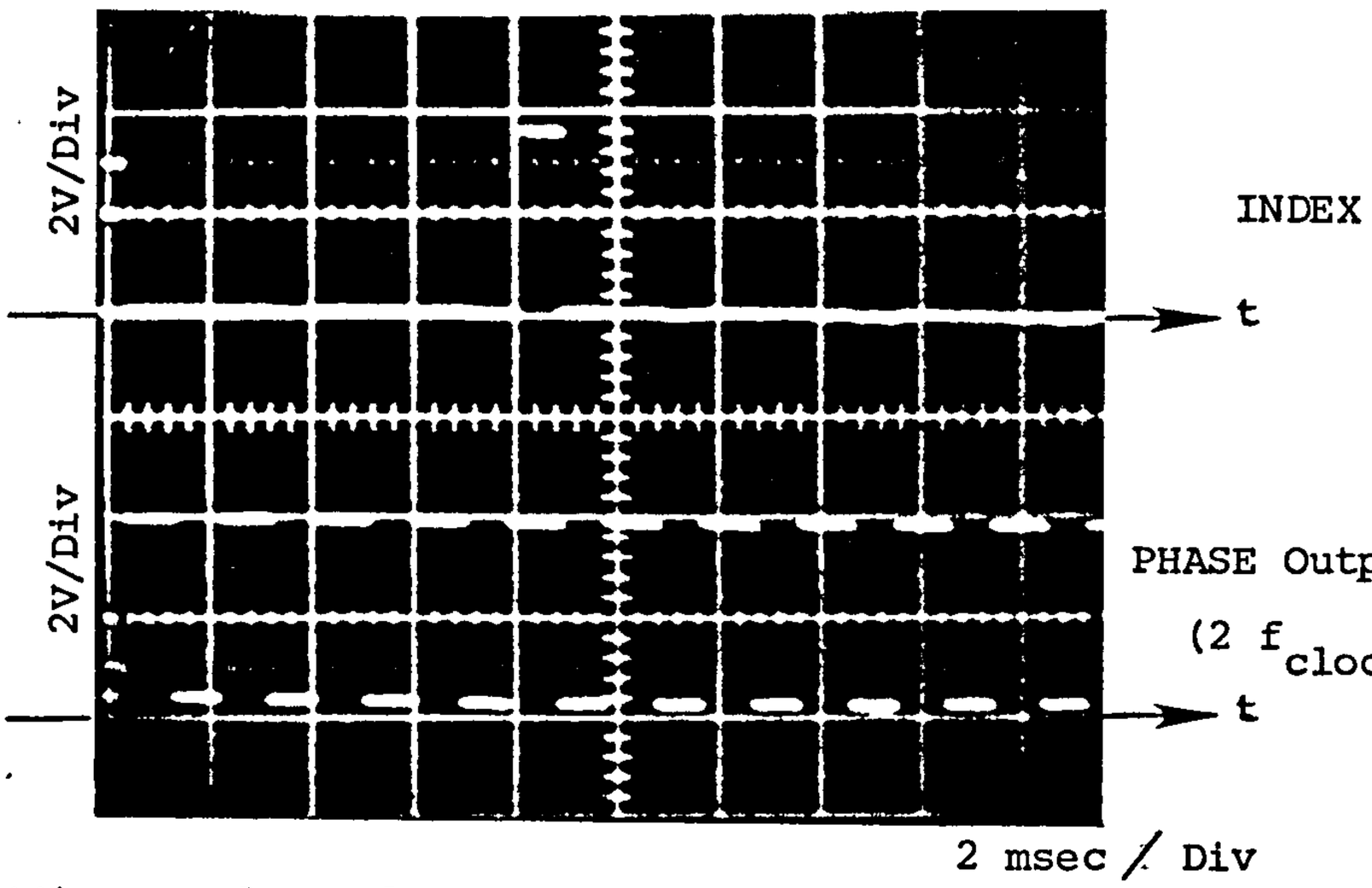

(ii) Encoder Pulse Shaping Circuit Output

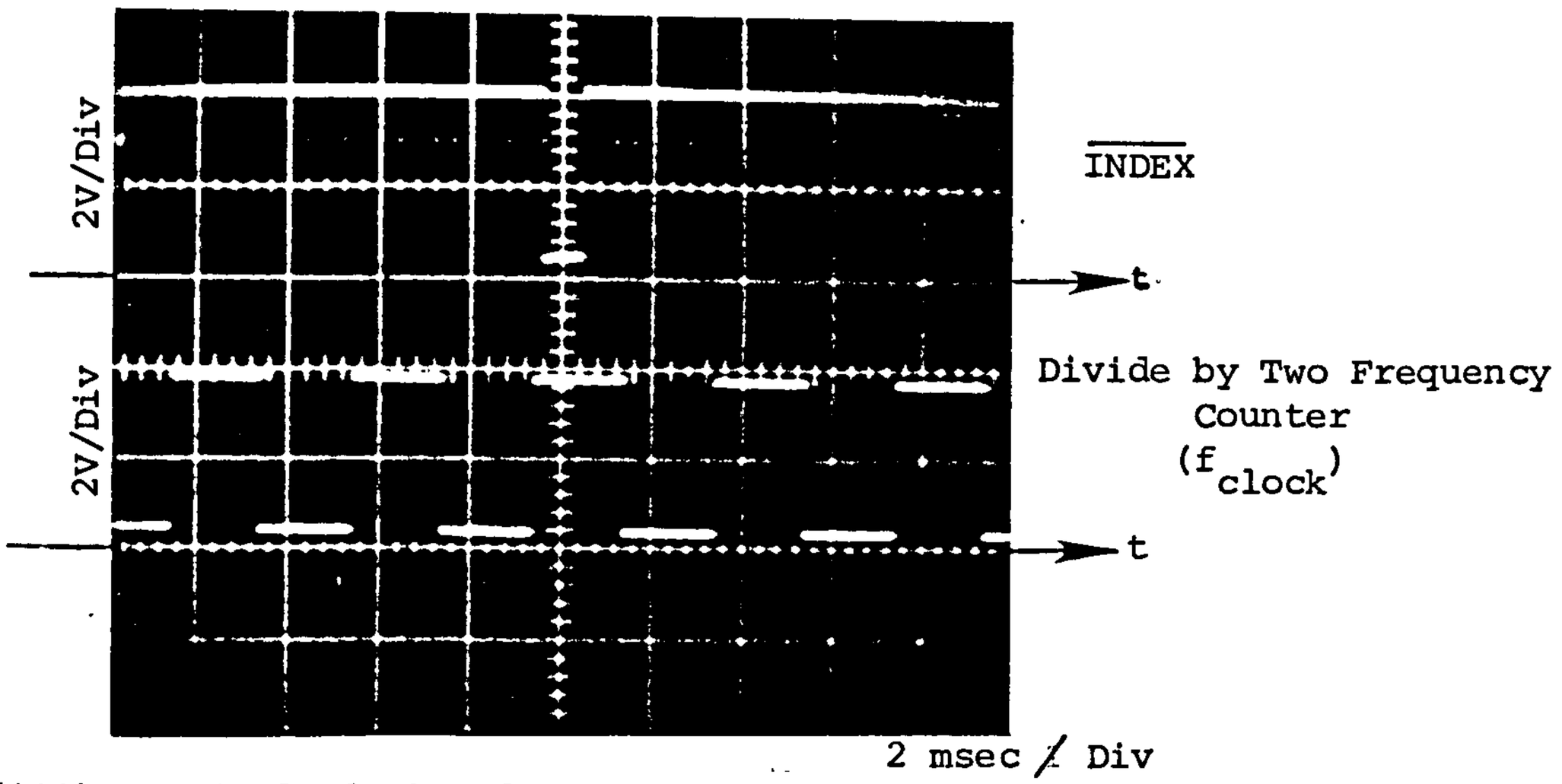

(iii) Digital Clock Pulses Proportional to Speed

Fig. 5.4 Oscillogram of Encoder Pulse Conditioning Circuit

used with one of its inputs connected to an RC network. The value of C_1 is fixed at 47 μF and the value of R_4 is adjusted to give the required frequency. The NAND gate is also a Schmitt trigger circuit which gives the necessary squaring of edges of the clock pulses. Using this circuit, the frequency can be changed within a certain range, if desired. The output frequency of the clock was fixed at 16 Hz. The division by two using the "divide by 2" frequency counter (section 5.4.4), will give 8 Hz. Therefore the shift register is initially clocked at a frequency of 8 Hz. The function of the low frequency clock was simply to get the rotor moving away from standstill and the frequency chosen was suitable to give this function.

5.4.3 SHAFT FEEDBACK TRANSITION ROUTINE

The circuit which performs the transition to the shaft feedback information is shown in Fig. 5.5. It utilises two counters C_1 and C_2, two D-type flip-flops F_1 and F_2, AND gates G_7, G_8, G_9, G_{10} and OR gates G_{11} and G_{12}. Switch S_R is the "resetting switch" for initialisation of the network. When S_R is reset, the output of F_2 (Q_{F_2}) is forced to go low and complement output of F_1 ($\bar{Q}_{F_1}$) goes to logic high. This "enables" the output of the low frequency clock to be available at G_8 (and therefore at 'e'). The clocking of the main shift register circuit (described in section 5.4.5, Fig. 5.6), is therefore initially done by the low frequency clock. Once the rotor has moved away from standstill, output will be available from 'a', 'b' and 'c' of the encoder signal processing circuit. When the index pulse arrives at 'a', counter C_2 "ripple carry output" (Rc_2) goes high, forcing Q_{F_2} to go high, $\bar{Q}_{F_1}$ to go low. Therefore the

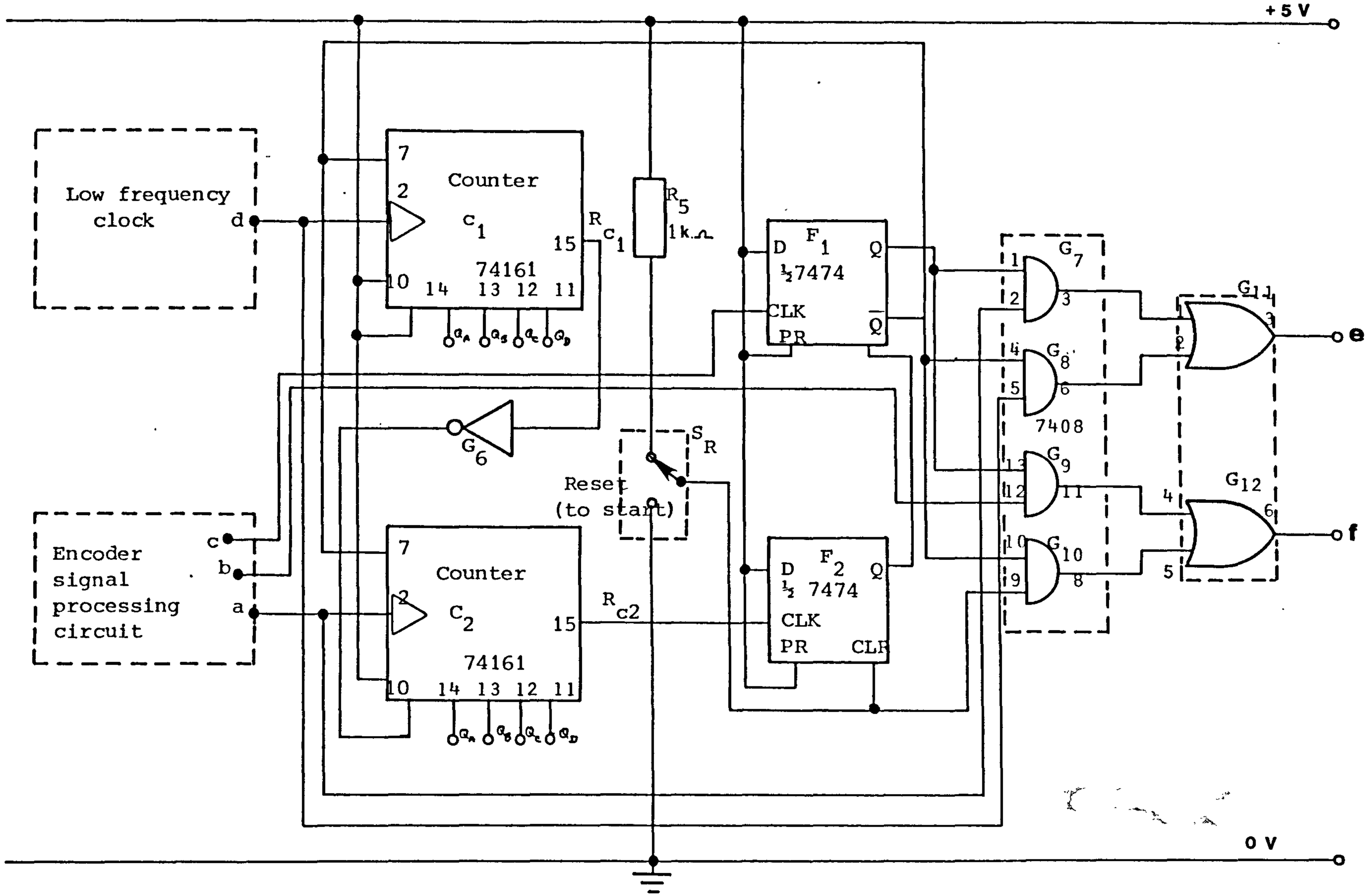

Fig. 5.5 Shaft feedback transition circuit

output of G_8 is disabled and G_7 outputs the shaft encoder clock pulses. Also G_{10} is disabled and the encoder index pulse is enabled at the output of G_9 .

To conclude, at starting the low frequency clock is available at 'e' and "reset" pulse at 'f'. These two are disabled immediately the index pulse is generated by the encoder, and thereafter, the encoder clock pulses are available at 'e' and index pulse at 'f'.

5.4.4"DIVIDE BY"TWO FREQUENCY COUNTER

With the resolution of the encoder at 96 pulses per revolution, it is clear that the encoder frequency {at 'a'-Fig. 5.3(i)} is twice that required for clocking the shift register; this can be deduced from the following :

Consider the rotor running at 1000 rpm :

Encoder output frequency at this speed (in Hz)

$$= 1000 \times 96/60 = 1600 \text{ Hz}$$

From the graph of Fig. 3.11 it is clear that the digital clock frequency required for this speed is 800 Hz.

Therefore it is necessary to halve the encoder frequency. This is achieved using an edge triggered J-K flip-flop (F_3) used in the toggle mode. The circuit for this is shown in Fig. 5.3(iii). Five Schmitt triggers (G_{14} - G_{18}) were used to obtain the clock pulses for the flip-flops of the shift register {the five Schmitt triggers are necessary to give low "fan-out" [65] on these gates}.

5.4.5 THE MAIN SHIFT REGISTER [67]

The function of this circuit is to generate the logic pulses which define the conduction periods of armature GTO thyristors. D-type edge triggered flip-flops are used in a ring counter as shown in Fig. 5.6. The shift register is designed in such a way that, under normal running conditions the output of Q1 goes to logic high when the shaft encoder index pulse is generated, corresponding to maximum torque angle of 90°.

The operating mode of the main shift register can best be understood by referring to the timing diagrams of Figures 5.8 and 5.9, and the main shift register circuit shown in Fig. 5.6.

Appropriate clock pulses are applied at points l, m, n, o and p (Fig. 5.6) obtained from the "divide by two" frequency counter circuit" (Fig. 5.3). These clock pulses have fast rising edges, each clock pulse defining an angular displacement of 7.5° (electrical). Under normal operating conditions, when the radial field of the armature winding is required to be in space quadrature with that of the main field winding, output Q_1 of flip-flop Dl is required to go high when the index pulse is generated, and all other outputs are required to be low.

i.e. Q_2, Q_3, ---- Q_{24} are at logic low, as shown in Fig. 5.8(i).

This is done by "presetting" flip-flop Dl (preset = logic high), and "clearing" flip-flops D2, D3 ---- D24 (clear = logic low) at the instant when the index pulse is generated. The outputs of the remaining flip-flops are thereafter sequentially generated at the positive edges of the clock pulses.

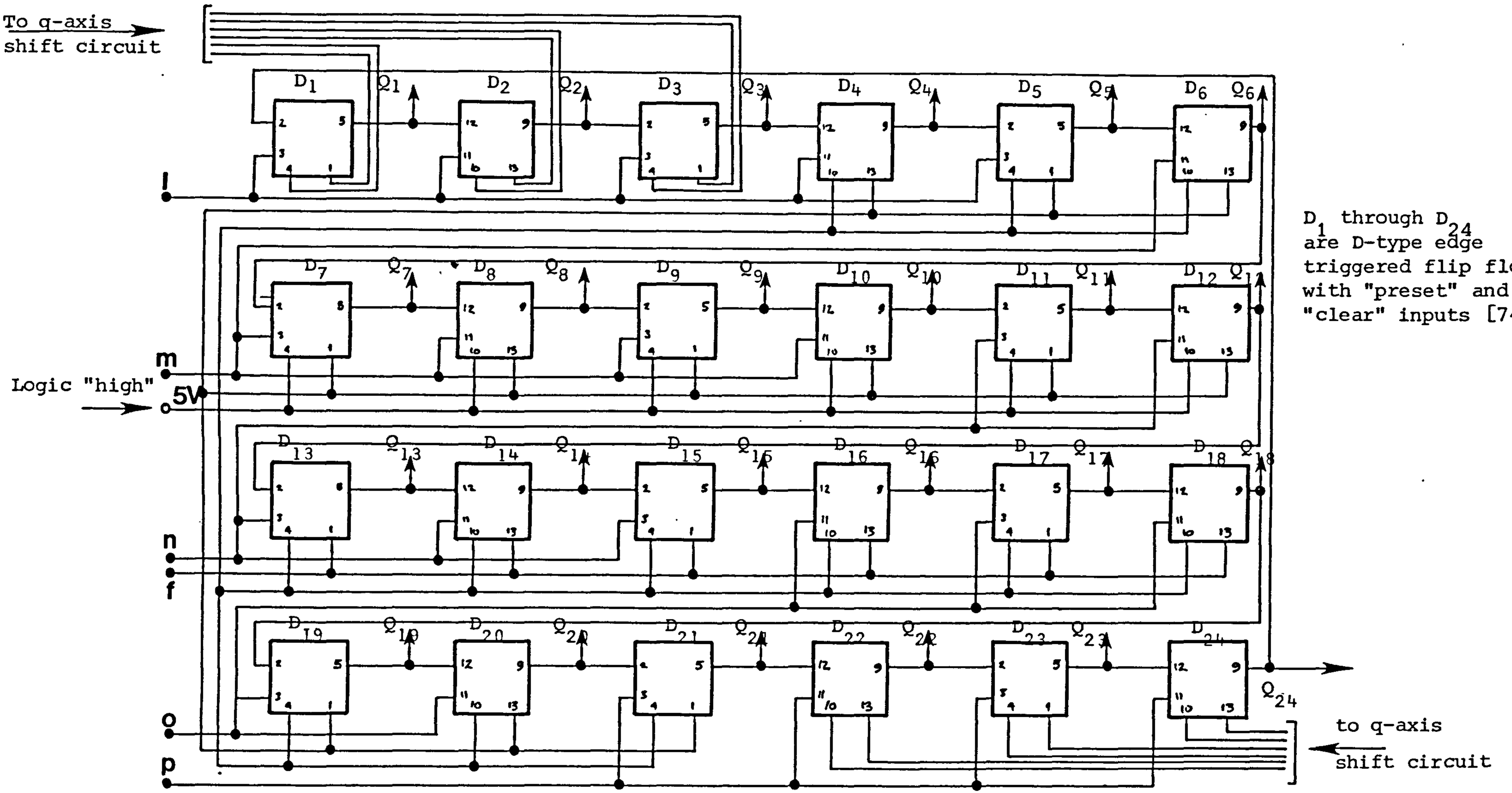

D_1 through D_{24} are D-type edge triggered flip flop with "preset" and "clear" inputs [7474]

Fig. 5.6 Main shift register circuit - 24 output logic generator

To ensure that the output logic signals of the main shift register are maintained in the correct sequence, the index pulse is used for resetting and synchronisation of the shift register flip-flops every single revolution of the rotor shaft. This safeguards against any possibility of malfunction occurring within the shift register and in this case, it also means that the correct GTO armature switch is pulsed to obtain the required torque angle. The generation of the correct pulses is clearly shown in the timing diagram of figures 5.8 and 5.9.

5.4.6 CONTROLLED DEPARTURE FROM THE QUADRATURE-AXIS POSITION

The possibility of controlled departure of the axis of the radial field of the armature winding from the quadrature-axis position (i.e optimal torque angle) was incorporated using the circuit of Fig. 5.7, by the redirection of the index pulse using the "enabling" switches S1 to S6 and bi-stable latches B1 to B6 .

For a "forward" shift of the radial field of the armature winding from the quadrature axis, the outputs of flip-flop D1 and D2 (i.e. Q_1 and Q_2) are made to go high when the index pulse is generated. This is done by initialisation of bistable latches B4 and B5 to logic high, and all the other latches (i.e. B1, B2, B3, B6) to logic low. This will result in the index pulse being "directed" to "preset" of flip-flops D1 and D2, and to "clear" of all the other flip-flops in the shift register. This will give a forward shift of 7.5° (one clock pulse). The timing diagram for this case is shown in Fig. 5.9(i).

For a "backward" shift of the radial field of the armature winding from the q-axis, the output of flip-flops D23 and D24 (i.e.

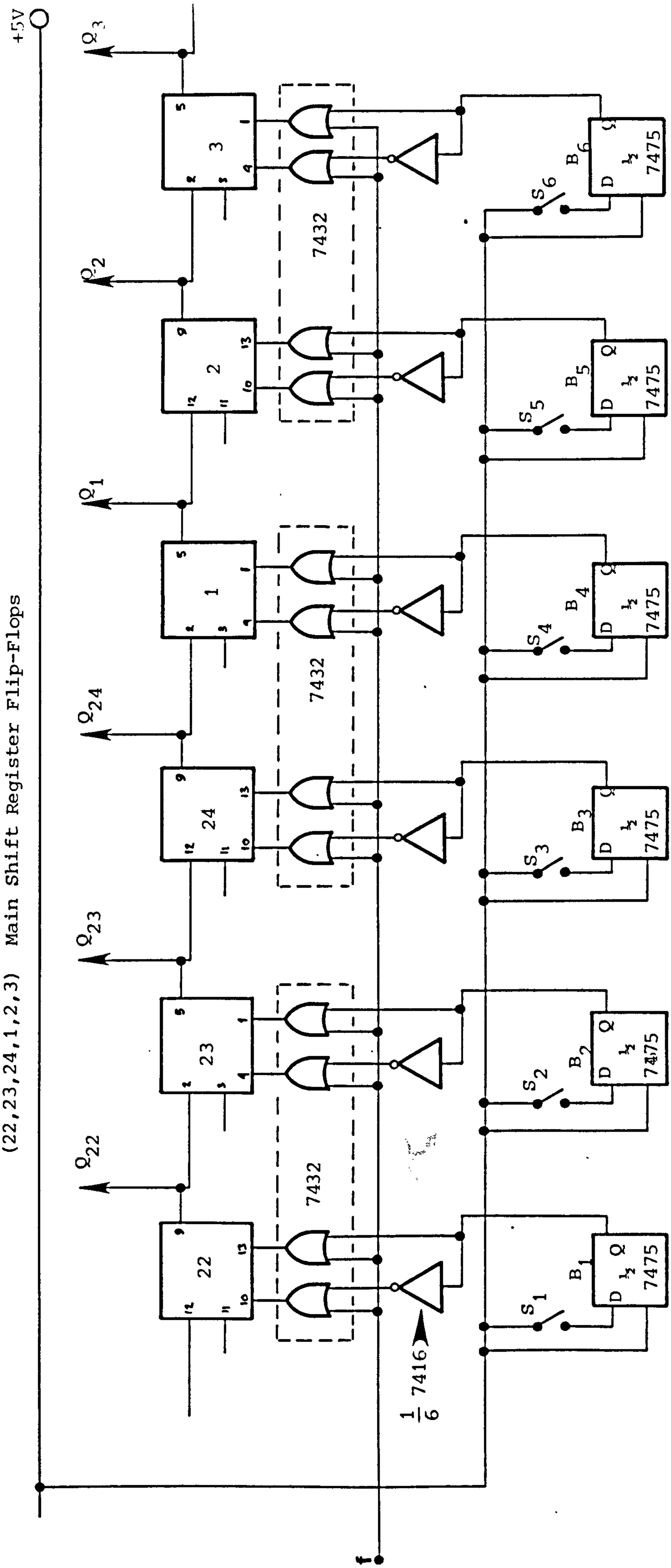

(22,23,24,1,2,3) Main Shift Register Flip-Flops

Fig 5.7 Circuit for controlled departure from the q-axis

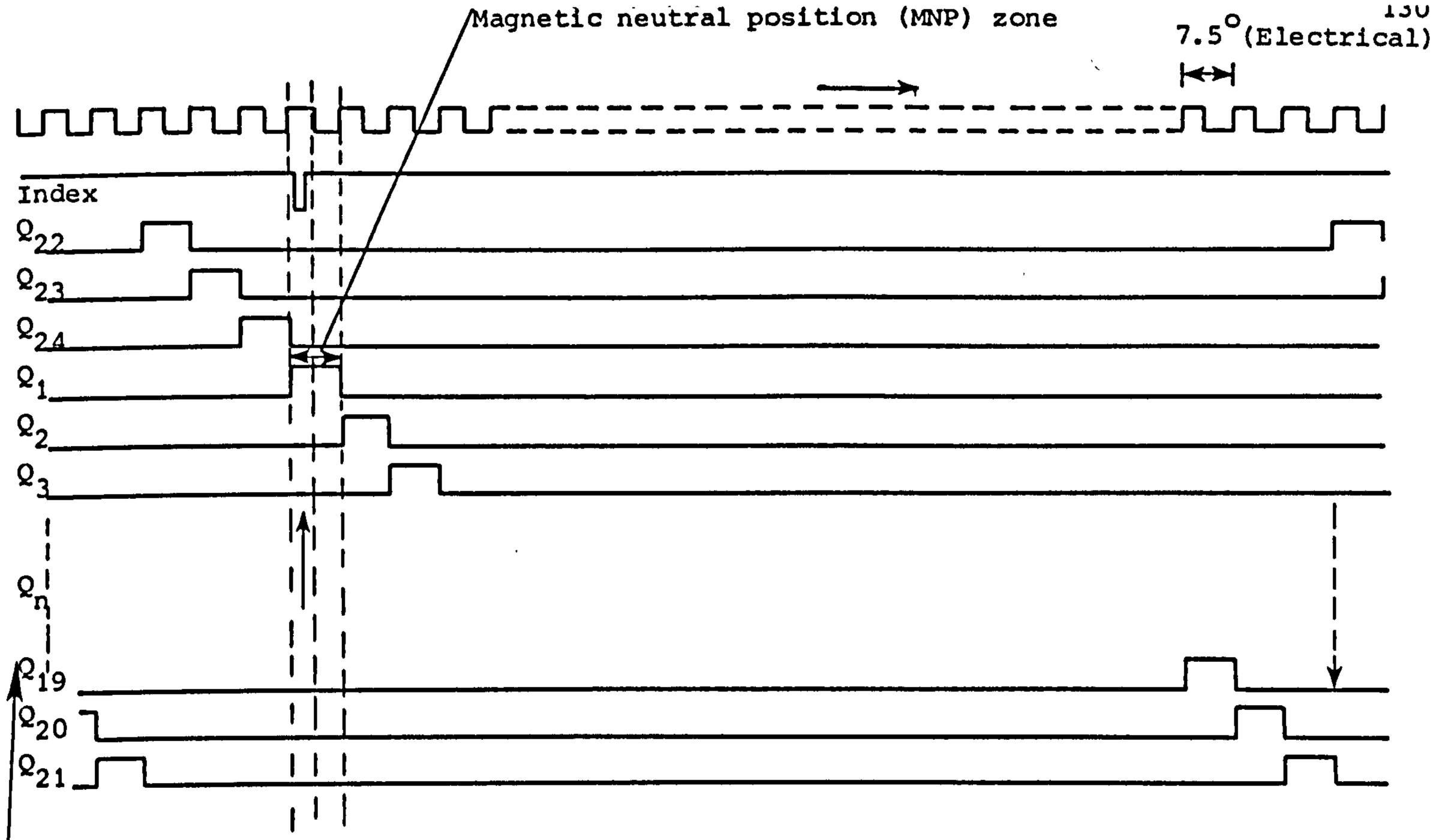

(i) Index pulse coincident with MNP zone - Q_1 High at q-axis

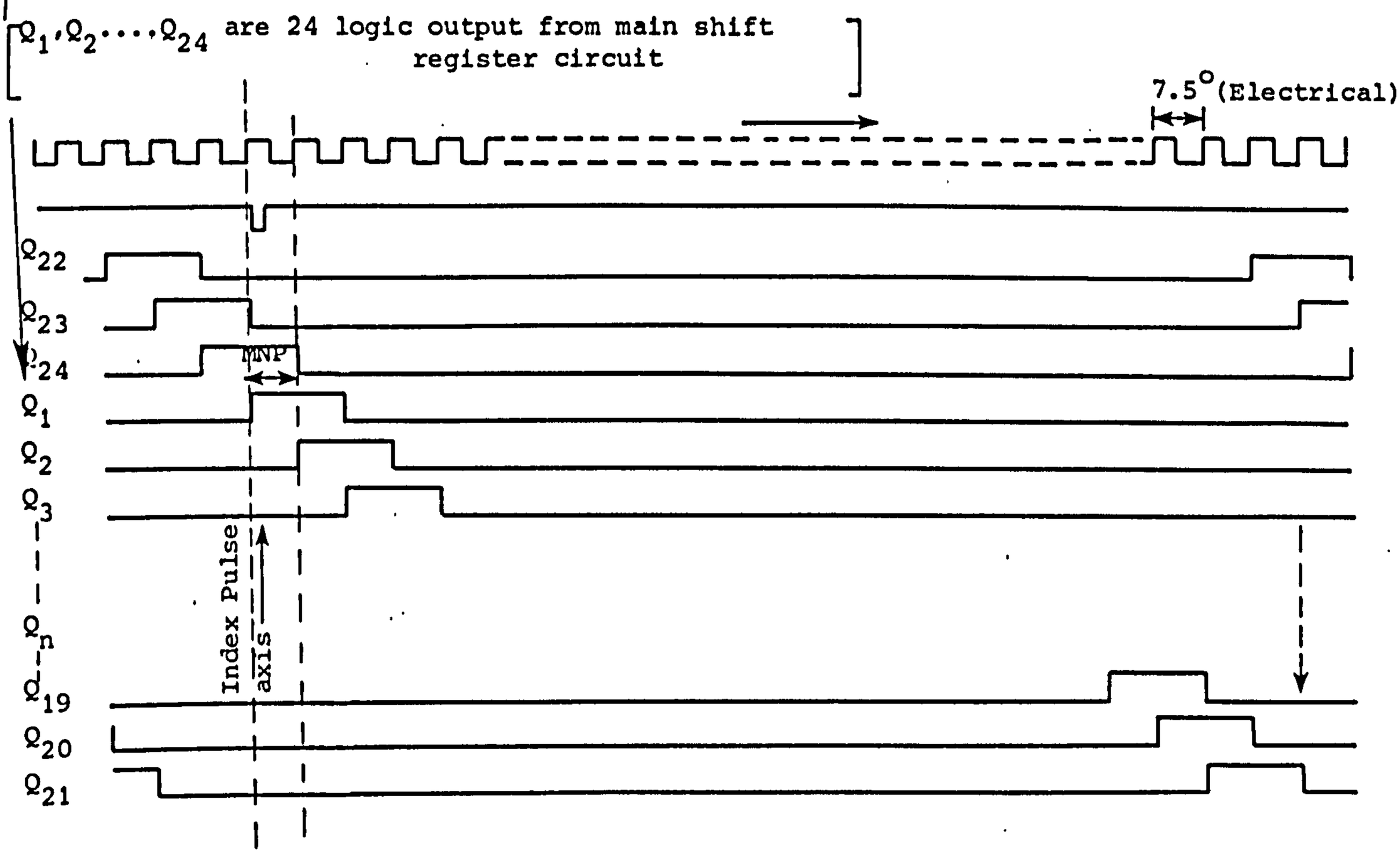

(ii) Index pulse coincident with MNP zone - Q_1 & Q_{24} high at q-axis

Fig. 5.8 Timing diagram - maximum torque angle

Q_{23} and Q_{24}) are made to go high when the index pulse is generated. In a similar way, bistable latches B2 and B3 are initialised to logic high and all the other latches (B1, B4, B5, B6) to logic low. This will "direct" the index pulse to "preset" of flip-flops D23 and D24 and to "clear" of all the other flip-flops in the shift register circuit, giving a backward shift of 7.5°. The timing diagram for this case is shown in Fig. 5.9(ii). Table 5.1 shows few examples of various other possibilities with the timing diagram of four of these possibilities shown in figures 5.8 and 5.9.

Fig. 5.10 depicts oscillograms of the logic control circuit output, illustrating an example of forward shift of the axis of the index pulse with respect to the quadrature axis. The sequential triggering pulses applied to the opto-isolation circuits of armature GTOs (T_1,S_{13}) and (T_2,S_{14}) is shown in Fig. 5.10(iii).

5.5 DETERMINATION OF QUADRATURE-AXIS OF THE MACHINE

During normal running conditions of the machine, the axis of the radial field of the stator (armature) winding is maintained in space quadrature with the radial field of the rotor (field) winding. In a conventional DC machine, this corresponds to the setting of the brushes on the geometric neutral or quadrature axis.

It is therefore necessary to determine the instantaneous position of the quadrature axis in order to maintain the 90° relationship between stator and rotor radial fields. This axis is physically marked and subsequently during setting-up procedures the shaft encoder is adjusted so that the index pulse appears when this marked

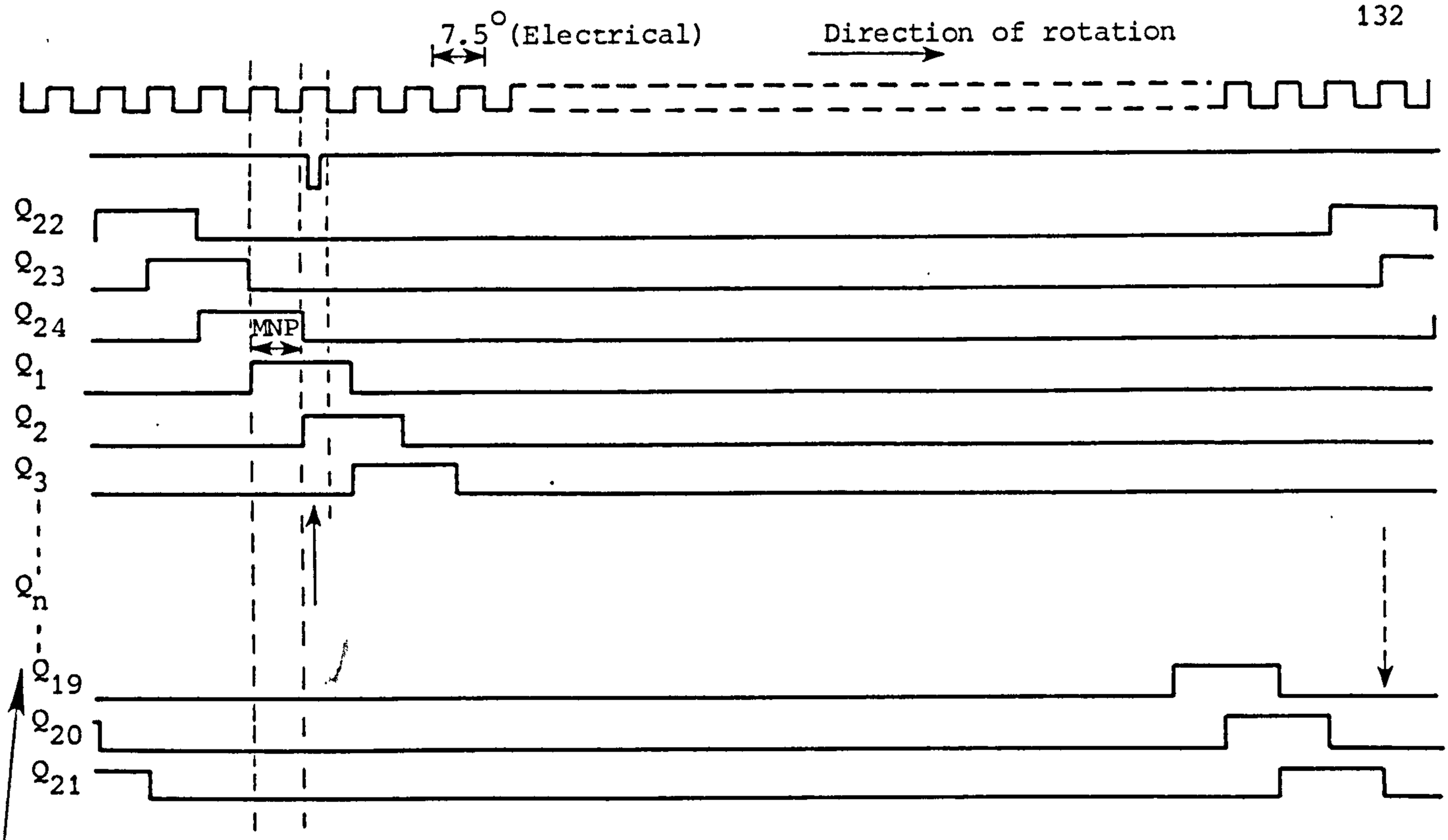

(i) Forward shift of index pulse axis w.r.t. q-axis position

[Q_1, Q_2....Q_{24} are 24 logic output of main shift register]

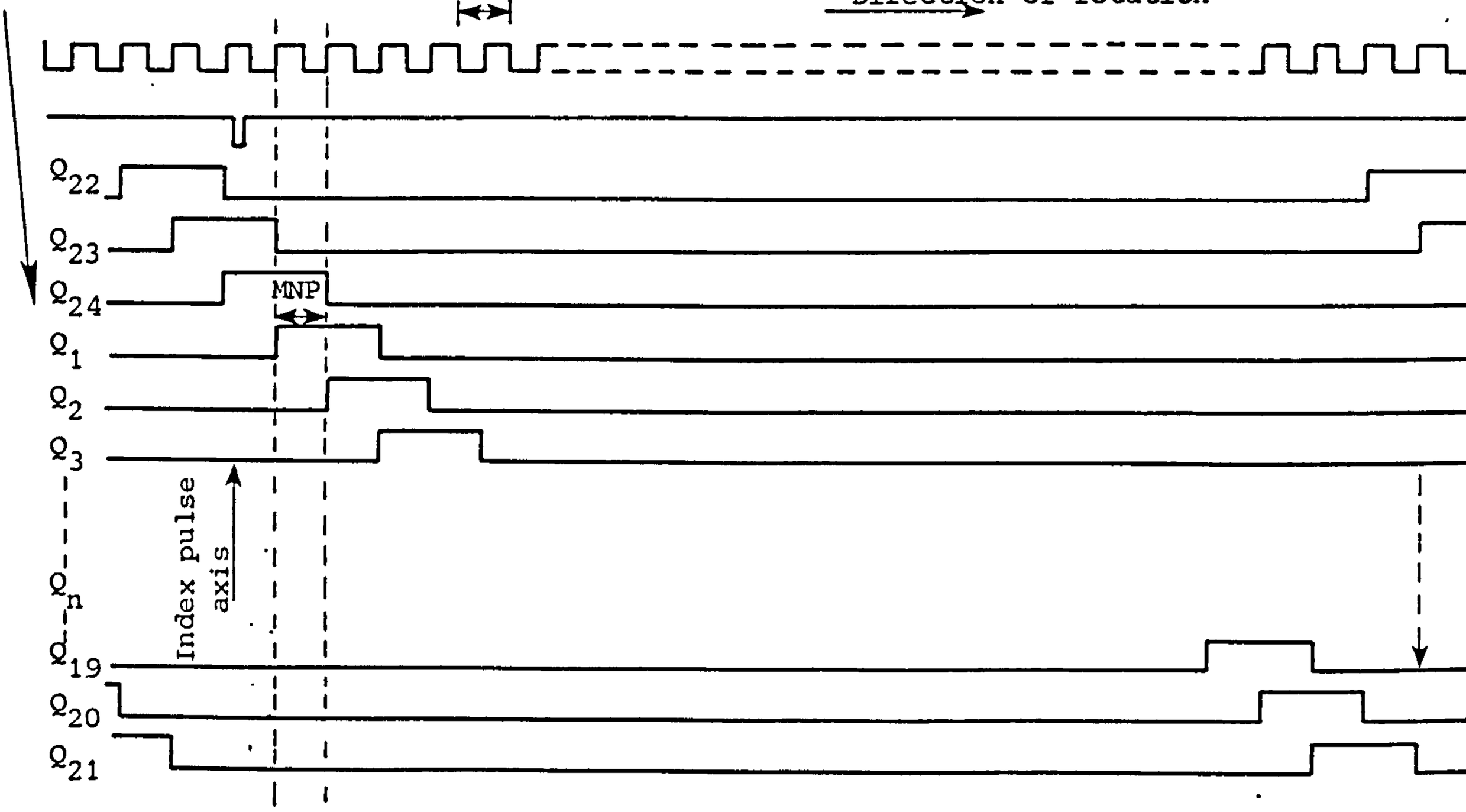

(ii) Backward shift of index pulse axis w.r.t. q-axis position

Fig. 5.9 Timing diagram - "Forward" and "Backward" shift of index pulse axis

Output high at index axis		Controlled Shift with respect to q - axis position
S1,S2=H	*Q22,Q23=H	
S2,S3=H	*Q23,Q24=H	Backward shift of index pulse axis, Fig.5.9(ii)
S3,S4=H	*Q24,Q1 =H	index pulse coincident with q-axis, Fig.5.8(ii)
S4,S5=H	*Q1 ,Q2 =H	Forward shift of index pulse axis, Fig.5.9(i)
S5,S6=H	*Q2 ,Q3 =H	
S2=H	** Q23=H	Backward shift of index pulse axis (-15°)
S3=H	** Q24=H	Backward shift of index pulse axis (-7.5°)
S4=H	** Q1 =H	index pulse coincident with q-axis position Figure 5.8 (i) - maximum torque angle
S5=H	** Q2 =H	Forward shift of index pulse axis (+7.5°)
S6=H	** Q3 =H	Forward Shift of index pulse axis (+15°)

* Two shift register outputs high at index Pulse axis - overlapping .

** One shift register output high at index pulse axis - sequential triggering .

TABLE 5.1

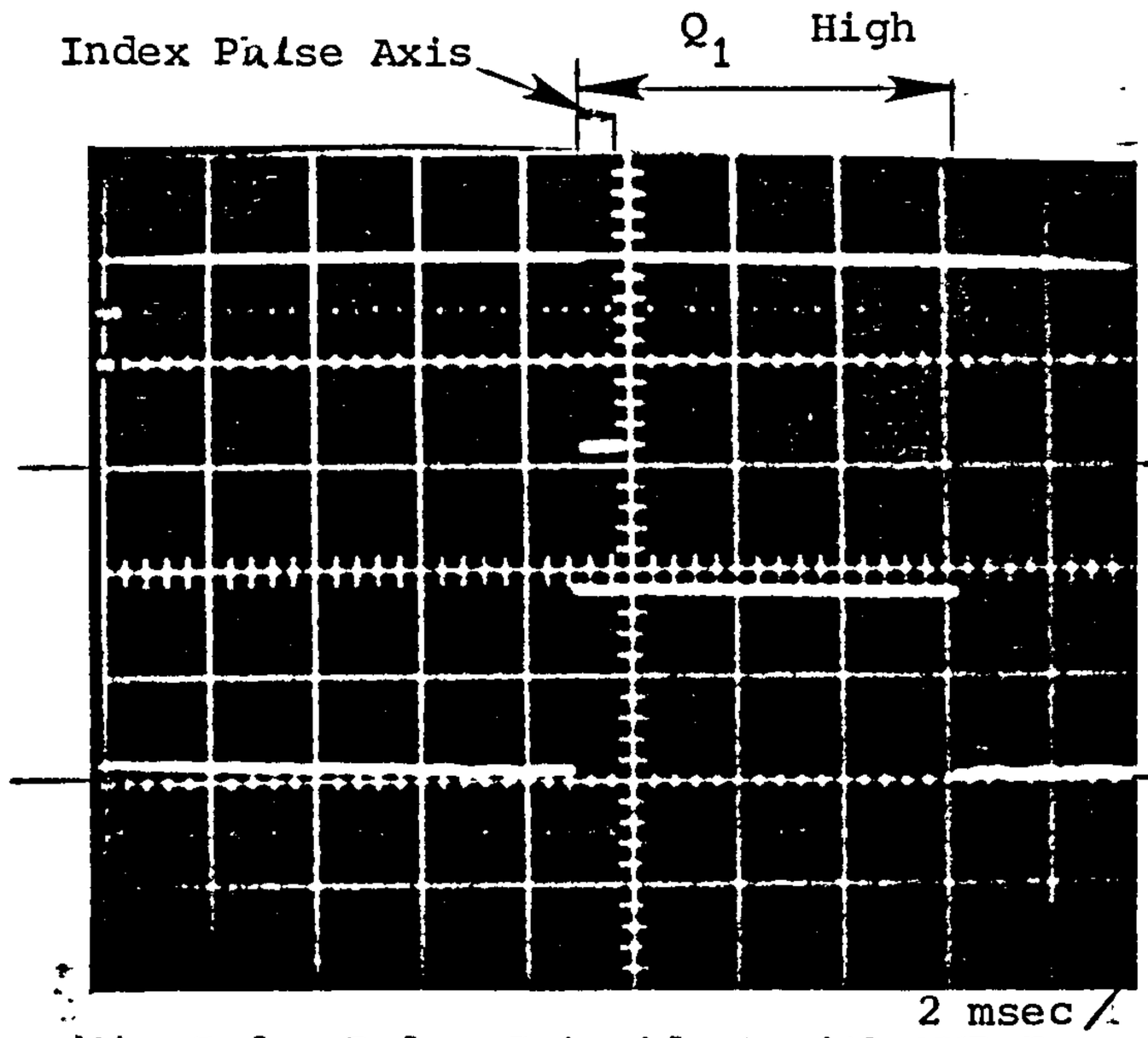

(i) Index Pulse Coincident with MNP Zone

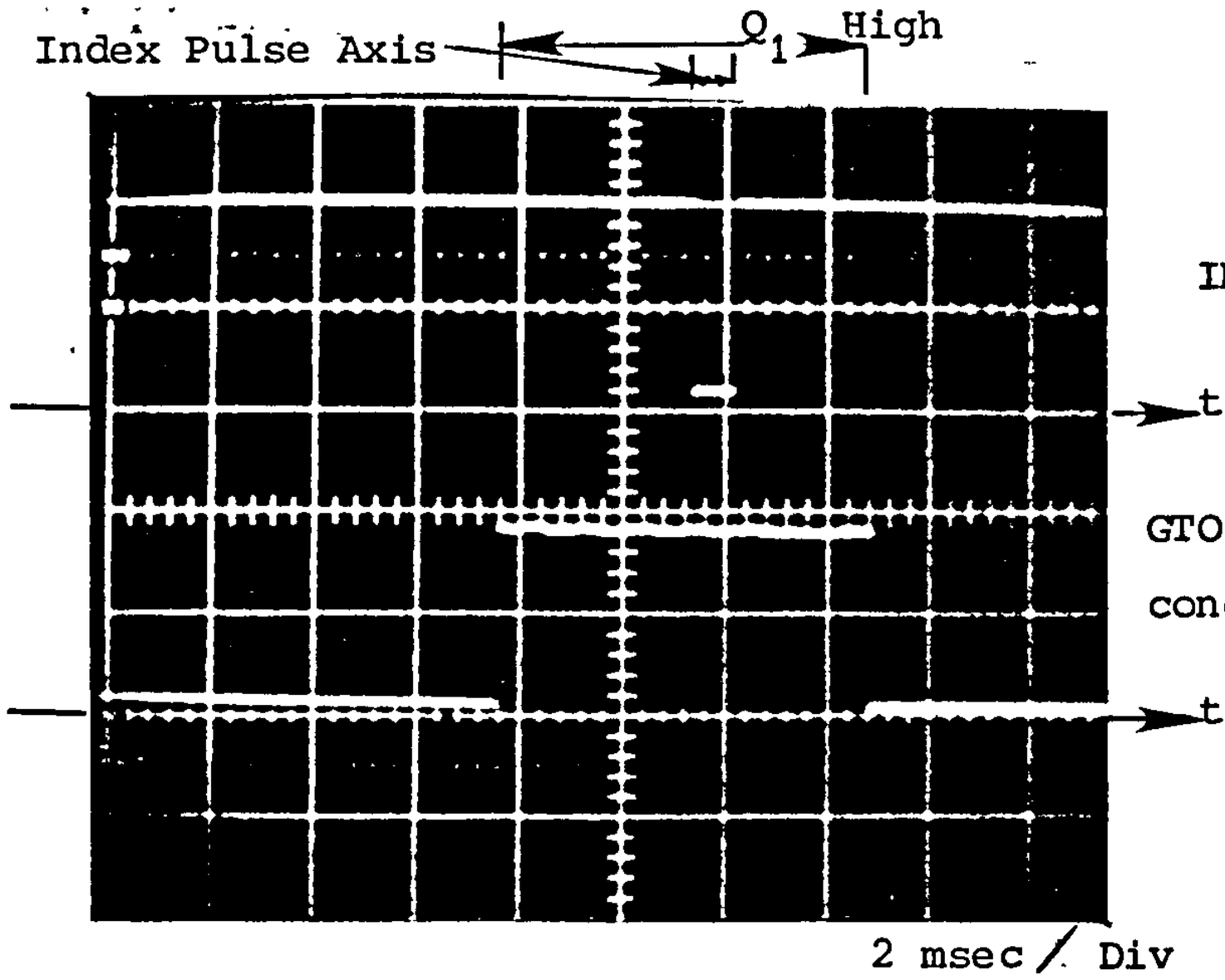

(ii) Forward Shift of Index Pulse Axis

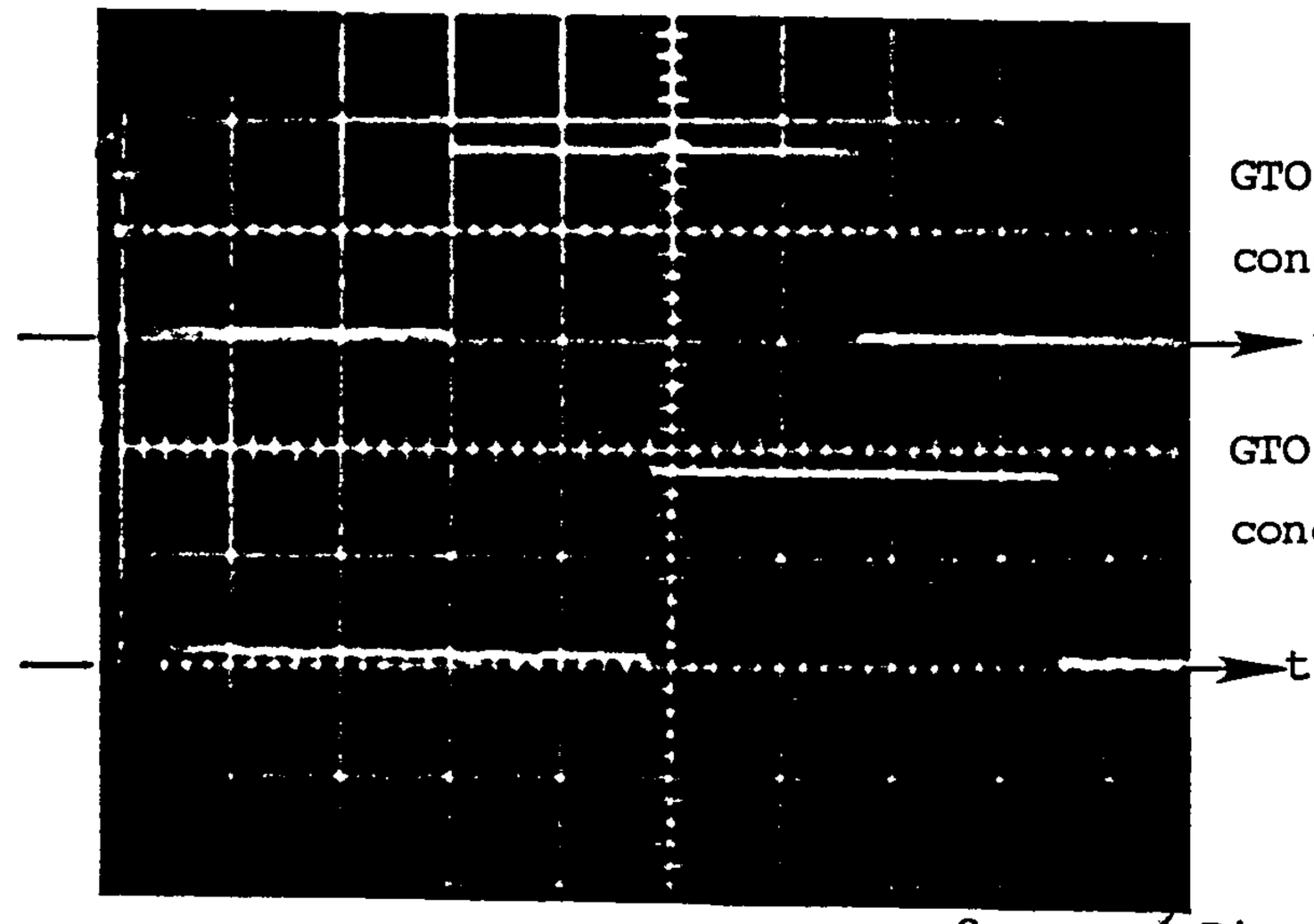

(iii) Sequential Triggering Pulses Applied to Armature Switching Devices

Fig. 5.10 Oscillogram of Control Circuit Output

position is traversed.

A "static kick test" [69] is the method used to determine the neutral or quadrature axis position. Fig. 5.11 shows the circuit used. Two tappings on the armature winding which are a pole pitch apart (x - x`, Fig. 5.11), are connected to a detector (centre zero millivoltmeter) while the field circuit is connected to a DC supply via a potential divider. The supply to the field circuit is opened and closed and the deflection on the detector is observed. The rotor is rotated by hand until a position is obtained when there is no "kick" on the detector. An error one way gives a positive kick while an error the other way gives a negative kick. Once the q-axis position is determined, the shaft encoder index pulse is carefully adjusted to appear at that marked position. The design of the digital control circuit is such that a particular pair of armature GTO thyristors are fired (in this case GTO T_1 and its output counterpart S_{13}) when the index pulse has arrived, to give the required maximum torque angle. Controlled departure of the radial field of the armature winding from the q-axis is made possible by redirection of the index pulse as discussed in section 5.4.6.

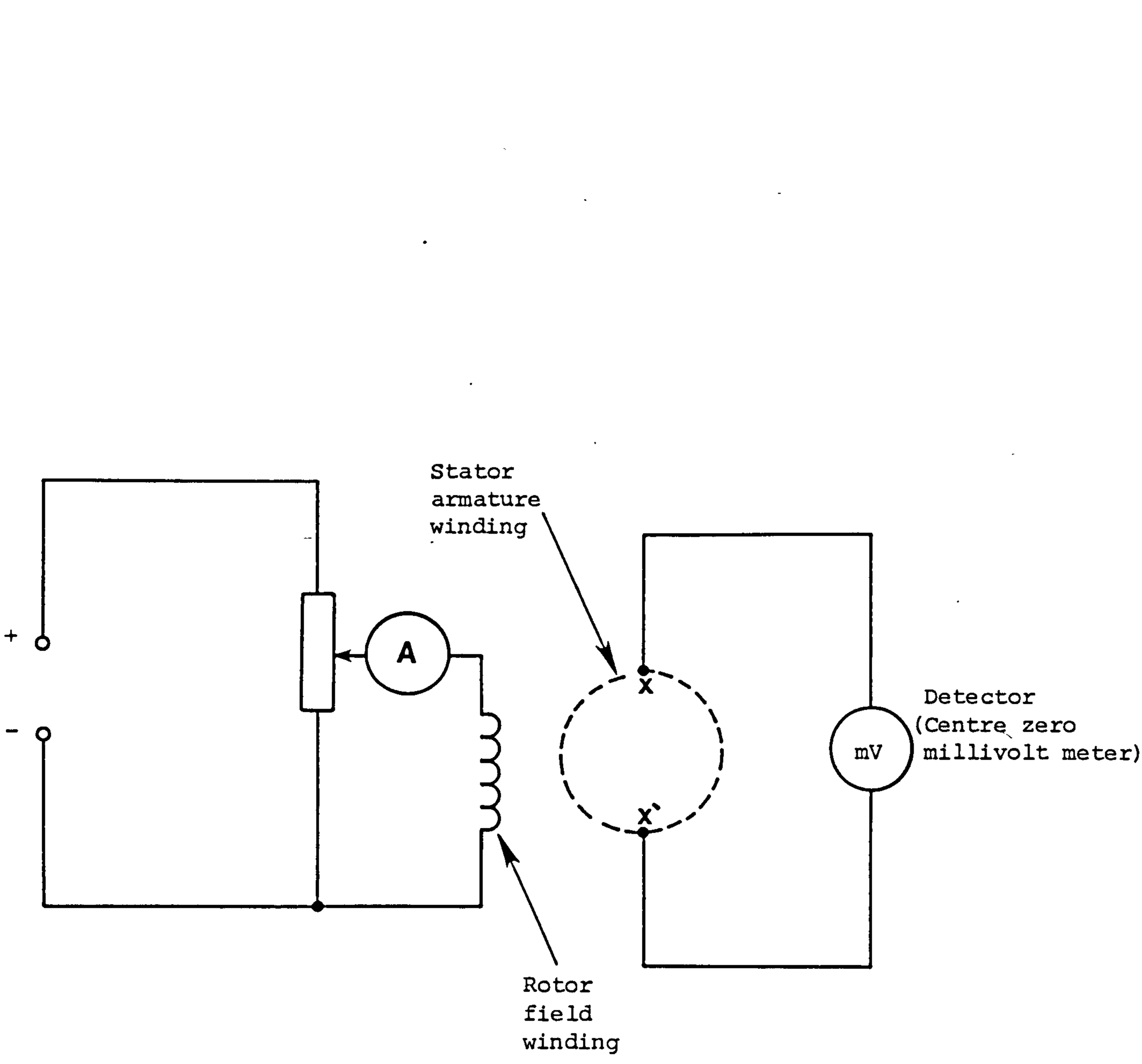

Fig. 5.11 Circuit diagram to determine the position of the neutral axis

CHAPTER SIX

EXPERIMENTAL RESULTS AND ANALYSIS

CHAPTER SIX

EXPERIMENTAL RESULTS AND ANALYSIS

6.1 INITIAL DEVELOPMENT TESTS

In chapter 4 the overall layout of the GTO armature switches was described and the digital control scheme for controlling the GTO devices was explained in chapter 5. Output logic pulses available from the control circuit (these are designated as Q_1, Q_2, Q_3 ------- etc. shown in Fig. 5.6) are required to be interfaced to the appropriate (i.e corresponding) firing circuit of the armature circuit GTO thyristor as shown in Fig. 4.4(i). The digital control circuit output logic pulses are generated in the correct order and care is necessary to ensure that this correct sequence is maintained when interfacing these outputs to the appropriate firing circuits.

To confirm the validity of the proposed interconnections and phasing a few initial tests were carried out. First, the DC work machine was used to rotate the shaft and, using an oscilloscope the sequence of the logic pulses was checked. On confirmation of the correct sequence of logic pulses, the armature circuit was connected to a DC source and the armature circuit GTO thyristors sequentially triggered using feedback information derived from the shaft encoder. The necessary requirement is that each armature switch should conduct at the appropriate angular position of the shaft and for a

defined period. This was checked using an oscilloscope by observing the conduction period of a particular device relative to the change in rotor position. The next step was to energise the field winding (using separate excitation), testing operation of the loaded machine in the both motoring and generating modes. Of interest is an observation of the resultant radial field distribution in the airgap of the machine and analysis and comparison of this with the theoretical distribution. Using the available flexibility incorporated within the digital control circuit, it was possible to examine various possibilities such as: (i) the controlled departure, forwards and backwards, from the q-axis of the coil sides undergoing commutation and (ii) overlapping the conduction periods of two adjacent armature GTO thyristors. The term overlapping' here refers to the condition when two armature GTO switches are allowed to conduct at the same time, during the commutation period of a particular armature coil. For example, GTOs S_{13} and S_{14}, Fig. 4.5(i), are allowed to conduct simultaneously during the commutation period of coils connected between the anodes of these two devices, i.e. between armature tapping points "c" and "d". This feature is analogous to a brush short-circuiting two adjacent commutator segments on a conventional DC machine.

Tests were carried out to observe and analyse the effect of both of these actions. The latter case was of particular interest as the possibility of sharing of armature current between the two overlapped GTO devices was being investigated, in the interest of improving the switching duty on the armature switching devices. Current sharing was not achieved naturally at other than very low armature current and rotational speeds. Analysis was carried out to

establish the reason for this. The machine rotor system incorporated an interpole winding as previously described in section 3.4.1. The effect of exciting this winding was investigated together with any consequence that it might have on the current sharing between the adjacent devices.

In this chapter, experimental results relevant to each case are presented, together with any corresponding theoretical analysis.

6.2 OPERATION OF THE MACHINE IN THE MOTORING AND GENERATING MODES

In chapter three, the basic configurations of the machine original and inverted format were described. In the inverted format, the current excitation for both the stator (armature winding) and rotor (field winding) which provides equal electric loading as given by the original format of the machine was obtained. The corresponding current value for the main field winding is around 6 A and for the armature winding around 4.5 A. For initial test purposes, the machine was run at these values of field and armature current to give rated torque as given by the original format of the machine. However, operation at those values of current for rotor and stator meant that the machine operates at reduced speed because lower speeds are obtained for high values of field current as demonstrated by the graph of Fig. 6.1. The machine has subsequently been run as a separately-excited motor at armature voltage (V_a) up to 140 V and speeds up to 1500 rpm.

Speed control when motoring was possible either by varying supplied armature voltage (V_a) or by changing current excitation to

the main field winding (I_f). Fig. 6.1 shows speed control of the machine by varying the armature voltage supplied for two values of field current. It is clear from this figure that higher speed is obtained by reducing the field current (field weakening).

The machine is primarily intended to operate as a motor and various oscillograms were recorded for operating the machine in this mode. The oscillogram shown in Fig. 6.2(a) refers to the voltage typically developed between anode and cathode terminals of a GTO thyristor connected to the positive rail of the DC armature supply, e.g. GTO T_1 shown in Fig. 3.7 or 4.5(i). The voltage waveshape is nearly sinusoidal with a peak-to-peak value approximately equal to the supply voltage; the reason for this distribution will be explained in section 6.3, from elementary considerations of the resultant radial field distribution in the airgap of the machine. Superimposed on the sinusoidal variation there are twenty four switching voltage transients per rotation of the armature field through a double pole pitch. The brief period when the device is conducting is apparent when the voltage across the device is equal to V_T(anode to cathode on-state voltage, as specified by the device manufacturer data sheets, $V_T < 3V$).

Fig. 6.2(b) is included to demonstrate the slight negative excursion of fundamental of the voltage waveform across the GTO device due to controllable displacement of the armature switch tapping point from the quadrature axis of the coil sides undergoing commutation. i.e. the voltage curve will go further negative for further departure from the q-axis position.

When the GTO is turned off, this results in an overshoot

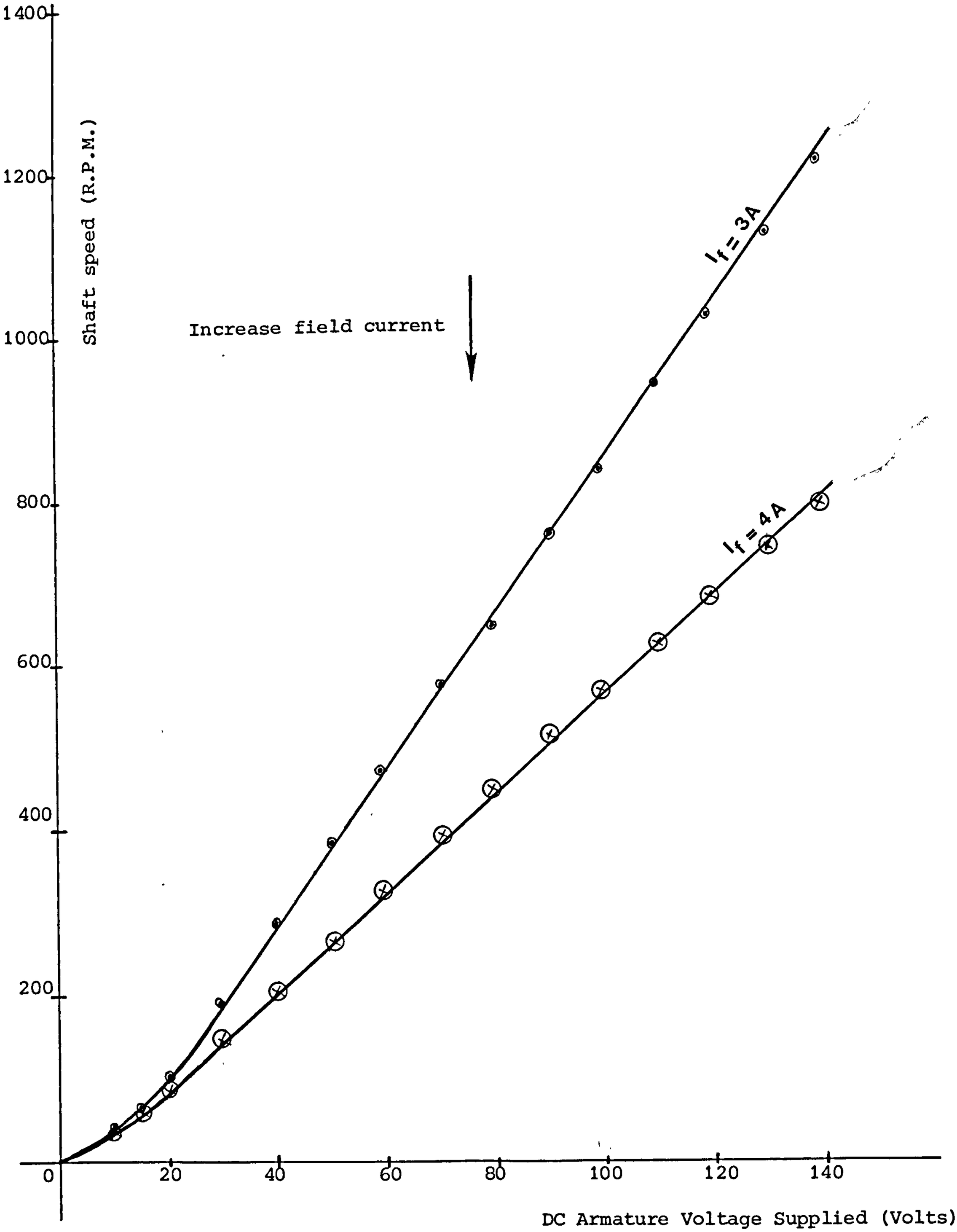

Fig. 6.1 Speed control by varying armature voltage (shaft torque constant)

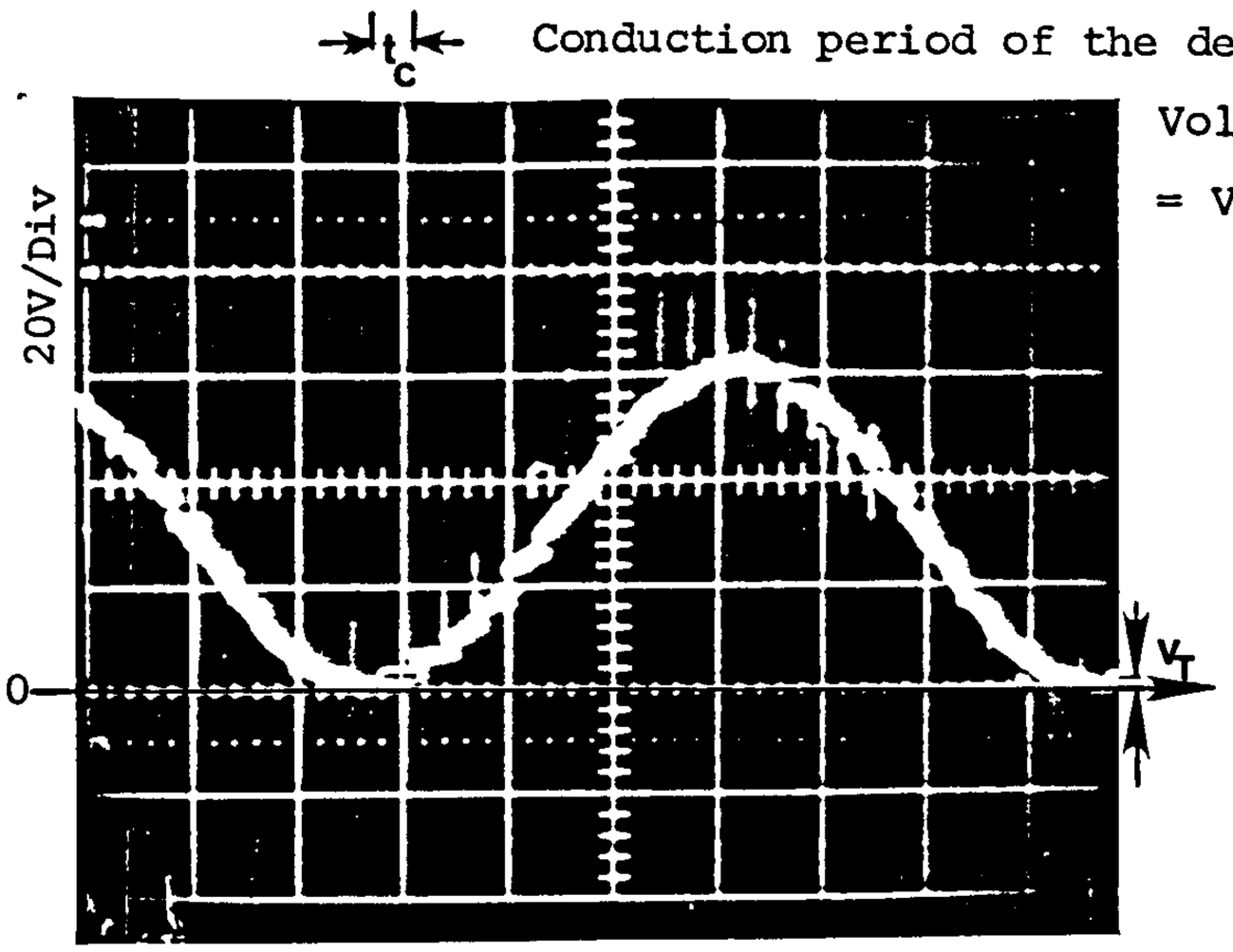

(a) GTO voltage waveform

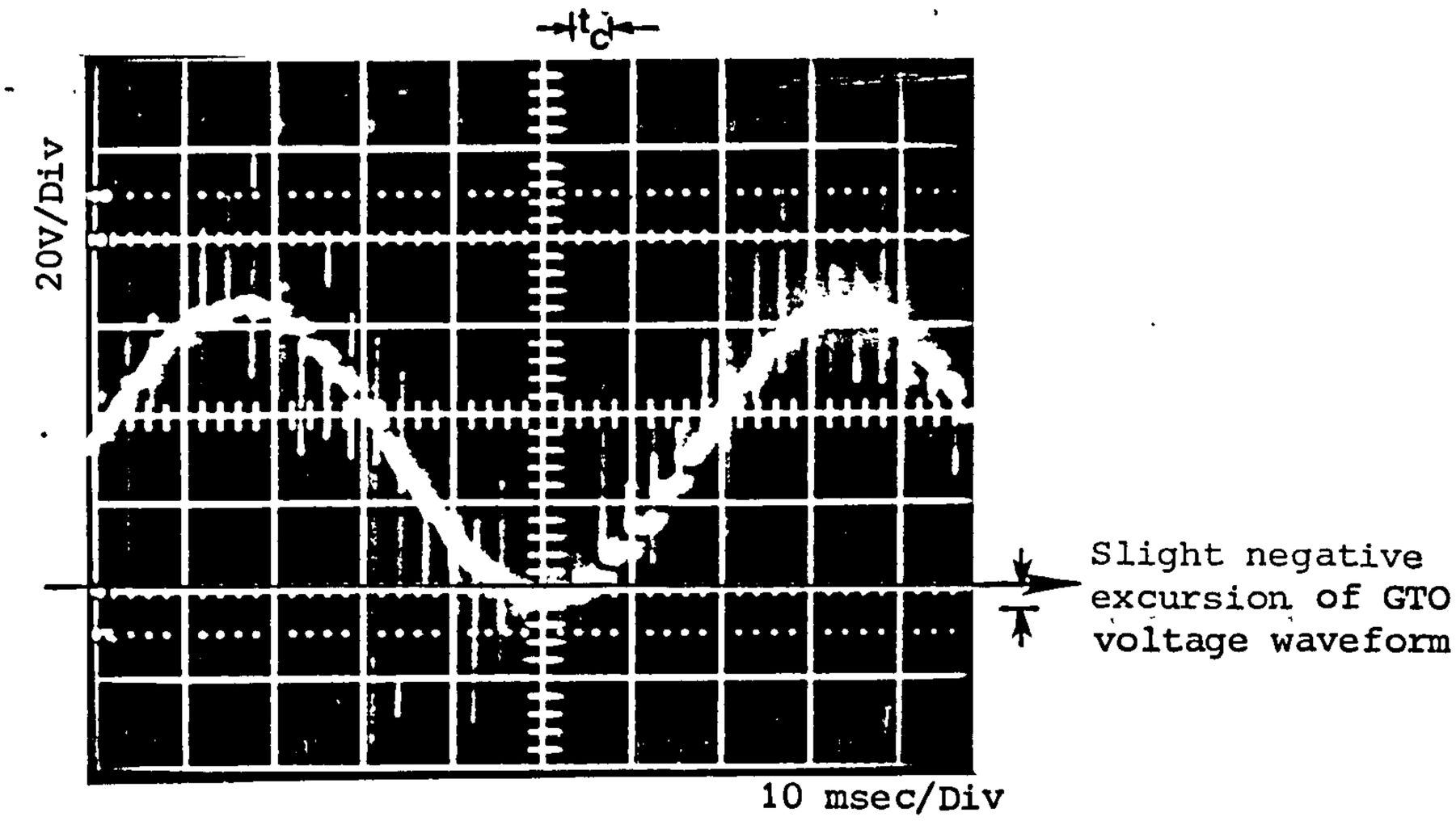

(b) GTO voltage waveform for a slight departure from q-axis position

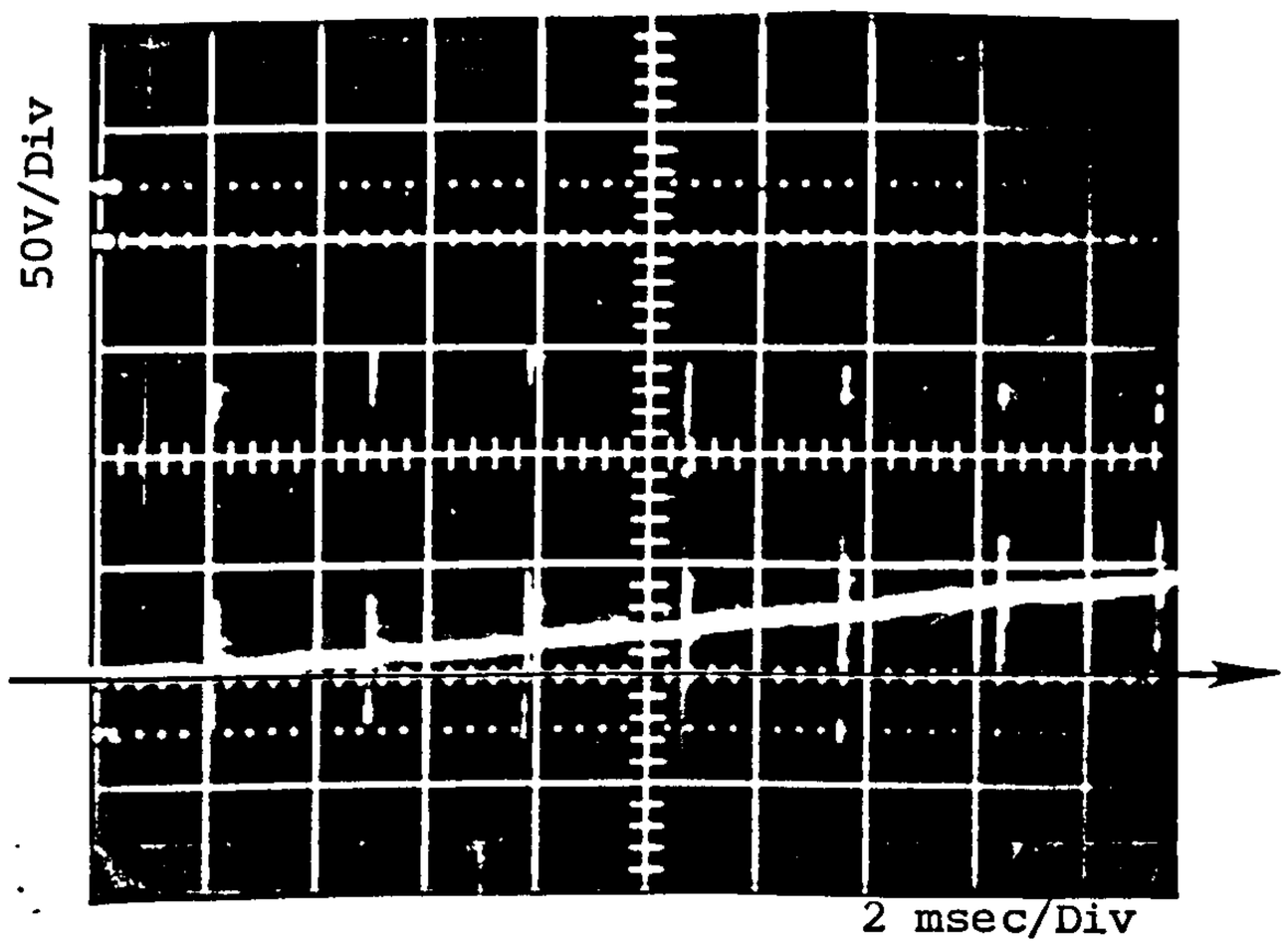

(c) GTO voltage waveform - expanded time scale

Fig. 6.2 Voltage waveform across a GTO thyristor (T_1)

(transient) voltage whose magnitude is related to the armature current being commutated and the parameters of the commutated circuit. In chapter four, a relationship (equation 4.12) was derived to relate these quantities based on the assumptions previously discussed in section 4.4.

$$(\Delta V) = (I_a/2)\sqrt{L_1/C_s}$$

Where: (ΔV) = peak value of overshoot voltage

I_a = armature load current

L_1 = the self inductance of the commutated coil

i.e. the combined inductance of coil (1,13) and (25,37) undergoing commutation, shown in Fig. 4.5 (= 2.26 mH, measured experimentally).

C_s = value of snubber capacitor = 22 nF.

If the armature current supplied is 1.0 A

$$(\Delta V) = (1/2)\sqrt{2.26 \times 10^{-3}/\ 22 \times 10^{6}} = 160\ V \qquad (6.1)$$

The oscillogram of Fig. 6.2(c) was recorded to a different time scale to that given in Fig. 6.2(a) and (b), showing the waveform of the voltage across GTO T_1. The peak transient voltage recorded is around 150 V for an armature current of 1.0 A. Comparison of the calculated value with that obtained experimentally shows close agreement, the slight difference may be due to either assumptions made in the derivation of equation 4.12 or error incurred during the measurement of the self-inductance of the commutated coil.

The waveform of GTO on-state current is shown in Fig. 6.3(a) in which the rapid switching action of the GTO thyristor is clearly seen. Typical turn-on and turn-off times for this device, as stated in the data sheets, are of the order 1 μs or less; the switching

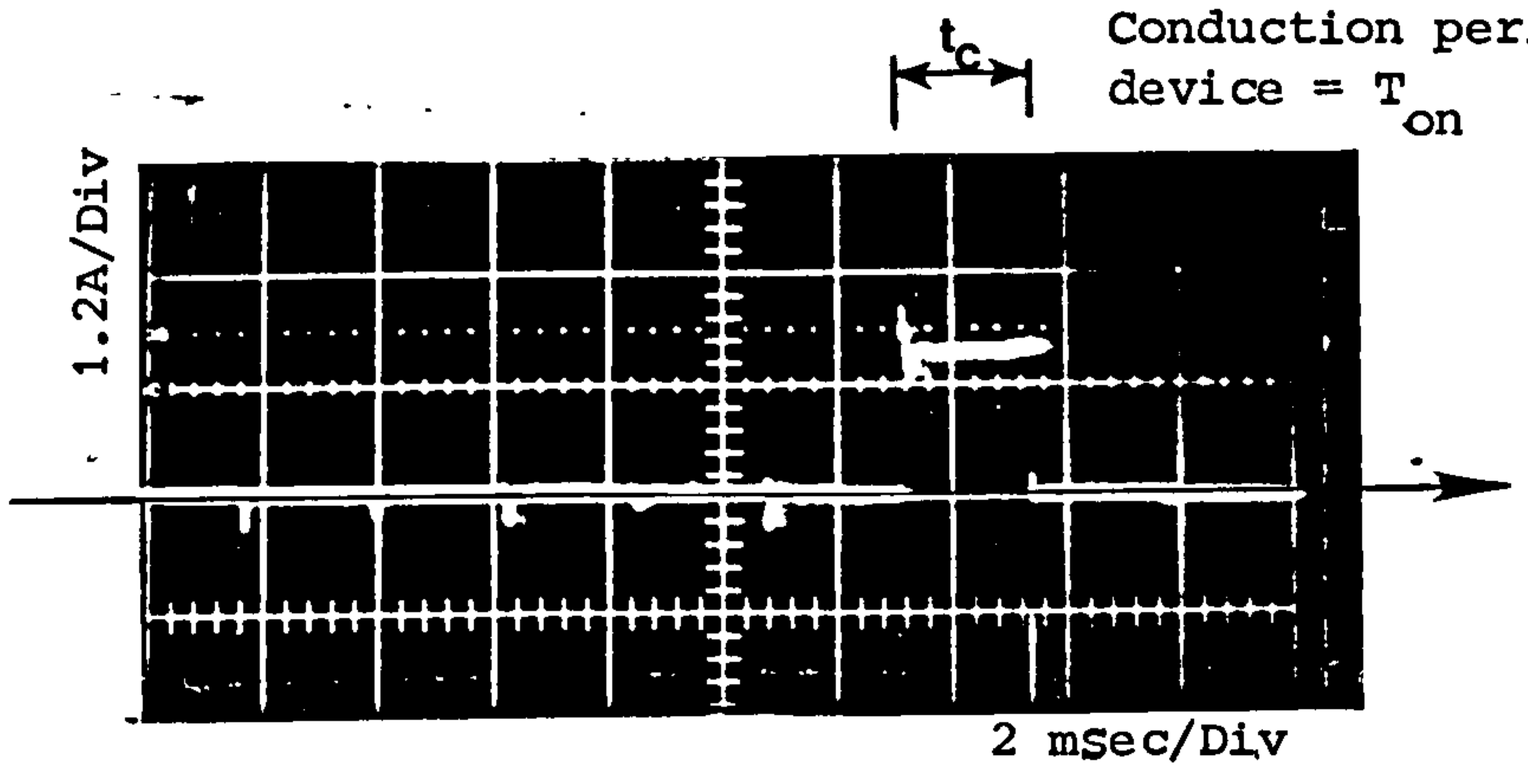

(a) Waveform of GTO on-state current

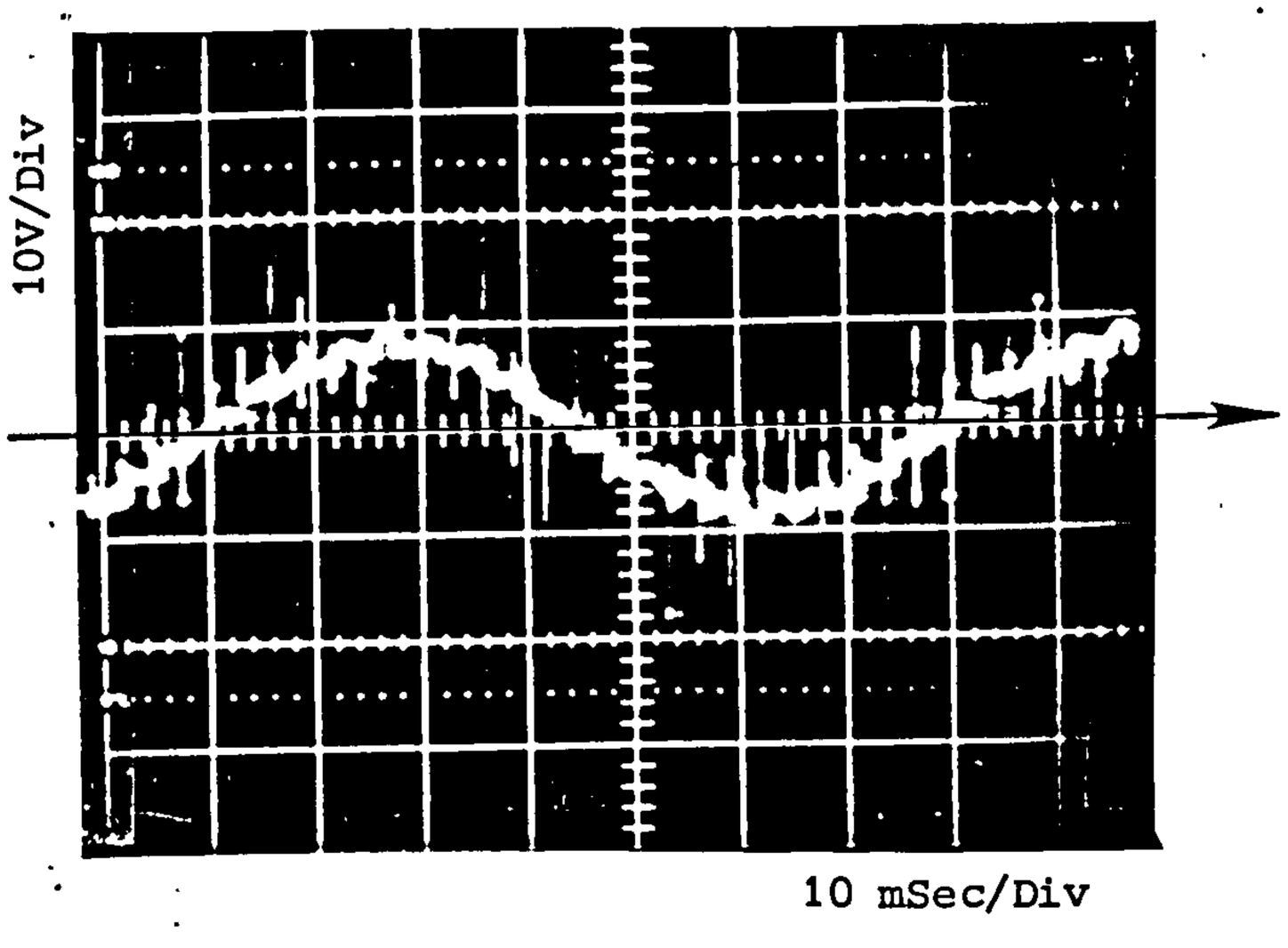

(b) Voltage waveform across an armature coil
(recorded between points a & b, Fig. 4.5(i))

Fig. 6.3 Oscillogram of GTO on-state current and armature coil voltage

times depend on various factors such as the gate drive current, both at turn-on and turn-off, and the ambient temperature - Fig. 12 and 14 (Appendix E) respectively.

The waveform of the voltage developed across a full-pitch armature coil {between points "a" and "b", Fig. 4.5(i)} is shown in Fig. 6.3(b). The motional e.m.f. component alternates in time with a waveform precisely matching the resultant radial field distribution in the airgap at the rotor surface. The resultant radial field distribution in the airgap of the machine will be considered in section 6.3.

When the machine was operated solely in the motoring mode, the reverse blocking diodes BY249 shown in Fig. 4.3(i) were not needed because the voltage across the GTO switching devices was always in the forward bias direction. (The GTO was reverse biased by a few volts for a slight departure from the q-axis position as previously discussed in this section). The machine when loaded as a motor gave the torque/speed characteristics shown in Fig. 6.4. The maximum torque as given by the original format of the machine was achieved but at reduced speed. In chapter seven, proposals are made to up-rate the machine in terms of speed and armature voltage.

When satisfactory operation of the machine in the motoring mode had been completely verified, the possibility of regenerative operation was investigated. Most DC machines are built for a basic motoring duty with the prospect of regenerating into a DC power supply, or dissipating energy within resistance during braking.

If the polarity of the supply voltage is reversible, regeneration is possible without the need to duplicate the armature switching

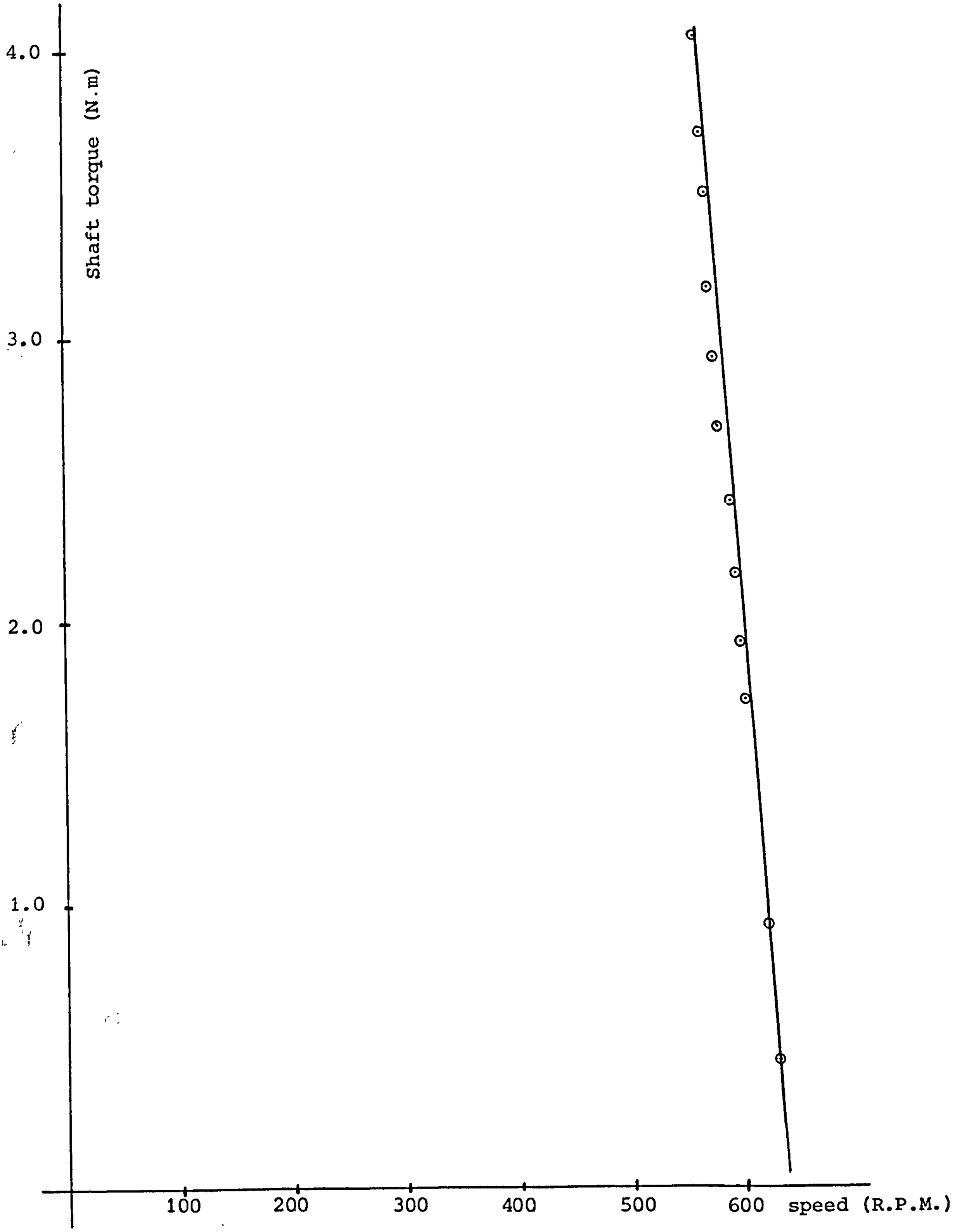

Fig. 6.4 Torque/speed characteristics for the developed machine, Operation in the motoring mode [V_a = 140V, I_f = 6A]

devices. Reversal of the polarity of the supply voltage in the generating mode means that reverse blocking diodes are required as discussed in section 4.3.4. These are identified as diodes BY249-600 shown in Fig. 4.3(i).

6.3 THE DISTRIBUTION OF THE RESULTANT RADIAL FIELD IN THE AIRGAP

In chapter 3, the radial field distributions in the airgap of the machine due to current excitation of main field, armature and interpole windings were derived from basic considerations of the layout of the machine.

The idealised theoretical distributions of radial field of main field and armature winding are plotted in Fig. 6.5(i) together with their resultant (i.e. the instantaneous sum of Hn_f and Hn_a at every position in the airgap). The idealised distributions are deduced on the assumptions that the conductors are uniformly spread over the appropriate iron/airgap boundary. The resulting distributions are as follows :

- Ideal trapezoidal radial field distribution due to main field winding excitation, labelled "a".
- Ideal triangular radial field distribution due to current excitation to the armature winding, labelled "b".
- The resultant of these two distributions labelled "c", for the case when the interpole winding is not energised.

Fig. 6.5(ii) depicts the oscillogram of the e.m.f. induced in a full pitch search coil located in a pair of slots on the stator of the machine. The value of the resultant radial field can be

calculated theoretically and compared to the distribution obtained experimentally, as in section 3.6, chapter 3.

For the machine operating in the motoring mode with a field winding excitation of 4.0 A and an armature load current 1.0 A, the resultant radial airgap field distribution can be deduced from component peak values calculated as follows:

$$Hn_f(max) = (n \times I)/(2 \times g) \qquad \{equation\ 3.15\}$$

$$= (7 \times 13)(4)/(2 \times 0.508 \times 10^{-3}) = 358268\ A/m$$

$$Hn_a(max) = (12 \times 31)(1/4)/(2 \times 0.508 \times 10^{-3}) = 91535\ A/m$$

The radial field distributions of main field and armature windings are plotted as shown in Fig. 6.5(i). Addition of these two waveforms gives the distribution of the resultant radial field in the airgap (Hn_r), labelled "c". The peak theoretical value of Hn_r is 378610 A/m.

The peak value of the e.m.f. induced in the search coil is approximately 300 mV, Fig. 6.5 (ii).

The oscillogram was recorded for a rotor speed of 400 rpm.

$$v = 3.17 \quad m/sec \qquad (using\ 3.16)$$

Using equation 3.13, the maximum value of the resultant radial flux density in the airgap, $Bn_r(max)$, can be calculated.

$$300 \times 10^{-3} = 2\ (Bn_r(max) \times 101.6 \times 10^{-3} \times 3.17)$$

$$Bn_r(max) = 0.4656\ Wb/m^2$$

Also using the relationship $\{Bn = \mu o \times Hn\}$

$$0.4656 = (4\pi \times 10^{-7}) \times Hn_r(max)$$

$$Hn_r(max) = 370000 \quad A/m$$

This represents the maximum value of the resultant radial field in the airgap of the machine, obtained experimentally.

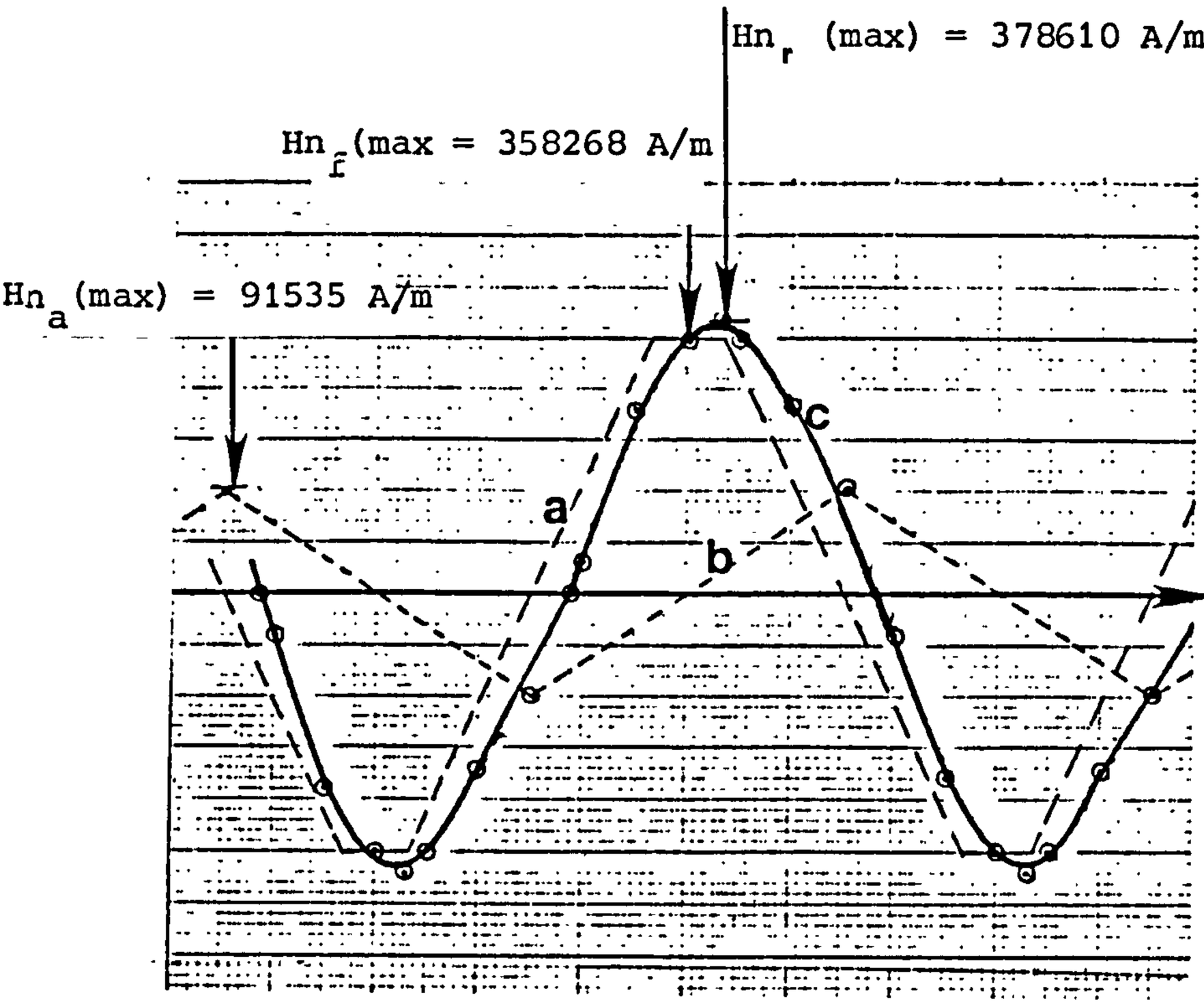

(i) Theoretical distribution

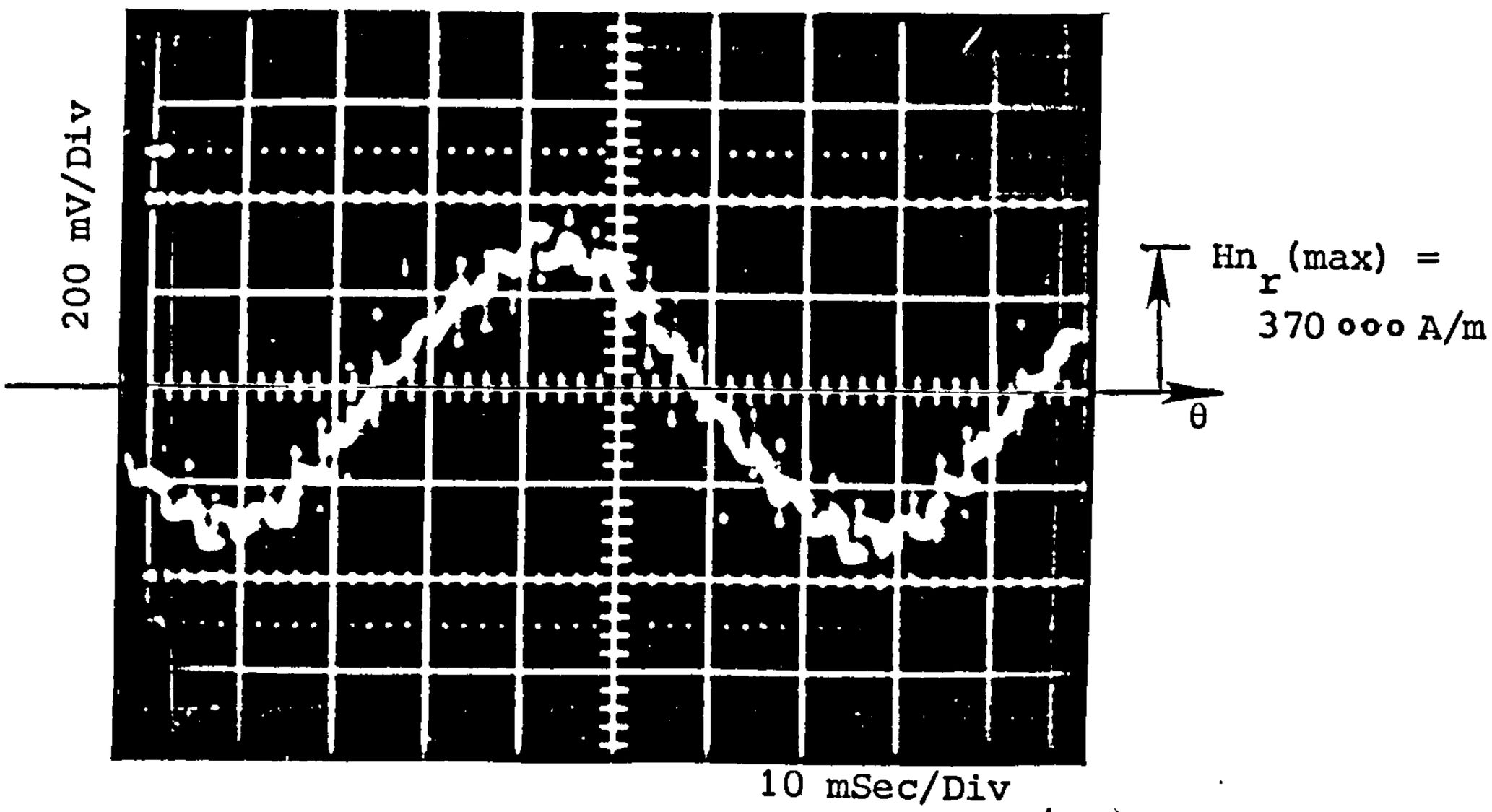

(ii) Experimental Result

Fig. 6.5 Resultant airgap radial field distribution due to current excitation to both armature and main field windings of the machine

Comparing the theoretical peak value of Hn_r (378610 A/m) with the experimental value (370 000 A/m), it is clear that close agreement has been achieved. Also, the waveshape of theoretical distribution of Hn_r shown in Fig. 6.5(i) agrees with the result obtained experimentally, shown in Fig. 6.5(ii).

6.4 ANALYSIS AND CALCULATION OF ARMATURE GENERATED E.M.F.

When current is passed through the armature winding of a DC machine, and its field coils are excited, torque is established. The configuration here is such that the main field winding rotates with the rotor shaft when the machine is in motion.

The rotating main field winding induces a dynamic e.m.f. in the statically commutated armature winding. An equivalent circuit for this is shown in Fig. 6.6(i). The statically commutated armature winding is shown as dotted to discriminate it from the conventional notation of representing rotating armature windings, shown as a circle with two quadrature-axis brushes. R_a is the armature resistance.

If the numerical value of the applied armature voltage = V_a Volts

and the numerical value of armature generated e.m.f. between two tapping points which are a pole pitch apart = E_a Volts

Then from Kirchoff's Law, the voltage equation of the DC motor circuit at steady state :

$$V_a = E_a + (I_a)(R_a) \qquad (6.2)$$

applies, where I_a = armature load current.

The value of the V_a, I_a and R_a can all measured experimentally, hence the value of E_a can be evaluated using equation 6.2.

The value of the armature generated e.m.f. (E_a) can also be determined from first principles from ordinary consideration of main field winding radial field distribution, number of series-connected armature conductors and speed.

The aim of the following analysis is to calculate and compare the value of the armature generated e.m.f. (E_a) from experimental measurement of V_a, I_a and R_a using equations 6.2, comparing this with the theoretical value obtained from basic consideration of radial field distribution.

From first principles, in order to calculate the mean or average value of e.m.f. developed between two armature tappings which are a pole pitch apart {points "a" and "c", Fig. 4.5(i)}, it is necessary to calculate the sum of the mean values of the e.m.f.s in each of the conductors connected in series between these two armature tappings, during the interval separating any one instant of commutation from the next.

Thus, during the interval between any successive pair of commutation instants, the average e.m.f. between the two armature tappings due to "N_a" series connected armature conductors, designated 1 to N_a is given by:

$$E_a = E_{av} = (e_1 av + e_2 av + \text{----------} + e_{N_a} av) \qquad (6.3)$$

{Where $e_k av$ is the mean or average e.m.f. induced in the k^{th} armature conductor}.

The main field winding of the machine was excited with a current

of I_f = 4A. The armature load current recorded was I_a = 0.925A, with a rotor speed of approximately 820 r.p.m.

First, the armature generated e.m.f. will be theoretically calculated from the knowledge of main field winding radial field distribution and equation 6.3, as follows:

The diagram of Fig. 6.6(i) shows the armature winding of the inverted machine supplied with an armature voltage (V_a) of 140V.

The main field winding has a total of 7 coils per pole as previously described in section 3.4, Fig. 3.5. The remaining two coils were identified with the optional interpole winding, unexcited in this case.

For the present analysis, the "stepped" radial field distribution previously described in Fig. 3.8(i) is assumed; this is shown in Fig. 6.6(ii). This distribution is derived on the assumptions previously discussed in section 3.6.1.

The normal component of the magnetic field intensity (Hn) due to current excitation of the main field winding can be evaluated by the application of Ampere's Law, equation 3.15. This component has a maximum value $Hn_f(max)$ which occurs midway along the pole face and is given by :

$$Hn_f(max) = (7 \times 13)(4)/(2 \times 0{:}508\times10^{-3}) = 358268 \text{ A/m}$$

The corresponding peak value of flux density is given by

$$Bn_f(max) = \mu o \times 358268 = 0.4502 \text{ Wb/m}^2$$

The e.m.f. induced in an armature coil of n_c turns whose sides are axially-directed of length "l" , situated a pole pitch apart in

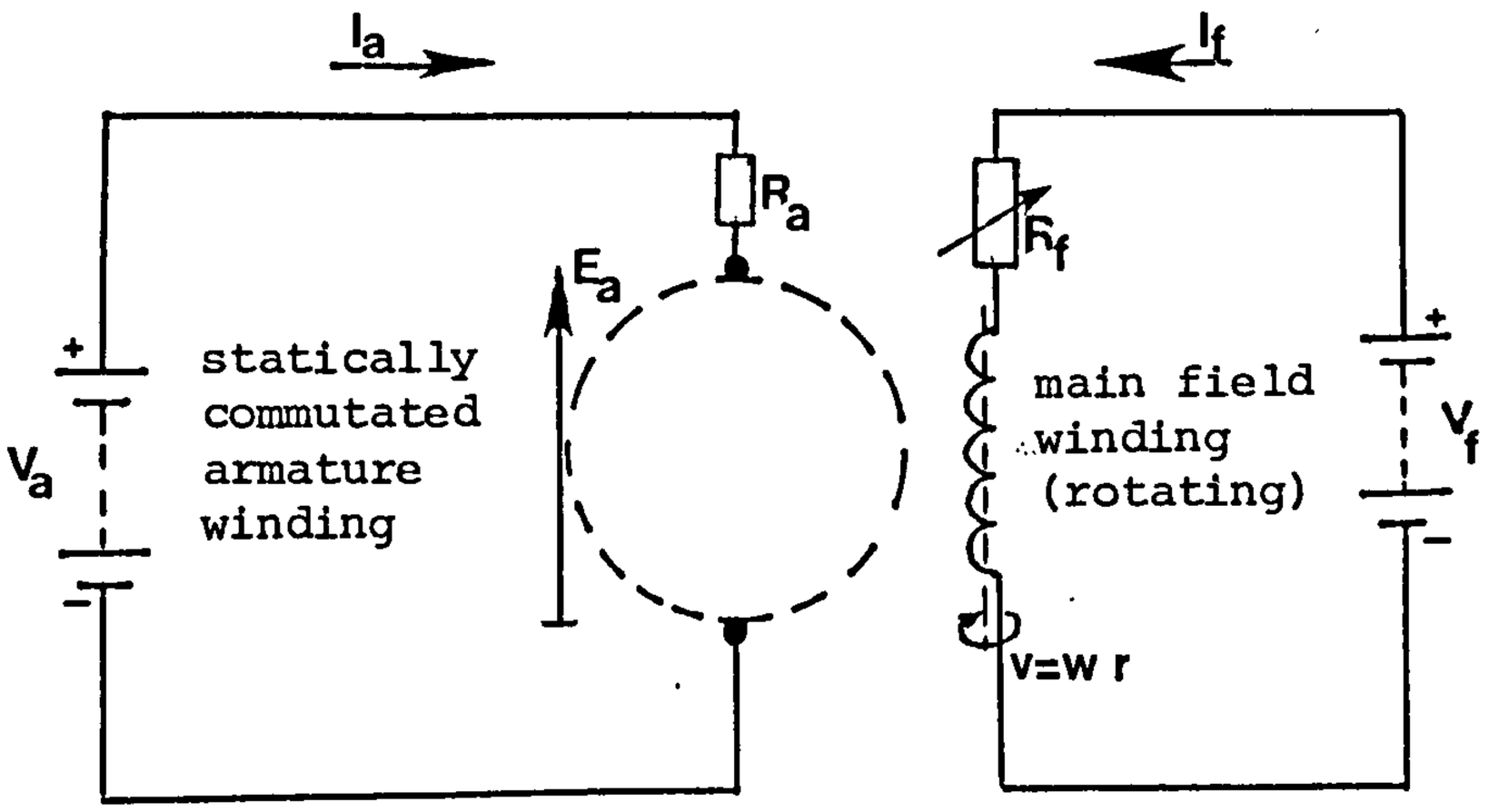

(i) Separately excited - GTO thyristor commutated DC machine equivalent circuit

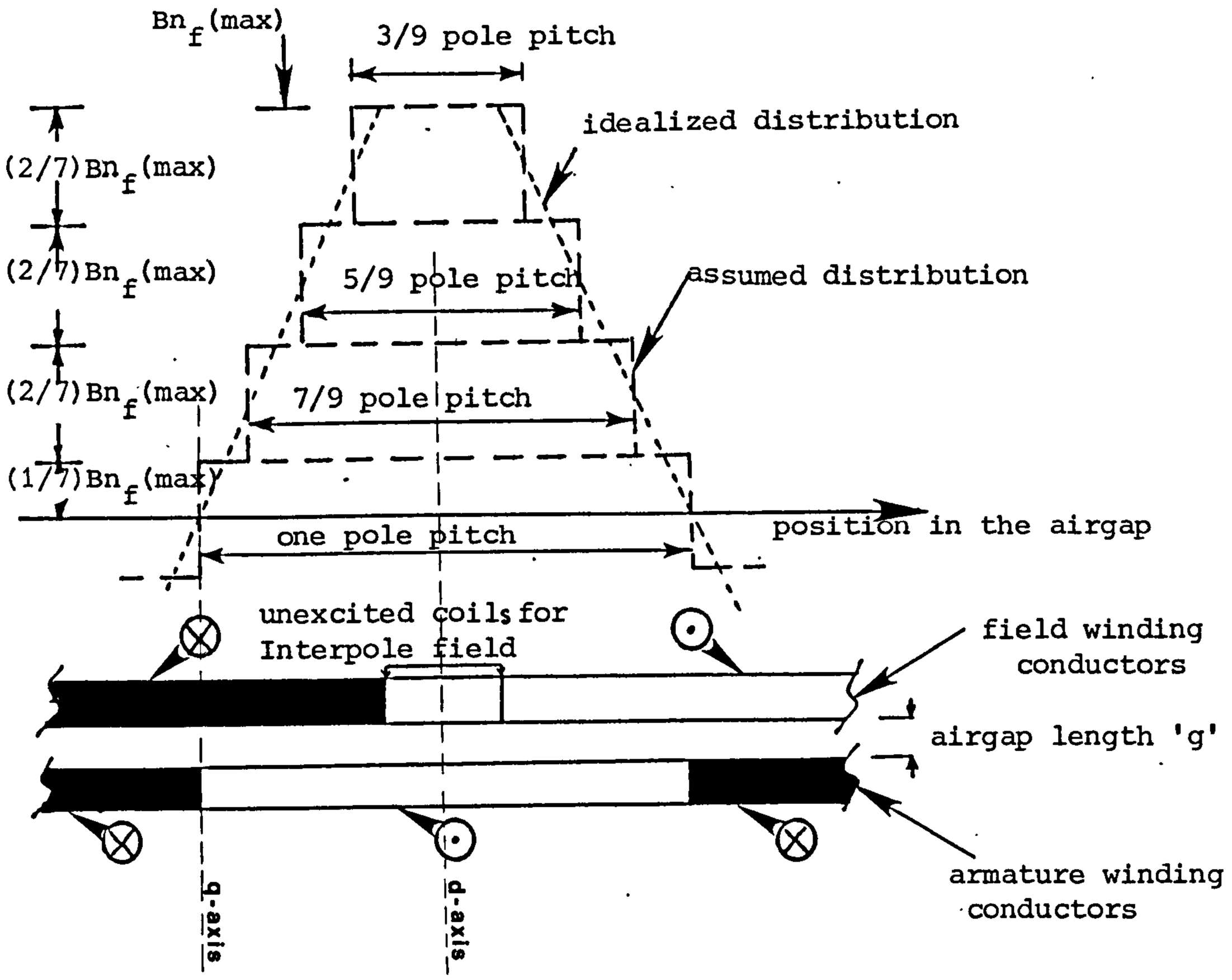

(ii) Radial field distribution due to main field winding excitation

Fig. 6.6

a stationary field system of radial flux density of instantaneous value $Bn(\theta)$ is given by equation 3.13 :

$$e_n(\theta) = 2 \times n_c \times Bn(\theta) \times 1 \times v \qquad (6.4)$$

The average e.m.f. induced in one armature coil as it moves over a pole pitch is given by :

$$e_{av} = \int_{}^{\text{Pole Pitch}} \{ e(\theta) \}\, d\theta \qquad (6.5)$$

The instantaneous value of the radial flux density $Bn(\theta)$ can be deduced from the knowledge of $Bn_f(max)$, Fig.6.6(ii), as follows:-

The radial flux density shown in Fig. 6.6(ii) is represented as 4 "dotted" blocks of radial flux density.

* Height of the first block is $(\frac{1}{7})Bn_f(max)$ extending over the whole pole pitch.

* Height of the second block is $(\frac{2}{7})Bn_f(max)$ extending over $\frac{7}{9}^{th}$ pole pitch.

* Height of the third block is $(\frac{2}{7})Bn_f(max)$ extending over $\frac{5}{9}^{th}$ pole pitch.

* Height of the fourth block is $(\frac{2}{7})Bn_f(max)$ extending over $\frac{3}{9}^{th}$ pole pitch.

These are the instantaneous values of radial flux density, $Bn(\theta)$, the corresponding value of the $e_k(\theta)$ can be calculated and summed to give e_{av} (equation 6.3, 6.4 and 6.5).

Shaft radial velocity for a speed of 820 rpm, v = 6.5 m/sec.

Using equation 6.4, the instantaneous values of e.m.f induced in an armature coil of 31 turns $\{e_k(\theta)\}$ can be calculated as follows :

$$e_1(\theta) = 2 \times 31\{ (0.064316) \times (101.6 \times 10^{-3})(6.5)\} = 2635 \text{ mV}$$

$$e_2(\theta) = 2 \times 31\{(0.128632 \times \tfrac{7}{9})(101.6 \times 10^{-3})(6.5)\} = 4092 \text{ mV}$$

$$e_3(\theta) = 2 \times 31\{(0.128632 \times \tfrac{5}{9})(101.6 \times 10^{-3})(6.5)\} = 2930 \text{ mV}$$

$$e_4(\theta) = 2 \times 31\{(0.128632 \times \tfrac{3}{9})(101.6 \times 10^{-3})(6.5)\} = 1752 \text{ mV}$$

Summation of these four quantities give the average e.m.f. induced in one armature coil, equation 6.5:

$$e_{av} = \sum_{k=1}^{4} e_k(\theta) = 11.41 \text{ V}$$

Referring to Fig. 4.5(i), the e.m.f. induced between the two armature tapping points "a" and "c" (i.e. considering an instantaneous period when GTOs T_1 and S_{13} are conducting) can be obtained using equation 6.3:

The armature has a total of 12 coils per pole

$$E_a = E_{av} = 12 \times 11.41$$

$$E_a = 136.5 \text{ V.}$$

Alternatively, the armature generated e.m.f. between these two armature tappings ("a" and "c") can be obtained using equation (6.2) and the values of V_a, I_a and R_a, measured experimentally.

"R_a" is the value of armature d.c. resistance measured experimentally, R_a= 2.45 ohms.

$$V_a = E_a + I_a R_a$$

$$140 = E_a + (0.925)(2.45)$$

$$E_a = 137.75 \text{ V.}$$

The values of armature generated e.m.f. calculated theoretically using equation 6.3 (136.5 V) shows a good agreement with the value obtained experimentally using equation 6.2 (137.75 V) and this identification was found to hold true for other values of V_a, I_a and speed.

6.5 ANALYSIS OF RESULTANT POTENTIAL DIFFERENCE ACROSS A COIL UNDERGOING COMMUTATION

With the available flexibility incorporated within the digital control circuit, it is possible to examine various effects on the commutation of a particular armature coil.

The analysis detailed below considers the effects of the three following variations on procedure:

(1) "Sequential triggering" of the armature GTO thyristor switches such that a conducting device is turned-off at the same precise instant when the next (following) device (in the sequence, in the direction of rotation) is turned-on. This case can be best explained by referring to Fig. 6.7(a) which depicts an instant when a particular armature GTO device (S_{13}) is conducting and it is required to switch-off this device and switch-on the next device in the sequence (S_{14}); this resulting in the commutation of current in the two coils connected in parallel, between the anodes of these two devices, viz coil $C_{1,37}$ and $C_{13,25}$ (for convenience, these two coils will be referred to as coils C_k and C_{kk} respectively).

(2) Overlapping the conduction periods of two adjacent armature GTO thyristors. Overlapping refers to the condition when two adjacent armature GTO switches are allowed to conduct at the same time, during the commutation of a particular armature coil. This condition can be explained by referring to Fig. 6.8(a) and considering an instant when GTO thyristors S_{13} and S_{14} are conducting during the commutation period of coil C_k, then for equal current sharing between these two armature GTO devices, the potential difference across coil C_k should ideally be zero.

(3) Departure of the commutation axis of a particular armature coil from the quadrature axis position.

Both coils C_k and C_{kk} are identical, full pitch armature coils of equal number of turns, located in identical slots and distant a double pole pitch apart. Paralleling (equalising) connections are placed across these two coils as previously described in section 3.4.2 of chapter three.

Option (2) is of particular interest as the possibility of current sharing between the two adjacent armature GTO devices was being investigated in the interest of improving the switching duty on the armature switching devices.

The following analysis details the effect of each of the above actions, presenting experimental measurement and theoretical analysis to illustrate the effect in each case.

Considering coil 1,37 (coil C_k) undergoing commutation, the value of the resultant potential difference across this coil is partially contributed by the dynamic e.m.f. induced in this coil due to the radial fields which exist in the commutation space, as shown in Fig. 6.7(b). Three components of radial field exist, these are due to:-

(a) Radial fringe field of the main field winding.

(b) Radial field intensity of the armature winding.

(c) Radial field intensity of the interpole winding (this exists for the case when the interpoles are excited).

The values of each of these radial field components can be calculated and added together to obtain the resultant radial field in the commutation zone of this armature coil (coil C_k). From this,

the value of the flux density and hence the dynamic (or motional) e.m.f. induced in the commutating coil can be calculated. The following analysis is based on the radial field distributions derived in section 3.6. Further assumption is that the length of the airgap is assumed uniform and constant.

Two further voltage components contribute to the resultant potential difference across the coil undergoing commutation. During the period when an armature coil is short circuited by two adjacent conducting armature switches, the current in the short circuited coil, initially equal in magnitude to the current flowing in one of the parallel paths through the armature, has to reverse its direction of flow. This will cause a small but finite resistive voltage drop across the commutating coil. The other component is due to the current changing during the commutation period (t_c); the current variation will give rise to an e.m.f. of self induction, proportional to the rate of change of current:

$$e_l = l(\Delta i/\Delta t) \qquad (6.6)$$

Once each individual component has been determined, they can be added together to obtain the resultant potential difference across the commutating coil. The equivalent circuit shown in Fig. 6.7(a) depicts the instant when the parallel combination of coil C_k and C_{kk} are undergoing commutation, showing the three components of e.m.f. across these coils; these are as follows :

e_1 is the dynamic e.m.f induced due to the resultant radial field in the commutation zone.

e_l is the e.m.f. of self induction of the coil undergoing commutation.

V_r is the resistive voltage drop across the resistance of the

commutating coil.

In the following analysis, several cases are considered to determine the effect of such factors as introduction of the interpoles and shifting the axis of the radial field of the armature winding from the q-axis position by the redirection of the "index" pulse as explained in section 5.4.6 of chapter five.

6.5.1 CASE ONE: COMMUTATION OCCURS PRECISELY WHEN THE RADIAL FIELDS OF THE ARMATURE AND MAIN FIELD WINDING ARE IN SPACE QUADRATURE {SEQUENTIAL TRIGGERING OF THE ARMATURE SWITCHES}

Fig. 6.7(b) illustrates this case where the radial field of the armature winding (Hn_a) is in space-quadrature with that due to the main field winding (Hn_f). The commutation period of coil C_k is clearly shown which occurs when the radial field of the main field winding (Hn_f) crosses the zero axis. Hence at the start of commutation of coil C_k, Hn_f is negative increasing to zero and positive by the end of the commutation period.

The radial field intensity in the commutation zone can be determined from the knowledge of the current excitation to the windings.

The main field winding is interconnected with 7 coils per pole (as previously described in section 3.3.1) with a current excitation of 3.5A to the winding.

The maximum value of radial field intensity due to main field winding excitation is given by:-

$$Hn_f \text{ (max)} = (7 \times 13)(3.5)/(2 \times 0.508\times10^{-3}) = 313484 \text{ A/m}$$

The radial field in the commutation zone has a value which changes from $-\frac{1}{7} Hn_f(\text{max})$ to $+\frac{1}{7} Hn_f(\text{max})$.

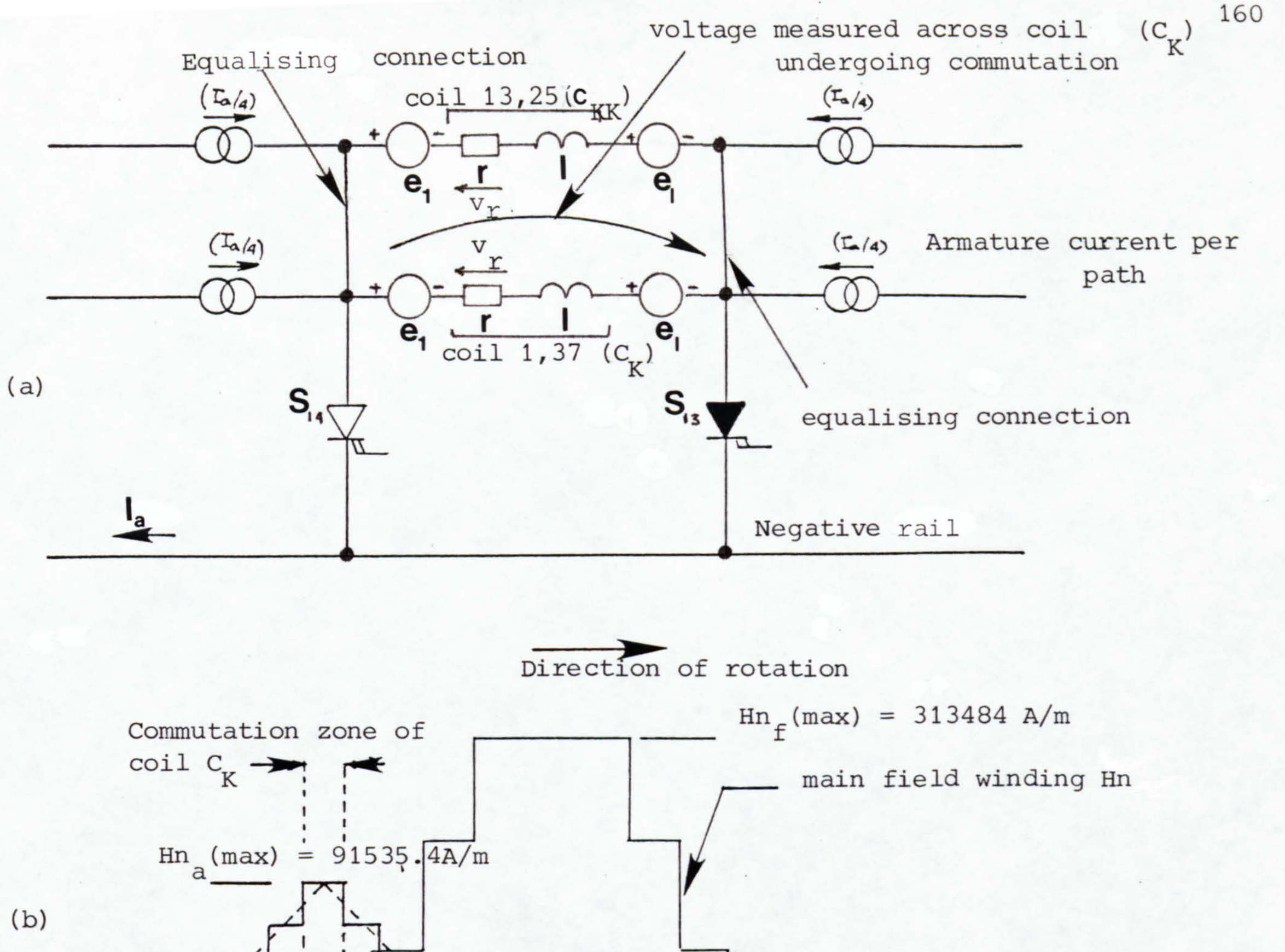

Fig. 6.7 Radial field distribution of armature winding in space quadrature with that due to main field winding.
Sequential triggering - Interpoles not excited.

The radial field intensity due to armature winding excitation is maximum at the quadrature axis position where armature coil C_k is undergoing commutation.

For an armature load current of 1.0 A, $Hn_a(max)$ = 91535.4 A/m

Referring to Fig. 6.7(b), it is possible to determine the resultant value of the radial field (Hn_r) in the commutation zone of coil C_k as follows:

$$Hn_r = Hn_f + Hn_a$$

Therefore at the start of commutation of coil C_k

$$Hn_r = (-44783.5) + (91535.4) = + 46752 \quad A/m.$$

The flux density corresponding to this value of Hn_r can be calculated using equation 2.11 :

$$Bn_r = \mu o \times (46752) = 0.05875 \quad Wb/m^2$$

The e.m.f. induced in coil C_k corresponding to this value of flux density in the commutation region can be calculated using equation 3.13:

$v = 3.488$ m/sec (rotor speed 440 rpm)

Therefore $e_1 = 2 \times 31\ (0.05875)(101.6\times10^{-3})(3.488) = + 1.29083$ V.

By the end of the commutation period "t_c", Hn_f is positive

$$Hn_r = (+44783.5) + (91535.4) = + 136319 \text{ A/m.}$$

$$Bn_r = 0.1713 \quad Wb/m^2$$

$$e_1 = 2 \times 31\ (0.1713)(101.6\times10^{-3})(3.488) = + 3.7638 \text{ V.}$$

Current in the coil undergoing commutation is initially (1/4) of the total armature current "I_a", giving a resistive voltage drop

$$V_r = (-I_a/4) \times r$$

The measured value of the d.c. resistance of coil C_k is 0.3733 ohm.

$$V_r = - 0.0933 \quad V$$

The oscillograms of Fig. 6.7(c) is recorded for the case when the armature GTOs were sequentially triggered but not overlapped. The current in coil C_k reverses direction very rapidly when S_{14} is closed and S_{13} is opened. The current in the commutated coil C_k doesnot change during the conduction period of GTO S_{13}:

i.e. $(\Delta i/\Delta t) = 0.0$ {during period tc}

Inductive voltage component $(e_l) = l(\Delta i/\Delta t) = 0.0$ V

Addition of these three components of voltage gives the resultant voltage across coil C_k as it undergoes commutation. The direction of the three component of voltage is clearly shown in the equivalent circuit of Fig. 6.7(a). These directions are deduced on the basis of sequential triggering of armature GTOs such that S_{13} conducts before S_{14} in a cycle.

Hence at the start of commutation period

$$V\ (total) = e_1 + V_r + e_l$$
$$= (1.29083) + (-\ 0.0933\ ) + (0.0) = 1.20\ V$$

And at the end of the commutation period

$$V\ (total) = (3.7638) + (-\ 0.0933) + (0.0) = 3.67\ V$$

The oscillogram of Fig. 6.7(c) confirms this voltage variation during the conduction period of GTO S_{13}, from around 1.20 V at the start of the period rising to 3.6 V at the end of it.

The case just considered is of particular interest since the armature devices were sequentially triggered, therefore the current in the commutated coil reverses when GTO S_{13} is turned-off and S_{14} is turned-on. The rapid current reversal in the commutated coil results in a transient overshoot voltage across the device which has been turned-off because of the large $(\Delta i/\Delta t)$ in the commutated coil.

From section 6.1 of this chapter, it was calculated and verified that the peak overshoot voltage at turn-off is of the order of 150V, for an armature load current of 1 A. The current in the coil C_k undergoing commutation changes from a value $(- I_a/4)$ to $(+ I_a/4)$ in a time (Δt).

Therefore $\Delta t = 15\ \mu sec$

i.e. current reversal in the commutated coil occur in a time of around 15 μsec.

6.5.2 CASE TWO: SAME AS CASE ONE - OVERLAPPING TWO ARMATURE GTO SWITCHES

In the interest of improving the switching duty on the armature GTO devices, the possibility of current sharing between two adjacent devices was investigated. Two armature GTO thyristors, typically S_{13} and S_{14} Fig. 6.8(a), were allowed to conduct during the commutation period tc of coil C_k. This condition is referred to as overlapping, as previously explained.

The ideal condition is that each GTO carry equal share of total armature current supplied; this is only possible if the potential difference across coil C_k is zero during period t_c.

The oscillogram of Fig. 6.8(c) shows a constant voltage of around 1.2 V across coil C_k during its commutation period t_c.

A comparable value is now theoretically calculated from the knowledge of the various voltage component contributions.

Referring to Fig. 6.8(b), commutation of coil C_k occurs when fringe field of the main field winding is negative.

The value of this radial field was previously calculated to be

$$Hn_f = (-1/7) \times Hn_f(max) = - 44783.5\ A/m$$

The value of Hn_a is constant during period t_c, as previously

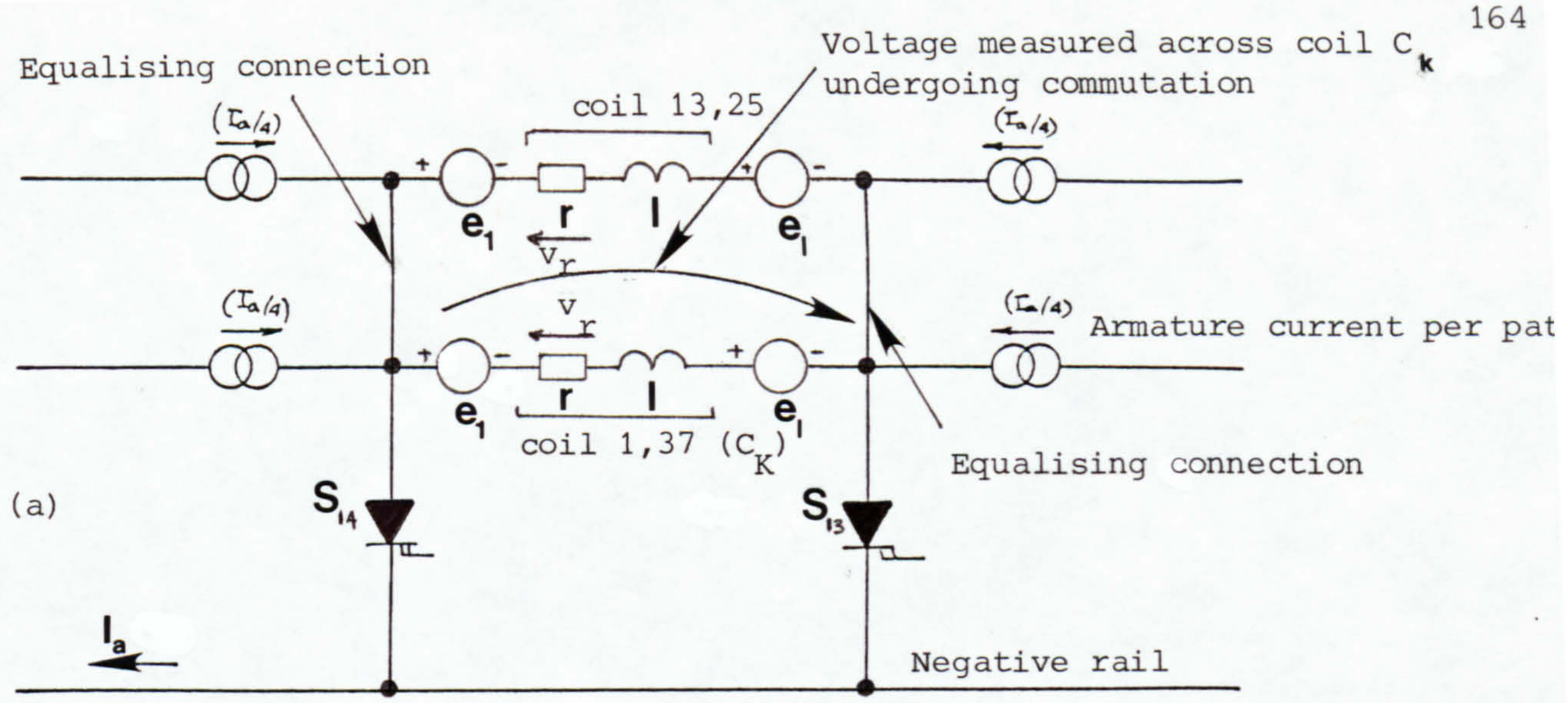

Fig. 6.8 Radial field distribution of armature winding in space quadrature with that of main field winding.
overlapping - Interpoles not excited

calculated.

$Hn_a(max) = 91535.4$ A/m

Addition of these two values of radial field components gives the resultant radial field for the commutation zone of coil C_k

$$Hn_r = Hn_f + Hn_a = 46752 \text{ A/m}$$

The corresponding value of flux density

$$Bn_r = 0.05875 \text{ Wb/m}^2$$

The dynamic e.m.f. induced in the coil undergoing commutation, coil C_k

$$e_1 = 2 \times 31(0.05875)(101.6\times10^{-3})(3.488) = 1.2908 \text{ V}$$

The resistive voltage drop is the same as that calculated for case 1

$$V_r = -0.0933 \text{ V}$$

In this case, although two adjacent armature GTO devices were allowed to conduct during the commutation period (t_c) of coil C_k, current sharing was not achieved at other than very low speeds due to the finite potential difference across coil C_k. This is demonstrated by the oscillogram of Fig. 6.8(c), the current clearly does not change direction during period t_c.

$\therefore (\Delta i/\Delta t) = 0.0$ during period t_c, giving $e_1 = 0.0$ V

Fig. 6.8(a) gives the polarity of these three components of voltage (as in case one). Addition of these components give the resultant potential difference across commutated coil C_k.

V (total) = 1.198 V.

Fig. 6.8(c) confirms the voltage across the coil undergoing commutation to be around 1.2 V.

Again in this case, the rapid current reversal in the commutated coil C_k at the end of period t_c results in a transient overshoot voltage of similar magnitude as that calculated for case one.

6.5.3 CASE THREE: SAME AS CASE TWO BUT WITH THE INTERPOLES EXCITED

The position of commutation of coil C_k is exactly the same as described in case two but with the interpole winding excited with a current of around 2.0 A.

In this case, three components of radial field exists in the commutation zone of coil C_k ; these are due to radial field distribution of the main field, armature and interpole winding as shown in Fig. 6.9(b).

One immediate observation from this figure is that the interpole winding is not local in its action. This means that the winding doesnot develop radial field (Hn) confined to the commutation zone (q-axis) only, but rather its radial field extends over almost the whole pole face. Energisation of the interpole winding constructed in this manner will therefore lead to slight distortion of resultant radial field in the airgap of the machine.

Since the condition for this case in the same as that for case two (section 6.5.2), the values of Hn_f and Hn_a remain the same as previously calculated.

$$Hn_f = -44783.5 \quad A/m$$

$$Hn_a = 91535.4 \quad A/m$$

The third component of radial field due to interpole winding excitation can be calculated in a similar manner. The interpoles are connected such that in the motoring case, their polarities are opposite of the main pole in advance (in the direction of rotation), Fig. 6.9(b).

Hence the radial field of the interpole (Hn_{cp}) is directly opposite that due to the armature winding.

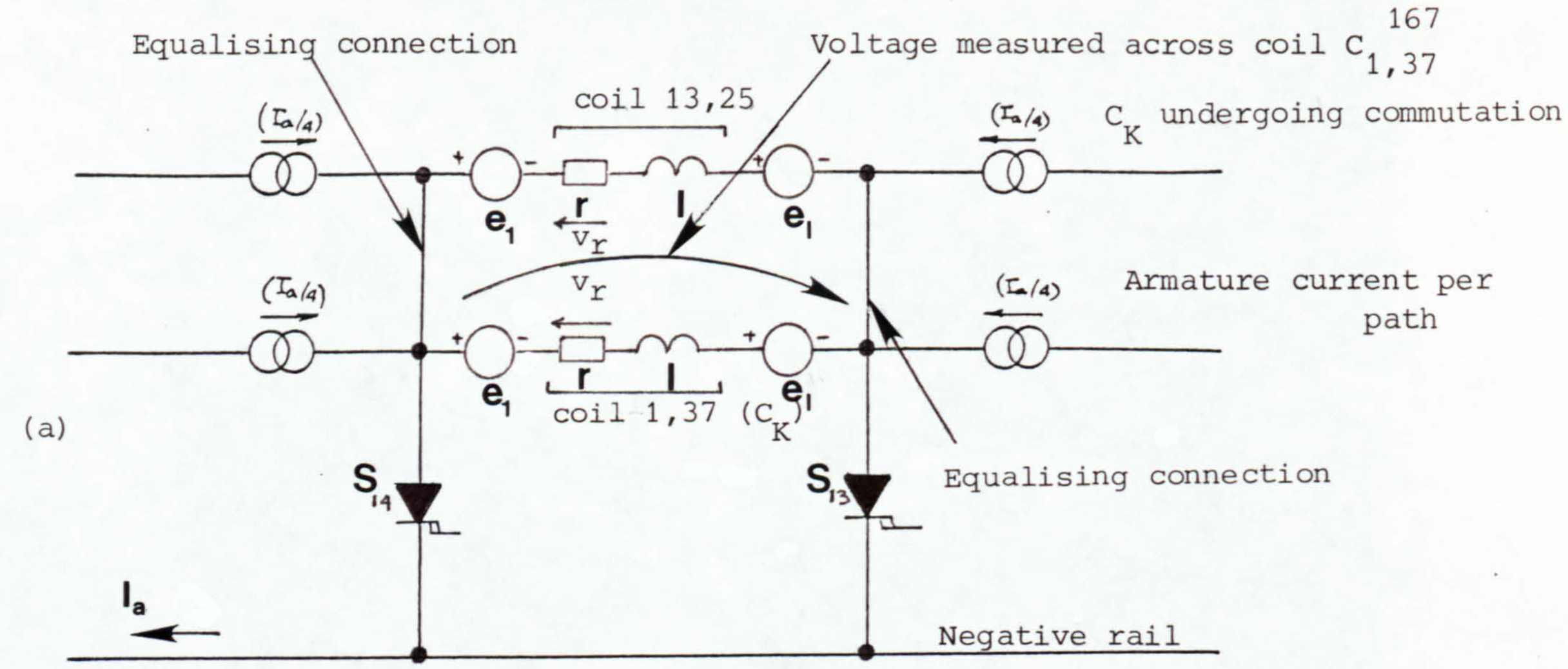

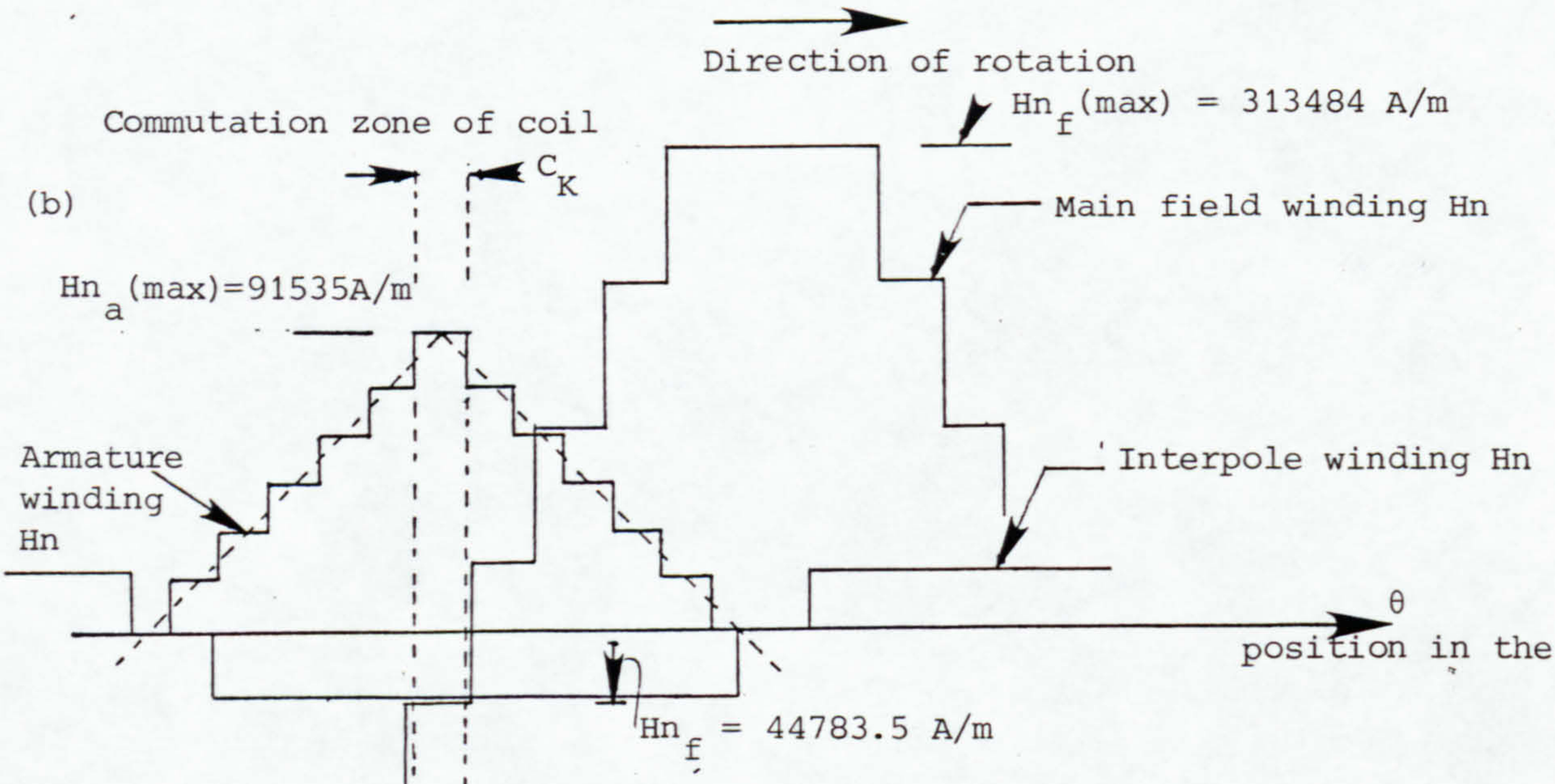

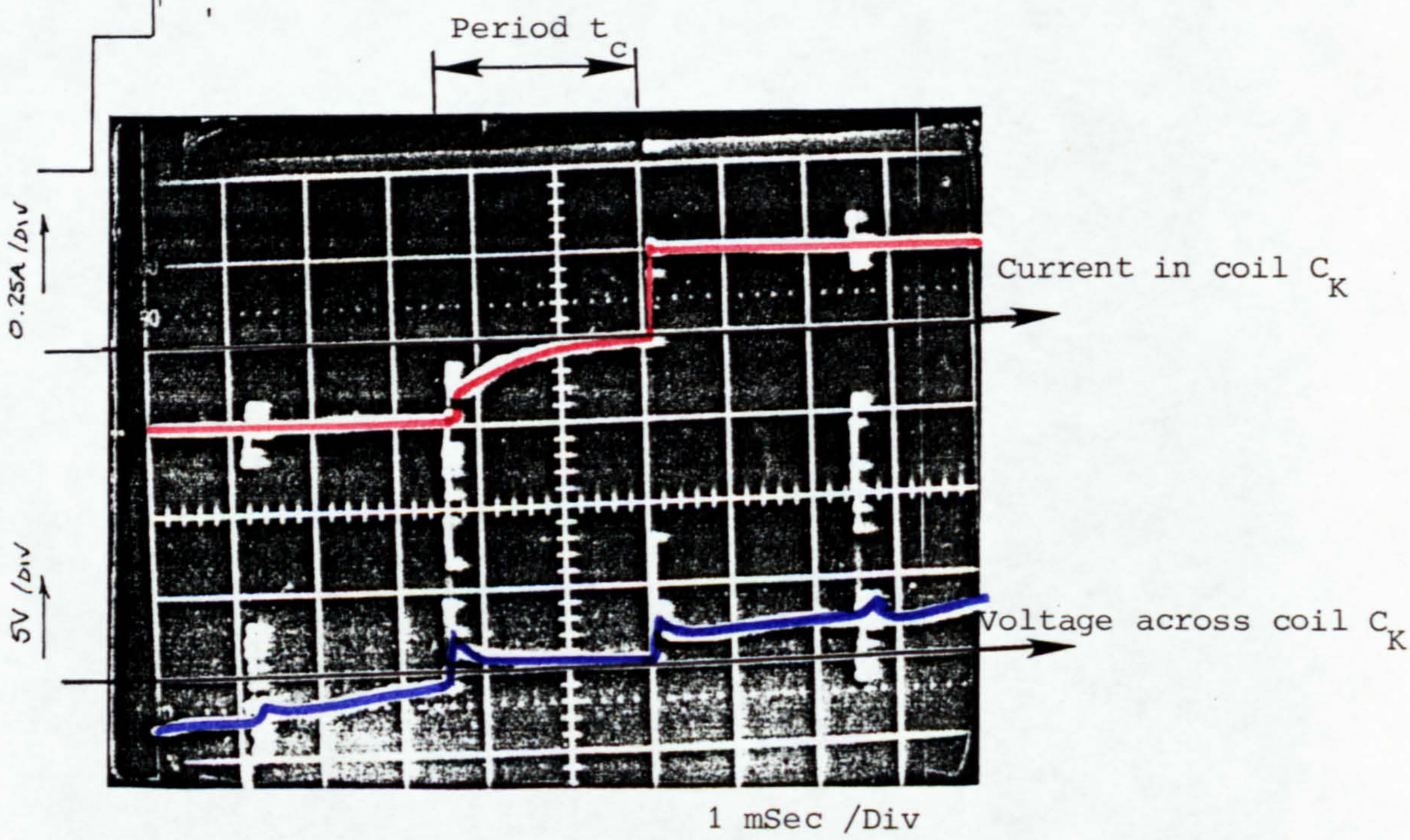

Fig. 6.9 Same as Case (2) but with the Interpoles excited

The radial field due to current excitation of 2.0 A to the interpole winding is given by

$$Hn_{cp} = (n)(I_{cp})/(2g)$$

$$= (2 \times 13)(2.0)/(2 \times 0.508\times10^{-3}) = - 51181 \quad A/m$$

Addition of these three components of radial field gives the resultant radial field in the commutation zone of coil C_k.

$$Hn_r = Hn_f + Hn_a + Hn_{cp}$$

$$= 4429.2 \ A/m$$

The flux density in the commutation zone of coil C_k

$$Bn_r = 0.00557 \quad Wb/m^2$$

The dynamic e.m.f. induced in coil C_k undergoing commutation

$$e_1 = 2 \times 31(0.00557)(101.6\times10^{-3})(3.488) = + 0.0512 \ V.$$

Clearly, the radial field set-up by the interpole winding has substantially reduced the dynamic e.m.f. in the coil undergoing commutation (coil C_k). Ideally, if the resultant potential difference across coil C_k is reduced to zero then current will be shared equally between the two adjacent conducting GTOs.

Inspection of the oscillogram of Fig. 6.9(c) shows the effect of the interpoles in improving the current sharing between two adjacent overlapped thyristors. The oscillogram also shows that the current in the commutated coil decays from a value $(-I_a/4)$ to nearly 0.0 A during the commutation period t_c .

Hence an inductive voltage given by

$$e_l = l \ (\Delta i/\Delta t)$$ must be considered.

The value of a coil C_k inductance is 4.52 mH

$(\Delta t) = t_c = 2.84$ msec (from equation 3.17, for n=440 rpm)

$$\therefore \quad e_l = 4.52\times10^{-3}(-I_a/4)/(2.84\times10^{-3}) = - 0.398 \ V$$

The resistive voltage drop is the same as calculated for case

two, $V_r = -0.0933$ V.

Addition of these components of voltage give the resultant voltage across coil C_k during its commutation period t_c .

$$V\ (\text{total}) = (0.0512)+(-0.0933)+(-0.398)$$

$$= -0.44\ V$$

The oscillogram of Fig. 6.9(c) confirms the improved current sharing during period t_c, between the two adjacent GTO thyristors when the interpoles are excited. The voltage across the commutated coil is clearly reduced to nearly zero during the commutation period t_c . Experimental tests on the machine also showed that the transient overshoot voltages across armature GTO switching devices were significantly reduced (almost halved) for this case when the interpoles were excited. This agrees with the theoretical consideration of this condition : When the interpoles are excited (in the correct polarity) then the current is shared between the adjacent conducting devices.

i.e. each device will carry half armature current (for the case of ideal current sharing).

Hence 50% reduction in the transient spike voltage. This result is significant.

6.5.4 CASE FOUR: FORWARD SHIFT OF COIL C_k COMMUTATION AXIS

This is accomplished by forward movement (in the direction of rotation) of the Index pulse axis. Fig. 6.10(b) illustrates this condition. The commutation of coil C_k is now moved into the positive fringe field of the main field winding.

The voltage induced in coil C_k due to this radial fringe field is positive adding to that due to armature winding radial field.

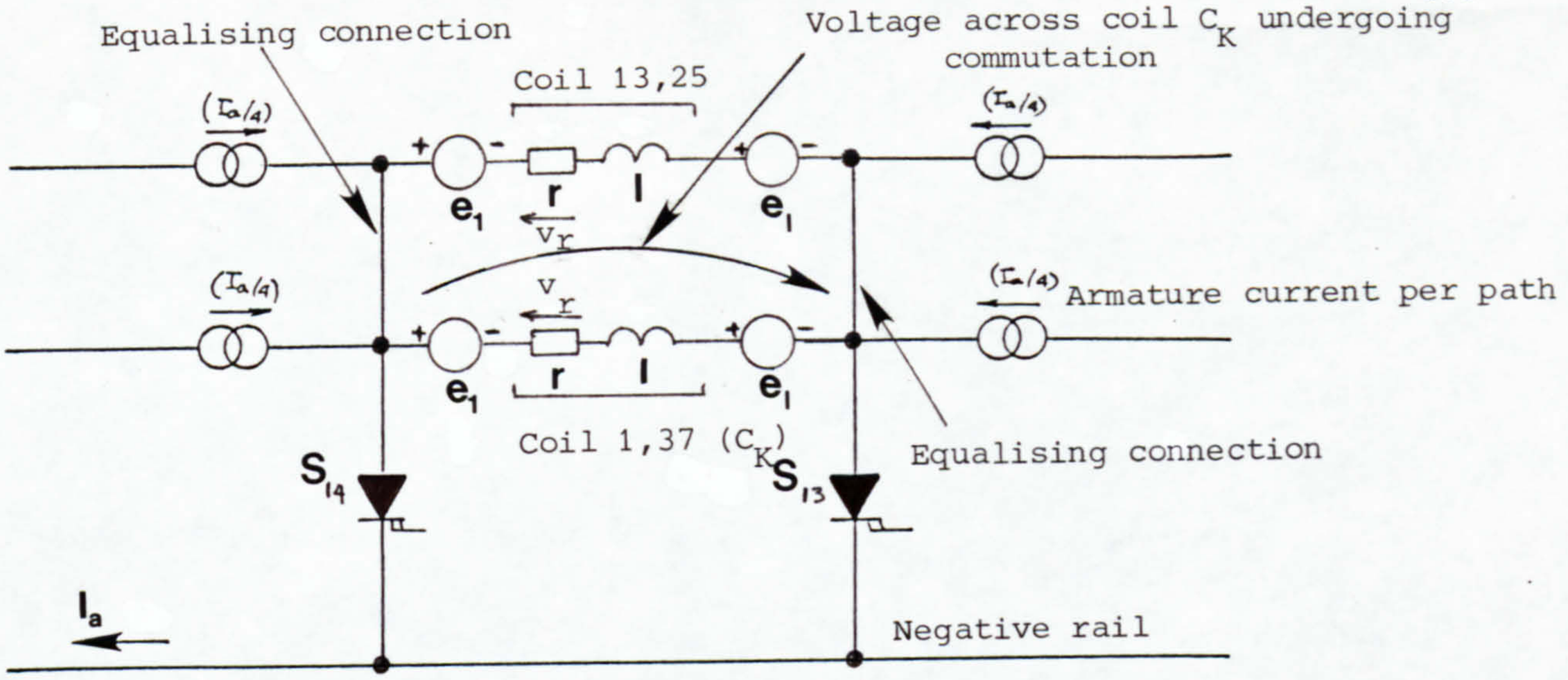

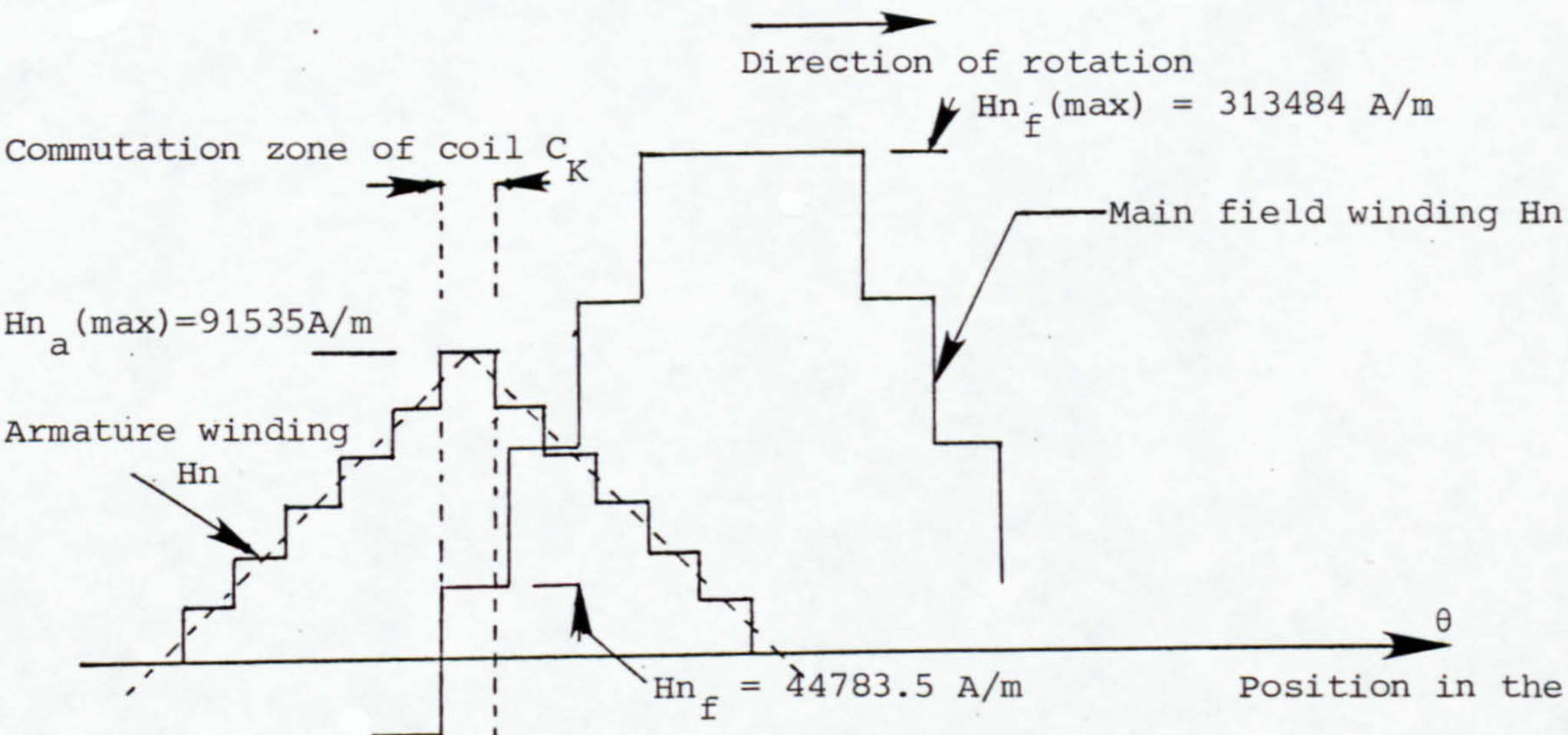

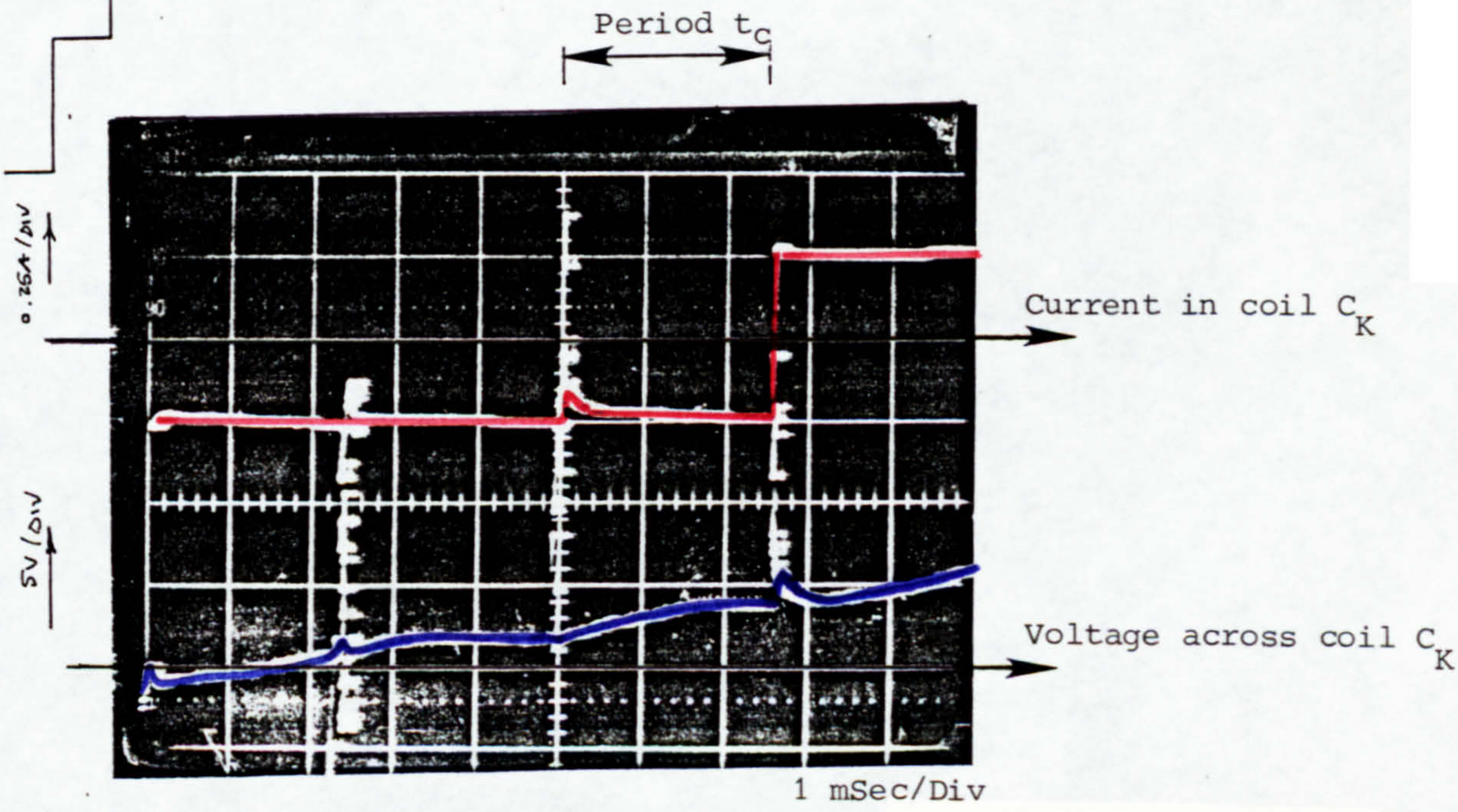

Fig. 6.10 Forward shift of axis of coil undergoing commutation - overlapping
- Interpoles not excited

The result is a larger positive voltage which will impair the current sharing between the two adjacent overlapped GTO thyristors.

oscillogram of Fig. 6.10(c) clearly shows this where the voltage across commutating coil (C_k) rises from around +1.5V to +4.0V during the period t_c .

The position of commutated coil C_k is shown on the radial field distribution diagram, Fig. 6.10(b). From this it can be seen that commutation of coil C_k starts when the value of Hn_f is negative and finishes when Hn_f is positive.

$Hn_f = (-1/7)xHn_f(max) = -44783.5$ A/m {at the start of period t_c}

$Hn_f = (+1/7)xHn_f(max) = +44783.5$ A/m {at the end of period t_c}

The value of $Hn_a(max)$ (maximum radial field due to armature winding excitation) is the same as previously calculated.

$Hn_a = 91535.4$ A/m

The interpoles are not excited in this case; $Hn_{cp} = 0.0$ A/m

The resultant value of Hn_r in the commutation zone of coil C_k varies from

(-44783.5 + 91535.4) = 46752 A/m {at the start of period t_c}

(+44783.5 + 51535.4) = 136319 A/m {at the end of period t_c}

The corresponding value of flux density can be calculated

$Bn_r = 0.05875$ Wb/m^2 {at the start of period t_c}

$Bn_r = 0.1713$ Wb/m^2 {at the end of period t_c}

The motional e.m.f. induced in coil C_k undergoing commutation due to these value of flux density is calculated as follows:-

At the start of commutation of period t_c

$e_1 = 2 \times 31\ (0.05875)(101.6x10^{-3})(3.488) = 1.2908$ V

At the end of commutation period t_c

$e_1 = 3.764$ V

The resistive voltage drop across coil C_k remains the same as previously calculated {V_r = - 0.0933 V }.

Current sharing cannot be achieved in this case because of the finite potential difference across coil C_k during period t_c .

The current reverses direction rapidly only at the end of commutation period tc, e_1 = 0.0 V

Adding these components of e.m.f.s gives the resultant potential difference across coil C_k during its commutation period.

At the start of commutation of coil C_k, V (total) = 1.20 V

At the end of commutation of coil C_k, V (total) = 3.67 V

This voltage variation across coil C_k is confirmed in the oscillogram of Fig. 6.10(c).

Hence with a forward shift of armature commutation axis, as in this case, current sharing between adjacent GTo thyristorscan not be obtained because, as verified, the voltage across the commutating coil is finite and large. The transient overshoot voltage due to rapid current reversal in the commutated coil is the same as that calculated for case one.

6.5.5 CASE FIVE: BACKWARD SHIFT OF COIL C_k COMMUTATION AXIS

The radial field distribution of Fig. 6.11(b) illustrates this case, the commutation zone of coil C_k is backward shifted in the main field winding fringe field of polarity opposite to that of the main pole in advance (in the direction of rotation). The maximum value of radial field due to current excitation to the main field winding is 313484 A/m. The radial fringe field in the commutation

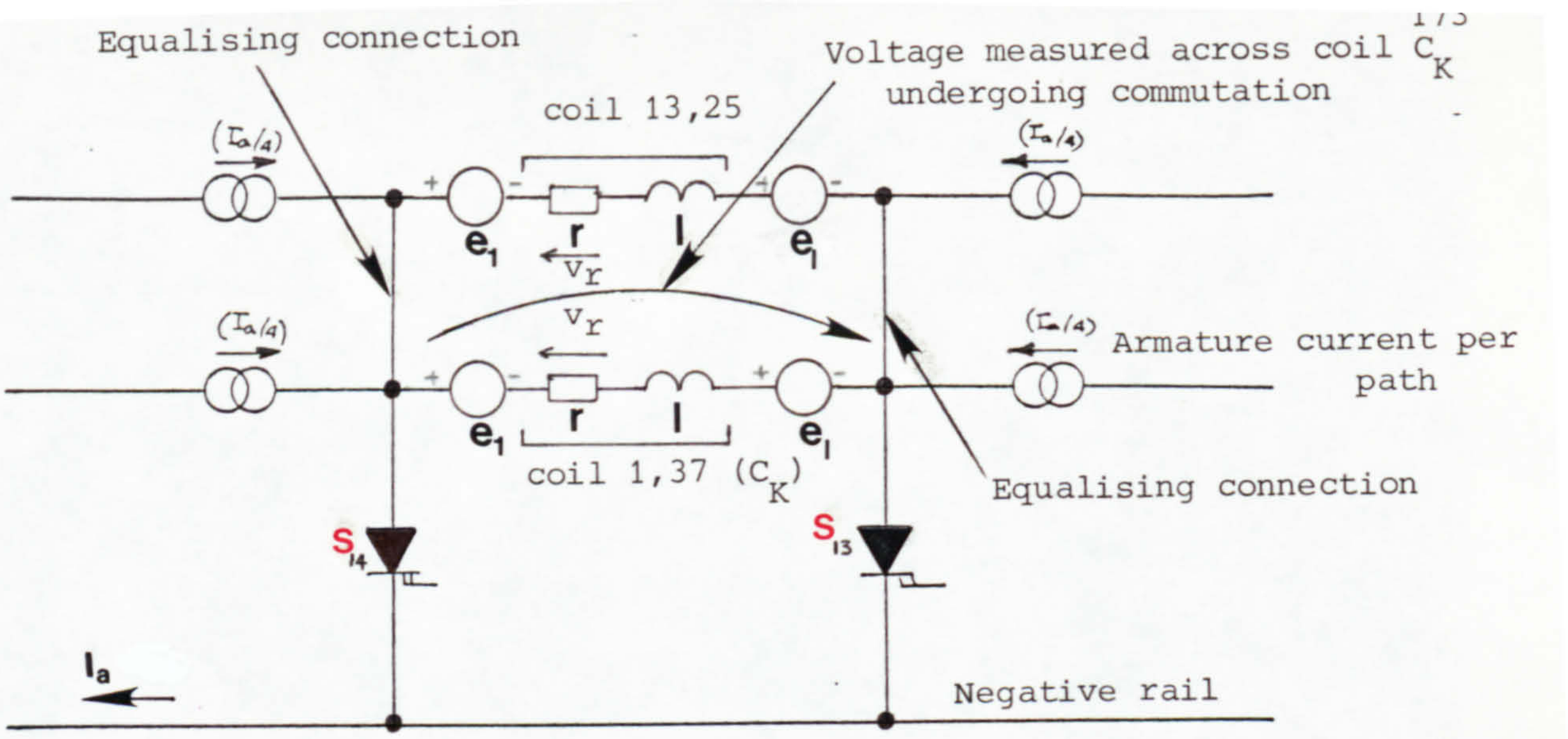

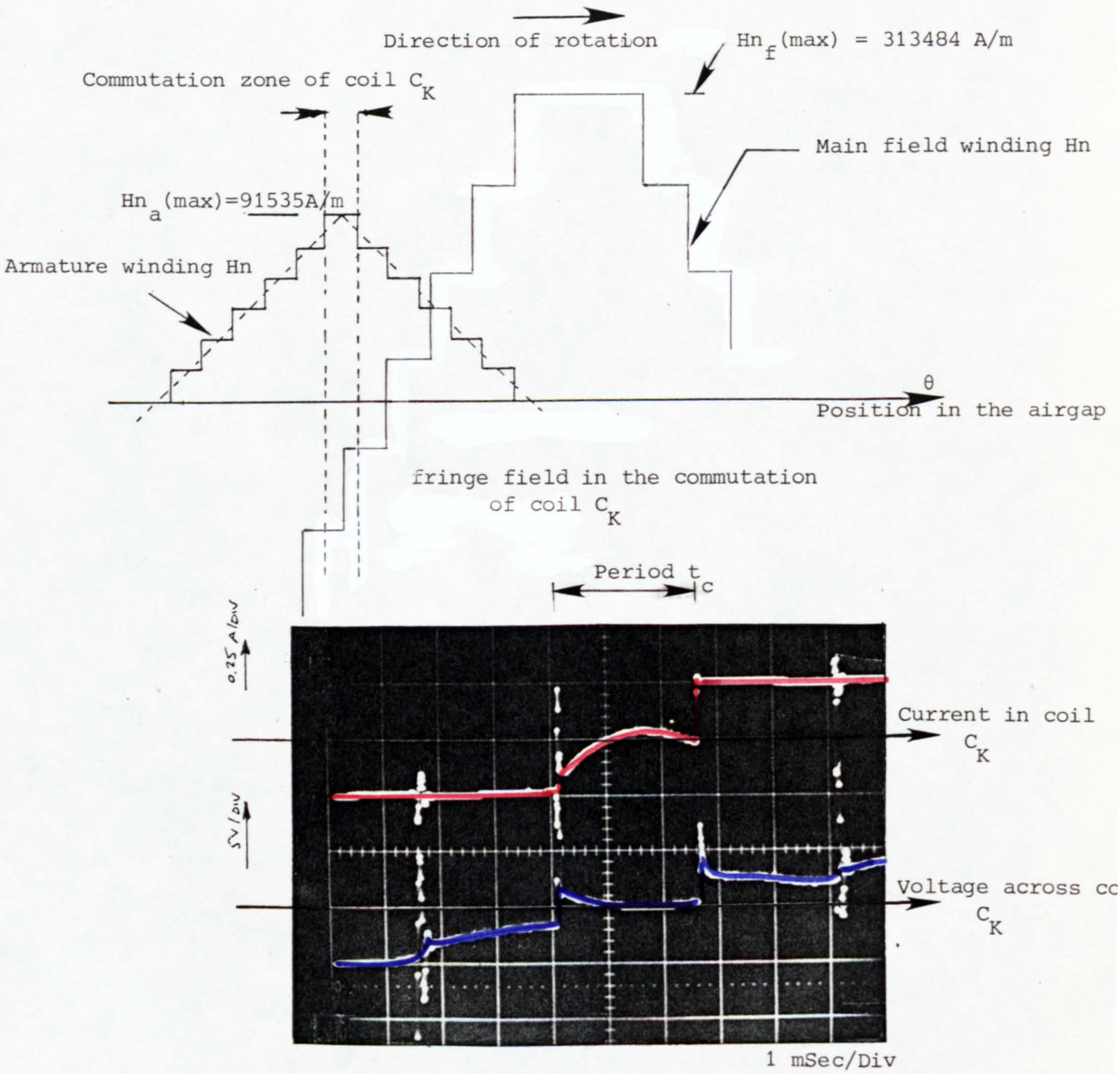

Fig. 6.11 Backward shift of axis of coil undergoing commutation overlapping - Interpoles not excited

zone of coil C_k has an average value (2/7)xHn_f(max).

i.e. Hn_f = - 89567 A/m

The peak radial field intensity due to current excitation to the armature winding

Hn_a(max) = 91535.4 A/m

Resultant radial field in the commutation zone of coil C_k

Hn_r = (91535.4) + (-89567) = 1968 A/m

The corresponding value of flux density

Bn_r = 0.00247 Wb/m^2

The dynamic e.m.f. induced in coil C_k due to this radial flux

e_1 = 2 x 31 (0.00247)(101.6x10^{-3})(3.488)

= + 0.0543 V

The resistive voltage drop (V_r) = -0.0933 V

The oscillogram of Fig. 6.11(c) clearly shows the current change from a value ($-I_a/4$) to zero during period t_c.

The e.m.f. of self induction of coil undergoing commutation is

e_1 = 1($\Delta i/\Delta t$) = 4.52x10^{-3}($-I_a/4$)/(2.84x10^{-3})

= -0.398 V

Hence the resultant potential difference across coil C_k undergoing commutation for this case is

V (total) = - 0.437 V

This case clearly verifies that with a backward shift, the effect is similar to the introduction of the interpoles: the resultant radial field in the commutation zone of an armature coil is effectively reduced to zero, resulting in the reduction of the potential difference across the coil.

The above analysis on current commutation in an armature coil

provided some interesting results. Reflecting on the five cases considered, the following concluding comments can be made:

(a) With the armature GTO devices sequentially triggered but not overlapped, the current in the coil undergoing commutation reverses rapidly at the instant of switching transition when the conducting GTO device is turned off and the next device (in the sequence, in the direction of rotation) is turned on. The rapid current reversal in the commutated coil results in a transient overshoot voltage across the anode-cathode terminals of the device which has been switched-off whose magnitude is determined by the e.m.f of the self induction of the commutated coil, $l(\Delta i/\Delta t)$. Equation 4.12 gives an analytical expression for determining the peak value of overshoot voltage due to current commutation in a particular armature coil.

(b) When armature GTO devices were pulsed in overlapped sequence, current sharing was not achieved between the two adjacent conducting devices. To achieve current sharing, it is necessary to reduce the resultant radial field in the commutation zone of an armature coil to nearly zero. In the foregoing analysis, it was verified that excitation of the interpole winding can accelerate and control the process of current reversal in the short circuited coil by inducing a dynamic e.m.f. (of the correct polarity) in the coil sides due to its passage in the interpole radial flux density. For the case of motoring, the polarity of the e.m.f. should be opposite to that about to be experienced by the coil as it emerges after commutation {see the radial field distribution diagram of Fig. 6.9(b)}.

(c) The process of current commutation in an armature coil is impaired if the axis of the commutating coil is moved in a direction

such that the main field winding radial field in the commutation zone is positive (for the motoring case), i.e. forward movement of the index pulse axis. This will lead to increased dynamic e.m.f. developed across the commutating coils, increasing the resultant potential difference across the coil. Clearly, this does not lead to current sharing between adjacent staggered devices. For the case when the axis of the commutated coil is backward shifted, in a direction where the radial fringe field has a polarity opposite to that of the main pole field ahead (in the direction of rotation), current sharing between the adjacent overlapped devices was achieved. This feature can be utilised for improving the current commutation in an armature coil as an alternative to using interpoles, as explained in chapter seven.

CHAPTER SEVEN

CONCLUSIONS AND SUGGESTIONS FOR FUTURE WORK

CHAPTER SEVEN

CONCLUSIONS AND SUGGESTIONS FOR FUTURE WORK

7.1 CONCLUSIONS

The subject of this thesis, the development of a DC machine with a statically switched armature winding, capable of being operated as a motor or as a generator has been successfully achieved. The subject matter details the overall description of the developed machine with a comprehensive analysis of the experimental results obtained.

The developed machine has its armature winding located on the stator, interconnected in "lap" configuration with "paralleling" connections on similar coils a double pole pitch apart as described in section 3.4.2 of chapter 3. The paralleling connections not only "equalise" the e.m.f.s at those points which are a double pole pitch apart, but also halves the required number of armature GTO switching devices, for the case of the 4-pole configuration.

In the initial development stage, the machine was required to operate in the motoring mode, this mode was successfully achieved without the use of the series connected diodes described in section 4.3.4, Fig. 4.3(i). This is because, when operating as a motor, the voltage across the thyristors is always in the correct forward-bias direction. Reversal of the polarity of the supply of the main field winding in the generating mode, will lead to the reversal of the

voltage across the GTO thyristor devices, and since GTOs cannot block significant voltages, it was necessary to connect a diode of the type BY 249 - 600 rated at 6.5 A - mean forward current, in series with each armature GTO thyristor as shown in Fig. 4.3(i), chapter 4.

The pulses which define the conduction periods of the armature GTO thyristors are generated by the digital control logic circuit in conjunction with an incremental shaft encoder. The rotary encoder provides output pulses corresponding to increments of rotor displacement, together with a reference "index" pulse generated once per revolution and used as a "reference marker" of the instantaneous position of the quadrature axis. The relevant details of the encoder, how the index pulse was set-up and adjusted to serve as the quadrature axis marker, and also subsequently used for resetting and synchronisation of the bistables in the logic control circuit shift register, are given in chapter five. The digital control circuit designed by the writer is capable of organising correctly the switching sequence of all the armature GTO switching devices, defining the absolute switching period of a particular device. The control circuit is designed such that to obtain optimal torque angle during the normal running condition of the machine, the axis of radial field of the armature winding is maintained in space-quadrature with that of the rotor main field winding, as is normal for operating conventional DC machines with quadrature axis brushes. The added flexibility incorporated within the digital control circuit permitted the investigation of the following effects on the commutation of the current in an armature coil:

(a) The switching of the armature GTO thyristors to obtain the

required space-quadrature relationship between the axis of the radial fields of the armature and main field windings, such that a conducting GTO device is turned-off at the same precise instant when the following device (in the sequence, in the direction of rotation) is switched-on; this is referred to as "sequential triggering", the timing diagram for this case is given in Fig. 5.8(i) of chapter five with the relevant analysis given in section 6.5.1 of chapter six.

(b) Simultaneous conduction of two adjacent armature GTO devices during the commutation period of a particular armature coil while ensuring the space quadrature relationship between the axis of the radial fields of the armature and main field field winding. This condition is referred to as overlapping, the timing diagram for this case is given in Fig. 5.8(ii) with the relevant analysis and discussion given in section 6.5.2 of chapter six.

(c) The effect of exciting the interpole winding for the case of overlapping the conduction periods of two armature GTO switches, discussed in section 6.5.3 of chapter six.

(d) Controlled departure of the axis of the radial field of the armature winding from the quadrature axis of the main field winding, both in the forward direction (section 6.5.4) and backward direction (section 6.5.5), accomplished by the redirection of the index pulse within the digital control circuit - the relevant timing diagrams given in Fig. 5.9 of chapter five.

For the case of sequential switching of the armature GTO devices - Fig. 6.7, the current in the coil undergoing commutation reverses when the switching occurs. The current reversal is rapid (typically

in a time of 15 μsec), occurring precisely at the instant of switching transition. This rapid current reversal in the coil undergoing commutation results in an e.m.f. of self induction which appears across the anode cathode terminals of the device which has been turned-off. In chapter four, section 4.4 an empirical formula was derived (equation 4.12) relating the peak overshoot voltage at turn-off of the device to the parameters of the commutated circuit. Oscillograms of the anode-cathode voltage recorded across an armature GTO device shown in Fig. 6.2(c) show a peak overshoot voltage typically of the order 150 V for an armature load current of 1 A; this result closely agrees with the value calculated theoretically using equation 4.12 as discussed in section 6.2 of chapter six. The peak overshoot voltage across the terminals of the device can be controlled by the value of the capacitor in the slow-rise (snubber) circuit.

The requirement for current sharing between two adjacent armature GTO devices when allowed to conduct during the commutation period of a particular armature coil, stems from the fact that it not only leads to improvement of the switching duty of the armature switches, but also reduces the peak overshoot voltage on the devices at turn-off. Current sharing between the adjacent overlapped devices was not achieved for the cases when the resultant radial field in the commutation zone is finite and has a polarity the same as that of the main pole ahead. However, current sharing was achieved in the cases when the resultant radial field in the commutation zone was reduced to zero by using the interpole facility or shifting, as explained below.

The main field and interpole windings located in the rotor of the

inverted machine has its coils distributed in slots as previously described in section 3.4.1 of chapter 3. This gives the windings the following features:

(i) The radial field due to current excitation to the interpole winding is not confined to the "interpolar space" where commutation is occurring, but extends over approximately (3/4) of a pole pitch (for the case when 2 coils per pole are utilised for the interpole winding - see Fig. 3.10 or 6.9). Ideally the interpole winding should develop radial field precisely confined to the commutation zone of an armature coil (the commutation zone for the inverted format of the machine occupies (1/12) of a pole pitch). In the experimentation carried out it was observed that substantial current excitation of the interpole winding, although leading to the improvement in the current sharing between the adjacent overlapped devices, resulted, on account of its distributed nature, in the distortion of the resultant radial field in the airgap of the machine.

(ii) The radial field due to current excitation of the main field winding, although zero at the "precise" d-axis, is finite as experienced by an armature coil during the period of its commutation, changing from a certain "positive" value in one direction to a certain "negative" value in the opposite direction as clearly demonstrated in the radial field diagram of Fig. 6.7, chapter six. Therefore commutation occurs in a finite radial fringe field. This feature is useful because, considering the case of motoring, when the commutation zone of an armature coil is backward-shifted in a fringe field of polarity which effectively cancels the radial field of the armature winding, then the resultant radial

field in the commutation zone may be effectively reduced to zero with the consequence of improving the the current sharing between the armature overlapped devices - Case (5), chapter six. The controlled shift required can be calculated for total cancellation of armature radial field in the commutation zone.

Throughout the work, the performance and characteristics of the developed format of the machine were fully investigated by observing and analysing the radial field distribution due to current excitation of both the stator and rotor windings of the machine. The radial field due to current excitation to the main field winding was derived in section 3.6.1 of chapter 3, that of the armature and interpole winding in section 3.6.2 and 3.6.3 of the same chapter, respectively. The distribution of the resultant radial field in the airgap of the machine for operation in the motoring mode was analysed in section 6.2 of chapter six. In each case, the theoretical distribution derived, based on certain assumptions and the experimental result given. It is clear that the theoretical and experimental results in each case are in close agreement, confirming the validity of the assumptions made.

This study carried out by the writer clearly demonstrates the feasibility of using solid-state devices such as gate turn-off thyristors for current commutation in the armature coils of a DC machine, eliminating many of the problems encountered in the previous designs { Zabar [16], see also section 1.5 of chapter one }.

Future development should include:

(i) The use of a rotor system in which the main field winding

poles are excited by field currents in concentrated coils i.e. a rotor of salient pole structure. The advantage of such rotor system will be the increased flux per pole with the available rotor diameter. The poles can be shaped to obtain finite fringe field in the quadrature axis. The method of "digital controlled departure" of the armature switch tapping points from the quadrature axis can then be used for improving commutation, hence dispensing with the requirement for the interpole facility on the machine.

(ii) The number of armature switching devices needed in solid-state commutation is twice the number of commutator segments. Since the peak overshoot voltage (at turn-off) on the electronic switches can be controlled by the designer, the number of armature tappings may be reduced to a more economical level. Two schemes are possible with the available layout of the existing stator winding:

(a) The number of armature tappings can be reduced to eight, requiring eight positive rail and eight negative rail connected GTO devices as shown in scheme 1, Fig. 7.1.

(b) Alternatively, the number of armature tappings can be made asymmetrical by using six GTO devices connected to the positive rail and, twice this number connected to the negative rail as shown in scheme 2, Fig. 7.2. Since individual power supplies are needed for the positive rail GTO gate drive circuits, this scheme is economical because only six isolated power supplies are needed for the positive rail GTOs while the twelve negative rail GTOs can be supplied from a common unit. The timing diagram for the case of sequential triggering for this scheme is given in Fig. 7.3, from which it can be seen that two negative rail

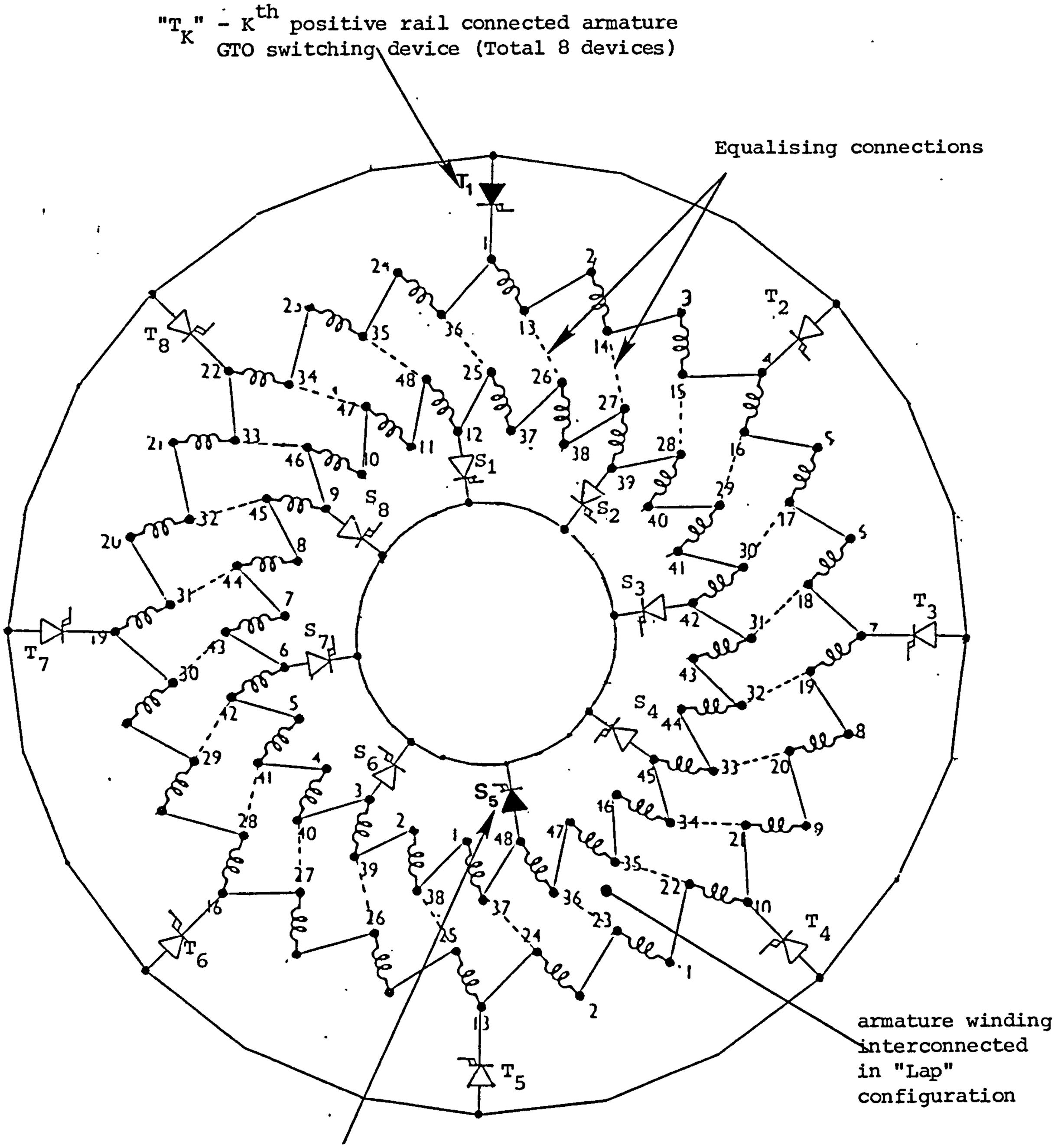

Fig. 7.1 Scheme 1

"T_K" - K^{th} positive rail connected armature GTO switching device
(Total 6 devices)

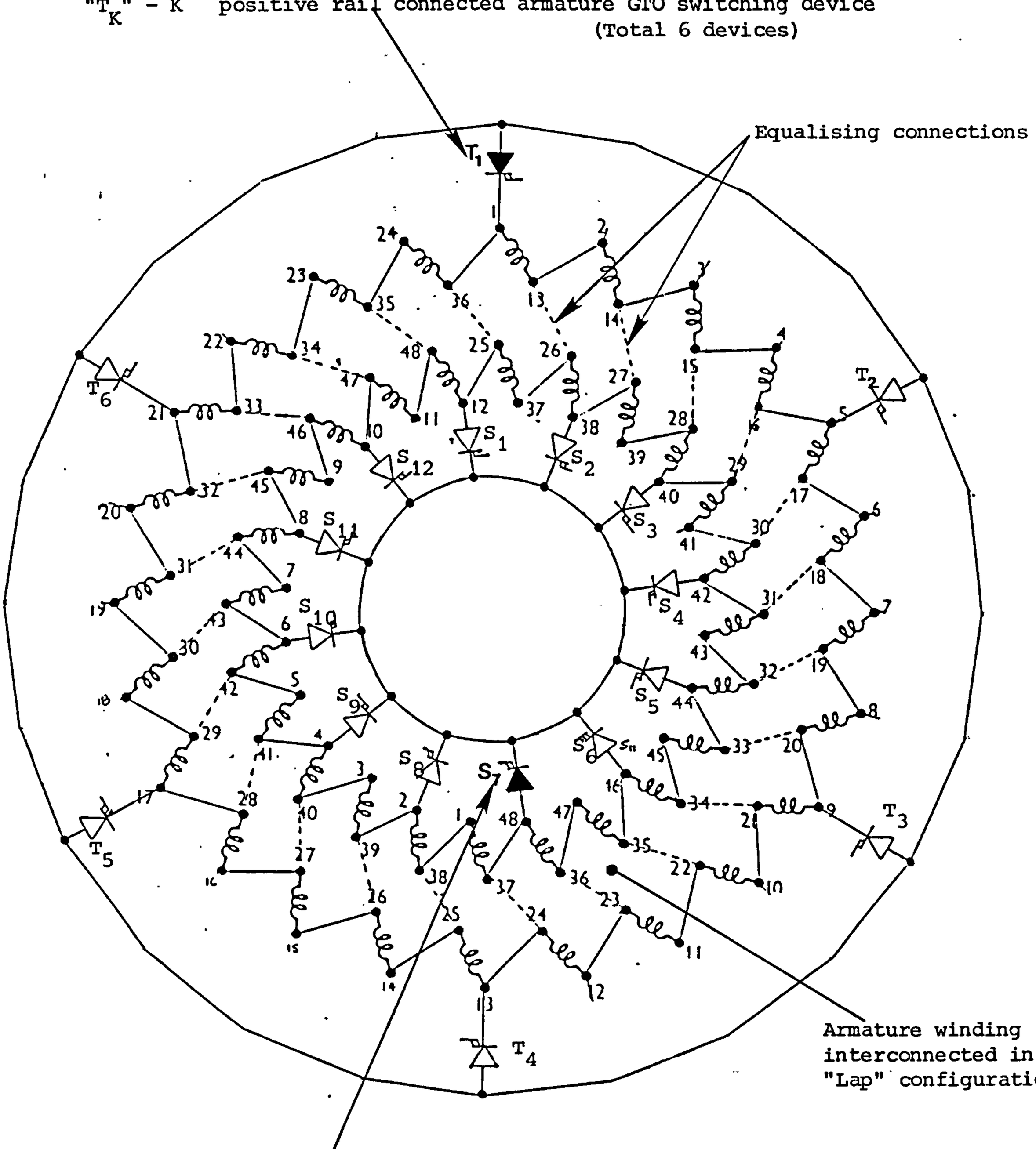

"S_K" - K^{th} negative rail connected armature GTO switching device
(Total 12 devices)

Fig. 7.2 Scheme 2

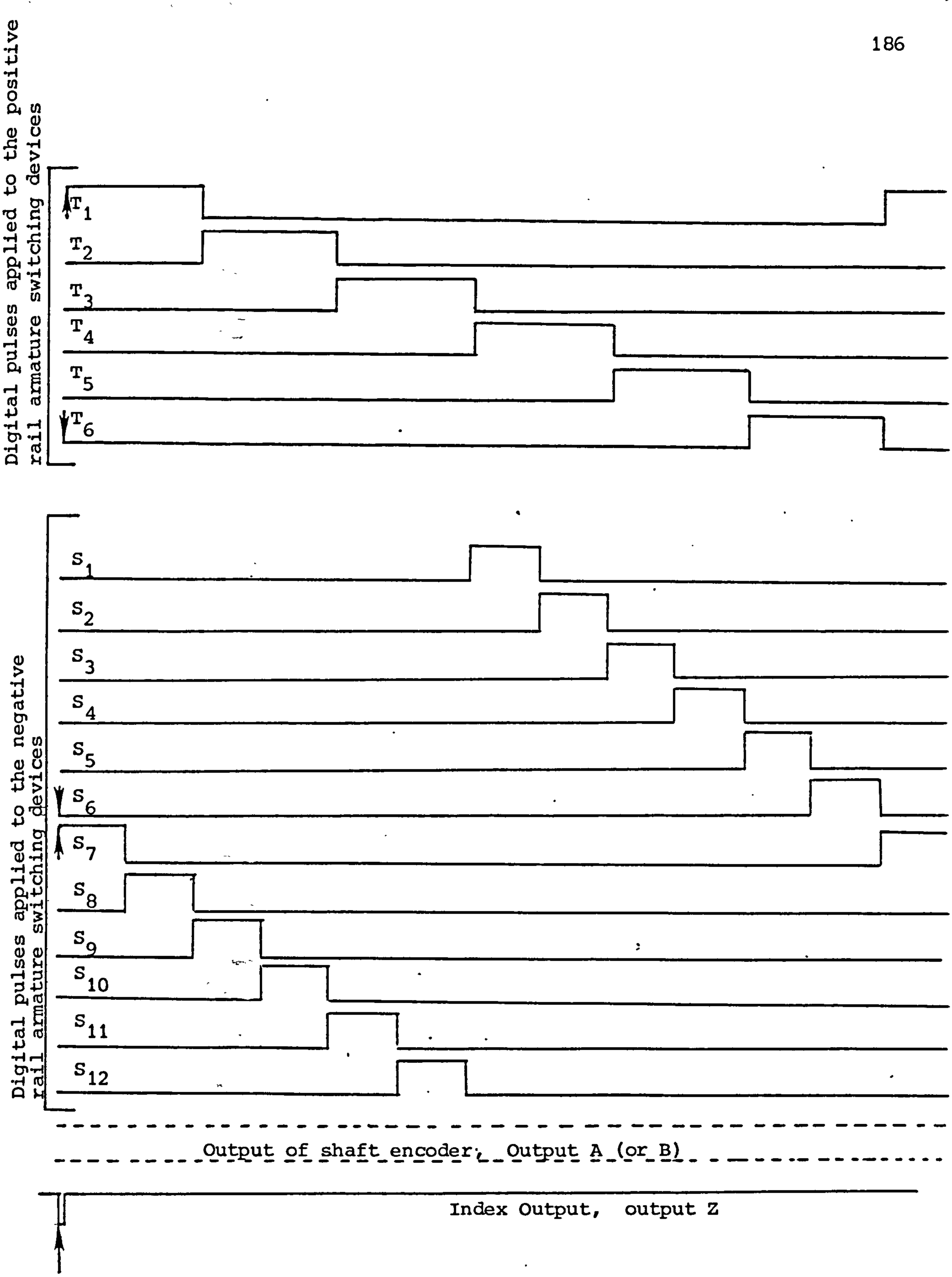

Fig. 7.3 Timing diagram for armature switching devices for Scheme 2

connected GTO devices conduct during the conduction period of one positive rail connected device. The reduced number of armature tappings in either of the two schemes leads to an advantage to be gained when the method of "digital controlled departure" is used for improving commutation, since each "departure step" brings the commutation zone of an armature coil in a substantially larger radial fringe field.

(iii) Uprating the machine in terms of speed as detailed in section 7.2.

(iv) Investigation into the use of a microprocessor to fulfil and perform the functions of the digital control logic circuit while at the same time serving as a fully digital speed control scheme to provide a four-quadrant drive capability.

Commutation using gate turn-off thyristors as proposed by the writer eliminates many of the limitations of conventional variable speed DC drives. In the experimentation carried out by the writer, it was confirmed that the controlled departure of the axis of the radial field of the armature winding from the quadrature axis position, gives rise to a change of speed. Such "digital controlled departure" of the radial field of the armature can be the subject for further investigation for possible use for speed control of the machine, as an alternative to field current or armature voltage variation.

7.2 DESIGN SPECIFICATION FOR FUTURE DEVELOPMENT

In the presentation of the experimental results in section 6.2 of chapter six, it was stated that the inverted machine as tested was capable of developing full load torque but at reduced speed. This is because of the high value of field current, calculated on the basis of equal electric loading as given by the original format of the machine, resulting in the machine operating at lower speeds (the machine speed decreases with increasing field current, as is normal for DC machines; see Fig. 6.1 of chapter six).

To obtain rated speed of 2400 r.p.m. as given by the original format of the machine, it is necessary to operate the machine at a reduced field current and possibly increase the applied armature voltage.

The following analysis details the evaluation of the required field current excitation, full load armature current, corresponding semiconductor switching device rating and protection requirements, assuming that the machine is to be supplied with an armature voltage of 240 V.

If the electric loading calculated for the main field winding in chapter 3 is halved, then that of the armature winding must be doubled to obtain rated torque.

Referring to section 3.5.2.1 of chapter three, the armature current required to obtain rated torque is 4.3 A. Therefore, armature current to obtain rated torque at rated speed = 2 x 4.3 = 8.6 A

Using the analysis given in section 6.4, but working backwards, current excitation to the field winding can be calculated from the

knowledge of the maximum value of the radial field:

The lap interconnected armature winding remains the same as previously discussed in chapter 3 except that the number of armature switching devices is reduced, as shown in Fig. 7.2, scheme 2.

The armature is to be directly connected to a 240 V DC supply, R_a = 2.45 ohms.

Using equation 6.2, the value of armature generated e.m.f. can be calculated. Thus:

$$E_a = V_a - I_a R_a$$

$$= 240 - (8.6)(2.45) = 220 \text{ V}$$

There are 12 series connected armature coils between two armature tappings which are a pole pitch apart, e.g. assuming the conduction period of armature GTO thyristors T_1 and S_7, Fig. 7.2 .

The average e.m.f. in one armature coil = 220/12 = 18.333 V.

Using equations 6.3, 6.4 and 6.5, the maximum value of radial flux density, hence peak radial field intensity of the main field winding can be calculated as follows :

$$e_c = 2 \times n_c \{ Bn_f(av) \times 1 \times v \}$$

The instantaneous value of radial flux density, $Bn(\theta)$, is known from the distribution previously described in Fig. 6.6 and the analysis given in section 6.4.

The average value of radial flux density can be calculated

$$Bn_f(av) = Bn_f(max)\{ \frac{1}{7} + \frac{2}{7} \times \frac{7}{9} + \frac{2}{7} \times \frac{5}{9} + \frac{2}{7} \times \frac{3}{9} \}$$

$$= 0.6190\ Bn_f(max)$$

Rotor peripheral speed for n = 2400 rpm

$$v = (\pi \times d)(2400/60) = 19.03 \text{ m/sec, hence}$$

$$e_c = 18.33 = 2 \times 31 \{ 0.6190\ Bn_f(max) \times 101.6 \times 10^{-3} \times 19.03 \}$$

$Bn_f(max) = 0.2471 \quad Wb/m^2$

The corresponding maximum value of radial field intensity

$Bn_f(max) = \mu o \times Hn_f(max)$

$Hn_f(max) = 196646 \quad A/m$

$= (n \times I_f)/2 \times g$

$I_f = 2.2 \ A$

Comparing this value of field current with that obtained in section 3.5.2.2 of chapter 3, it is clear that the field winding loading has been reduced by half; however the armature electric loading has been doubled in order to obtain the rated torque.

Armature current at full load, rated speed = 8.6 A

Allowing for 25% overload, the rated on-state current of the GTO armature switching devices will be around 10 A.

The Mullard GTO thyristor device in present use is the BTW 58 - 1300R, with average on-state current of 6.5 A. Since the duty cycle on the device is low (1/6 for the positive rail connected GTOs), this GTO can pulsed at 10 A, at reduced dV/dt (<200 V/μsec). Alternative devices are the BTV 58 - 1000R also available from Mullard, which can control the rated current at dV/dt not exceeding 300 V/μsec.

Assuming a peak dV/dt of 50 V/μsec, the size of the snubber capacitor needed can be calculated using equation 4.1 .

$C_s = I_T(pk)/(dV/dt)$

$= 10 \ / \ 50 \times 10^6 = 0.2 \ \mu F.$

An allowance should be made for the tolerance of the capacitor value. A suitable snubber capacitor is :

$C_s = 0.22 \ \mu F$, 1500 V (polypropylene)

It is expected that the reviewed design of the machine will be more attractive because of the reduced number of devices which will make the whole power electronics equipment more compact.

REFERENCES

REFERENCES

(1) Lander C.W: "Power Electronics", Book, McGraw-Hill Book Company, U.K., 1981.

(2) Shepherd W: "Thyristor control of AC circuits", Book, Bradford University press, England, 1976.

(3) Fitzgerald A.E, Kingsley C, Umans A: "Electric Machinery", Book. McGraw-Hill Kogakusha, Japan, 1983.

(4) Gray C.B, Howe D and O'Kelly D: "Modern electrical machine theory", Seminar notes, University of Bradford, September 1984.

(5) Wheeler A.R: "Comparison of electric variable speed drives", IEE PEVSD Conf. 234, London, May 1984, pp175-179.

(6) Lloyd M.R: "Survey of electric motors for use in variable speed drives", IEE PEVSD Conf. 234, London, May 1984, pp180-186.

(7) Tez E.S and Said W.M: "A Microcomputer-controlled reversible and regenerative drive system", IEE PEVSD Conf. 234, London, May 1984, pp199-202.

(8) Bhadra S.N, De N.K and Chattopadhay A.K: "Regenerative braking performance analysis of a thyristor chopper controlled DC service drive motor", IEEE Trans. Ind. electron. Contr. Instr., Vol. IECI-28, No. 4, Nov. 1981, pp342-347.

(9) Bose B.K and Jentzen K.J: "Digital speed control of a DC motor with phase locked-loop regulation", IEEE Trans. Ind. Gen. Appl., Vol. IGA-4, No. 4, July/Aug. 1968, pp396-409.

(10) Harris M.R: "Brushless Motors-A selective review", Proc. 1st European Conf. on Elect. Drives, Motors, Controls, Leeds-England, 1982, pp84-90.

(11) Bland R.J: "Factors Effecting the operation of a phase-controlled cycloconverter", Proc. IEE, 114, 12, 1967, pp1908-1916.

(12) Farrer W and Maskin J.D: "Quasi-sine wave fully regenerative inverter", Proc. IEE, 120, 9, Sept 1973.

(13) Persson E.K: "Brushless DC motors-A review of the state of art", Proc. 1st annual Int. Motor Conf., Chicago, June 1981, pp1-16.

(14) Alexanderson E.F.W and Mittag A.H. "The Thyratron motor", AIEE Trans., Vol. 53, 1934, pp1517-1523.

(15) Wilson T.G and Trickey P.H: "DC machine with solid-state commutation", Electrical Engineering, Vol. 81, Nov. 1962, pp879-884.

(16) Noat Y and Zabar Z: "Static commutator for DC motor", IEEE PES Winter Meeting & Tesla Symposium, Jan. 1976.

(17) Aichholzer G and Walzel G: "Commutatorless DC machine with auxiliary poles", Int. Conf. on Elect. Machines, Budapest, Sept. 1982, pp278-281.

(18) Radzwill W: "A highly efficient small brushless motor", Philips Tech. Review, Vol. 30, 1969, pp7-12.

(19) Ogawa T and Yoneda S: "Electronically commutated DC motor with Hall elements", Fuji Electronic Rev., Japan, 1974, pp 120-128.

(20) Radzwill W: "Small DC motors with controllable electronic commutators", IEE conference on small and special machines, Sept. 1981, pp 170-173.

(21) Yamaguchi M and Fujiwara H: "Analysis of commutatorless motors", Elect. Eng. in Japan, Vol. 89, No. 9, 1969, pp35-42.

(22) Stocken A.R: "Synchronous motor, variable speed, AC drive system", IEE Variable Speed drives conf., No. 179, London, Sept. 1979, pp 58-60.

(23) Matsui N, Yanagihara N and Tsunehiro Y: "DC commutatorless motor with a static var generator", IPEC Conf., Tokyo, 1983, pp969-980.

(24) Sato N: "Induced voltage commutation-type commutatorless motor", Elect. Eng. in Japan, Vol. 91, No. 3, 1971, pp114-124.

(25) Slabiak W and Collins G.C: "Brushless synchronous propulsion motor", S.A.E. paper no. 680455.

(26) Ohno E, Kishimoto T and Akamatu M: "The thyristor commutatorless motor", IEEE Trans. on Magnetics, Vol. MAG-3N03, 1967 .

(27) Morsy-shanab M.A: "Speed characteristics of commutatorless motors", IEEE/IAS annual meeting-Part II, Sept. 1980, pp 871-876.

(28) Frankl G and Walzel G: "The digital control of a commutatorless DC machine for an electric vehicle", CONUMEL 80, LYON-France, 1980, pp I/70-I/79.

(29) Gray C.B and Karim A.M.H: "Brushless DC machine with GTO thyristor switching", Proceedings 20th UPEC, Huddersfield Polytechnic, April 1985, pp 179-182.

(30) Say M.G and Taylor E.O: "Direct Current Machines", Book, Pitman-London, 1980.

(31) Kenjo T and Naganmori: "Permanent-magnet and brushless DC motors", Book, Clarendon press, Oxford, 1985.

(32) Kwecken J.A: "Solid-state motors control", Book, Tab books, USA, 1980.

(33)"DC motors-speed controls-servo systems", Book, Electro-Craft Corporation, July 1980.

(34) Bates J.J: "Thyristor-assisted commutation in electrical machines", Proc. IEE, Vol. 115, No. 6, June 1968, pp791-801.

(35) Bates J.J: "Using thyristors and diodes to improve commutation", IEEE Spectrum, Vol. 8,No. 1, Jan. 1971, pp38-47.

(36) Bates J.J, Stanway J and Sansum R.F: "Contact problems in machines using thyristor assisted commutation", Proc. IEE, Vol. 117, No. 2, Feb. 1970, pp387-397.

(37) Mawdsley's Generalized Electrical Machine-operating and maintenance handbook, Mawdsley's Ltd., Dursley, Gloucestershire, England.

(38) Wood P: "Switching power converters", Book, Westinghouse Electric Corporation, Research & Development Centre, Pittsburgh, USA.

(39) Foster A: "Trends in power electronics", IEE PEVSD conf., London, May 1984, pp 1-6.

(40) Stefanovic V.R: "Present trends in variable speed drives", IPEC Conf., Tokyo, Japan, March 1983, pp 438-449.

(41) Pelly B.R: "Power semiconductor devices-a status review", IEEE/IAS International Semiconductor Power Converter conf., 1982, pp 1-9.

(42) Technical literature: "Power MOS-Field-Effect Transistor", Motorola Semiconductor products Inc., No. SG 56 R2.

(43) Technical literature: "Switching power transistors", SanRex power semiconductors, Sansha Electric MFG Co., Tokyo, Japan.

(44) Taylor P.D: "future trends in GTO thyristors", IEE colloquium on GTO devices and applications, London, May 1985, pp 4/1-4/3.

(45) Burgum F.J: "The GTO-a new power switch", Electronics & Power, May 1982, pp 389-392.

(46) Bosterling W, Ludwig H, Schimmer R and Tscharn M: "Gate turn-off thyristors : their properties and applications", AEG Telefunken technical information, Oct. 1983.

(47) Hall J.K: "Characteristics of gate turn-off thyristors", 19th UPEC conf., University of Dundee, April 1984, Paper No 9.1.

(48) Woodworth A and Burgum F: "Simple rules for GTO circuit design", Mullard Tech. Pub. # M83-0137, Oct. 1983.

(49) Grant D: "Applying gate turn-off thyristors", IEE colloquium on GTO devices and applications, London, May 1985, pp 1/1-1/8.

(50) Ikeda Y: "Gate turn-off thyristors", Hitachi review, Vol 31 (1982) No. 4, pp 169-172.

(51) Hall J.K, Manning C.D and French P st J.R: "Switching properties of gate turn-off thyristors", IEE PEVSD conf., London, May 1984, pp 58-61.

(52) Matsuda Y and Fukui H: "Application engineering of gate turn-off thyristors", Hitachi Review, Vol 31 (1982) No.4, pp 173-178.

(53)"Understanding GTO data as an aid to circuit design", Mullard Tech. Pub. No. M81-0046, April 1981.

(54) Ikeda Y and Sakurada S: "Gate turn-off thyristor and drive circuits", Hitachi Review, Vol 29 (1980) No. 3, pp 127-130.

(55) Burgum F, Nijhof E.B.G and Woodworth A: "Gate turn-off switch", Mullard Tech. Pub. No. M81-0075, July 1981.

(56)"Colloquium on GTo Devices and their Applications", IEE - London, May 1985.

(57) Steigerwald R.L: "Application techniques for high power gate turn-off thyristor", IEEE conf. Pub. IAS meeting 1980, pp 165-174.

(58)"Rules for GTO circuit design : Part I & II", Electronic product design, April 1984, pp 79-85.

(59) Ohashi H: "Snubber circuits for high power gate turn-off thyristors", IEEE Trans. on Ind. Appl., Vol. IA-19, No. 4, July/ August 1983, pp 655-664.

(60) Barton T.H: "Snubber circuits for thyristor converters", IEEE Conf. Rec. IAS annual meeting, Toronto, Oct. 1980, pp 871-876.

(61) Technical literature for rotary encoder: "Sharp GP-1R52", Sharp Corporation, Electronic Component Group, Oct. 1982.

(62) Technical literature: "Design and operational considerations for the HEDS-5000 and HEDS-6000 incremental shaft encoder", Application note 1011, Hewlett Packard.

(63)"Encoder direction sensing and pulse rate quadrupling", Electronic product design, Feb. 1985.

(64)"Commutation chip keeps DC brushless motors out of harm's way", Electronic Design, April 1985, pp 183-188.

(65) Dempsey J.A: "Basic digital electronics with MSI applications", Book, Addison-Wesley Publishing Co., Reading, Mass., 1977.

(66) Millman J and Halkias C.C: "Integrated electronics: analogue and digital circuits and systems", Book, McGraw-Hill Kogakusha Ltd, Japan, 1972.

(67) Gaskell T: "Digital design techniques, part 5, Advanced sequential circuits", Practical Electronics, Dec. 1981, pp 38-41.

(68) Gray C.B and Karim A.M.H: "GTO thyristor commutated DC machine", Proceedings 21st UPEC, Imperial College, London, U.K, April 1986, pp 456-459.

(69) Bourne R: "Electrical rotating machine testing", Book, ILIFFE Books Ltd, 1967.

(70) Grimshaw K.P: "The electromagnetic principles of commutation in DC machine", Int. Journal Elect. Eng. Educ., Vol. 2, pp 56-69.

(71) Technical data: "Opto-isolaters and opto-coupled SCR/ Triacs", RS data sheet No. 3958, Nov. 1984.

(72) El-Sheikh-Mahmoud M: "A microprocessor thyristor-controlled DC drive incorporating regenerative braking", Ph.D Thesis, Bradford University, 1985.

(73) Slemon G.R and Straughen A: "Electric Machines", Book, Addison-Wesley Publishing Co., USA, 1980.

A P P E N D I C E S

APPENDIX A

PHOTOGRAPH OF THE OVERALL LAYOUT OF THE DEVELOPED MACHINE

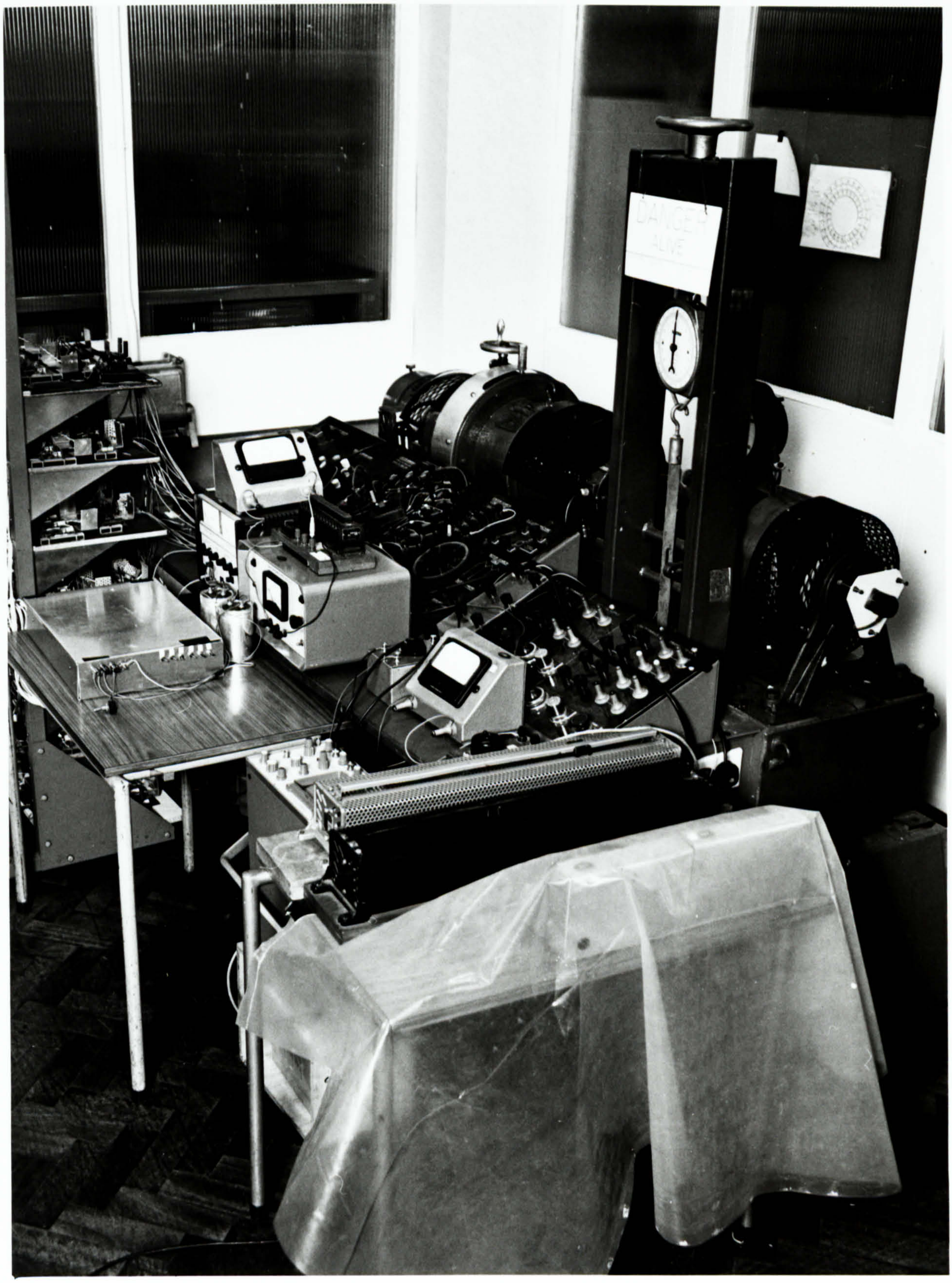
DANGER
ALIVE

APPENDIX B

PHOTOGRAPH OF THE MECHANICALLY COUPLED "INVERTED" MACHINE, DC WORK MACHINE AND ROTARY SHAFT ENCODER

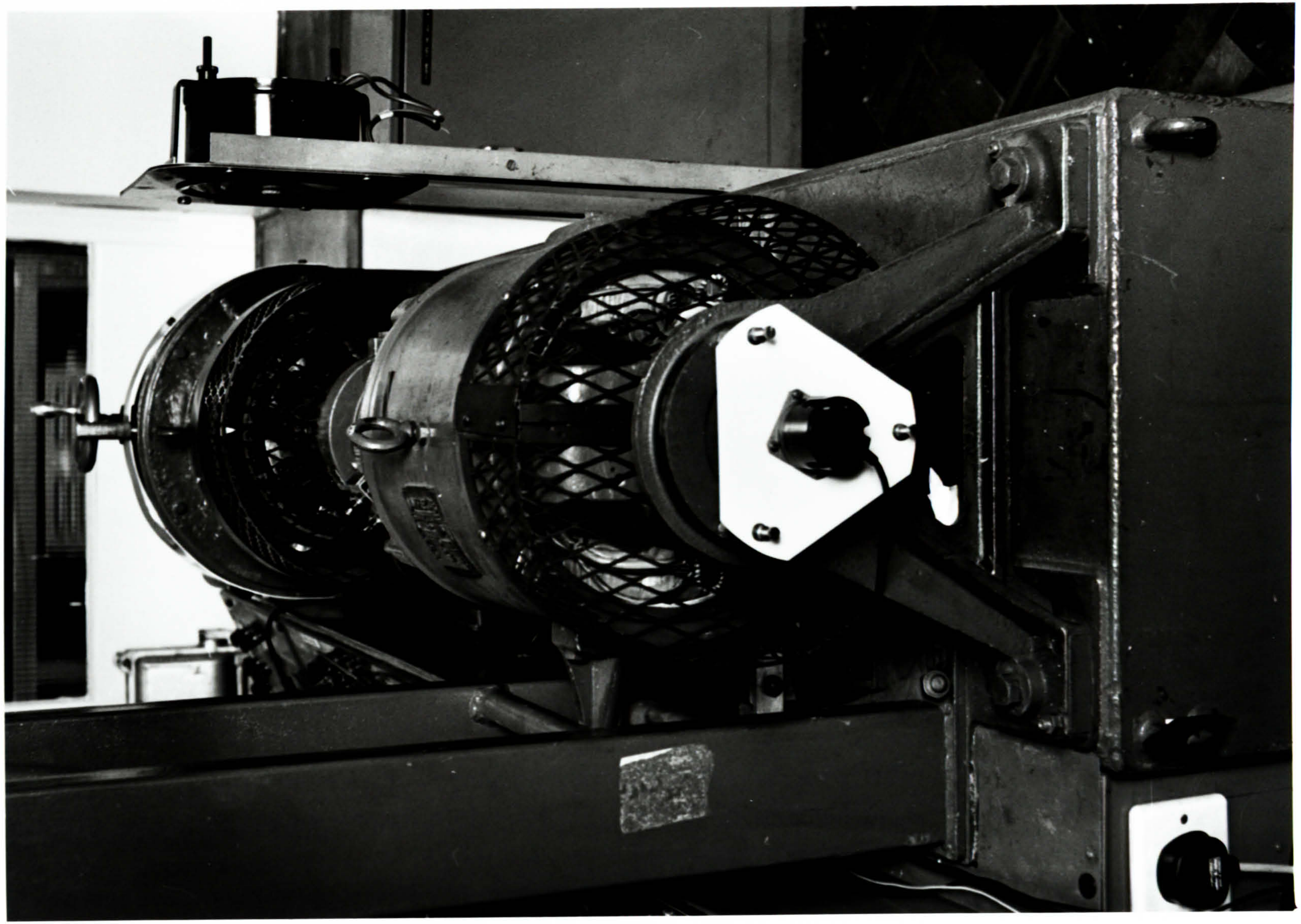

APPENDIX C

SCHEDULE OF DESIGN DATA FOR MAWDSLEY'S GENERALISED MACHINE

MAWDSLEY'S LTD

SCHEDULE OF DESIGN DATA

	Stator	Rotor
Number of slots	48	36
Number of coils	48	36
Type of winding	Double layer	lap
Coil pitch	1-13	1-10
Length of mean turn (metres)	$73.5 \cdot 10^{-2}$	$59.5 \cdot 10^{-2}$
Slot skew	1 slot pitch	nil
Number of commutator segments	-	144
Carter coefficient	1.19	1.18

Diameters (metres)		Axial lengths (metres)		Flux path lengths (metres)	
D_1	$279.0 \cdot 10^{-3}$	L_s	$101.6 \cdot 10^{-3}$	Stator teeth, l_{ts}	$26.4 \cdot 10^{-3}$
D_2	$205.2 \cdot 10^{-3}$	L_{es}	$96.5 \cdot 10^{-3}$	Rotor teeth, l_{tr}	$26.16 \cdot 10^{-3}$
D_3	$152.4 \cdot 10^{-3}$	L_r	$108.0 \cdot 10^{-3}$	Radial air-gap, l_g	$0.508 \cdot 10^{-3}$
D_4	$99.06 \cdot 10^{-3}$	L_{er}	$102.6 \cdot 10^{-3}$		
D_5	$57.15 \cdot 10^{-3}$	L_g	$102.9 \cdot 10^{-3}$	Flux path areas ($metres^2$)	
D_6	$203.0 \cdot 10^{-3}$				
	$114.3 \cdot 10^{-3}$	Lamination thickness, t $0.457.10^{-3}$		Stator core, A_{cs}	$7.16 \cdot 10^{-3}$
				Rotor core, A_{cr}	$4.30 \cdot 10^{-3}$
				Air-gap surface area, A_s	$46.80 \cdot 10^{-3}$

Width of Teeth (metres)				Width of Slot (metres)			
Stator		Rotor		Stator		Rotor	
W_{ts1}	$4.59 \cdot 10^{-3}$	W_{tr1}	$5.35 \cdot 10^{-3}$	W_{1s}	$2.54 \cdot 10^{-3}$	W_{1r}	$3.175 \cdot 10^{-3}$
W_{ts2}	$3.22 \cdot 10^{-3}$	W_{tr2}	$3.87 \cdot 10^{-3}$	W_{2s}	$5.59 \cdot 10^{-3}$	W_{2r}	$7.62 \cdot 10^{-3}$
W_{ts}	$3.68 \cdot 10^{-3}$	W_{tr}	$4.36 \cdot 10^{-3}$	W_{3s}	$10.185 \cdot 10^{-3}$	W_{3r}	$4.775 \cdot 10^{-3}$

Flux Path Volumes ($metres^3$)			
Stator core, U_{cs}	$2.73 \cdot 10^{-3}$	Rotor core, U_{cr}	$0.53 \cdot 10^{-3}$
Stator teeth, U_{ts}	$0.45 \cdot 10^{-3}$	Rotor teeth, U_{tr}	$0.42 \cdot 10^{-3}$

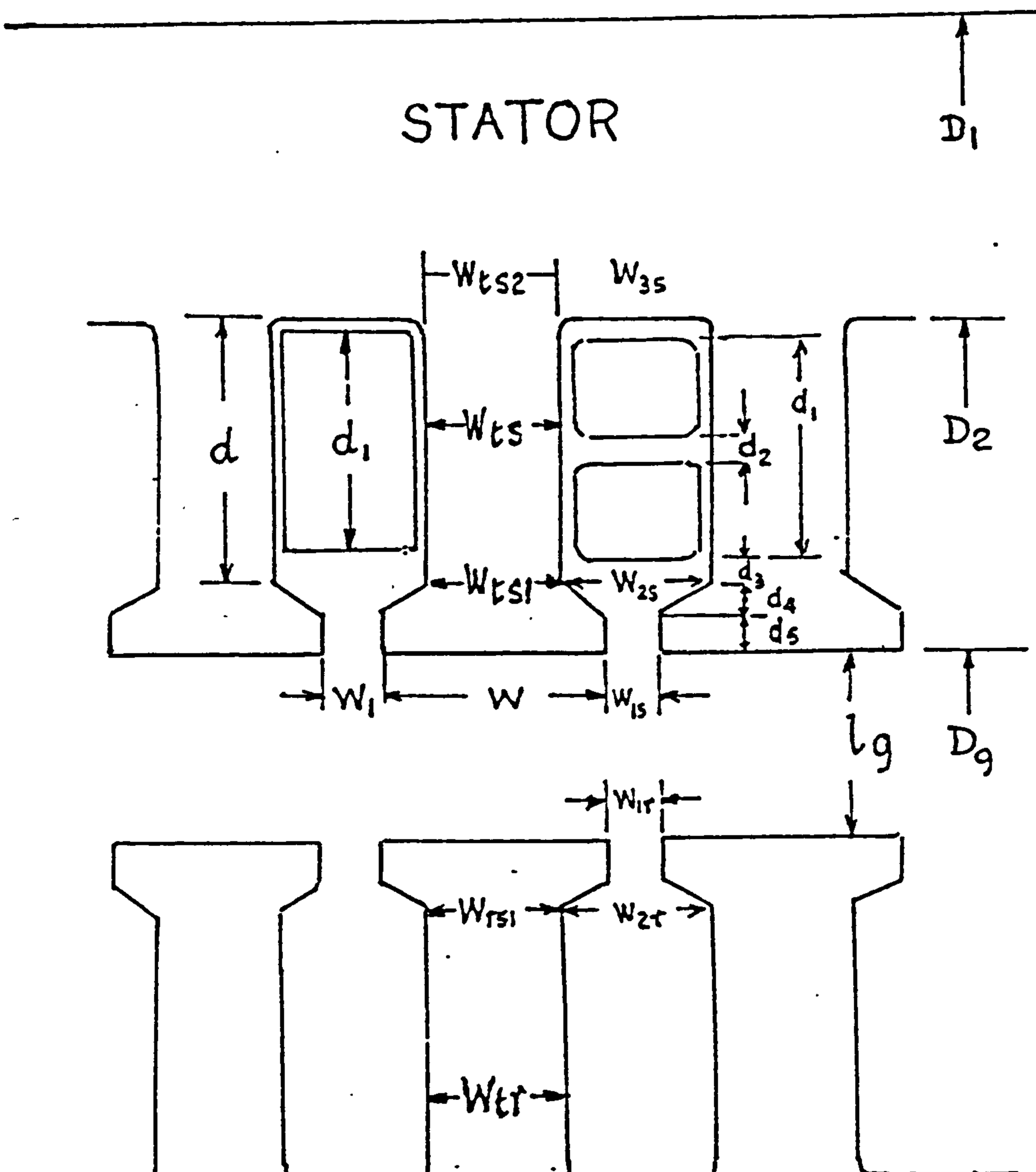

KEY TO STATOR AND ROTOR LAMINATION DIMENSIONS

APPENDIX D

COMPARISON OF PROPERTIES OF G.T.O, SYMMETRICAL THYRISTOR AND DARLINGTON TRANSISTOR.

COMPARISON OF PROPERTIES OF G.T.O, SYMMETRICAL THYRISTOR AND DARLINGTON TRANSISTOR

Designation \ Component		Fast Thyristor (symetrical)	GTO (asymetrical)	Darlington Transistor (npn)
Symbol		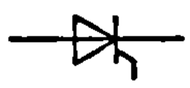	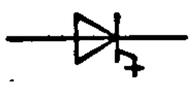	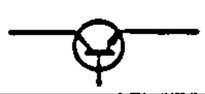
Schematic Representation of Layer Structure in the Silicon		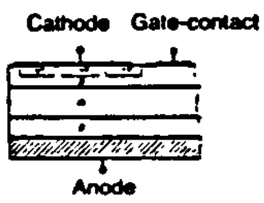	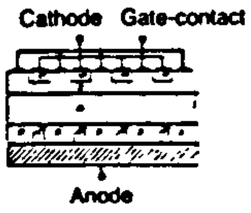	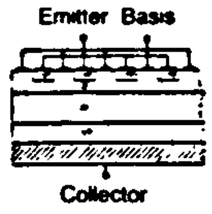
Circuit Diagram of a Self Commutating Converter		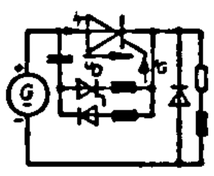	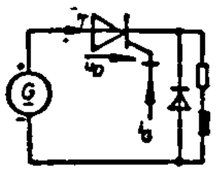	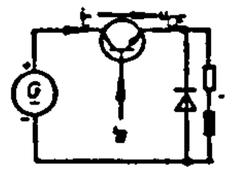
Current and Voltage Loading of the Component vs Time (Schematic)	Main Current			
	Main Voltage			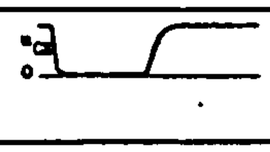
	Gate Current			
Electrical Properties	Turn-on Behavior	low latching current low turn-on power losses turn-on current behavior good	latching current fairly high low turn-on power losses turn-on current behavior good	no latching current low turn-on power losses turn-on current behavior average
	on-state Behavior	on-state power losses low over-current behavior good	on-state power losses average over-current behavior average	on-state power losses low no over-current loading permissible
	Turn-off Behavior	Long turn-off-time Commutation necessary with high power losses	Short turn-off time turn-off power losses average	Short turn-off time turn-off power losses average
	Blocking Capability	Symmetrical in both directions, or more seldom asymmetrical	Often only in forward direction; seldom symmetrical	Only in forward direction
Protection Measures	over-current	Turn-off via fuses or fast contactors	Fast turn-off via gating, delayed turn-off via fuse	Super-fast turn-off via neg. basis current delayed turn-off prohibited
	over-voltage	RC-circuit at equipment input or at the thyristor	RCD-circuit on the GTO with additional circuit at equipment input	RCD-circuit on the transistor with additional electronic voltage monitor
Repetition Frequency		low	Fairly High	Fairly High
Area of Silicon Element		small	average	large

APPENDIX E

DATA SHEETS FOR THE MULLARD BTW 58 - 1300R GATE TURN-OFF THYRISTOR ARMATURE SWITCHES

FAST GATE TURN-OFF THYRISTORS

Thyristors in TO-220AB envelopes capable of being turned both on and off via the gate. They are suitable for use in high-frequency inverters, power supplies, motor control, horizontal deflection systems etc. The devices have no reverse blocking capability. For reverse blocking operation use with a series diode, for reverse conducting operation use with an anti parallel diode.

QUICK REFERENCE DATA

			BTW58–1000R	1300R	1500R	
Repetitive peak off-state voltage	V_{DRM}	max.	1000	1300	1500	V
Controllable anode current	I_{TCRM}	max.		25		A
Average on-state current	$I_{T(AV)}$	max.		6.5		A
Fall time	t_f	<		250		ns

MECHANICAL DATA

Dimensions in mm

Fig.1 TO-220AB

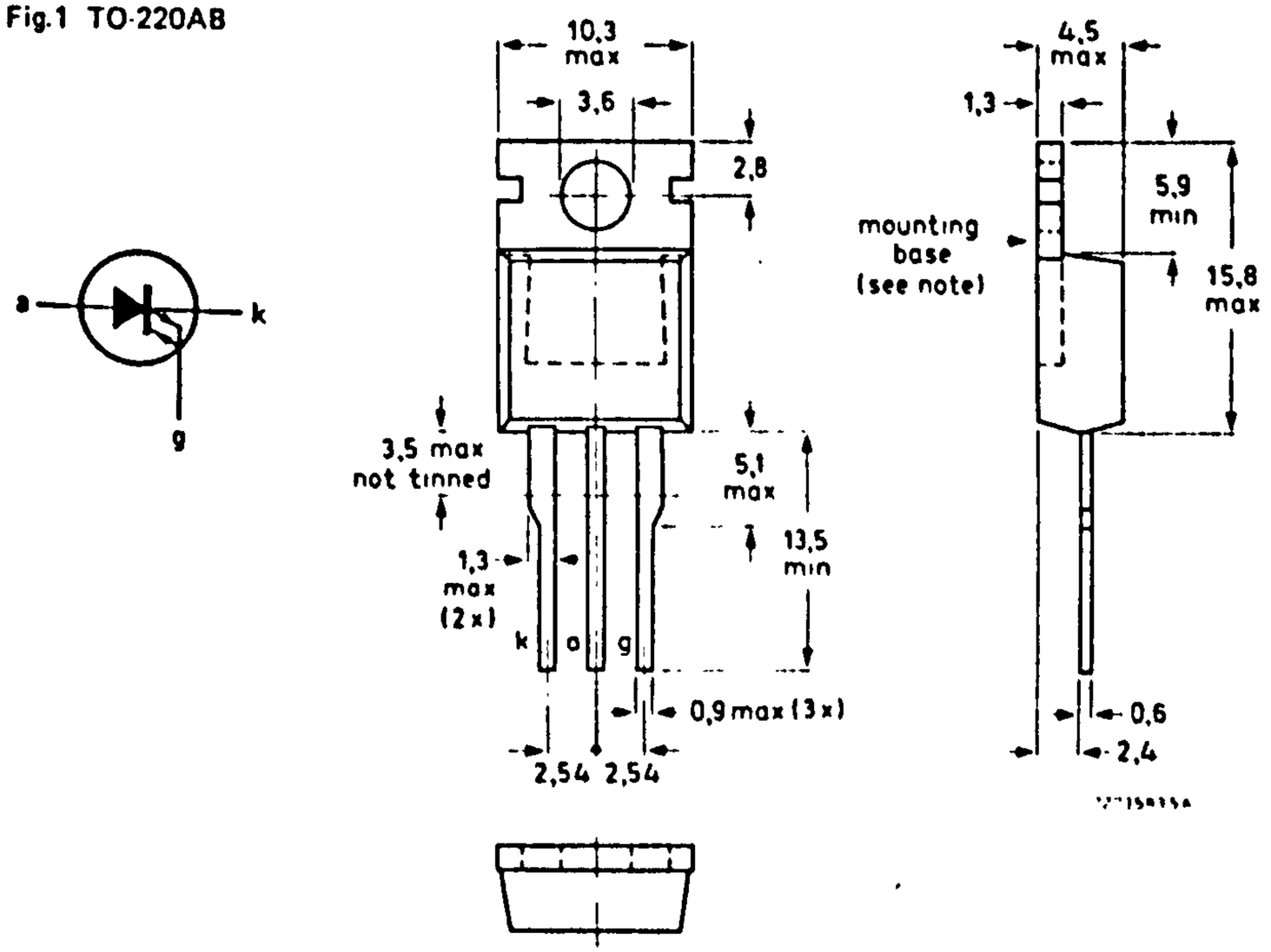

Net mass: 2 g

Note: The exposed metal mounting base is directly connected to the anode.

Accessories supplied on request: see data sheets Mounting instructions and accessories for TO-220 envelopes.

RATINGS

Limiting values in accordance with the Absolute Maximum System (IEC134)

Anode to cathode			BTW58–1000R	1300R	1500R	
Transient off-state voltage	V_{DSM}	max.	1200	1500	1650	V*
Repetitive peak off-state voltage	V_{DRM}	max.	1000	1300	1500	V*
Working off-state voltage	V_{DW}	max.	650	1200	1300	V*
Continuous off-state voltage	V_D	max.	650	750	800	V*

Average on-state current (averaged over any 20 ms period) up to T_{mb} = 85 °C	$I_{T(AV)}$	max.	6.5	A
R.M.S. on-state current	$I_{T(RMS)}$	max.	7.5	A
Controllable anode current	I_{TCRM}	max.	25	A
Non-repetitive peak on-state current t = 10 ms; half-sinewave; T_j = 120 °C prior to surge	I_{TSM}	max.	50	A
I^2t for fusing; t = 10 ms	I^2t	max.	12.5	A^2s
Total power dissipation up to T_{mb} = 25 °C	P_{tot}	max.	65	W
Gate to cathode				
Repetitive peak on-state current T_j = 120 °C prior to surge				
gate-cathode forward; t = 10 ms; half-sinewave	I_{GFM}	max.	25	A
gate-cathode reverse; t = 20 μs	I_{GRM}	max.	25	A
Average power dissipation (averaged over any 20 ms period)	$P_{G(AV)}$	max.	2.5	W
Temperatures				
Storage temperature	T_{stg}		−40 to +150	°C
Operating junction temperature	T_j	max.	120	°C

THERMAL RESISTANCE

From junction to mounting base	$R_{th\ j\text{-}mb}$	=	1.5	°C/W
From mounting base to heatsink with heatsink compound	$R_{th\ mb\text{-}h}$	=	0.3	°C/W
with 56367 alumina insulator and heatsink compound (clip-mounted)	$R_{th\ mb\text{-}h}$	=	0.8	°C/W

*Measured with gate-cathode connected together.

CHARACTERISTICS

Anode to cathode

On-state voltage I_T = 5A; I_G = 0.2A; T_j = 120 °C	V_T	<	3.0	V*
Rate of rise of off-state voltage that will not trigger any off-state device; exponential method V_D = 2/3 V_{Dmax}; V_{GR} = 5 V; T_j = 120 °C	dV_D/dt	<	10	kV/μs
Rate of rise of off-state voltage that will not trigger any device following conduction; linear method; I_T = 5A; V_D = V_{Dmax}; V_{GR} = 10 V; T_j = 120 °C	dV_D/dt	<	1.5	kV/μs
Off-state current V_D = V_{Dmax}; T_j = 120 °C	I_D	<	3.0	mA
Latching current; T_j = 25 °C	I_L	<	1.5	A**

Gate to cathode

Voltage that will trigger all devices V_D = 12 V; T_j = 25 °C	V_{GT}	>	1.5	V
Current that will trigger all devices V_D = 12 V; T_j = 25 °C	I_{GT}	>	200	mA
Maximum reverse leakage current V_{GRM} = 10 V	I_{GRM}	<	1.0	mA

Switching characteristics

Turn on when switched to I_T = 5A from V_D = 250 V with I_{GF} = 500 mA delay time	t_d	<	0.25	μs
rise time	t_r	<	1.0	μs
Turn-off when switched from I_T = 5A to V_D = 250 V with $-V_{GG}$ = 10 V storage time	t_s	<	0.5	μs
fall time	t_f	<	0.25	μs

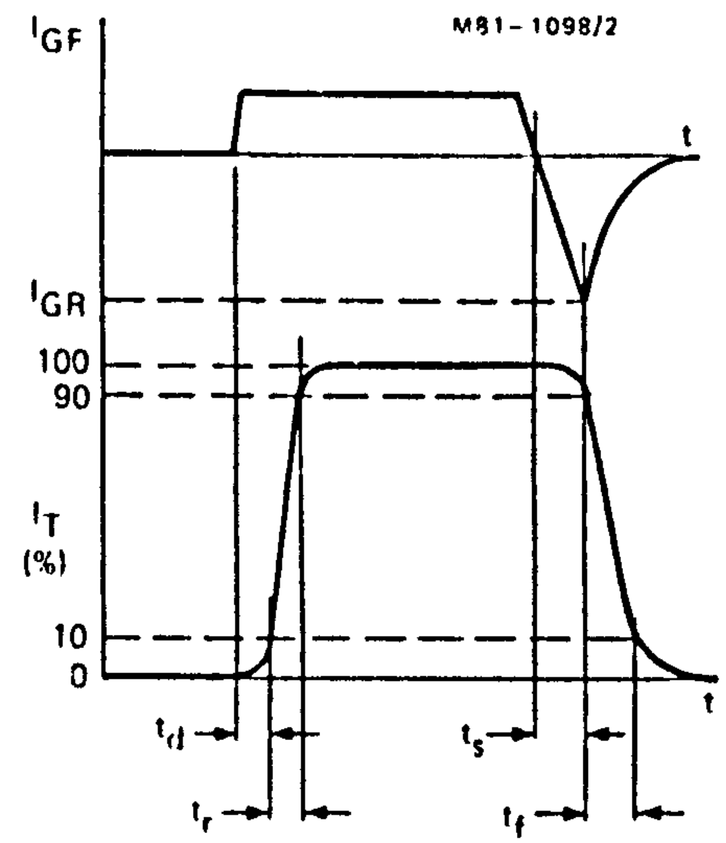

Fig 2 Waveform

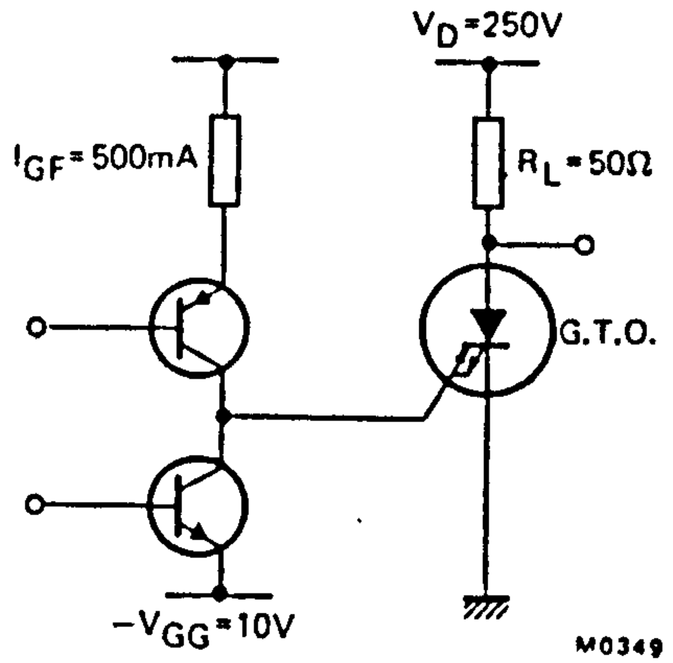

Fig.3 Test circuit

* Measured under pulse conditions to avoid excessive dissipation.

** Below latching level the device behaves like a transistor with a gain dependant on current; see Fig 8.

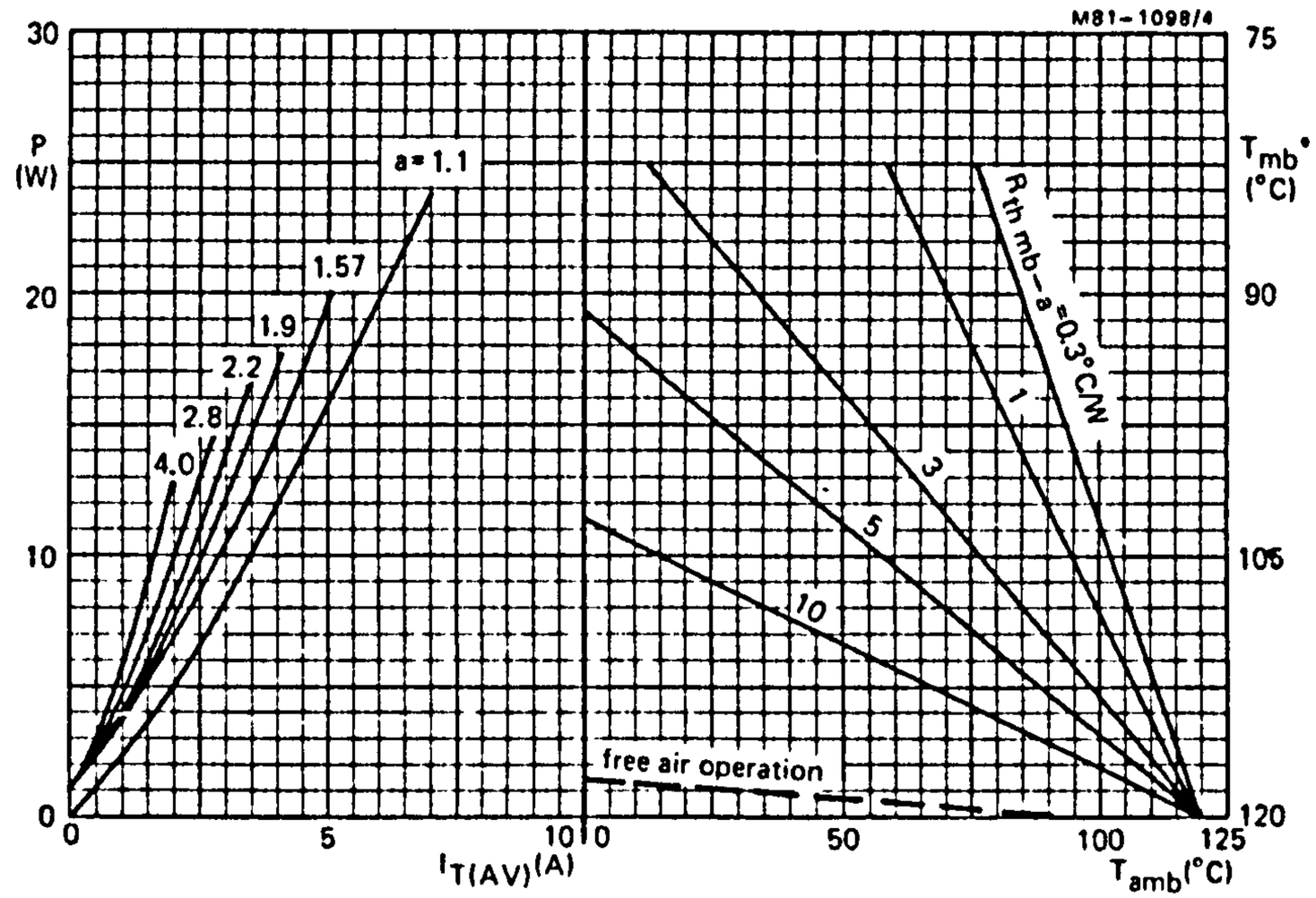

Fig.4 The right hand part shows the interrelationship between the power (derived from the left-hand part) and the maximum permissible temperatures.

a = form factor = $\frac{I_{T(RMS)}}{I_{T(AV)}}$

*T_{mb} scale is for comparison purposes and is correct only for $R_{th\ mb\text{-}a} < 9.6$ °C/W.

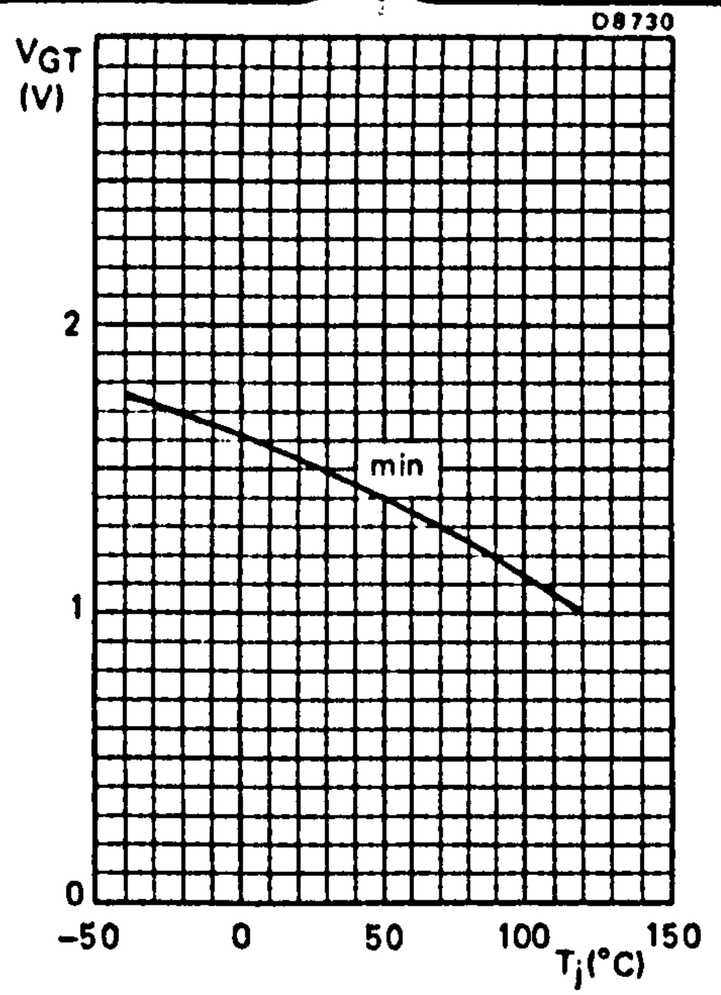

Fig.5 Minimum gate voltage that will trigger all devices as a function of junction temperature.

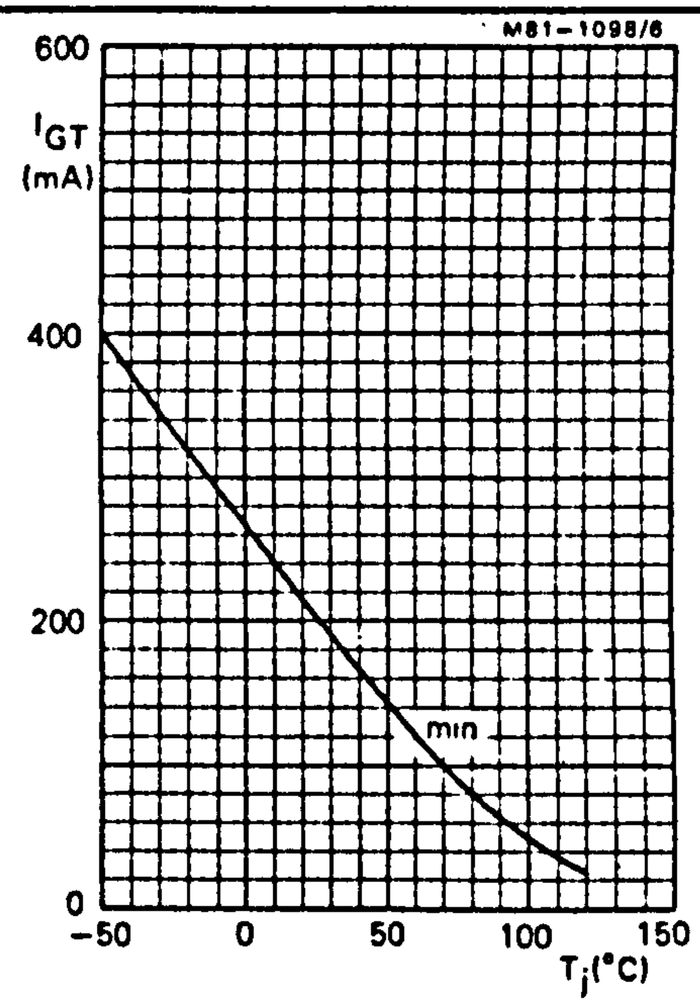

Fig.6 Minimum gate current that will trigger all devices as a function of junction temperature.

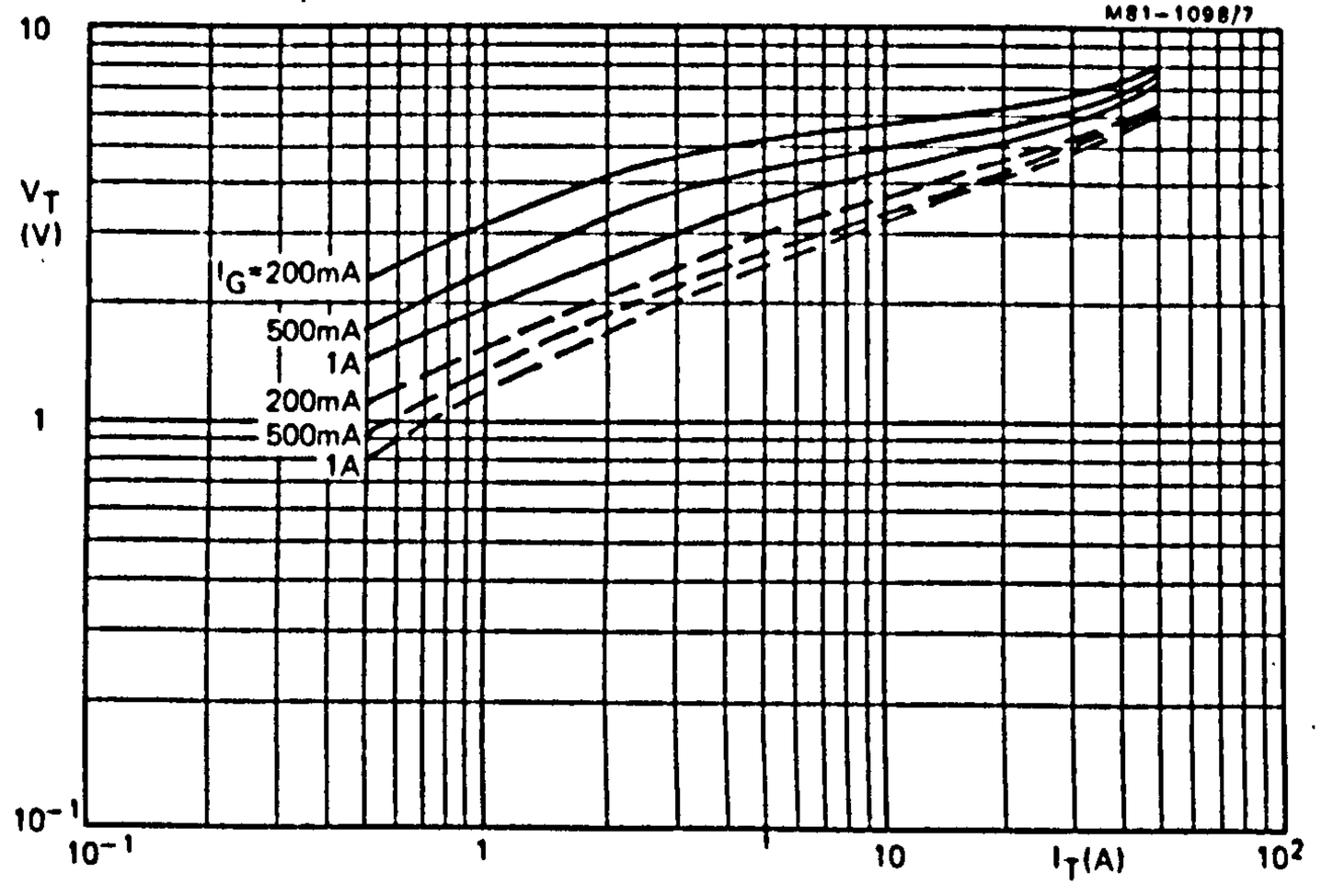

Fig.7 Maximum V_T versus I_T; —— T_j = 25 °C; - - - - T_j = 120 °C.

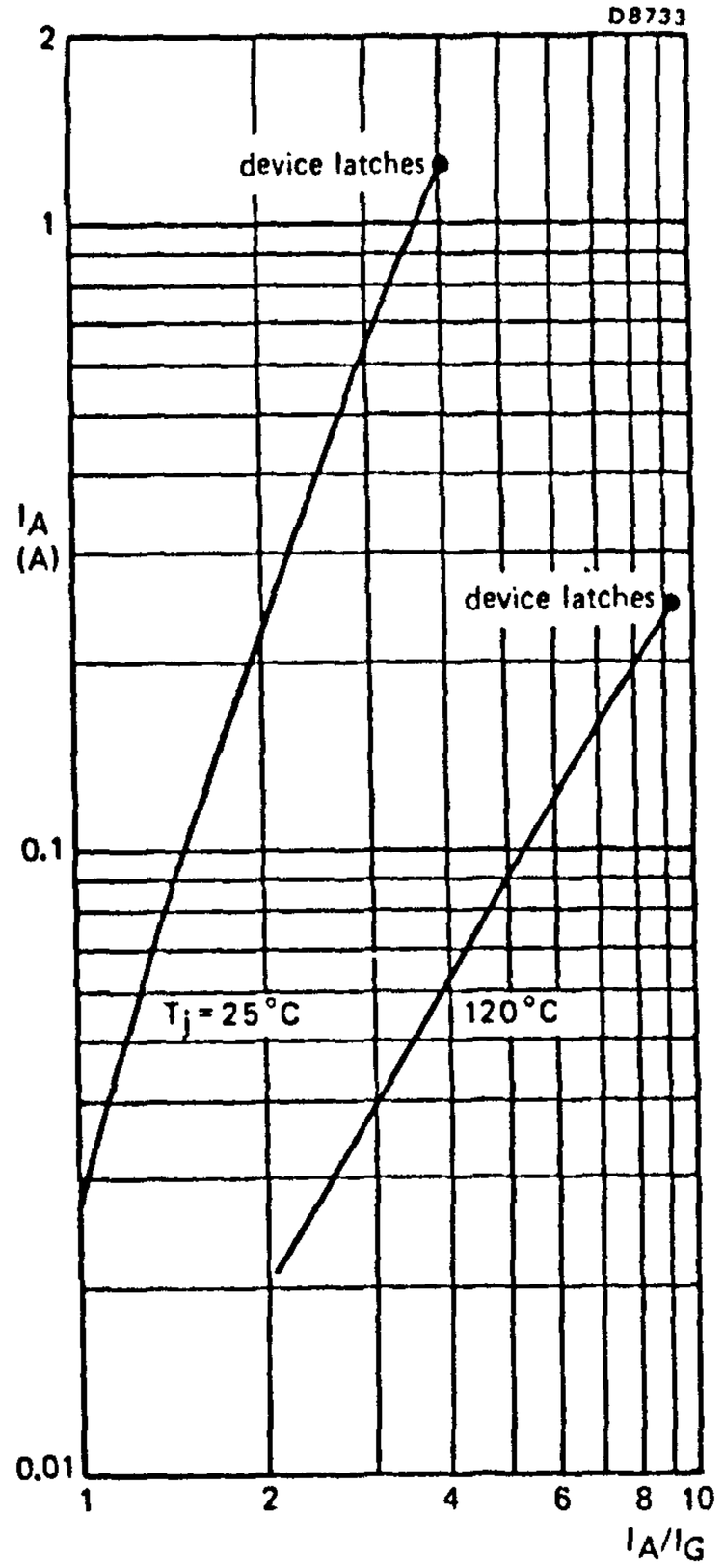

Fig 8 Typical latching behaviour

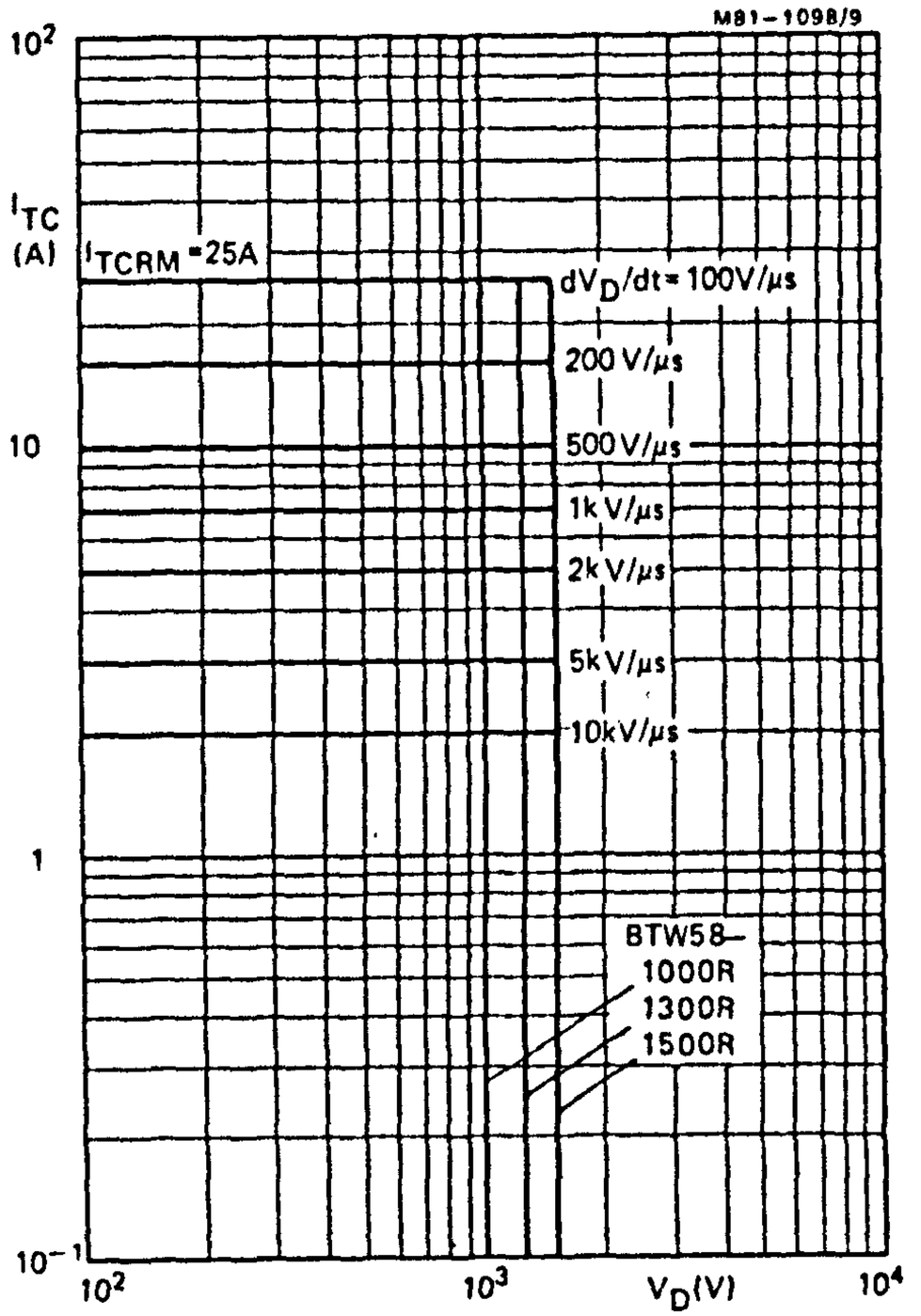

Fig.9 Anode current which can be turned off versus anode voltage. Inductive load; V_{GR} = 10 V; T_{mb} = 85 °C.

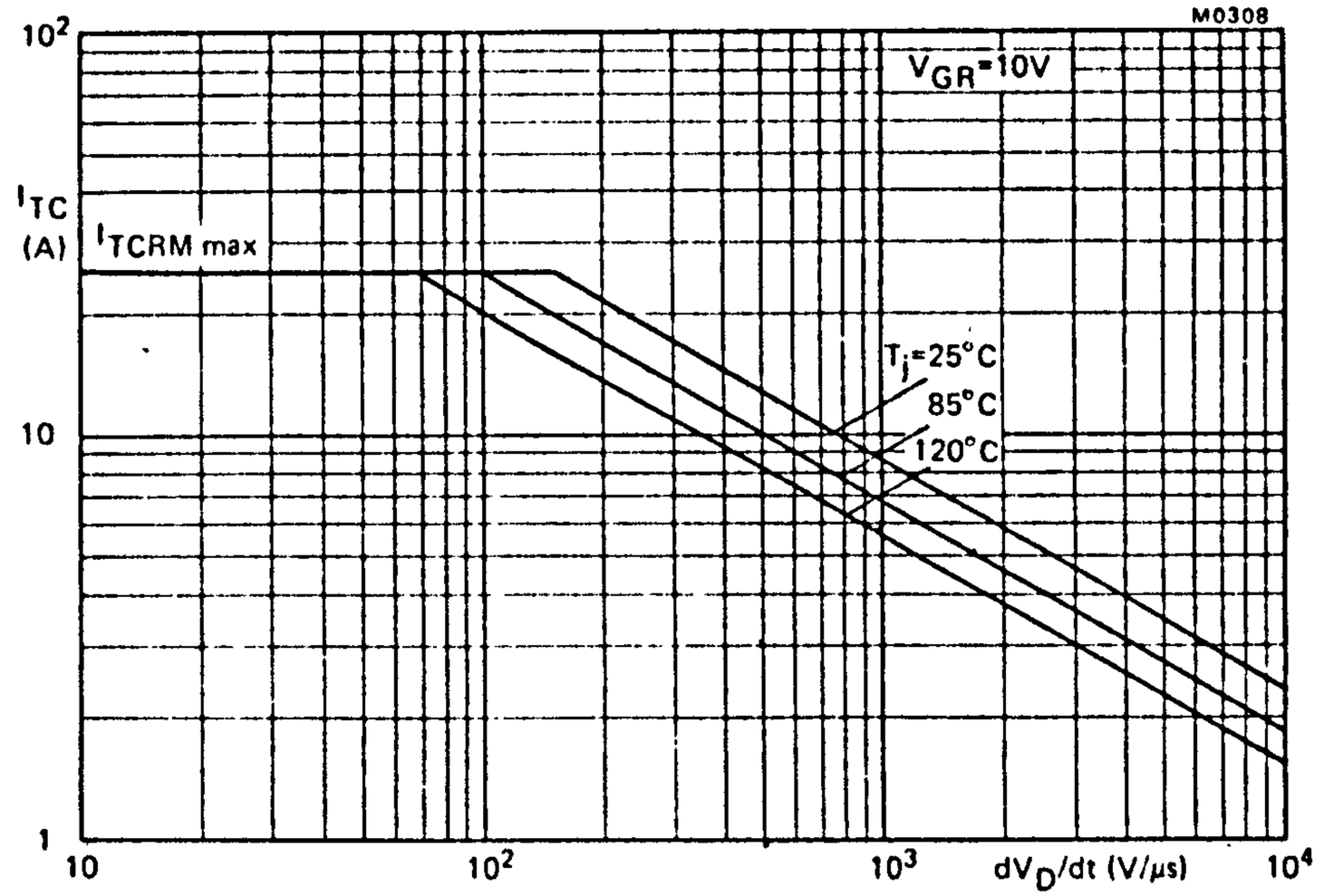

Fig. 10 Anode current which can be turned off versus applied dV_D/dt; inductive load; V_{GR} = 10 V.

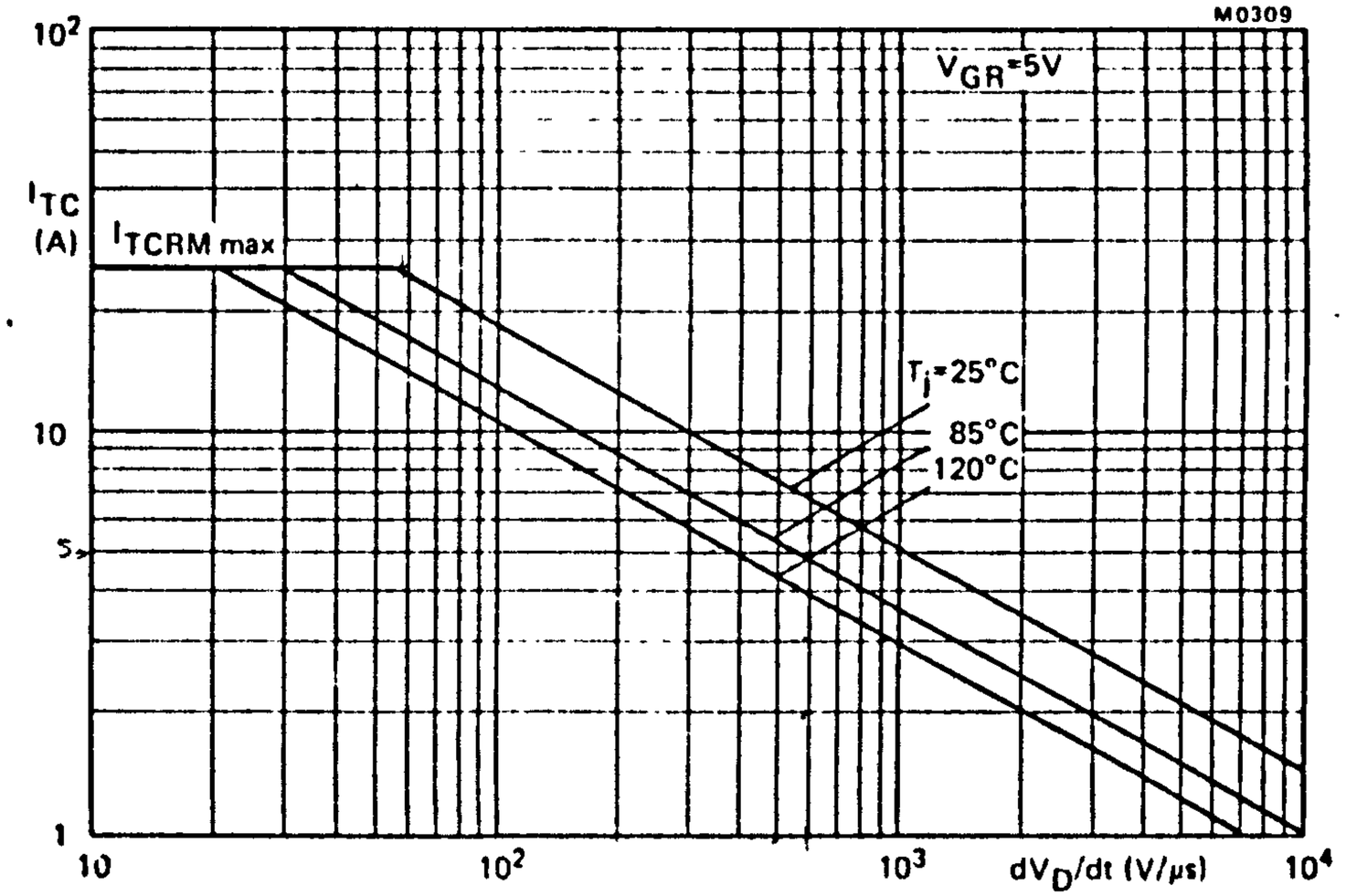

Fig. 11 Anode current which can be turned off versus applied dV_D/dt; inductive load; V_{GR} = 5 V.

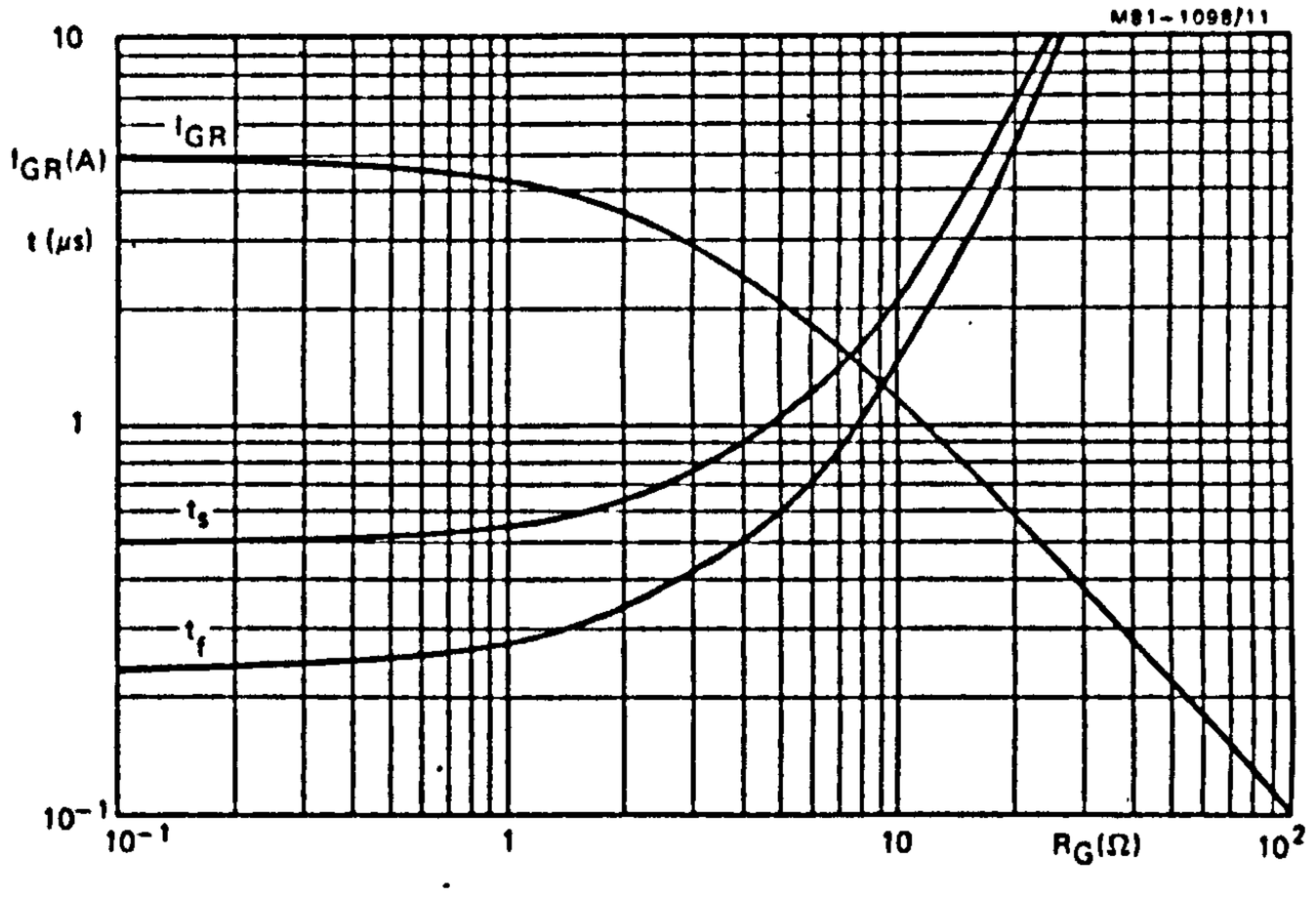

Fig. 12 Reverse gate current, storage time and fall time versus series gate resistance. Resistive load; I_T = 5 A; V_{GR} = 10 V; T_{mb} = 25 °C. Maximum values.

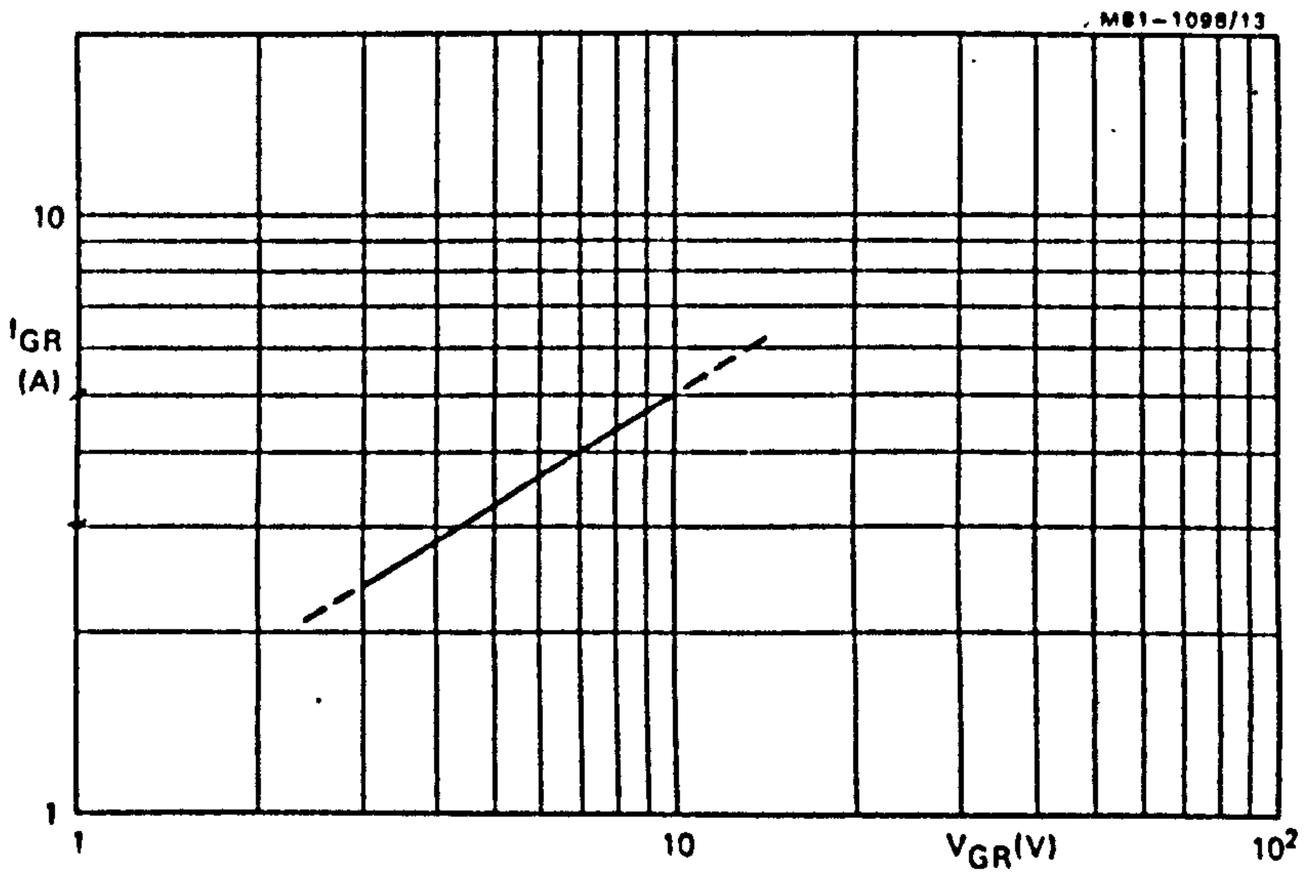

Fig. 13 Reverse gate current versus applied reverse gate voltage. Resistive load; I_T = 5 A; R_G = 0 Ω; T_{mb} = 25 °C. Maximum values.

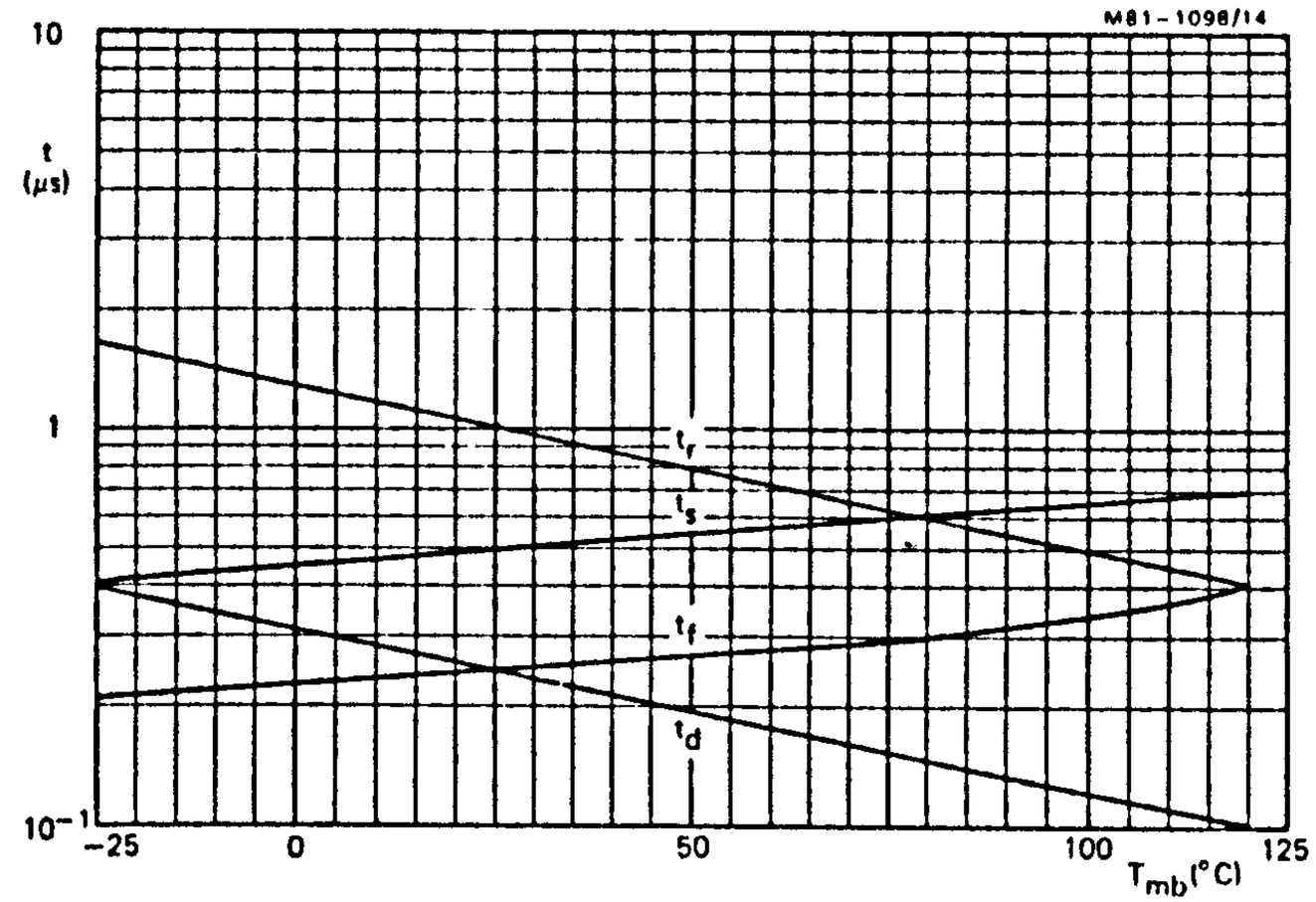

Fig. 14 Delay time, rise time, storage time and fall times as a function of temperature. Resistive load; I_T = 5 A; V_{GR} = 10 V; R_G = 0 Ω. Maximum values.

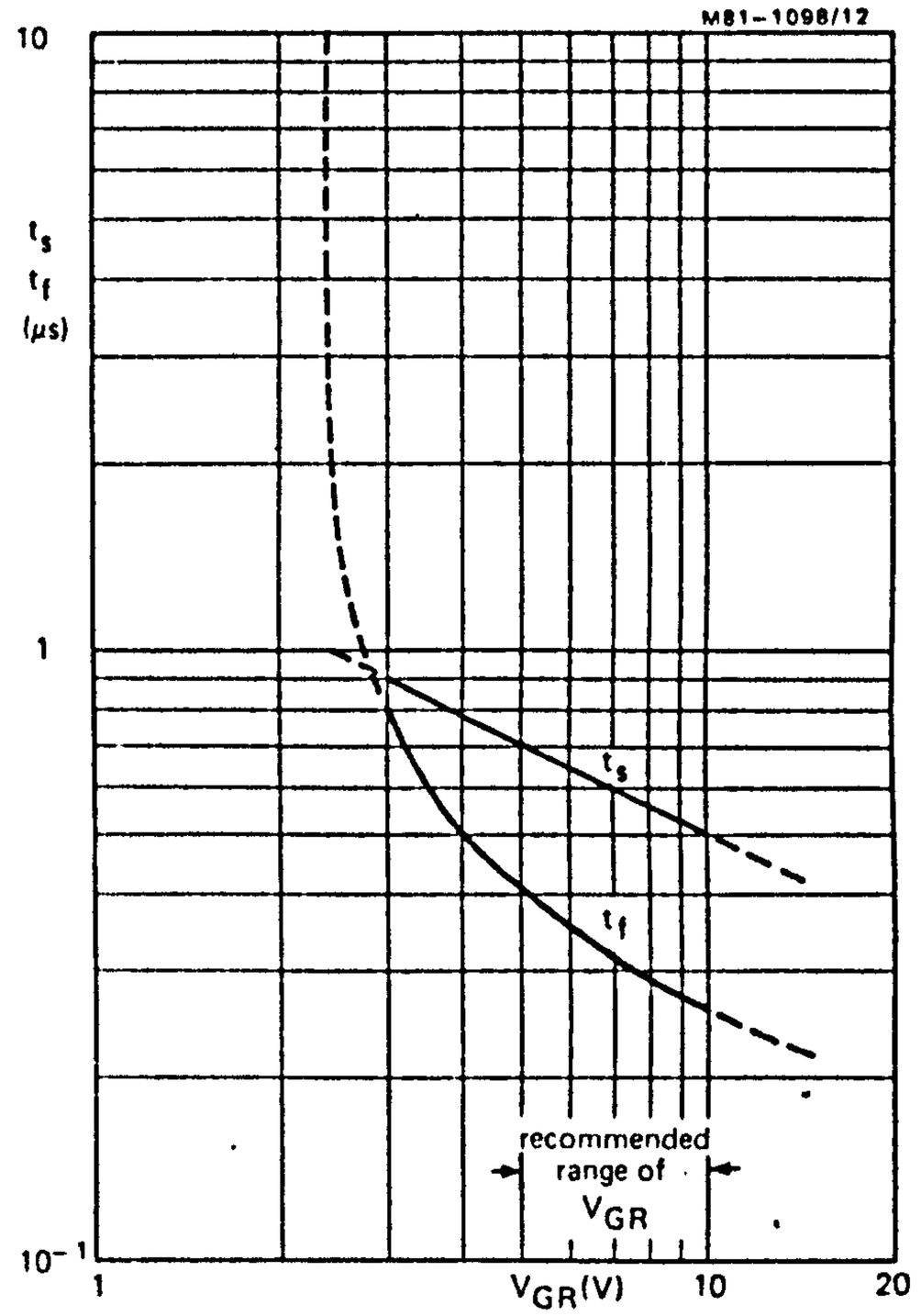

Fig. 15 Storage and fall times versus applied reverse gate voltage. Resistive load, I_T = 5 A; R_G = 0 Ω; T_{mb} = 25 °C. Maximum values.

APPENDIX F

DATA SHEETS FOR SHARP GP1R52 INCREMENTAL ROTARY ENCODER FOR ROTOR POSITION FEEDBACK

214

SHARP CORPORATION

No. KS-82543

TECHNICAL LITERATURE

FOR

Rotary Encoder

MODEL NO. GP-1R52

DATE October 26, 1982

Hero Electronics Limited,
Dunstable Street,
Ampthill,
Bedfordshire, MK45 2JS,

Telephone 0525 405015
Telex 825906

HERO

** The technical literature is subject to be changed without notice **

SHARP CORPORATION
ELECTRONIC COMPONENTS GROUP

SHARP

1. Application

This specification applies to the structures and characteristics of Model No. GP-1R52.

2. Outline

Refer to the attached drawing SOG89172.

3. Ratings and characteristics

3-1. Test circuit

- Supply Voltage : V_{CC}=5V±5%
- Load Resistance on Output Side : R_L=10kΩ±5%

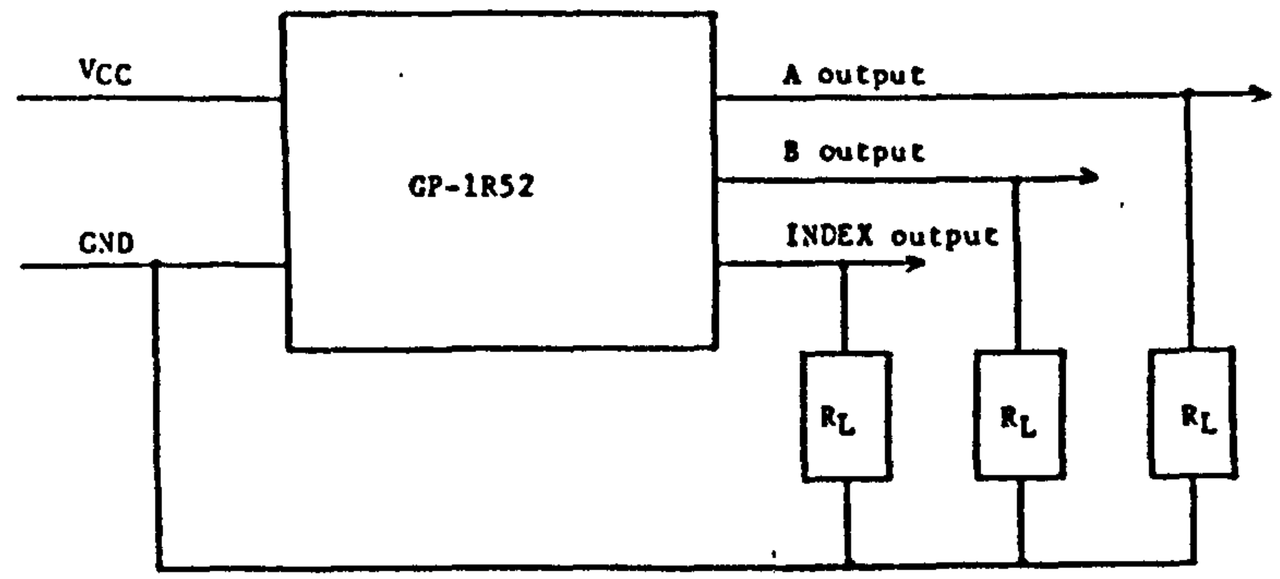

3-2. Absolute maximum ratings

Ta = 25°C

Parameter	Symbol	Ratings	Unit	Remarks
Supply Voltage	V_{CC}	8	V	Note 1)
Min. Load Resistance on Output Side	R_L	5.0	kΩ	
Operating Temperature	Topr	0 ∿ +70	°C	
Storage Temperature	Tstg	-40 ∿ +80	°C	
Max. Allowable Number of Rotations	RPMmax.	5000	rpm	

SHARP

3-3 Electrical Characteristics

V_{CC}=5.0V, R_L=10KΩ, Ta=25°C

Parameter	Symbol	Conditions	MIN.	TYP.	MAX.	UNIT
Cycle	$\frac{T_1}{T_3}$	V_{TH} = 1.5V T_3 = DC~0.5msec (A output)	0.45	0.50	0.55	
	$\frac{T_2}{T_3}$	V_{TH} = 1.5V T_3 = DC~0.5msec (A output)	0.45	0.50	0.55	
	$\frac{T_6}{T_8}$	V_{TH} = 1.5V T_3 = DC~0.5msec (B output)	0.45	0.50	0.55	
	$\frac{T_7}{T_8}$	V_{TH} = 1.5V T_8 = DC~0.5msec (B output)	0.45	0.50	0.55	
Phase Difference	$\frac{T_4}{T_3}\times 360°$	T_3 = DC~5msec (A, B output)	75	90	105	deg
	$\frac{T_5}{T_3}\times 360°$	T_3 = DC~5msec (A, B output)	75	90	105	deg
Index Voltage	V_H	T_3 = DC~5msec	1.00	1.25	1.50	V
	V_L	T_3 = DC~5msec	—	—	0.6	V
Dissipation Current	I_{TOTAL}	————	—	—	70	mA

Note 1) The resolution of the encoder shall be 96 P/R.

Note 2) Supply voltage shall be V_{CC}=5V±5%.

MODEL No. GP-1R52 | PAGE

SHARP

3-4. Output Waveform

a) A Output

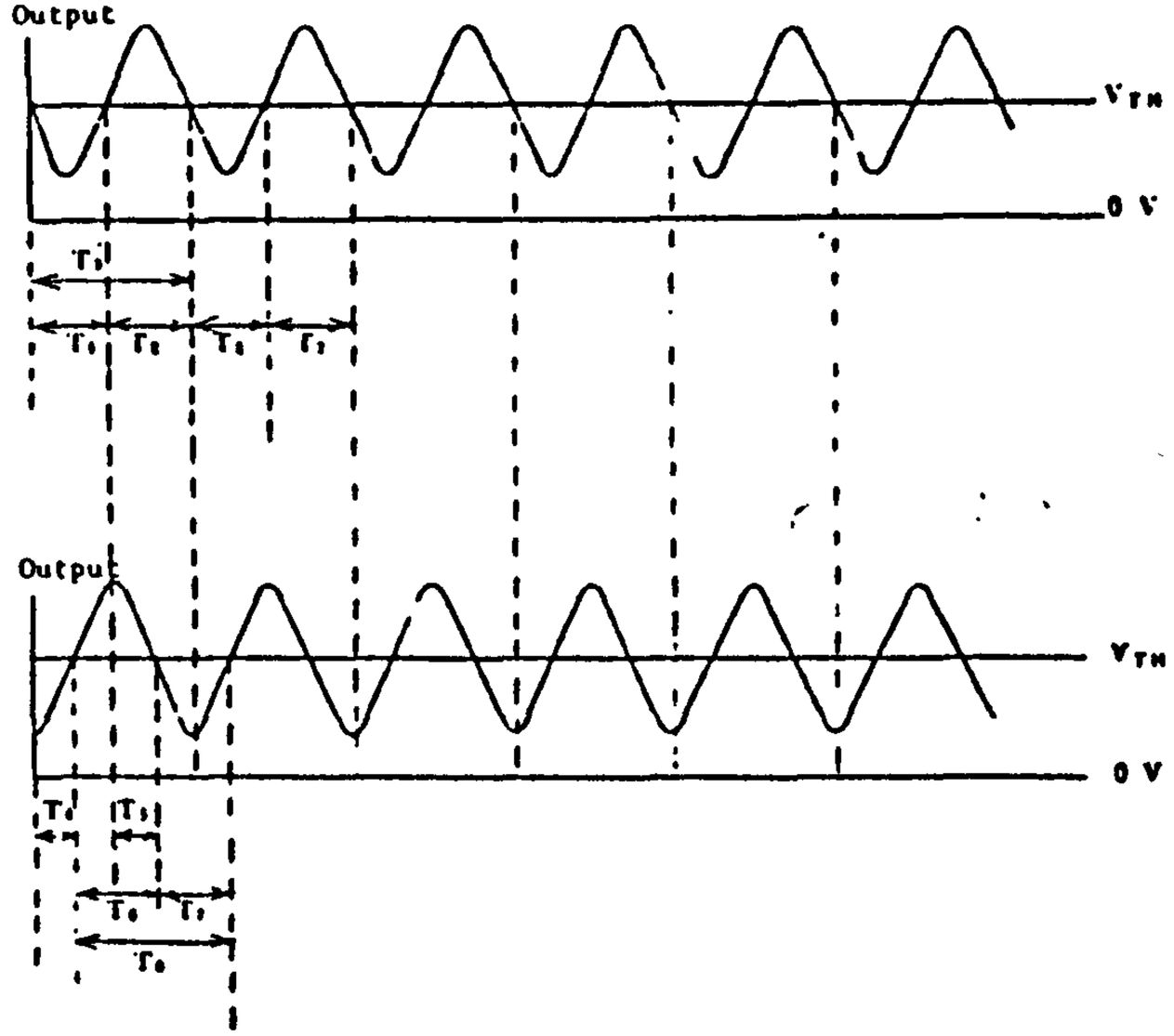

b) B Output

c) INDEX Output

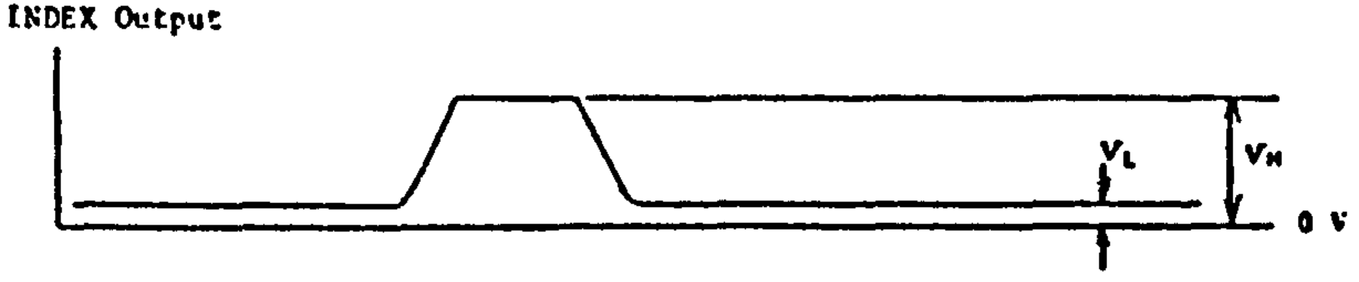

- Rotational direction : Clockwise when seen from the light emitting diode.
- T_1 : Average time required for A output to fall below V_{TH}.
- T2 : Average time required for A output to rise over V_{TH}.
- $T_4 \sim T_8$: Average time for above waveforms.

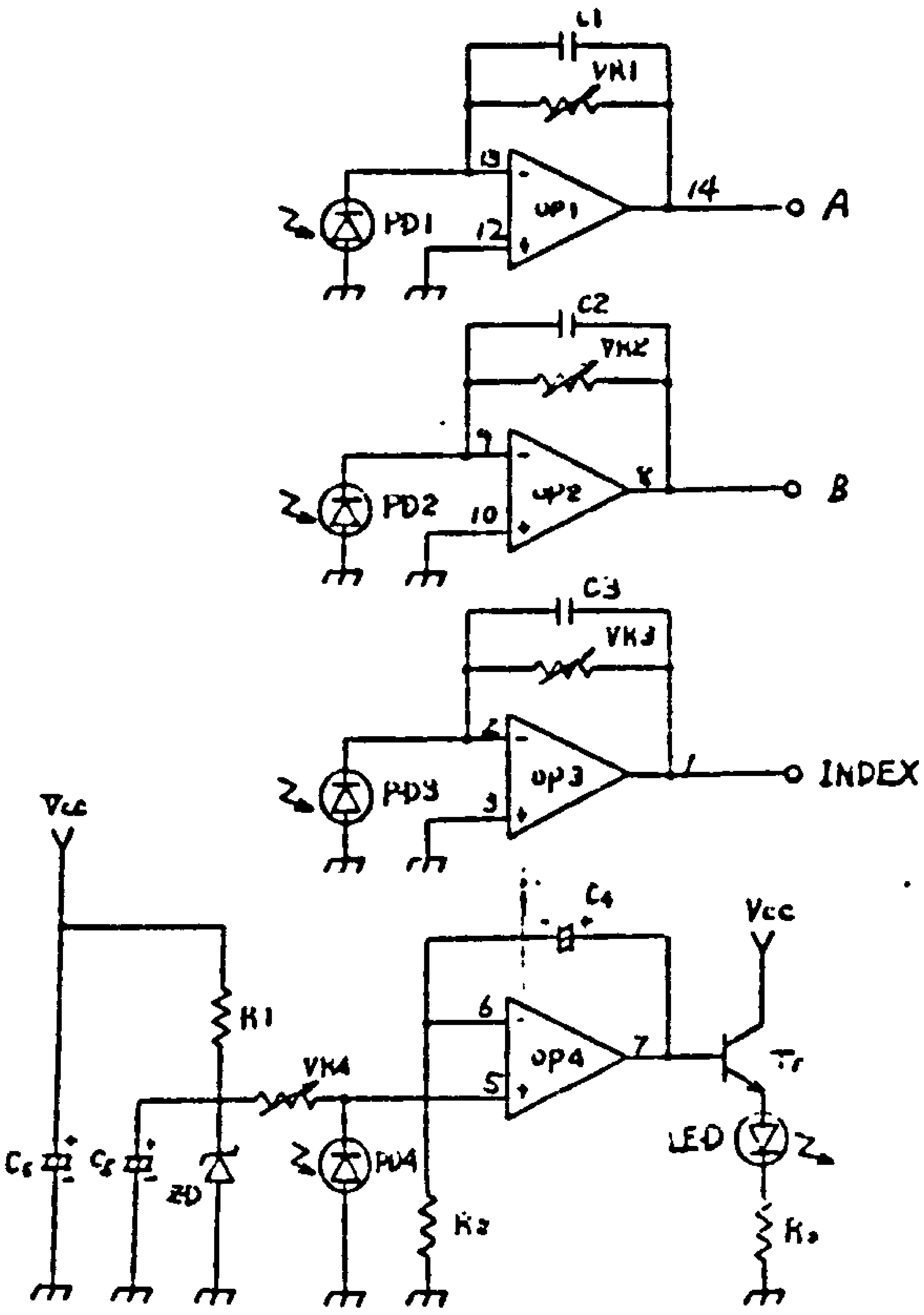

OP1 ∿ OP4 : IR3702

PD1 ∿ PD4 : Photodiode PD-004

VR1 ∿ VR4 : Trimming resistor (4 elements)

R1 : 200Ω 1/4W±5% }
R2 : 150kΩ 1/4W±5% } Carbon resistor
R3 : 33Ω 1/2W±5% }

C1 ∿ C3 : Ceramic capacitor 33pF

C4 ∿ C6 : Tantalum capacitor 0.1μF

ZD : 05Z30

Tr : 2SC1214, 2SC1213A

LED : GL-515

Page